Pontifícia Universidade Católica do Rio Grande do Sul
FACULDADE DE ENGENHARIA
PROGRAMA DE PÓS-GRADUAÇÃO EM ENGENHARIA E TECNOLOGIA DE MATERIAIS

DESIGN DE NOVOS MATERIAIS POLIMÉRICOS PARA CAPTURA DE CO_2

FRANCIELE LONGARAY BERNARD
QUÍMICA INDUSTRIAL E LICENCIADA
MESTRE EM ENGENHARIA E TECNOLOGIA DE MATERIAIS

TESE PARA A OBTENÇÃO DO TÍTULO DE DOUTOR EM ENGENHARIA E TECNOLOGIA DE MATERIAIS

Porto Alegre

Junho, 2017

Pontifícia Universidade Católica do Rio Grande do Sul
FACULDADE DE ENGENHARIA
PROGRAMA DE PÓS-GRADUAÇÃO EM ENGENHARIA E TECNOLOGIA DE MATERIAIS

DESIGN DE NOVOS MATERIAIS POLIMÉRICOS PARA CAPTURA DE CO_2

FRANCIELE LONGARAY BERNARD
QUÍMICA INDUSTRIAL E LICENCIADA
MESTRE EM ENGENHARIA E TECNOLOGIA DE MATERIAIS

ORIENTADOR: PROF(a). DR(a). SANDRA MARA DE OLIVEIRA EINLOFT
CO-ORIENTADOR: Prof. Dr. FELIPE DALLA VECCHIA

Tese realizada no Programa de Pós-Graduação em Engenharia e Tecnologia de Materiais (PGETEMA) da Pontifícia Universidade Católica do Rio Grande do Sul, como parte dos requisitos para a obtenção do título de Doutor em Engenharia e Tecnologia de Materiais.

O presente trabalho de tese foi alcançado em cooperação com a Hewlett-Packard Brasil Ltda. e com recursos provenientes da Lei de Informática (Lei nº 8.248, de 1991).

Porto Alegre
Junho, 2017

Pontifícia Universidade Católica do Rio Grande do Sul
FACULDADE DE ENGENHARIA
PROGRAMA DE PÓS-GRADUAÇÃO EM ENGENHARIA E TECNOLOGIA DE MATERIAIS

DESIGN DE NOVOS MATERIAIS POLIMÉRICOS PARA CAPTURA DE CO2

CANDIDATA: FRANCIELE LONGARAY BERNARD

Esta Tese de Doutorado foi julgada para obtenção do título de DOUTOR EM ENGENHARIA E TECNOLOGIA DE MATERIAIS e aprovada em sua forma final pelo Programa de Pós-Graduação em Engenharia e Tecnologia de Materiais da Pontifícia Universidade Católica do Rio Grande do Sul.

DRA. SANDRA MARA OLIVEIRA EINLOFT - ORIENTADORA

DR. FELIPE DALLA VECCHIA - CO-ORIENTADOR

BANCA EXAMINADORA

DR. CARLOS ARTHUR FERREIRA - DO PPGE3M - UFRGS

DRA. OFÉLIA DE QUEIROZ FERNANDES ARAÚJO - ESCOLA DE QUÍMICA DA UNIVERSIDADE FEDERAL DO RIO DE JANEIRO, DEPARTAMENTO DE ENGENHARIA QUÍMICA - UFRJ

DR. RUBEM MÁRIO FIGUEIRÓ VARGAS - DO PGETEMA/FENG - PUCRS

PUCRS
Campus Central
Av. Ipiranga, 6681 - Prédio 30 - Sala 103 - CEP: 90619-900
Telefone: (51) 3353.4059 - Fax: (51) 3320.3625
E-mail: engenharia.pg.materiais@pucrs.br

”Cada sonho que você deixa pra trás, é um pedaço do seu futuro que deixa de existir”

(Steve Jobs)

DEDICATÓRIA

Ao meu querido avô Nôrmio Longaray (in memoriam), por ter desempenhado esplendidamente o papel de pai e avô na minha vida, transmitindo sempre bons conselhos, amor e alegria. A Minha amada mãe Liége T.B.Longaray, meu exemplo, a quem considero a minha melhor amiga e grande responsável por esta trajetória acadêmica. Ao meu amado esposo Diego Nardin, pelo seu amor, aconchego, apoio, incentivo e por estar sempre ao meu lado, tornando meus dias mais felizes. Por fim, mas não menos importante, a minha querida avó Angelina Bernar pelo seu amor, ternura e cuidados.

AGRADECIMENTOS

A minha família, em especial a minha mãe Liége e aos meus avôs Nôrmio e Angelina por todo amor, carinho, ensinamentos e por sempre acreditarem no meu potencial, incentivando e apoiando minhas decisões.

Ao meu esposo Diego que torna meus dias mais alegres e a minha vida mais leve com seu amor, carinho, apoio, incentivo, companheirismo e compreensão nos momentos de ausência.

A minha orientadora, professora Sandra pela confiança, imensa dedicação e apoio ao longo deste trabalho.

Ao meu co-orientador, professor Felipe pelo incentivo e contribuições durante o desenvolvimento deste trabalho.

Ao Professor Vitaly Chaban pela realização dos estudos computacionais apresentados neste trabalho.

Aos queridos colegas e amigos do grupo de pesquisa Fabiana Cobalchini, Maria Carolina Fialho, Marina Schwab, Barbara Polesso, Daniela Rodrigues, Henrique Ferrari, Rafael Duczinski e Marisol Rojas, pelo apoio, companhia e colaboração no desenvolvimento deste trabalho.

A Fabiana Gonçalves, Marisol Rojas, Rafael Duczinski e Leonardo Moreira pela grande parceria, amizade e momentos de descontração, indispensáveis em um dia a dia de pesquisa.

Ao Nelson Goes e Luciane München pela boa vontade e disposição em ajudar com os materiais e equipamentos utilizados neste trabalho.

A PETROBRAS pelo financiamento do projeto

A Hewlett-Packard Brasil Ltda pela bolsa de mestrado

Por fim, a Deus por iluminar meu caminho e proporcionou-me a realização de mais uma conquista.

SUMÁRIO

LISTA DE FIGURAS

LISTA DE TABELAS

LISTA DE SÍMBOLOS

[bmpyrr][Cl]	Cloreto de 1-butil-1-metilpirrolidinio
$[Bmim]^+$	Cátion 1 butil - 3 – metilimidazólio
[bmim] $[PF_6]$	Hexafluorofosfato de 1-butil-3-metilimidazólio
[BMIM] $[TF_2N]$	Bis(trifluorometilsulfonil)imida de 1-butil-3-metilimidazólio
[bmim] $[BF_4]$	1-butil-3-metilimidazolio tetrafluoroborato
$[BF_4]^-$	Ânion Tetrafluoroborato
DEA	Dietanolamina
GEE	Gases Efeito Estufa
LIs	Líquidos iônicos
MEA	Monoetanolamina
MDEA	Metil dietanolamina
Mn	Massa molar ponderal média
OTf	Ânion Triflato ($CF_3SO_3^-$)
OTs	Ânion Tosilato ($H_3CC_6H_4SO_3^-$)
PLIs	Poli (líquidos iônicos)
P[VBTMA][BF_4]	Poli [p-(vinilbenzil)-trimetilamônio tetrafluorborato]
P[MATMA][BF_4]	Poli [2- (metacriloiloxi)etil-trimetilamônio tetrafluorborato]
P[VBTMA][BF_4]	Poli [p-(vinilbenzil)-trimetilamônio tetrafluorborato]
P[VBBI][BF_4]	Poli [p-(vinilbenzil)-3-butilimidazólio tetrafluorborato]
P[VBTEA][PF_6]	Poli [4-(vinilbenzil)-trietilamônio hexafluorofosfato]
P[MABI][BF4]	Poli [2- (metacriloiloxi)etil-3-butilimidazólio tetrafluorborato]
(PVBIT)	Poli[1-p-(vinilbenzil)-3-butilimidazolio tetrafluoroborato]
(PVBIH)	Poli[1-p-(vinilbenzil)-3-butilimidazolio Hexafluorofosfato]
(PBIMT)	Poli [2-(metacriloiloxi)etil-3-butilimidazolio tetrafluoroborato]
$[TF_2N]^-$	Ânion bis(trifluorometilsulfonil)imida
TBAB	Brometo de tetra-n-butilamônio
TBPB	Brometo de tetrabutilfosfonio

RESUMO

BERNARD, FRANCIELE. L. **Design de Novos Materiais Poliméricos Para Captura de CO_2.** Porto Alegre. 2017. Tese. Programa de Pós-Graduação em Engenharia e Tecnologia de Materiais, PONTIFÍCIA UNIVERSIDADE CATÓLICA DO RIO GRANDE DO SUL.

O desenvolvimento de materiais de baixo custo e com design inteligente para a separação de CO_2 de gases exaustos é um dos principais focos de pesquisa na atualidade. A absorção química utilizando soluções aquosas de aminas como solventes tem sido extensivamente estudada e utilizada na indústria há décadas. No entanto, a degradação do solvente, a corrosão de equipamentos e o elevado consumo energético necessário para etapa de regeneração são os principais problemas relacionados ao uso destes solventes. Poli (líquidos iônicos) (PLIs) e aminas suportadas têm sido apontados como materiais promissores para captura de CO_2. PLIs combinam as características úteis dos líquidos iônicos (LIs) tais como a seletividade ao CO_2, propriedades ajustáveis, estabilidade química e térmica com as propriedades dos polímeros. A adsorção usando aminas suportadas em sólidos oferece vantagens, como por exemplo: a facilidade de manuseio, estabilidade térmica, eliminação do processo de corrosão dos equipamentos, baixo consumo de energia na etapa de regeneração, baixo custo operacional e cinética rápida. Neste trabalho, foram sintetizados PLIs baseados em polímeros sintéticos (poliuretano) e naturais (celulose extraída da casca de arroz). A fim de comparar aminas e polieteraminas, estas também foram suportadas em celulose extraída da casca de arroz. Os materiais obtidos foram caracterizados por FTIR, RMN, DRX, TGA, DSC, GPC e AFM e MEV-FEG, PTGA ou célula de decaimento de pressão. Estudos com simulações computacionais também foram realizados com o propósito de investigar a interação do CO_2 e os grupos funcionais presentes nos materiais sintetizados. Dentre todos os materiais sintetizados neste trabalho, os PLIs celulósicos CL-TBA e $[CelEt_3N][PF_6]$ e com o PLI base PU-imida HPIL-02-TBA demostraram maior afinidade pelo CO_2, aliado a boa estabilidade térmica e reciclabilidade.

Palavras-Chaves:Poli (líquidos iônicos), dióxido de carbono, aminas suportadas, celulose.

ABSTRACT

BERNARD, FRANCIELE. L **Design of New Polymeric Materials for CO_2 Capture** Porto Alegre. PhD Thesis. Graduation Program in Materials Engineering and Technology, PONTIFICAL CATHOLIC UNIVERSITY OF RIO GRANDE DO SUL.

The development of low-cost materials with intelligent design to be used in CO_2 separation from flue gases is one of the main research focuses in this field. Absorption using amines solutions as solvents have been extensively studied and used in industry for decades. However, solvent degradation, equipment corrosion, and the high regeneration energy penalty are the main problems in this process. Poly(ionic liquids) (PILs) or supported amines has been pointed as promising materials for CO_2 capture. PILs combine the useful features of ionic liquid (IL), such as affinity for CO_2, thermal and chemical stability and adjustable properties, allied to the intrinsic polymer properties. Adsorption using amine supported in solid sorbents offers advantages such as easy handling, thermal stability, elimination of corrosion processes, low regeneration energy, lower operating costs and fast kinetics. In this work, synthetic based (polyurethane) as well natural based (cellulose from rice husk) poly(ionic liquids) were synthesized. Aiming to compare amines and polyetheramines, both were also supported in cellulose extracted from rice husk. The obtained materials were characterized by FTIR, NMR, XDR, TGA, DSC, GPC, AFM, MEV-FEG and PTGA or decay pressure cell in order to evaluate their structure, thermal stability, morphology and sorption capacity. Computational simulation was also performed in order to investigate the interaction of CO_2 with functional groups present in the synthesized materials. Among all synthesized materials cellulosic PLIs CL-TBA e $[CelEt_3N][PF_6]$ and PU-imide based PIL HPIL-02-TBA presented higher CO_2 affinity allied to good thermal stability and reusability.

Key-words: Poly(ionic liquids), carbon dioxide, supported amines, cellulose.

1. INTRODUÇÃO

O nível crescente da concentração de dióxido de carbono (CO_2) na atmosfera, decorrente da produção e utilização de combustíveis fósseis, tem gerado grande preocupação da sociedade devido à sua implicação no aquecimento global (MONTZKA; DLUGOKENCKY; BUTLER, 2011; SONGOLZADEH et al., 2014; BRUHN; NAIMS; OLFE-KRÄUTLEIN, 2016; YAUMI; ABU BAKAR; HAMEED, 2017). Diferentes estratégias têm sido consideradas e adotadas por diversos países com o objetivo de redução da emissão do CO_2. Dentre elas destacam-se a melhoria da eficiência energética, o aumento do uso de combustíveis de baixa emissão de carbono, energias renováveis ou energia nuclear, aplicação de abordagens da geoengenharia e tecnologias de captura de carbono (GARCES et al., 2013; LEUNG; CARAMANNA; MAROTO-VALER, 2014; TOME; MARRUCHO, 2016).

Dentre estas diferentes estratégias a captura de carbono é considerada crucial, pois reduz a emissão de dióxido de carbono de grandes fontes de emissão (TOME; MARRUCHO, 2016). As tecnologias comerciais mais empregadas para captura são a pós-combustão, pré-combustão e oxi-combustão (MONDAL; BALSORA; VARSHNEY, 2012; SONGOLZADEH et al., 2014; KETZER; IGLESIAS; EINLOFT, 2015). Além do ponto de vista ambiental, a captura de carbono pode fornecer CO_2 para diversas aplicações industriais, tais como a recuperação avançada de petróleo, produção de uréia, fertilizantes, gelo seco ou até mesmo o uso como solvente no estado supercrítico (SONGOLZADEH et al., 2014; BRUHN; NAIMS; OLFE-KRÄUTLEIN, 2016).

Absorção química com o uso de soluções aquosas de aminas é o processo mais empregado comercialmente em plantas de captura de CO_2 (BACHELOR; TOOCHINDA, 2012; ARIAS et al., 2016). Embora, este método seja considerado economicamente viável para separação de CO_2 de diversas correntes de misturas

gasosas (RIVERA-TINOCO; BOUALLOU, 2010; BACHELOR; TOOCHINDA, 2012; RAMDIN et al., 2014), a utilização de soluções aquosas de aminas como solvente oferece uma série de inconvenientes operacionais, sendo as mais preocupantes a corrosão de equipamentos, volatilidade, degradação e alto consumo de energia (BACHELOR; TOOCHINDA, 2012; YAUMI; ABU BAKAR; HAMEED, 2017). Desta forma, a obtenção de materiais de baixo custo para a captura tornou-se um dos principais focos de pesquisa neste campo (ZULFIQAR; SARWAR; MECERREYES, 2015a).

Os sorventes empregados na captura de CO_2 precisam ser econômicos e operacionais. Para tal, o ideal seria que apresentassem alta capacidade de sorção com elevada seletividade, estabilidade, resistência química e térmica, baixo consumo de energia, cinética de sorção/dessorção rápida e baixo custo (YAUMI; ABU BAKAR; HAMEED, 2017). No entanto, é muito raro que um sorvente cumpra todos os critérios. Assim, os melhores sorventes são aqueles que podem capturar o CO_2 de forma efetiva e econômica (YAUMI; ABU BAKAR; HAMEED, 2017). O aperfeiçoamento ou desenvolvimento de Poli (líquidos iônicos) (PLIs) ou aminas suportadas em materiais sólidos têm sido relatado em diversos trabalhos, como opções promissoras para separação de CO_2 de diversos tipos de correntes gasosas (WATABE; YOGO, 2013; ZULFIQAR; SARWAR; MECERREYES, 2015b; QIAN; TEXTER; YAN, 2017; YAUMI; ABU BAKAR; HAMEED, 2017).

A captura de CO_2 utilizando aminas suportadas em materiais sólidos requer menos energia para a etapa de regeneração quando comparadas com soluções aquosas de aminas, pois não existe a necessidade de água no processo. Além disso, também demonstram maior estabilidade térmica e resistência a contaminantes presentes nos gases de combustão (BACHELOR; TOOCHINDA, 2012; YU; HUANG; TAN, 2012; WATABE; YOGO, 2013; YAUMI; ABU BAKAR; HAMEED, 2017). No entanto, o alto custo dos suportes comerciais é um desafio que ainda precisa ser superado para a consolidação do uso destes materiais em plantas de captura (BACHELOR; TOOCHINDA, 2012).

Poli(líquidos iônicos) ou líquidos iônicos polimerizados (PLIs) são uma subclasse de polieletrólitos que apresentam uma espécie de líquido iônico em cada

unidade de repetição, conectados através de uma estrutura polimérica para formar uma estrutura macromolecular (ZULFIQAR; SARWAR; MECERREYES, 2015a; TOME; MARRUCHO, 2016; QIAN; TEXTER; YAN, 2017). Estes compostos combinam os benefícios da utilização dos líquidos iônicos (LI) com as propriedades dos polímeros (YUAN; ANTONIETTI, 2011; TOME; MARRUCHO, 2016; QIAN; TEXTER; YAN, 2017). Outra característica importante destes materiais deve-se ao fato da sorção e dessorção de CO_2 ser completamente reversível e ocorrer de forma mais rápida do que nos líquidos iônicos (TANG et al., 2005a; ZULFIQAR; SARWAR; MECERREYES, 2015a).

Neste contexto, este trabalho visou à síntese e avaliação do potencial para captura de CO_2 de diferentes tipos de Poli (líquidos iônicos), baseados em polímeros sintéticos (poliuretano e poliuretano-imida) e naturais (celulose extraída da casca de arroz). Também foi avaliado a solubilidade do CO_2 em aminas e polieteraminas suportadas em celulose extraída da casca de arroz, com o propósito de produzir adsorventes químicos de baixo custo e contribuir para a redução da geração de resíduos agrícolas.

2. OBJETIVOS

Este trabalho tem como objetivo principal a síntese e a avaliação da capacidade de sorção de CO_2 de diferentes materiais poliméricos que contenham líquidos iônicos ou aminas em sua estrutura.

2.1. Objetivos Específicos

- Sintetizar poli (líquidos iônicos) aniônicos baseados em polímeros sintéticos (poliuretano ou poliuretano-imida);
- Extrair celulose a partir da casca de arroz por meio de métodos químicos
- Sintetizar poli (líquidos iônicos) catiônicos e aniônicos base celulose;
- Investigar a influência dos grupos funcionais presentes nos materiais sintetizados sobre a sorção de CO_2, utilizando dados experimentais e simulação computacional.

3. REVISÃO BIBLIOGRÁFICA

3.1. Tecnologias para mitigação da emissão de CO_2

A emissão de gases de efeito estufa de origem antropogênica, especialmente o CO_2, resultam de um amplo conjunto de atividades humanas, principalmente aquelas associadas com a geração de energia na área de transportes, ambientes urbanos e setores industriais (MONTZKA; DLUGOKENCKY; BUTLER, 2011; SONGOLZADEH et al., 2014; WANG et al., 2015; BRUHN; NAIMS; OLFE-KRÄUTLEIN, 2016; YAUMI; ABU BAKAR; HAMEED, 2017). As emissões de CO_2 para atmosfera continuam aumentando em ritmo acelerado e tem provocado alterações profundas no ecossistema (NOAA – NATIONAL ORGANIC & ATMOSPHERIC ADMINISTRATION, 2017; YAUMI; ABU BAKAR; HAMEED, 2017). A Figura 3.1, apresenta um gráfico que demonstra a taxa de crescimento da concentração de CO_2 em ppm/ano, medido em Mauna Loa no Havaí.

Estima-se que a concentração atmosférica global de dióxido de carbono tenha aumentado desde 1750 (pré- revolução industrial) de um valor de cerca de 280 ppm para 379 ppm em 2005, com um aumento da temperatura média global da terra de 0,6 °C para 1,0 °C dentro deste período (YAUMI; ABU BAKAR; HAMEED, 2017). As projeções do Painel Internacional de Alterações Climáticas (IPCC) indicam que, até 2100, a concentração atmosférica global de CO_2 atinja 570 ppm com um aumento médio de temperatura de 1,9°C (YAUMI; ABU BAKAR; HAMEED, 2017). Nos dias atuais, Janeiro de 2017, a concentração alcançou valores próximos a 406,13 ppm (Figura 3.1), com tendência de aumento, devido à enorme demanda global por combustíveis fósseis (NOAA – NATIONAL ORGANIC & ATMOSPHERIC ADMINISTRATION, 2017; YAUMI; ABU BAKAR; HAMEED, 2017).

Logo, do ponto de vista ambiental, reduzir os níveis crescentes de CO_2 na atmosfera torna-se essencial para mitigar os impactos causados pelo aquecimento global e as mudanças climáticas imprevisíveis (CHENG et al., 2015; ZULFIQAR; SARWAR; MECERREYES, 2015b; TOME; MARRUCHO, 2016).

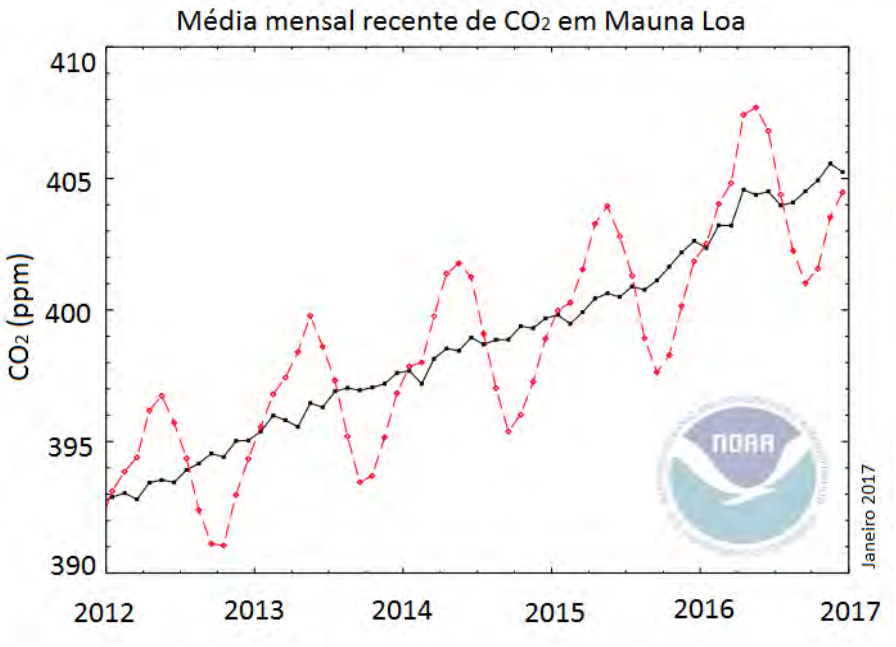

Figura 3.1. Aumento da concentração de CO_2 e as mudanças climáticas. Fonte: (NOAA – NATIONAL ORGANIC & ATMOSPHERIC ADMINISTRATION, 2017). A linha vermelha tracejada representa os valores médios mensais e a linha preta representa o mesmo, após correção para a média do ciclo sazonal.

O uso de tecnologias de captura de carbono tem sido indicado como um meio capaz para mitigar as emissões de CO_2 de grandes fontes geradoras de energia (TOME; MARRUCHO, 2016). As rotas tecnológicas para captura de CO_2 mais discutidas atualmente para instalações que utilizam combustíveis fósseis ou biomassa são: Pós - combustão, Pré -combustão e Oxi - combustão (Figura 3.2) (FIGUEROA et al., 2008; OLAJIRE, 2010; MONDAL; BALSORA; VARSHNEY, 2012; SONGOLZADEH et al., 2014; KETZER; IGLESIAS; EINLOFT, 2015; YAUMI; ABU BAKAR; HAMEED, 2017).

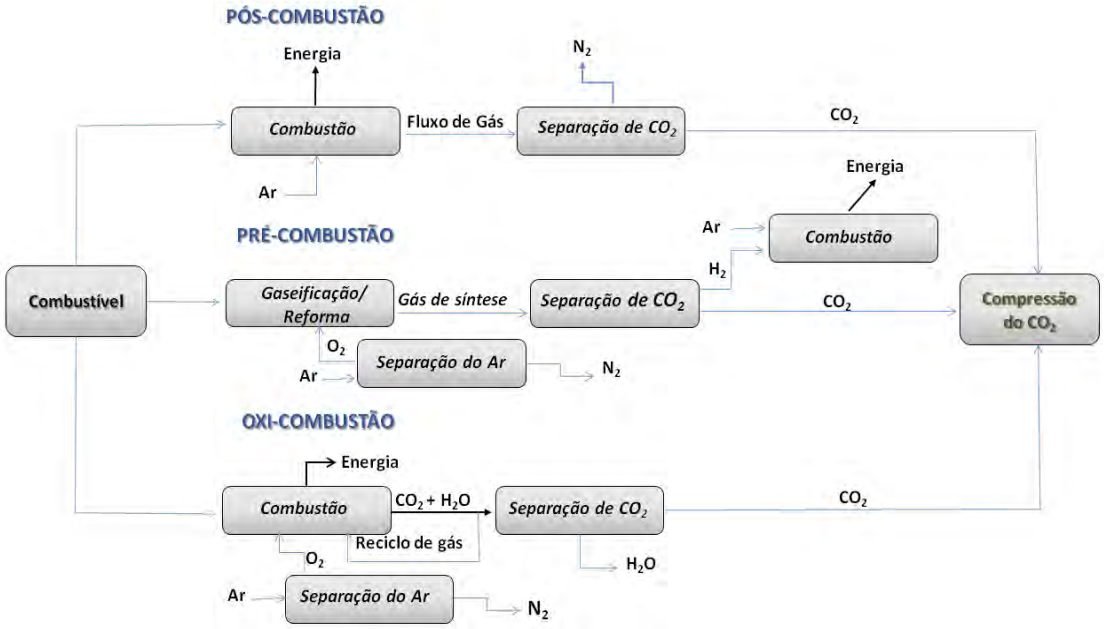

Figura 3.2. Fluxograma das tecnologias de captura de CO_2. Fonte: Adaptação (FIGUEROA et al., 2008).

A remoção do dióxido de carbono de gases produzidos e emitidos para a atmosfera em processos de queima de combustível fóssil ou biomassa é normalmente realizada pela tecnologia de Pós-combustão. Os gases de combustão, normalmente apresentam baixas concentrações de CO_2 (3 - 15 % para usinas de carvão, 7 - 8 % para usinas de gás (por volume)) (MONDAL; BALSORA; VARSHNEY, 2012; SONGOLZADEH et al., 2014) e saem à pressão atmosférica e a temperaturas entre 47°C e 127°C (SONGOLZADEH et al., 2014). A condição desfavorável dos gases de combustão (pressão e concentração baixas) para captura de CO_2 é apresentada como a principal desvantagem desta tecnologia (FIGUEROA et al., 2008; OLAJIRE, 2010; SONGOLZADEH et al., 2014) e a sua principal vantagem está relacionada ao uso de processos de baixo custo (SONGOLZADEH et al., 2014). Processos de absorção química se adaptam melhor a esta tecnologia (MONDAL; BALSORA; VARSHNEY, 2012), soluções aquosas de aminas (monoetanolamina (MEA), dietanolamina (DEA) e metildietanolamina (MDEA) destacam-se como os solventes mais empregados (YANG et al., 2008; BACHELOR; TOOCHINDA, 2012; RAMDIN et al., 2014; KETZER; IGLESIAS; EINLOFT, 2015; YAUMI; ABU BAKAR; HAMEED, 2017). Contudo, o uso deste tipo de solvente oferece algumas desvantagens operacionais, dentre as quais podem-se destacar o elevado consumo de energia (necessário para a etapa de regeneração), a corrosão

de equipamentos causada pela formação de subprodutos corrosivos, a necessidade de absorvedores de grande volume, além de custos operacionais adicionais devido à substituição de solventes decorrente da degradação (YANG et al., 2008; BACHELOR; TOOCHINDA, 2012; RAMDIN et al., 2014; SEO et al., 2014; KETZER; IGLESIAS; EINLOFT, 2015; YAUMI; ABU BAKAR; HAMEED, 2017). Outros processos de separação também podem ser empregados, como por exemplo: separação por membranas e adsorção em sólidos (OLAJIRE, 2010; BACHELOR; TOOCHINDA, 2012).

A captura de CO_2 de gases produzidos no sistema de pré-combustão ocorre a partir da produção de uma mistura gasosa contendo principalmente CO e H_2 (gás de síntese). Esta mistura é produzida pela reação do ar ou oxigênio com vapor, o monóxido de carbono produzido é colocado em contato com vapor de água resultando na produção de mais hidrogênio e CO_2 (teores na faixa de 15 a 60 % vol) a alta pressão. Finalmente o dióxido de carbono é separado e o hidrogênio pode ser usado como combustível (FIGUEROA et al., 2008; OLAJIRE, 2010; MARKEWITZ et al., 2012; SONGOLZADEH et al., 2014; KETZER; IGLESIAS; EINLOFT, 2015). Embora o principal inconveniente do sistema de pré-combustão esteja relacionado com o alto custo necessário para a instalação, a alta pressão e a concentração de CO_2 permitem a diminuição dos custos nas etapas de carga e compressão, bem como o emprego de processos de separação de CO_2 que necessitem de baixo consumo de energia na etapa de regeneração (ex, absorventes e adsorventes físicos) (FIGUEROA et al., 2008; OLAJIRE, 2010).

Na oxi-combustão, ao invés do ar, usa-se oxigênio praticamente puro (pureza >95%) para realização da combustão. Inicialmente o O_2 é separado do ar, em seguida o combustível é queimado com O_2 e uma mistura de gás de combustão rico em CO_2 e vapor de água é obtida e reciclada. Os gases de combustão contém CO_2 com teor superior a 80% vol., assim a água pode ser facilmente removida por condensação (FIGUEROA et al., 2008; OLAJIRE, 2010; MARKEWITZ et al., 2012; SONGOLZADEH et al., 2014; KETZER; IGLESIAS; EINLOFT, 2015). A maior vantagem desta tecnologia é a alta pressão parcial do CO_2 que permite sua fácil separação dos gases exaustos (KETZER; IGLESIAS; EINLOFT, 2015). No entanto,

esta tecnologia necessita de grande consumo de O_2, o qual tem custo elevado para produção (FIGUEROA et al., 2008; OLAJIRE, 2010; SONGOLZADEH et al., 2014).

3.2. Líquidos iônicos e seu potencial para captura de CO_2

Os Líquidos iônicos (LIs) são uma classe de sais orgânicos, formados pela combinação de cátions orgânicos e ânions inorgânicos ou orgânicos, que possuem temperatura de fusão inferior a 100 °C (WILKES, 2002; FIGUEROA et al., 2008; PRIVALOVA et al., 2012; BABAMOHAMMADI; SHAMIRI; AROUA, 2015; SHAPLOV et al., 2016). Estes compostos exibem propriedades únicas como a capacidade de não inflamar, pressão de vapor extremamente baixa e boa estabilidade térmica (WILKES, 2002; FIGUEROA et al., 2008; HASIB-UR-RAHMAN; SIAJ; LARACHI, 2010; RAMDIN; DE LOOS; VLUGT, 2012; QIAN; TEXTER; YAN, 2017). Além disso, são versáteis e menos prejudiciais ao meio-ambiente do que os solventes orgânicos convencionais. A grande variabilidade estrutural de cátions e ânions permite a criação de compostos com características e propriedades específicas para uma determinada aplicação (BABAMOHAMMADI; SHAMIRI; AROUA, 2015; DAI et al., 2016; TOME; MARRUCHO, 2016). A Figura 3.3 mostra as estruturas de alguns cátions e ânions comumente utilizados para obtenção de LIs.

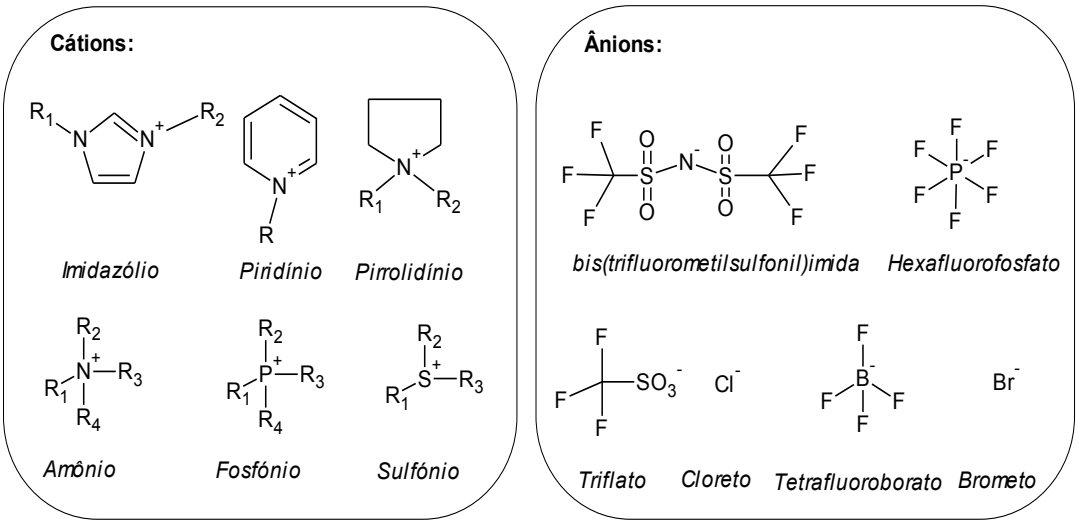

Figura 3.3. Exemplo de estruturas típicas de cátions e ânions comumente empregados em sínteses de líquidos iônicos. Fonte: Baseado em M. Hasib-ur-Rahman et al.,2010 (HASIB-UR-RAHMAN; SIAJ; LARACHI, 2010).

Em geral, os LIs são divididos em duas grandes categorias: Líquidos Iônicos à Temperatura Ambiente (RTILs: do inglês "*Room Temperature Ionic Liquids*") considerados como os LIs tradicionais ou convencionais e, os líquidos iônicos específicos (TSILs: do inglês "*task-specific ionic liquids*"), isto é, que apresentam grupos funcionais reativos em sua estrutura (HASIB-UR-RAHMAN; SIAJ; LARACHI, 2010; PRIVALOVA et al., 2012; BABAMOHAMMADI; SHAMIRI; AROUA, 2015; TOME; MARRUCHO, 2016).

Os LIs vem demonstrando potencial para captura de gases ácidos, como por exemplo, o CO_2 (HASIB-UR-RAHMAN; SIAJ; LARACHI, 2010; BABAMOHAMMADI; SHAMIRI; AROUA, 2015; TOME; MARRUCHO, 2016). Isto se deve principalmente às suas propriedades e características peculiares aliado ao fato da grande maioria dos LIs demonstrarem absorção seletiva para o CO_2 em uma mistura de gases (CADENA et al., 2004; ANTHONY et al., 2005; BABAMOHAMMADI; SHAMIRI; AROUA, 2015; TOME; MARRUCHO, 2016). Entretanto, existem alguns empecilhos que precisam ser superados para a sua ampla utilização em plantas de captura de CO_2, como por exemplo, o alto custo de produção em comparação com as soluções aquosas de aminas, a elevada viscosidade e a baixa taxa de absorção/dessorção de CO_2 (HASIB-UR-RAHMAN; SIAJ; LARACHI, 2010; KENARSARI et al., 2013). Avanços recentes sugerem que estas dificuldades podem ser superadas com o uso de líquidos iônicos polimerizados (ZULFIQAR; SARWAR; MECERREYES, 2015a; SADEGHPOUR; YUSOFF; AROUA, 2016).

Líquidos iônicos tradicionais ou convencionais são os mais investigados para utilização em processo de absorção de gases, em especial para o CO_2. É possível que este interesse esteja relacionado com o fato desta categoria de LIs apresentar comportamento típico de solvente físico, ou seja, a solubilidade dos gases tende a aumentar com o aumento da pressão e o processo de sorção/dessorção seja reversível (ANTHONY et al., 2005; HASIB-UR-RAHMAN; SIAJ; LARACHI, 2010; PRIVALOVA et al., 2012; RAMDIN; DE LOOS; VLUGT, 2012; BABAMOHAMMADI; SHAMIRI; AROUA, 2015).

Estudos sobre a interação do CO_2 com LIs tradicionais tem evidenciado que o ânion desempenha um papel chave na dissolução de CO_2, enquanto que o cátion

tem um papel secundário. Porém, em menor proporção, modificações no cátion envolvendo grupos alquil podem influenciar a capacidade de absorção de CO_2. Trabalhos relatam também que a fluoração do ânion e do cátion pode contribuir significativamente para o aumento da solubilidade do CO_2 nestes compostos (CADENA et al., 2004; ANTHONY et al., 2005; RAMDIN; DE LOOS; VLUGT, 2012; TOME; MARRUCHO, 2016).

3.3. Poli (líquidos iônicos) desenvolvidos para captura de CO_2

Poli (líquidos iônicos) ou líquidos iônicos poliméricos (PLIs) apresentam uma espécie de liquido iônico (LI) conectados através de uma estrutura polimérica para formar uma estrutura macromolecular (YUAN; MECERREYES; ANTONIETTI, 2013; ZULFIQAR; SARWAR; MECERREYES, 2015a; SHAPLOV et al., 2016; QIAN; TEXTER; YAN, 2017). Estes polímeros funcionais tornaram-se uma nova plataforma, extremamente versátil e ajustável para o desenvolvimento de uma grande variedade de sorventes para captura de CO_2 (TANG et al., 2009; HASIB-UR-RAHMAN; SIAJ; LARACHI, 2010; ZULFIQAR; SARWAR; MECERREYES, 2015a; TOME; MARRUCHO, 2016) combinando características notáveis dos líquidos iônicos (LIs), em especial, a possibilidade de variar suas propriedades físicas e químicas, por meio da combinação de cátions e ânions (YUAN; ANTONIETTI, 2011; TOME; MARRUCHO, 2016), com as propriedades dos polímeros (estabilidade mecânica, processabilidade e design macromolecular) (YUAN; ANTONIETTI, 2011; PRIVALOVA et al., 2012; TOME et al., 2013; YUAN; MECERREYES; ANTONIETTI, 2013; TOME; MARRUCHO, 2016).

Outra característica que deve ser ressaltada nestes materiais é o fato do processo de sorção e dessorção do CO_2 ser completamente reversível e ocorrer de forma mais rápida do que nos líquidos iônicos tradicionais (TANG et al., 2005a). Além disso, também tem sido reportado que a sorção de CO_2 em PLIs é seletiva (TANG et al., 2005a).

O método de síntese está diretamente ligado ao tipo de poli(líquidos iônico) que se deseja obter (YUAN; MECERREYES; ANTONIETTI, 2013). Em geral, a

síntese dos PLIs pode ser realizada por meio de duas rotas principais: a primeira consiste na polimerização direta de monômeros de LIs (TOME; MARRUCHO, 2016) e a segunda envolve basicamente reações de condensação, que podem ser conduzidas através da modificação de polímeros (SHAPLOV et al., 2016; TOME; MARRUCHO, 2016) ou via condensação do respectivo monômero (SHAPLOV et al., 2016). PLIs com diferentes estruturas podem ser produzidos, e certamente o tipo de rota selecionada pode afetar diretamente as características, propriedades e o custo destes materiais, acarretando em vantagens e desvantagens (YUAN; MECERREYES; ANTONIETTI, 2013).

3.3.1. Poli (líquidos iônicos) obtidos por polimerização radicalar direta

Seguindo a ideia dos LIs, a grande maioria dos PLIs sintetizados via polimerização radicalar direta é do tipo catiônico, ou seja, a estrutura da cadeia principal apresenta porções catiônicas enquanto que a parte móvel (contra - íon) é a aniônica (MECERREYES, 2011). O imidazólio é o cátion mais utilizado, podendo ser inserido na estrutura da cadeia principal do polímero a partir de estruturas como vinil, estireno, metacrilato entre outros (MECERREYES, 2011). O método de reação por troca aniônica de um monômero catiônico contendo contra-ânion do tipo haleto (Figura 3.4) é o mais empregado para obtenção de policátions (MECERREYES, 2011; SADEGHPOUR; YUSOFF; AROUA, 2016). Em geral, esta rota utiliza monômeros de LIs, Azobisisobutironitrila (AIBN) e solvente dimetilformamida (DMF) (SADEGHPOUR; YUSOFF; AROUA, 2016).

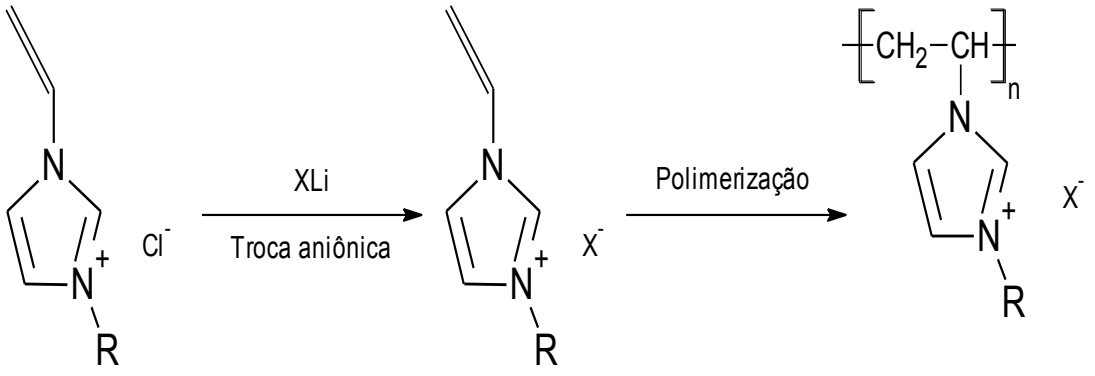

Figura 3.4. Rota sintética geral para obtenção de PLIs via reação por troca aniônica. Adaptação Mecerreyes,2011 (MECERREYES, 2011).

Os primeiros estudos sobre a solubilidade de CO_2 em PLIs obtidos via síntese radicalar foram reportados no ano de 2005 por Tang e colaboradores (TANG et al., 2005a, 2005b, 2005c, 2005d). Estes trabalhos despertaram um enorme interesse da comunidade científica e alavancaram as pesquisas sobre a utilização de PLIs para captura de CO_2.

Inicialmente Tang e co-autores investigaram o desempenho de três PLIs base imidazólio: poli[1-p-(vinilbenzil)-3-butilimidazolio tetrafluoroborato] (PVBIT), poli[1-p-(vinilbenzil)-3-butilimidazolio hexafluorofosfato] (PVBIH) e poli [2-(metacriloiloxi)etil-3-butilimidazolio tetrafluoroborato] (PBIMT). Surpreendentemente, como pode ser verificado na Figura 3.5, os PLIs exibiram capacidade de sorção superior à do líquido iônico 1-butil-3-metilimidazolio tetrafluoroborato ([bmim] [BF_4]) e de seus monômeros correspondentes (TANG et al., 2005a). Os PLIs sintetizados por Tang et. al., 2005 (TANG et al., 2005a) necessitaram de apenas alguns minutos para alcançar 90% da sua capacidade de sorção de CO_2 e cerca de 30 minutos para atingir o equilíbrio, enquanto que para o [bmim] [BF_4] foi necessário mais de 400 min para que a sua capacidade de sorção total fosse atingida (Figura 3.5).

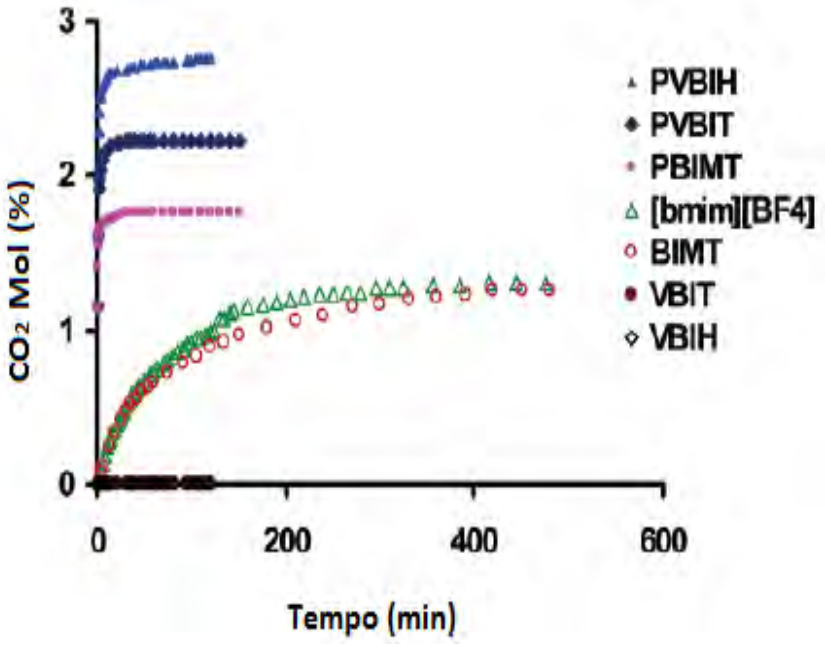

Figure 3.5: Sorção de CO_2 ao longo do tempo para os PLIs: PVBIH, PVBIT, PBIMT e seus respectivos monômeros (VBIT, VBIH, BIMT). Condições: (0,79 bar e 22 °C). Fonte: Tang et. al., 2005 (TANG et al., 2005a).

Ainda neste trabalho (TANG et al., 2005a), os PLIs PVBIT e PBIMT foram submetidos a quatro ciclos de sorção/dessorção (Figura 3.6a) e o PLI PVBIT foi avaliado quanto a sua seletividade (Figura 3.6b). Os resultados experimentais de sorção/dessorção apresentados na Figura 3.6a não demonstraram variação na capacidade de sorção de CO_2 dos PLIs PVBIT e PBIMT após a realização de cada ciclo. Isto sugere que a dessorção ocorreu de forma completa e que o processo é completamente reversível (TANG et al., 2005a). Também foi verificado que o PLI PVBIT é seletivo para CO_2, pois não foi observado nenhum ganho de massa quando este PLI foi exposto a N_2 ou O_2 (TANG et al., 2005a) (Figura 3.6b).

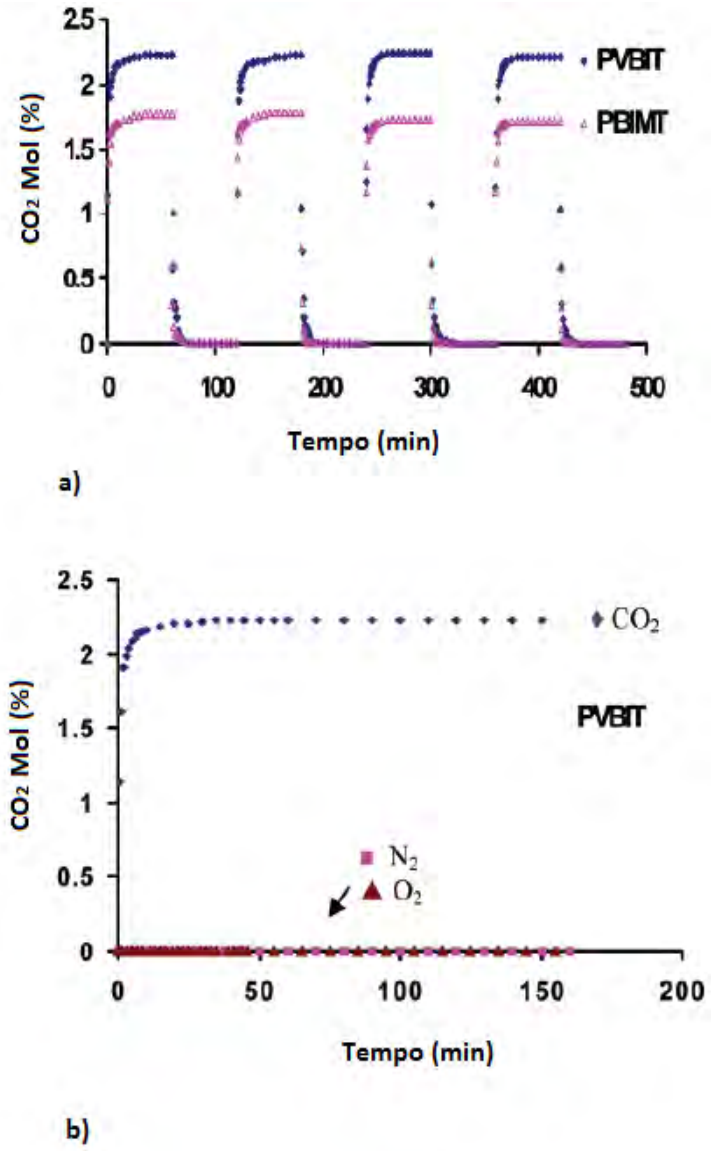

Figura 3.6. a) Ciclos de sorção (592,3 mmHg e 22 °C /dessorção com vácuo em PVBIT e PBIMT e b) Sorção dos Gases: CO_2, O_2 e N_2 em PVBIT .Condições : 592,3 mmHg e 22 °C.

Diversos estudos têm sido realizados sobre o uso de PLIs catiônicos sintetizados via polimerização radicalar direta de monômeros em captura de CO_2 (TANG et al., 2005a, 2005b, 2005d, 2009; SIMONS et al., 2010; BHAVSAR; KUMBHARKAR; KHARUL, 2012; CARLISLE et al., 2013; YU et al., 2014). Resultados experimentais de sorção de CO_2 demonstraram que além da pressão e temperatura (BLASIG et al., 2007) vários aspectos podem influenciar na solubilidade do CO_2 em PLIs. Neste cenário, o tipo de cátion, ânion e a estrutura da cadeia principal merecem destaque (ZULFIQAR; SARWAR; MECERREYES, 2015a; SADEGHPOUR; YUSOFF; AROUA, 2016; TOME; MARRUCHO, 2016; QIAN; TEXTER; YAN, 2017).

A maior parte do PLIs desenvolvidos para uso em captura e separação de CO_2 tem utilizado metacrilato (TANG et al., 2005b, 2005d, 2009; BARA et al., 2007; TOMÉ et al., 2015) e estireno (TANG et al., 2005d; BLASIG et al., 2007; BARA JASON E. , HATAKEYAMA EVAN S. , GIN DOUGLAS L., 2008; SIMONS et al., 2010) como estrutura da cadeia principal. No entanto, outras estruturas também têm sido exploradas, tais como o vinil (CARLISLE et al., 2013) e o dialildimetilamônio (BHAVSAR; KUMBHARKAR; KHARUL, 2012; TOMÉ et al., 2013, 2015).

Testes experimentais de sorção de CO_2 revelaram que a utilização do estireno ao invés de metacrilato pode aumentar a solubilidade de CO_2 em PLIs, provavelmente devido a sua estrutura mais rígida (TANG et al., 2005b, 2009). Por exemplo, o poli [p-(vinilbenzil)-trimetilamônio tetrafluorborato] (P[VBTMA][BF_4]) com estrutura principal formada por estireno mostrou capacidade de sorção de CO_2 superior ao poli [2- (metacriloiloxi)etil-trimetilamônio tetrafluorborato] (P[MATMA][BF_4]) desenvolvido a partir de metacrilato (TANG et al., 2005b, 2005d, 2009). Comportamento similar foi observado em PLIs de cátion imidazólio, onde o poli [p-(vinilbenzil)-3-butilimidazólio tetrafluorborato] (P[VBBI][BF_4]) demonstrou capacidade de sorção cerca de 20% (2.27 mol%) superior ao poli [2-(metacriloiloxi)etil-3-butilimidazólio tetrafluorborato] (P[MABI][BF_4]) (1.80 mol%) (TANG et al., 2005b).

A permeabilidade e seletividade ao CO_2 destes materiais também podem sofrer influência considerável da estrutura da cadeia principal empregada em sua síntese. Normalmente, PLIs à base de estireno e metacrilato tendem a ser mais seletivos para CO_2 que os a base de vinil (BARA et al., 2007; CARLISLE et al., 2013). Além disso, a permeabilidade do CO_2 em PLIs com a estrutura formada por estireno tende a ser mais elevada que os sintetizados com metacrilato e vinil (BARA et al., 2007; CARLISLE et al., 2013).

A influência da reticulação de PLIs catiônicos sobre a capacidade de sorção de CO_2 também tem sido avaliada (TANG et al., 2009; YU et al., 2014). Yu et al, 2014 (YU et al., 2014) sintetizou o PLI N,N-metilenobisacrilamida (MBA) reticulado - poli [4-(vinilbenzil)-trietilamônio hexafluorofosfato] (MBA-reticulado- P[VBTEA][PF_6]) e comparou seus resultados de sorção de CO_2 com o poli [4-(vinilbenzil)-trietilamônio hexafluorofosfato] (P[VBTEA][PF_6]). Conforme pode-se observar na Figura 3.7, o PLI (MBA-reticulado- P[VBTEA][PF_6]) demonstrou capacidade de sorção de CO_2 superior ao (P[VBTEA][PF_6]). Este comportamento está relacionado com o aumento da área específica e formação de poros promovida pela reticulação (YU et al., 2014).

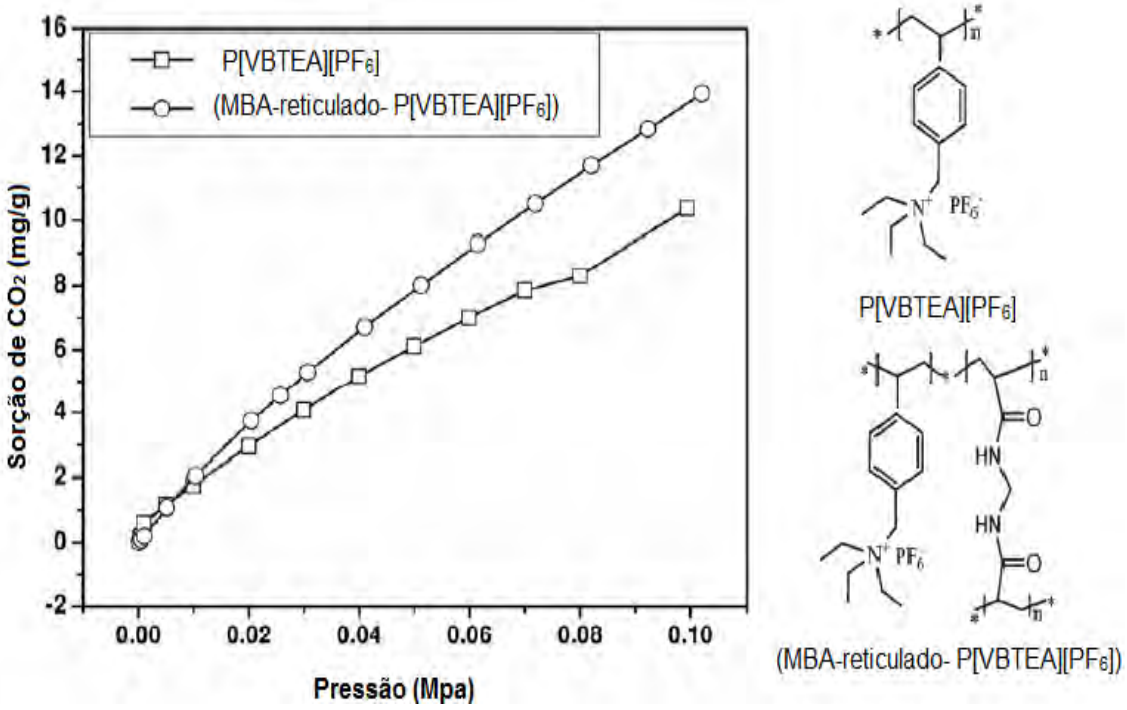

Figura 3.7. Isoterma de sorção de CO_2 do (MBA-reticulado- P[VBTEA][PF6]) e P[VBTEA][PF6]) a 25°C avaliando a influência da reticulação na capacidade de sorção de CO_2. Adaptação: Yu et al., 2014 (YU et al., 2014).

Comportamento distinto foi observado por Tang e colaboradores, 2009 (TANG et al., 2009) com a inserção de 5% de reticulação no poli [1-(p-vinilbenzil)-trimetilamônio tetrafluoroborato] (P[VBTMA]-[BF_4]). Neste caso, a rigidez decorrente da reticulação dificultou a interação do CO_2 com o PLI, e, consequentemente reduziu os valores de sorção de CO_2 (TANG et al., 2009).

Ao contrário do observado em líquidos iônicos convencionais, nos PLIs o ânion desenvolve um papel secundário sobre a sorção de CO_2 enquanto que o cátion desempenha o papel principal (TANG et al., 2005d, 2009). Estudos de simulação atomística (Figura 3.8 e 3.9) utilizando o policátion (1-vinil-3-butilimidazólio) $[VBIM]^+$ e diferentes ânions foram conduzidos por Fang et al.,2013 com o objetivo de compreender a interação entre o CO_2 e os PLIs catiônicos.

A Figura 3.8 ilustra as funções de distribuição radial g(r) do CO_2 no LI [BMIM] [TF_2N] e no poli [VBIM] [TF_2N] (FANG; LUO; JIANG, 2013). A tendência de distribuição radial em torno do $[TF_2N]^-$ do LI ou PLI é praticamente idêntica. No entanto, uma diferença é notada entre a distribuição radial obtida com o poli $[VBIM]^-$ e para o $[BMIM]^-$. Para o LI [BMIM] [TF_2N] tanto o cátion quanto o ânion demostram uma interação estreita com o CO_2, três picos acentuados são verificados, sendo dois picos para os átomos da extremidade do cátion $[BMIM]^-$ (C1 e C8) um pico para o átomo C1 do ânion [TF_2N]. Em contraste, no poli [VBIM] $[TF_2N]^-$ a distribuição radial g(r) do CO_2 é mais intensa para o átomo C1 do policátion. Isto sugere que o CO_2 interage mais fortemente com o átomo C1 do policátion do que com os outros átomos do cátion ou ânion. O átomo C1 do policátion está localizado na extremidade da cadeia polimérica, isto lhe confere elevada mobilidade e consequentemente grande volume livre disponível para acomodar o CO_2, enquanto que nesta configuração o átomo C8 não está acessível ao CO_2 (FANG; LUO; JIANG, 2013).

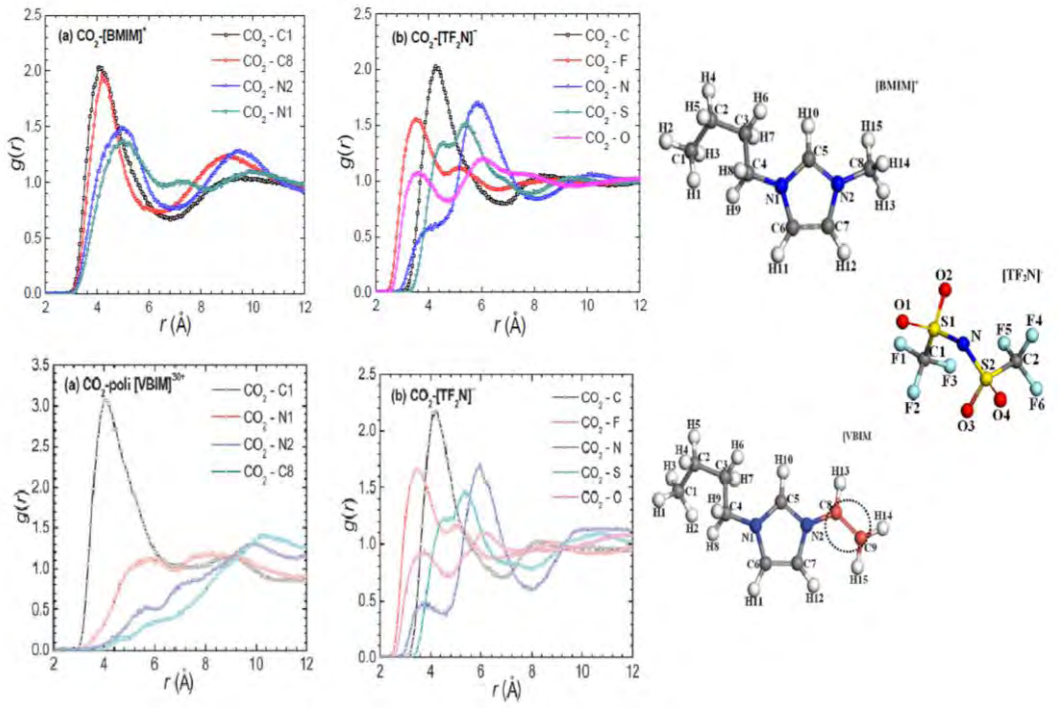

Figura 3.8. Funções de distribuição radial em [BMIM] [TF_2N] e poli [VBIM] [TF_2N].Fonte: (FANG; LUO; JIANG, 2013)

A avaliação da distribuição radial g(r) de CO_2 nos poli [VBIM] [PF_6] e [VBIM] [Cl] (Figura 3.9), demostrou comportamento semelhante ao observado no poli [VBIM] [TF_2N] (FANG; LUO; JIANG, 2013). O pico g(r) do CO_2 mostrou-se mais elevado em torno do átomo C1 do policátion. Este resultado corrobora a teoria de que o CO_2 possui maior afinidade pela cadeia lateral do policátion do que pelos átomos presentes na estrutura do ânion (FANG; LUO; JIANG, 2013).

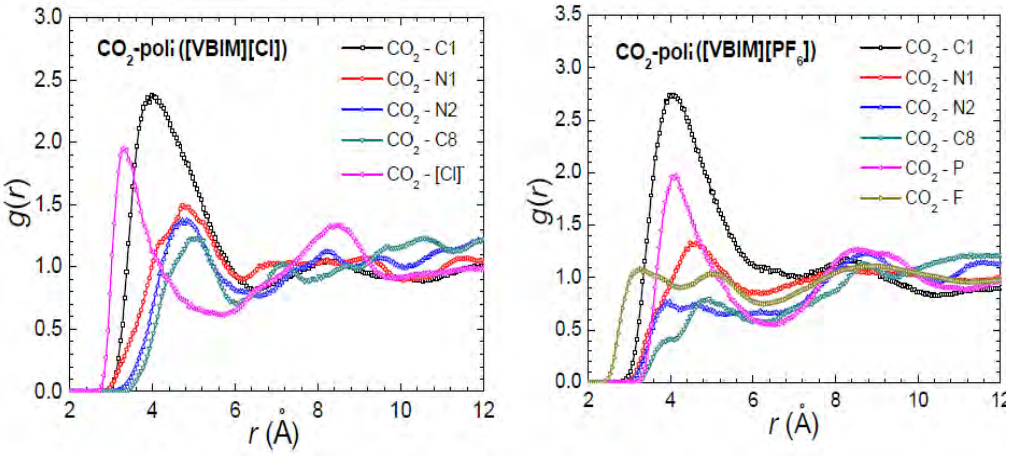

Figura 3.9. Funções de distribuição radial em poli [VBIM] [Cl] e poli [VBIM] [PF_6].Fonte: (FANG; LUO; JIANG, 2013)

Estudos sobre o efeito do tipo de cátion ou modificações na estrutura da cadeia lateral deste elemento, sobre a solubilidade do CO_2 têm sido relatados na literatura (TANG et al., 2005b, 2005c, 2005d, 2009, BARA et al., 2007, 2008; BARA JASON E. , HATAKEYAMA EVAN S. , GIN DOUGLAS L., 2008; SIMONS et al., 2010). Normalmente, PLIs contendo o cátion tetralquilamônio demonstram capacidade de sorção de CO_2 superior a PLIs com o cátion imidazólio (TANG et al., 2005b). Este fato possivelmente está relacionado à alta densidade de carga positiva do cátion tetralquilamônio que resulta em uma forte interação com o CO_2, em contraste a carga positiva deslocalizada do cátion imidazólio (TANG et al., 2005b).

Testes experimentais de sorção de CO_2 realizados em PLIs base estireno, contendo o ânion BF_4 e diferentes cátions (Amônio, Piridínio, Fosfônio, Imidazólio) também verificaram este comportamento, visto que a sorção de CO_2 diminuiu na seguinte ordem: Amônio> Piridínio> Fosfônio> Imidazólio (TANG et al., 2009). Além disso, assim como observado em LIs convencionais, a solubilidade de CO_2 é incrementada com o aumento da pressão (TANG et al., 2009).

A capacidade de sorção do CO_2 pode ser fortemente afetada por modificações na cadeia alquílica do cátion (TANG et al., 2005c, 2005d, 2009; QIAN; TEXTER; YAN, 2017). O aumento do comprimento da cadeia alquílica do cátion pode representar um obstáculo, devido ao surgimento do efeito estérico que dificulta a sorção do CO_2 (TANG et al., 2005c, 2009; QIAN; TEXTER; YAN, 2017).

Estudos mostraram que a introdução de cadeias longas no cátion amônio ou imidazólio comprometem a capacidade de sorção do CO_2 (TANG et al., 2005c, 2005d). A substituição do grupo metil por etil e butil no cátion amônio reduziu a capacidade de sorção de CO_2 em cerca de 53% e 70 %, respectivamente (TANG et al., 2005d). Comportamento similar foi encontrado para o cátion imidazólio, no qual a troca do grupo metil por butil provocou uma redução na solubilidade do CO_2 de aproximadamente 26 % (TANG et al., 2005c).

Em contrapartida, o aumento do comprimento da cadeia alquílica ou a introdução de substituintes, ramificados, cíclicos ou polares no cátion pode promover

melhorias na seletividade e permeabilidade ao CO_2 em correntes gasosas de CO_2/N_2 e CO_2/CH_4 (BARA et al., 2007, 2008; HORNE et al., 2014). Bara et al.,2007 (BARA et al., 2007) avaliaram o efeito do incremento da cadeia alquílica no cátion imidazólio de PLIs base estireno e acrilato sobre a permeabilidade de CO_2 (Figura 3.10).

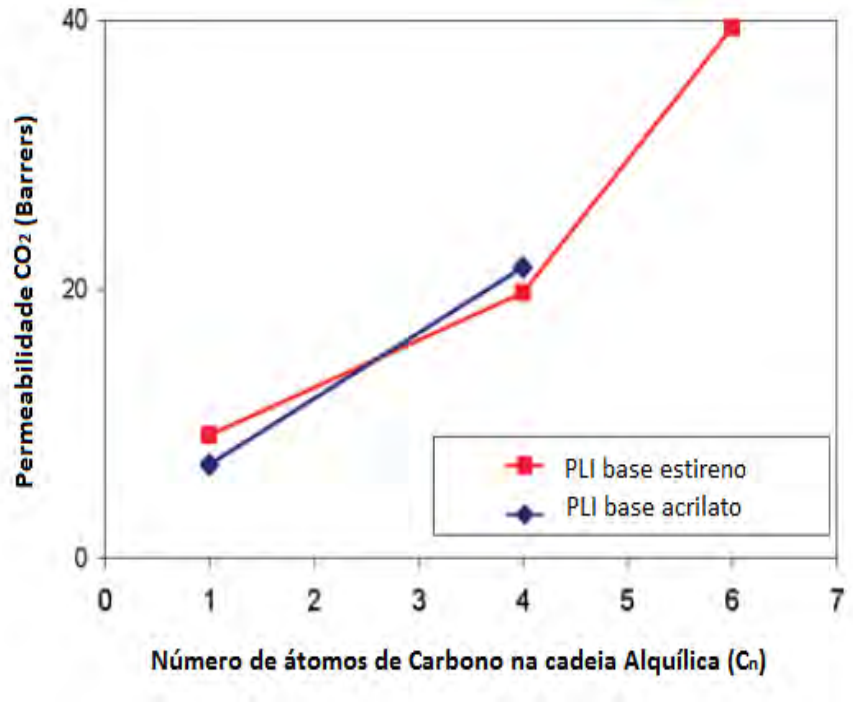

Figura 3.10. Tendências da permeabilidade de CO_2 em PLIs base estireno e acrilato. Barras de erro dentro de símbolos. Fonte: Bara et al.,2007

De acordo com os resultados apresentados na Figura 3.10 observar-se que o aumento do comprimento da cadeia alquílica do cátion tende a elevar drasticamente a permeabilidade ao CO_2. Este comportamento pode ser consequência do aumento do volume livre na rede polimérica, devido a um empacotamento ineficiente promovido pelas cadeias laterais alquílicas (BARA et al., 2007).

O efeito dos substituintes alquil na cadeia lateral do cátion imidazólio, sobre a permeabilidade e seletividade ao CO_2 em uma mistura de gases CO_2/CH_4 (50/50 vol.%), foi investigado por Simons et al., 2010 (SIMONS et al., 2010). A Figura 3.11 mostra a permeabilidade e seletividade ao CO_2 em função da pressão para os PLIs sintetizados com o ânion bis(trifluorometilsulfonil)imida (TF_2N) e diferentes substituintes alquila na cadeia lateral do cátion. C1 refere-se ao PLI com o grupo metil como substituinte, C4 ao PLI com o n-butil e C6 ao n-hexil.

Simons et al., 2010 observaram um incremento na permeabilidade dos PLIs com o aumento pressão parcial de CO_2 (Figura 3.11a). Em todas as pressões testadas, o substituinte mais longo (C6) apresentou maior permeabilidade ao CO_2, enquanto que o substituinte com cadeia mais curta (C1) demonstrou permeabilidade menor, devido a interações iônicas mais fortes dentro do material. O PLI contendo os grupos n-butil (C4) e n-hexil (C6) apresentaram comportamento semelhante e permeabilidades comparáveis (Figura 3.11a).

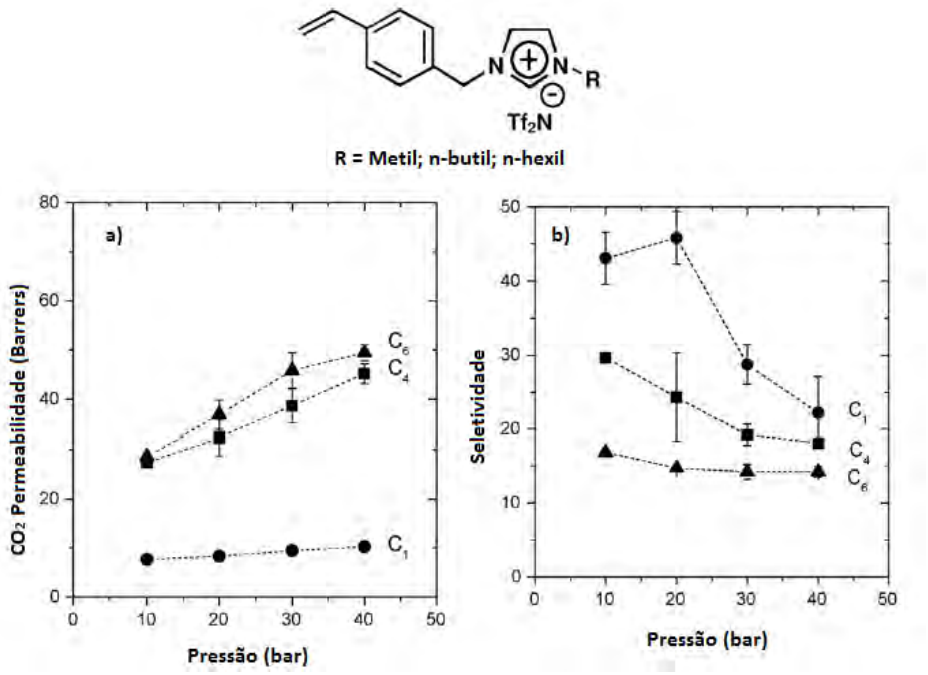

Figura 3.11. a) Permeabilidade ao CO_2 b) seletividade CO_2/CH_4, em função da Pressão. Condições: alimentação CO_2/CH_4 (50/50 vol.%) e temperatura de 20 °C. Adaptação Simons (SIMONS et al., 2010).

A Figura 3.11b mostra também que a seletividade depende fortemente do comprimento da cadeia lateral do cátion, além de sofrer influência da pressão de operação. Observa-se que a seletividade dos PLIs sintetizados com cadeias laterais mais longas (C4 e C6) reduz com o acréscimo da pressão. Isto pode estar relacionado com o fato de que o CO_2 interage preferencialmente com as cargas iônicas, ao contrário do CH_4 que possui grande afinidade pelas cadeias alquílicas, devido à maior hidrofobicidade, aliado ao fato de que substituintes mais longos possuem maior propensão ao inchamento (SIMONS et al., 2010).

O PLI sintetizado com uma cadeia lateral curta (C1) exibiu comportamento divergente dos demais PLIs (Figura 3.11b). Em pressões de até 20 bar, verificou-se um aumento da seletividade proporcionada pela restrição do inchamento do polímero com a incorporação de uma cadeia mais curta. Porém, em pressões superiores uma forte queda na seletividade foi notada, em consequência do aumento do inchamento e da permeabilidade ao CH_4 em relação ao CO_2 (SIMONS et al., 2010).

A introdução de grupos polares como, por exemplo -OR ou -CN na cadeia lateral do cátion foi investigada pelo grupo de pesquisa de Noble (BARA et al., 2007, 2008; BARA JASON E. , HATAKEYAMA EVAN S. , GIN DOUGLAS L., 2008). A Figura 3.12 ilustra as estruturas dos PLIs estudados e a Tabela 3.1 mostra os resultados de permeabilidade e seletividade encontrados para estes PLIs.

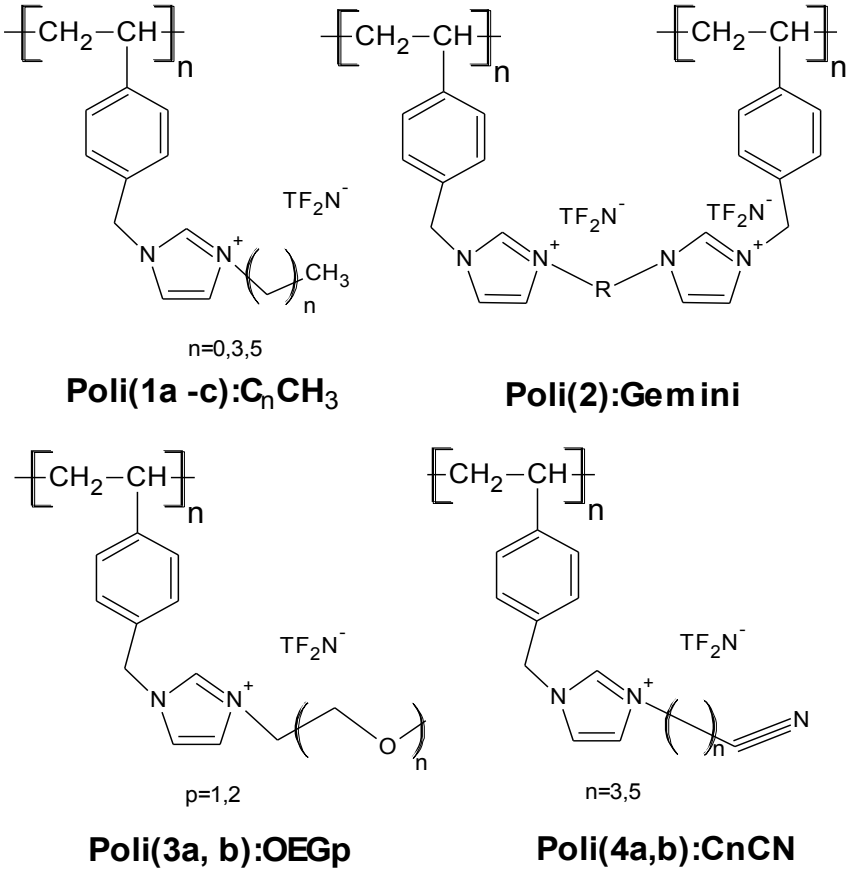

Figura 3.12: Estrutura das diferentes classes de PLIs sintetizadas pelo grupo de Noble Fonte: Bara et al., 2008 (BARA JASON E. , HATAKEYAMA EVAN S. , GIN DOUGLAS L., 2008).

Membranas de PLIs contendo grupos funcionais éter (R-O-R') na cadeia lateral do cátion imidazólio exibiram elevada permeabilidade ao CO_2 em comparação a PLIs que contém o grupo nitrila (-CN) e substituintes alquila. Além disso, a inserção de grupos funcionais éter também proporcionou valores de seletividade superiores ou similares aos alcançados com o aumento do comprimento da cadeia alquílica ou a introdução de grupos do tipo nitrila (-CN) (Tabela 3.1). Estes resultados demonstram que a inserção de grupos éter em PLIs pode ser uma abordagem interessante para melhorar a permeabilidade e seletividade destes materiais em processos de separação de CO_2.

Tabela 3.1. Valores de permeabilidade ao CO_2 e seletividade (CO_2/N_2; CO_2/CH_4) obtidas para as classes de PLIs estudadas pelo grupo de Noble. Fonte: Bara et al., 2008 (BARA JASON E. , HATAKEYAMA EVAN S. , GIN DOUGLAS L., 2008).

Membranas	Permeabilidade ao CO_2*	CO_2/N_2	CO_2/CH_4
Poli(1a –c):C_nCH_3	9-32	28-32	17-39
Poli(2):Gemini	4	22-28	27-32
Poli(3a, b):OEG_p	16-22	41-44	29-33
Poli(4a,b):C_nCN	4-8	37-40	30-37

* Permeabilidade ao CO_2 em Barrers. 1 Barrers = 10^{-10} $cm^3(STP)cm/cm^2$ s cm Hg.

Apesar da natureza do ânion exercer papel secundário sobre a afinidade do CO_2 com PLIs catiônicos, conforme mostrado no estudo de Fang et al., 2013 (Figura 3.8 e 3.9), a escolha do tipo de ânion é um fator que não pode ser desconsiderado na busca de PLIs catiônicos eficientes para separação de CO_2 (TANG et al., 2005d; CARLISLE et al., 2010; BHAVSAR; KUMBHARKAR; KHARUL, 2012; ZULFIQAR; SARWAR; MECERREYES, 2015b; SADEGHPOUR; YUSOFF; AROUA, 2016). O uso de vários tipos de contra ânions inorgânicos (Br^-, BF_4^-, PF_6^-,Tf_2N^- etc.), e orgânicos (Sac^-,Bz^-,Ac^- etc.) tem sido relatados na literatura para obtenção de PLIs catiônicos (TANG et al., 2005a, 2005b, 2005d, 2009; CARLISLE et al., 2010; BHAVSAR; KUMBHARKAR; KHARUL, 2012).

Estudos realizados com policátions de base amônio e imidazólio mostraram que diferentemente do observado em líquidos iônicos convencionais, a presença de

átomos fluorados em seus ânions não promove necessariamente um impacto direto na melhora da sorção de CO_2 (AKI et al., 2004; CADENA et al., 2004; TANG et al., 2005c, 2005d, 2009). Este comportamento pode ser evidenciado pelos resultados de sorção de CO_2 (Figura 3.13) obtidos para PLIs de base amônio, sintetizados com diferentes tipos de contra ânions inorgânicos fluorados (PF_6^-, BF_4^-, e Tf_2N^-) e com o ânion orgânico não fluorado Sac^-.

Conforme pode-se observar na Figura 3.13, a capacidade de sorção de CO_2 obtida para o PLI contendo o ânion TF_2N^- (2,85 mol%) foi muito menor que a encontrada para os PLIs com ânion PF_6^- (10,66 mol%), e BF_4^- (10,22 mol%) e semelhante a alcançada com o ânion não fluorado Sac (2,67 mol%) (TANG et al., 2005d).

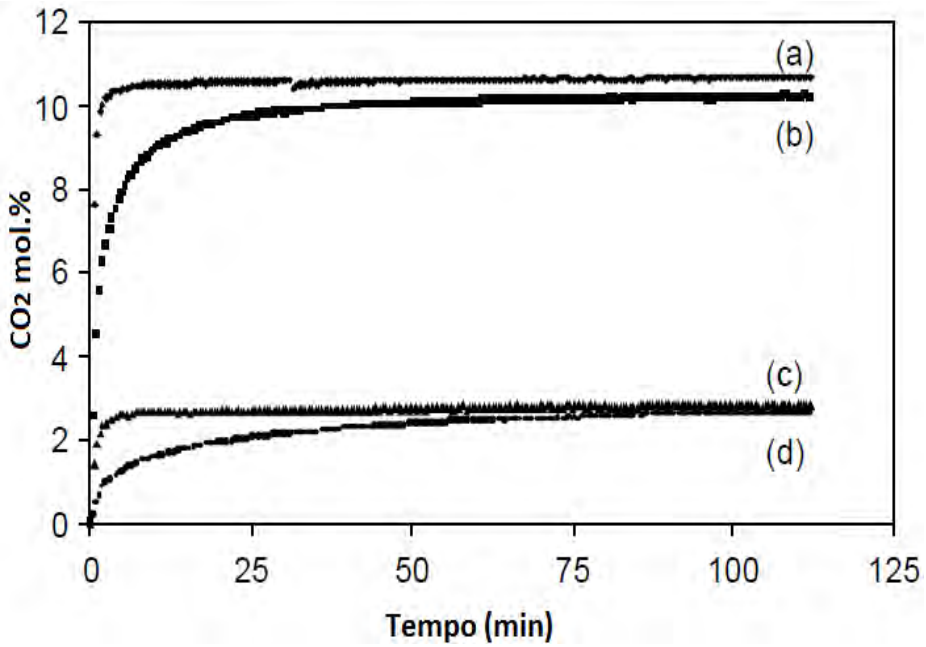

Figura 3.13. Isoterma de sorção de CO_2 em PLIs base amônio, sintetizados com diferentes ânions (22°C; 0,79 bar): (a) P[VBTMA][PF_6]; (b) P[VBTMA][BF_4]; (c) P[VBTMA [TF_2N]; (d) P[VBTMA [Sac]. Fonte: Tang et al.,2005(TANG et al., 2005d).

Uma série de policátions a base de dialildimetilamônio e amônio com diferentes ânions carboxilatos (Ac^-,$TFAc^-$,HFB^-,BZ^-), sulfonatos (MS^-, PTS^-, $TFMS^-$), sulfonamidas (TF_2N^-), e inorgânicos (Cl^-,NO_3^-,BF_4^-) ilustrados na Figura 3.14, foram investigados quanto a sua capacidade de sorção de CO_2 e seletividade (BHAVSAR; KUMBHARKAR; KHARUL, 2012). Os valores de coeficiente de solubilidade (SCO_2)

e seletividade (SCO_2/SH_2; SCO_2/SN_2) obtidos a 20 atm e 35°C podem ser vistos na Tabela 3.2.

Ao analisarmos o PLI P[DADMA] na Tabela 3.2 fica evidente que o ânion carboxilato AC proporcionou o maior coeficiente de solubilidade (SCO_2) (4,0) e seletividade de CO_2 em relação ao H_2 (SCO_2/SH_2 de 42,6) e N_2 (SCO_2/SN_2 de 114,3)(BHAVSAR; KUMBHARKAR; KHARUL, 2012). Observa-se ainda que o coeficiente de solubilidade (SCO_2) obtido para os PLIs com ânions carboxilatos aumenta na seguinte ordem [TFAc] < [HFB] < [Bz] < [Ac] de acordo com a tendência de incremento da sua basicidade (pKa do ácido conjugado = 4,8; 4,2; 0,4; 0,0 respectivamente). Este comportamento é semelhante ao observado em líquidos iônicos convencionais, onde o aumento da basicidade do ânion tende a elevar a sorção de CO_2 (BHAVSAR; KUMBHARKAR; KHARUL, 2012).

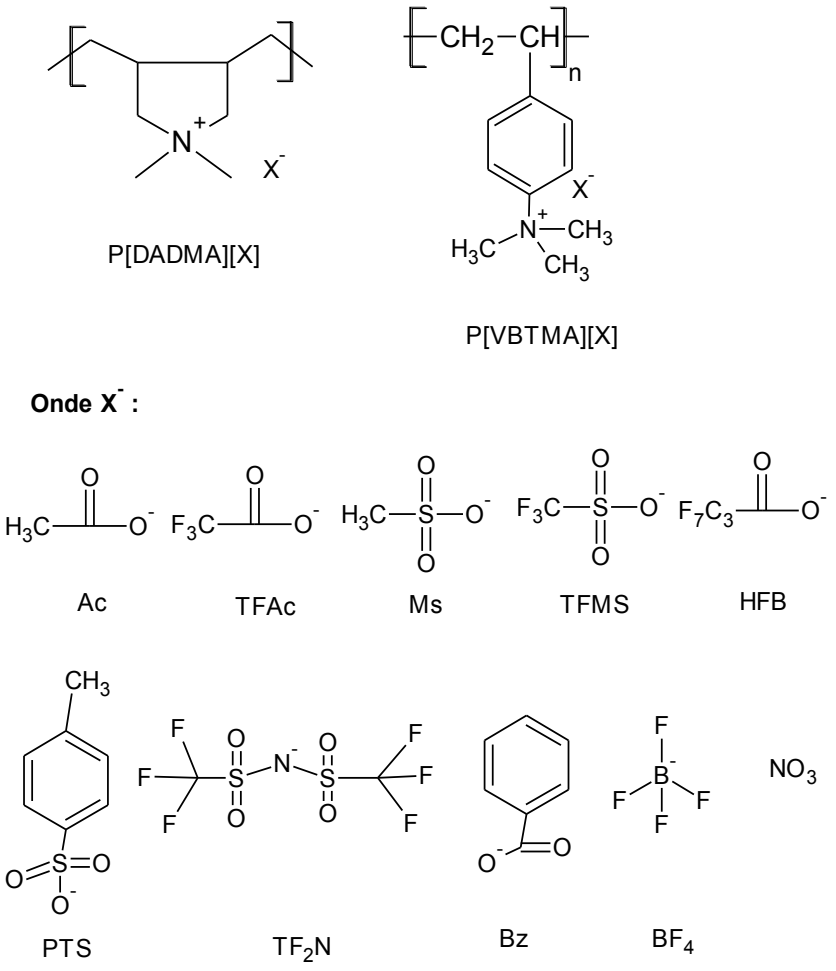

Figura 3.14. Estrutura de policátions e ânions utilizados no estudo de sorção e seletividade. Fonte: Bhavsar et al.,2012 (BHAVSAR; KUMBHARKAR; KHARUL, 2012).

No trabalho desenvolvido por Bhavsar et al., 2012 (BHAVSAR; KUMBHARKAR; KHARUL, 2012) verificou-se também que para PLIs com ânions sulfonados a basicidade do ânion não pode ser considerada como a única responsável pela melhora da seletividade e da capacidade de sorção de CO_2, outras propriedades como, por exemplo, a densidade e volume livre fracionário (VLF) também podem influenciar. O SCO_2 seguiu a seguinte variação $TFMS^- > PTS^- \approx MS^-$ e os valores de basicidade (pKa do ácido conjugado) foram: $TFMS^- = -13$, $PTS^- = -2,8$, $MS^- = -2,0$ (BHAVSAR; KUMBHARKAR; KHARUL, 2012). Em ânions inorgânicos tais como Cl^-, NO_3^-, BF_4^- o aumento da massa molar do ânion pode contribuir para o incremento no SCO_2, SCO_2/SH_2 e SCO_2/SN_2 (ver Tabela 3.2) (BHAVSAR; KUMBHARKAR; KHARUL, 2012)

Tabela 3.2. Coeficiente de solubilidade (SCO_2) e seletividade (SCO_2/SH_2; SCO_2/SN_2) a 20 atm, expresso em $cm^3(STP)/cm^3$ polímero.Fonte:Bhavsar et al.,2012 (BHAVSAR; KUMBHARKAR; KHARUL, 2012).

PLIs	**SCO_2**	**SCO_2/SH_2**	**SCO_2/SN_2**
P[DADMA][Cl]	0,12	1,6	2,3
P[DADMA][Ac]	4,00	42,6	114,3
P[DADMA][TFAc]	0,63	2,7	3,5
P[DADMA][MS]	0,25	2,4	1,4
P[DADMA][TFMS]	0,96	2,4	2,5
P[DADMA][PTS]	0,25	3,3	7,6
P[DADMA][HFB]	1,03	18,7	11,8
P[DADMA][Bz]	1,37	19,7	41,5
P[DADMA][NO_3]	0,42	3,6	4,8
P[DADMA][TF_2N]	0,73	8,2	12,8
P[DADMA][BF_4]	0,86	10,8	11,5
P[VBTMA][Cl]	0,67	-	4,5
P[VBTMA][Ac]	3,16	-	37,6
P[VBTMA] [BF_4]	1,45	-	14,6

3.3.2. Poli (líquidos iônicos) obtidos via polimerização por condensação/modificação

Recentemente tem aumentado o interesse de pesquisadores pela obtenção de PLIs via polimerização por condensação/modificação (SHAPLOV et al., 2016). Este método envolve basicamente reações de condensação, que podem ser conduzidas por meio da modificação de polímeros comerciais ou via condensação do respectivo monômero (BHAVSAR et al., 2014; SHAPLOV et al., 2016; TOME; MARRUCHO, 2016). Entretanto, na literatura, poucas são as classes de PLIs conhecidas sintetizadas por esta via para captura de CO_2: poliuretanos (PU) (MAGALHAES et al., 2014; FERNÁNDEZ et al., 2016), polibenzimidazol (PBI) (BHAVSAR et al., 2014; KUMBHARKAR; BHAVSAR; KHARUL, 2014), poliimidas (SHAPLOV et al., 2016) e a base de imidazólio contendo grupos éster e hidroxilas simétricas (XIONG et al., 2012).

A influência do ânion sobre a cinética e a sorção de CO_2 foi investigada em PLIs catiônicos base imidazólio ilustrados na Figura 3.14 (XIONG et al., 2012). O ânion PF_6 proporcionou uma capacidade de sorção superior quando comparada ao ânion BF_4 (Figura 3.15), possivelmente isto está relacionado à morfologia rugosa do PLI-PF_6 que pode promover uma área superficial maior e consequentemente uma sorção de CO_2 mais rápida e elevada (XIONG et al., 2012). Observa-se ainda na Figura 3.15, que, embora o tempo necessário para atingir o equilíbrio de sorção com os PLIs tenha sido inferior apenas ao alcançado com os LIs [bmim] [PF_6] (a) e [EEIM][PF_6] (c), a capacidade de sorção destes PLIs foi superior a uma série de LIs (XIONG et al., 2012).

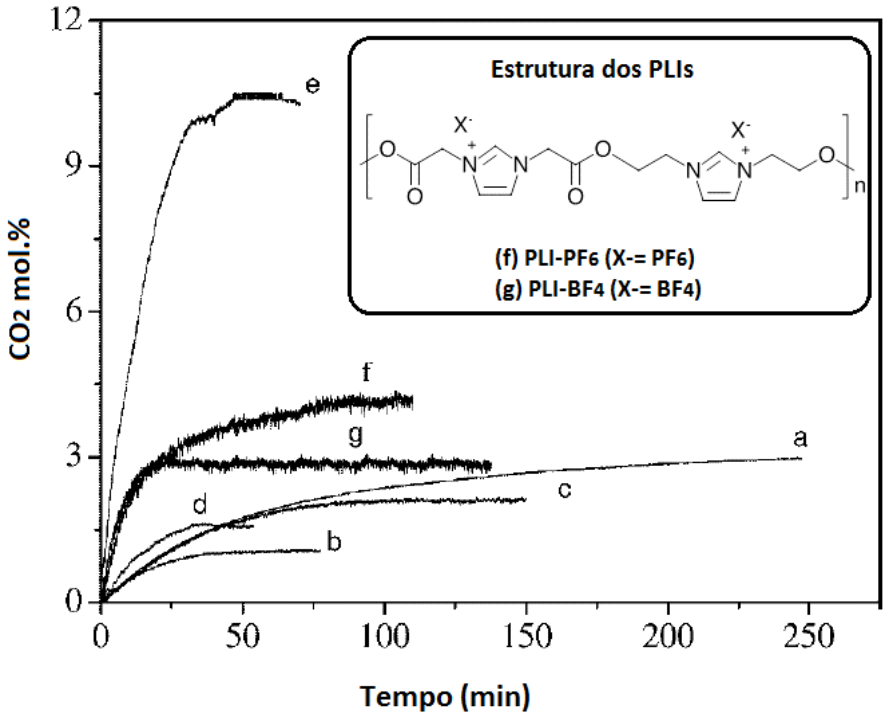

Figura 3.15. Cinética de sorção de CO_2 dos LIs e PLIs (25°C 648 mmHg): (a) [bmim] [PF_6]; (b) [EEIM][BF_4]; (c) [EEIM][PF_6]; (d)[HHIM][BF_4]; (e)[HHIM][PF_6]; (e) PLI-PF_6 e (f) PLI-BF_4. Fonte: Xiong, 2012 (XIONG et al., 2012)

O efeito do ânion e a estrutura do cátion sobre a solubilidade, seletividade e permeabilidade ao CO_2 também tem sido alvo de estudos em PLIs catiônicos baseados em polibenzimidazol (Figura 3.16) (BHAVSAR et al., 2014; KUMBHARKAR; BHAVSAR; KHARUL, 2014). Os coeficientes de solubilidade de CO_2 [$S(CO_2)$] e os resultados de permeabilidade e seletividades dos PLIs [TMPBI] [X] evidenciaram que o ânion possuiu um forte efeito sobre as propriedades de sorção de CO_2. A inserção do ânion TF_2N no PLI [TMPBI] [X] propiciou uma permeabilidade ao CO_2 mais elevada quando comparado ao BF_4. De acordo com Kumbharkar et al., 2014 (KUMBHARKAR; BHAVSAR; KHARUL, 2014) o ânion TF_2N proporciona maior volume livre na rede polimérica, devido a sua elevada mobilidade em comparação aos outros ânions (Ac^-,BF_4^- e I^-), o que resulta em uma melhora na difusão do gás.

Estudos desenvolvidos por Bhavsar et al 2014 (BHAVSAR et al., 2014) indicaram que modificações na estrutura do cátion também podem impactar na

solubilidade do CO_2, visto que a sorção de [TMPBI-BuI] [BF_4] foi superior a alcançada com os PLIs [TMPBI-I] [BF_4] e [DMABPBI] [BF_4] (Figura 3.16). Neste estudo, a forte influência do ânion sobre a sorção de CO_2 também foi observada. A troca do ânion iodeto (I) por tetrafluoroborato (BF_4) no PLIs [TMPBI-Iso] [X] e [DMABPBI] [X] promoveu o aumento da sorção de CO_2 (BHAVSAR et al., 2014).

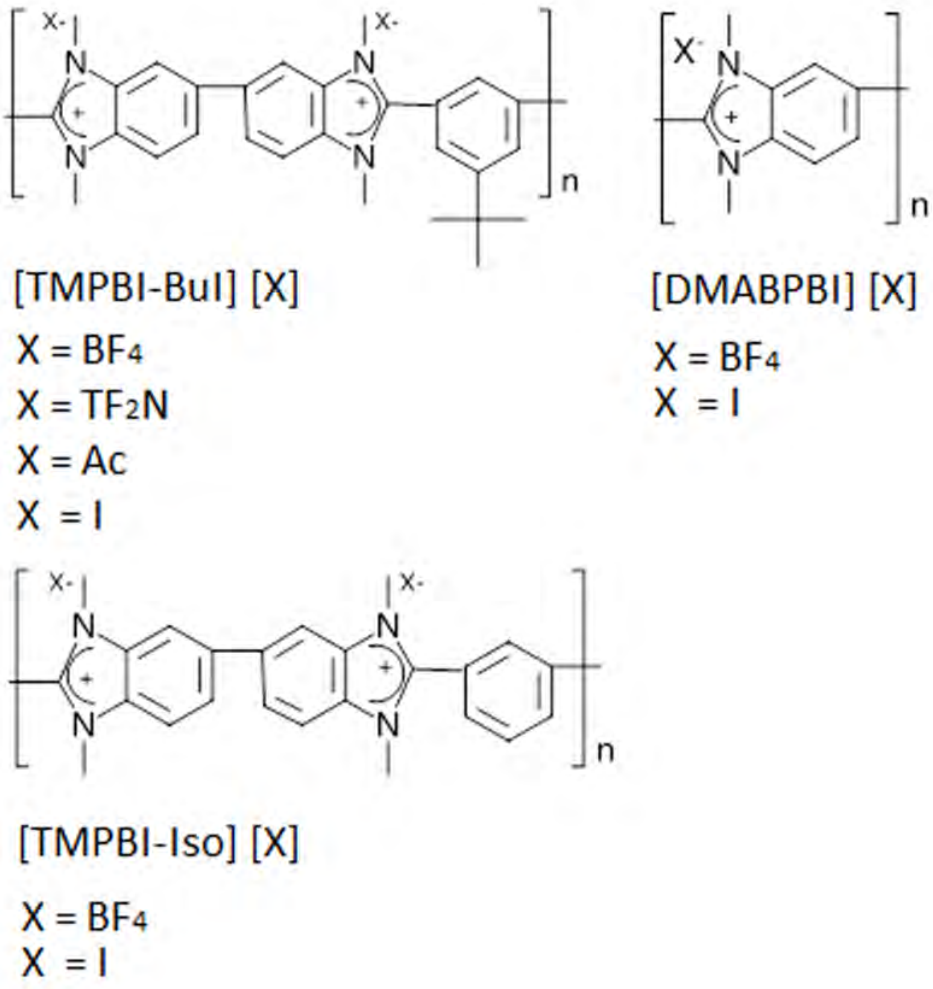

Figura 3.16. PLIs catiônicos baseados em polibenzimidazol. Fonte: Bhavsar et al.,2014(BHAVSAR et al., 2014) .

As isotermas de sorção de CO_2 obtidas para o PLIs base [TMPBI-BuI] [X] são apresentadas na Figura 3.17. Os resultados mostram que o aumento da sorção de CO_2 destes PLIs seguiu a ordem crescente de basicidade do ânion (pKa valor dos seus ácidos conjugados [Tf_2N] -4 < [BF_4] -0,44 < [Ac] 4,75) e que todos os PLIs [TMPBI] [X] apresentaram desempenho de sorção superior (cerca de duas a três

vezes maior) ao de membranas convencionais utilizadas, tais como a polissulfona (PSF) e policarbonato (PC)(KUMBHARKAR; BHAVSAR; KHARUL, 2014).

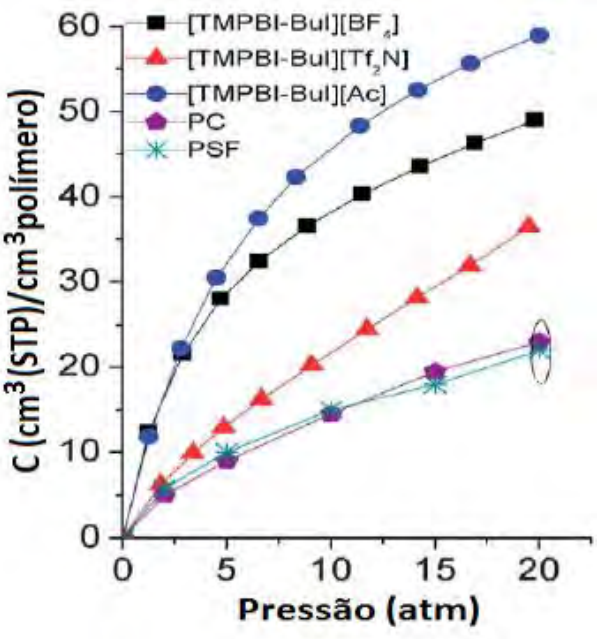

Figura 3.17. Isoterma de sorção de CO_2 a 35°C obtida para o PLI [TMPBI] [X] com diferentes ânions em comparação ao polímeros comerciais (polissulfona (PSF) e policarbonato (PC)).Fonte: Kumbharkar et al., 2014 (KUMBHARKAR; BHAVSAR; KHARUL, 2014)

O efeito da modificação estrutural da cadeia do cátion em PLIs catiônicos base poliimidas sobre a separação do CO_2 foi estudado. Foram testados a introdução de dois diferentes grupos (benzimidazole e azabiciclo[2.2.2]octano) no cátion. Membranas que continham grupos azabiciclo[2.2.2]octano demonstraram permeabilidade mais elevada ao CO_2. O incremento na permeabilidade com a presença do grupo azabiciclo[2.2.2]octano, pode estar associado ao fato deste ser mais volumoso que o benzimidazol, contribuindo assim para o desenvolvimento de uma membrana menos empacotada, com menor resistência à difusão de gás e consecutivamente maior permeabilidade aos gases (SHAPLOV et al., 2016).

A síntese e avaliação do desempenho de sorção de CO_2 de PLIs catiônicos e aniônicos base poliuretano também tem sido reportada na literatura (MAGALHAES et al., 2014; FERNÁNDEZ et al., 2016). Estes estudos mostraram que PLIs aniônicos apresentam capacidade de sorção de CO_2 mais elevada em comparação aos

catiônicos (MAGALHAES et al., 2014). O acréscimo da quantidade de grupos éter através do aumento da massa molar de 1000 para 2000 do polieter poli (tetrametileno glicol) (PTMG), empregado na síntese do PLI proporcionou uma elevação nos valores de sorção de CO_2 a 20 bar em cerca de 71%. Grupos éter possuem uma forte afinidade com o CO_2 e o aumento da distância entre os sítios iônicos pode promover a melhora na interação com o CO_2 e consecutivamente o aumento da solubilidade de CO_2 (MAGALHAES et al., 2014).

Ao contrário do esperado, a introdução de estruturas aromáticas no ânion do PLI aniônico através do uso do diisocianato m-tetrametilxileno diisocianato (TMXDI) ao invés de 1,6-hexametileno (HDI) não promoveu uma melhora significativa na solubilidade do CO_2. Em baixas pressões (5 bar), o PLI sintetizado com HDI apresentou uma capacidade de sorção 19% maior que a obtida com TMXDI na estrutura, em pressões mais elevadas (20 bar) a capacidade de sorção de CO_2 do PLI contendo a estrutura aromática foi levemente maior (cerca de 2%) que a atingida com a estrutura linear. A análise deste comportamento sugere que em baixas pressões, grupos aromáticos podem dificultar a interação do CO_2 com os grupos polares / iônicos da cadeia polimérica (MAGALHAES et al., 2014).

O poliânion sintetizado com PTMG de massa molar 2000 e HDI teve seus valores de sorção de CO_2 comparados com o PLI [VBTMA][BF_4] sintetizado via polimerização radicalar por Tang et al., 2005 (TANG et al., 2005b), solução aquosa de metildietanolamina (MDEA) 50 wt% e com o LI 1.butil-3-metilimidazólio bis(trifluorometil)-sulfonamida [bmim] [TF_2N]. Em 20 bar e 25°C, a capacidade de sorção de CO_2 atingida com o [bmim] [TF_2N] e MDEA foi de apenas 56% e 51% respectivamente, da alcançada com este PLI aniônico. A capacidade de sorção de CO_2 deste PLI aniônico também foi maior que a alcançada com o PLI [VBTMA][BF_4] (cerca de 77% maior)(MAGALHAES et al., 2014).

Normalmente, em LIs tradicionais a introdução de cadeias aquílicas ramificadas no cátion promove melhora na solubilidade de CO_2 (PENNLINE et al., 2008). No entanto, em PLIs aniônicos base PU esta tendência não foi observada, os resultados experimentais de sorção de CO_2 alcançados com o PLI de contra cátion

$[bmim]^+$(linear) foram levemente superiores ao obtidos com PLI contendo o contra cátion $[dmbmim]^+$(ramificado). Este comportamento pode estar relacionado com o impedimento estérico causado pela ramificação (MAGALHAES et al., 2014).

Em outro trabalho (FERNÁNDEZ et al., 2016), extensores de cadeia (dietanolamina (DEA) hidrazina (HYD) e etilenodiamina (EDA)) foram usados com o objetivo de aumentar a massa molar de PLIs aniônicos base PU. A massa molar ponderal média (Mn) dos PLIs obtida variou de 2413 a 10121 g/mol. A técnica de emulsificação múltipla também foi empregada para formação de micropartículas (μP) e nanopartículas (NP) de PLIs.

O comparativo dos resultados de sorção de CO_2 entre os PLIs sintetizados por Rojas et al.,2016 (FERNÁNDEZ et al., 2016) evidenciaram que o aumento da massa molar pode favorecer a solubilidade do CO_2, assim como a introdução de grupos amidas na estrutura do ânion. Verificou-se ainda que a capacidade de solubilizar o CO_2 baseia-se na estrutura, porém a morfologia e tamanho da partícula favorecem a sorção de CO_2. A capacidade de sorção de CO_2 das μP e NP foram similares a dos PLIs, no entanto, a formação das partículas proporcionou um aumento significativo na taxa de sorção. Os PLIs necessitaram de aproximadamente 6,7h para atingir 80% da sua capacidade total de sorção de CO_2. A baixa taxa de sorção pode estar relacionada com o fato de sua sorção ser principalmente superficial, em decorrência da sua morfologia lisa e não porosa (FERNÁNDEZ et al., 2016). Para a NP de PLI, o tempo fundamental para alcançar 82% do total de CO_2 capturado foi de apenas 50 min (4,936 mg/g a 25°C e 4 bar) (FERNÁNDEZ et al., 2016).

Poli (líquidos iônicos) aparecem como materiais promissores para captura de CO_2. Esta revisão apresentou uma visão geral sobre as tecnologias de captura de CO_2 e abordou de forma ampla o desenvolvimento de PLIs para captura de CO_2, explorando os principais aspectos da produção de PLIS, que afetam a capacidade de sorção, permeabilidade ou seletividade ao CO_2. Em resumo, os estudos mostraram que a área específica porosidade, massa molar, aumento da pressão e redução da temperatura tendem a aumentar a sorção de CO_2. Fatores como cátion,

ânion, introdução de grupos polares e modificações estruturais podem promover melhorias na sorção, seletividade e permeabilidade ao CO_2. Ultimamente, o interesse por PLIs obtidos via polimerização por condensação/modificação tem aumentado. Este comportamento está relacionado com o fato desta rota permitir o uso de polímeros comerciais e o uso de uma quantidade menor de LIs no processo de síntese, reduzindo assim o custo da produção de PLIs.

Neste cenário, este trabalho sintetizou e avaliou a capacidade de sorção de CO_2 de diferentes poli (líquidos iônicos) baseados em poliuretano, poliuretano-imida e celulose. Também buscou investigar o potencial para captura de CO_2 de aminas e polieteraminas suportadas em celulose.

4. PROCEDIMENTOS EXPERIMENTAIS E RESULTADOS

No presente trabalho foram sintetizados quatro tipos diferentes de poli (líquidos iônicos) baseados em polímeros sintéticos (PU e PU-imida) e na celulose, polímero natural extraído da casca de arroz. Todos os PLIs foram obtidos via polimerização por condensação/modificação, sendo de dois tipos (aniônico e catiônico) os produzidos a partir da celulose e apenas de um tipo (aniônico) os baseados em PU e PU-imida. Neste estudo, buscou-se correlacionar as propriedades mecânicas, térmicas, morfológicas e a capacidade de sorção de CO_2 com a estrutura de cada PLI produzido. Visando uma alternativa a estes PLIs, aminas e polieteraminas foram suportadas em celulose extraída da casca de arroz.

Nesta secção, em forma de artigos, serão apresentados os métodos, resultados e discussões pertinentes a esta tese, divididos da seguinte forma: Poli(líquidos iônicos) aniônicos base poliuretano (Capítulo I); Poli(líquidos iônicos) aniônicos base poliuretano-imida (capítulo II); Poli(líquidos iônicos) aniônicos celulósicos (capítulo III); Poli(líquidos iônicos) catiônicos celulósicos (capítulo IV) e aminas e polieteraminas suportadas em celulose (capítulo V). A Figura 4.1 mostra uma representação esquemática dos capítulos juntamente com os assuntos abordados. Na secção 5, será apresentado um comparativo dos principais resultados obtidos para os melhores materiais de cada grupo.

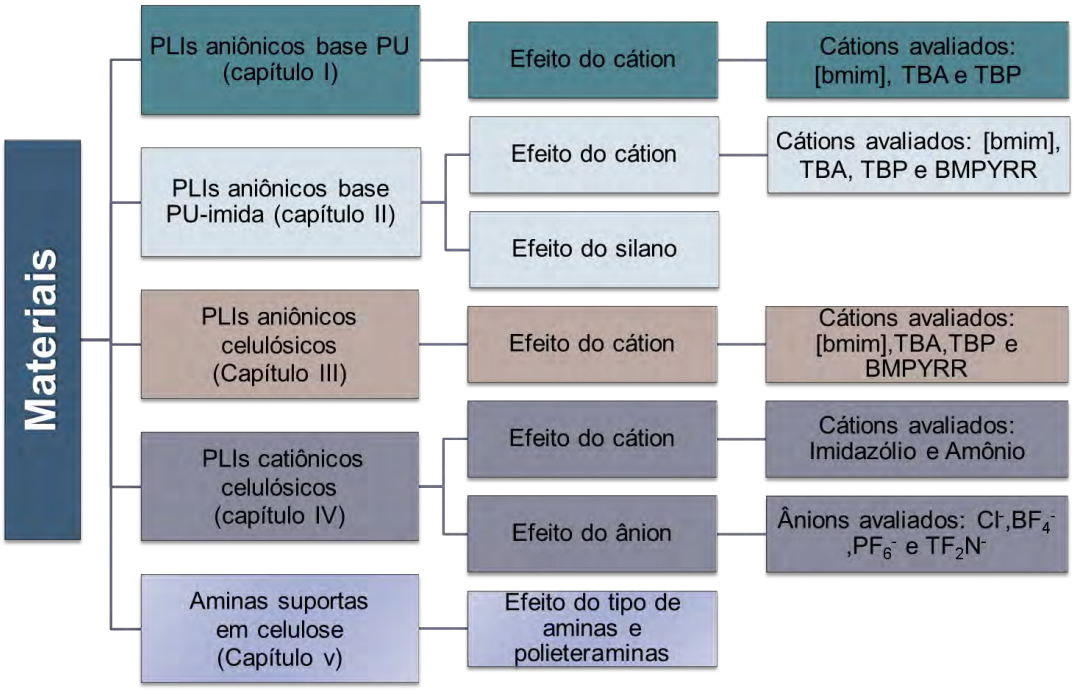

Figura 4.1. Representação esquemática dos capítulos e assuntos abordados.

4.1. Capitulo I: Poli (líquidos iônicos) aniônicos base poliuretano

Este capítulo descreve a síntese e caracterização de PLIs aniônicos base PU, por meio do artigo intitulado "*CO_2 capture: Tuning cation-anion interaction in urethane based poly(ionic liquids*" publicado na Polymer. Três tipos diferentes de cátions (imidazólio, fosfônio e amônio) foram usados para formação de PLIs. Os materiais obtidos foram caracterizados por FTIR, RMN, DSC, TGA, DMA, MEV-FEG e AFM. A capacidade de sorção de CO_2 foi avaliada a 303,15 K e pressões de 0,8 até 50 bar, utilizando uma PTGA. Simulações ab initio foram empregadas com o objetivo de compreender o papel dos principais grupos funcionais presentes na estrutura dos PLIs sobre a afinidade ao CO_2 . Os resultados mostraram a influência do tipo de contra-cátion sobre as propriedades térmicas, mecânicas e capacidade de sorção de CO_2. Ensaios experimentais e de simulação mostraram que cátions que coordenam fracamente o sítio COO^- (TBA e TBP) favorecem a sorção de CO_2. Os melhores desempenhos de sorção de CO_2 e propriedades mecânicas foram obtidos para os PLIs PU-TBP e PU-TBA (PU-TBP 15,7 mgCO_2/g e PU-TBA 16,1 mgCO_2/g a 30°C e 0,82 bar). Estes PLIs demostraram capacidade de sorção de CO_2 superior quando comparada a outros PLIs descritos na literatura.

Polymer 102 (2016) 199–208

Contents lists available at ScienceDirect

Polymer

journal homepage: www.elsevier.com/locate/polymer

CO_2 capture: Tuning cation-anion interaction in urethane based poly(ionic liquids)

Franciele L. Bernard [a, b], Barbara B. Polesso [c], Fabiana W. Cobalchini [c], Augusto J. Donato [b], Marcus Seferin [a, b], Rosane Ligabue [a, b], Vitaly V. Chaban [d], Jailton F. do Nascimento [e], Felipe Dalla Vecchia [c], Sandra Einloft [a, b, *]

[a] Post-Graduation Program in Materials Engineering and Technology, Pontifical Catholic University of Rio Grande do Sul – PUCRS, Brazil
[b] School of Chemistry, Pontifical Catholic University of Rio Grande do Sul – PUCRS, Brazil
[c] School of Engineering, Pontifical Catholic University of Rio Grande do Sul – PUCRS, Av. Ipiranga, 6681, Partenon, Porto Alegre, CEP: 90619-900, Brazil
[d] Institute of Science and Technology (ICT), Federal University of São Paulo (UNIFESP), São José dos Campos, SP, Brazil
[e] Petrobras / CENPES, Ilha do Fundão Qd. 07, Rio de Janeiro, RJ, Brazil

ARTICLE INFO

Article history:
Received 2 June 2016
Received in revised form
19 August 2016
Accepted 27 August 2016
Available online 8 September 2016

Keywords:
Poly(ionic liquids)
Ab inition simulations
CO_2 capture

ABSTRACT

The development of new urethane based poly(ionic liquids) (PILs) is a promising solution to address CO_2 capture. The obtainment of low cost polyurethane based PILs using different ionic liquids cations fosters the emergence of new materials for CO_2 capture. The synthesized PILs were characterized by GPC, FTIR, NMR, DSC, TGA, DMTA and AFM. CO_2 sorption capacity was gravimetrically assessed in a magnetic suspension balance. In addition, *ab initio* simulations were performed. Experimental and simulation results allow understanding the varying performance of the polymeric anion with the bmim, TBA, and TBP cations in CO_2 sorption. A successful compound for gas capture must exhibit the weakest possible cation-anion coordination and smaller molecular masses. Better CO_2 sorption capacity was achieved for the cation TBA as compared to TBP and bmim (the amounts of CO_2 sorption at 50 bar and 303.15 K were 162 $mgCO_2/g$ for the PU-bmim, 168 $mgCO_2/g$ for PU-TBP and 226 $mgCO_2/g$ PU-TBA). At lower pressures, these compounds present a high CO_2 sorption capacity (at 0.82 bar of pressure and 303.15 K PU-bmim presented a CO_2 sorption of 9.4 $mgCO_2/g$; PU-TBP 15.7 $mgCO_2/g$ and PU-TBA 16.1 $mgCO_2/g$). The compounds PU-TBP and PU-TBA presented higher sorption values as compared to literature.

1. Introduction

The growing atmospheric concentration of carbon dioxide (CO_2) continues to be a global issue due to the common awareness about the connection of this gas with global warning problem [1,2]. Traditionally, aqueous solutions of alkanolamines are widely used for CO_2 removal in capture plants [3,4]. However, there are some disadvantages in commercial use of these amines solutions, including the high energy consumption during regeneration, formation of corrosive by-products, amines loss (requiring solvent replacement) and the need of large volume absorber [3–6].

The development of versatile sorbents with smart design for CO_2 capture has become one of the main research focus in this field [2] and Poly(ionic liquid)s (PILs) appear as promising materials for CO_2 capture [2,7–9]. Poly(ionic liquids) or polymerized ionic liquids are a subclass of polyelectrolytes, in which each repeating unit is ionic. The units are connected through a polymeric backbone forming a macromolecular structure [8,10]. These compounds combine the benefits of ILs (high ionic conductivity, chemical and thermal stability) with the polymer properties (mechanical stability, processing and tunable macromolecular design) [8,11–13].

The PILs offer an extremely versatile and adjustable platform for designing sorbents, mainly for CO_2 separation from the flue gas (CO_2/N_2) and natural gas purification (CO_2/CH_4) [2,11].

It was described elsewhere [7] that polymers synthesized from the IL monomers present a higher sorption capacity as compared to room-temperature ILs (RTILs). It was also highlighted that the sorption/desorption of these polymers is higher than that of RTILs being completely reversible. A large number of studies have reported the solubility of CO_2 in different types of PILs [11,14–19]. Recently, we reported the synthesis of versatile and inexpensive

* Corresponding author. Post-Graduation Program in Materials Engineering and Technology, Pontifical Catholic University of Rio Grande do Sul – PUCRS, Brazil.
E-mail address: einloft@pucrs.br (S. Einloft).

http://dx.doi.org/10.1016/j.polymer.2016.08.095
0032-3861/

polyurethane based PILs designed for CO_2 capture [18]. Two different approaches were used for the synthesis of this material. The first one produces anionic PILs with the introduction of the imidazolium as a cation. The second one synthesizes cationic polyurethanes. The anionic PILs presented higher CO_2 sorption capacity as compared to the cationic polymers. It was also observed that PILs based in 1-butyl-3-methylimidazolium, $[bmim]^+$, as a cation achieved higher CO_2 sorption than PIL with 1-dimethylbutyl-3-methylimidazolium, $[dmbmim]^+$ as a cation. This behavior can probably be due to the steric hindrance of the branched alkyl side chain of imidazolium structure compared with the linear structure. The anionic PILs also showed superior performance when compared with the IL [bmim] $[Tf_2N]$, MDEA 50% (w/w) as well as the PILs as described in literature [20]. The use of anionic PU chain to produce PILs allows an easy way to obtain different materials to be tested in CO_2 sorption. The CO_2 affinity by RTILs is influenced by the cation type. The same behavior must be expected for PILs.

The present work was undertaken on the same line, i.e., to develop new anionic polyurethanes introducing three different types of cations (imidazolium-, phosphonium- and ammonium-based cations). Quantum mechanical simulations were employed to understand the varying performance of the polymeric anion with the 1-butyl-3-methylimidazolium (bmim), tetrabutylammonium (TBA), and tetrabutylphosphonium (TBP) cations.

2. Experimental

2.1. Materials

Poly(tetramethylene ether) glycol (PTMG, Mn 2000 g/mol, Sigma-Aldrich), hexamethylene diisocyanate (HDI, 99%, Merck), dimethylol propionic acid (DMPA, 99%, Perstorp), dibutyl tin dilaurate (DBTDL, Miracemanuodex), N-methy-2-pyrrolidone (NMP, 99,92%,Neon), methylethylketone (MEK, 99%, Mallinckrodt), tetrahydrofuran (THF, 99%, Vetec), potassium hydroxide (KOH, ≥85%,Sigma-Aldrich) were used as received. The tetrabutylammonium bromide (TBAB, 99%, Acros Organics), tetrabutylphosphonium bromide (TBPB, 98%, Sigma Aldrich), were dried under vacuum for 12 h at 60 °C. The ionic liquid 1-butyl-3-methylimidazolium chloride (bmim Cl) was synthesized following procedures well described in literature [21–23]. The ionic liquid (bmim Cl) was characterized by Fourier transform infrared spectroscopy (FTIR), using a Perkin-Elmer spectrophotometer model Spectrum 100 FT-IR with full attenuated reflectance model (ATR), as well as by proton nuclear magnetic resonance (1H NMR) on a Varian Spectrophotometer, model VNMRS 300 MHz, using DMSO-d_6 as solvent and glass tubes of 5 mm in diameter and are in accordance with the literature. 1H NMR (300 MHz, DMSOd6, 25 °C) δ (ppm): 1.01 (m, CH_3), 1.29 (m, CH_2CH_3), 1.83 (m, CH_2), 3.97 (s, CH_3), 4.25 (t, CH_2N), 7.79 (s, H5), 7.91 (s, H4), 9.48 (s, H2). FTIR ν (cm^{-1}): 3141 (N–H of imidazolium group), 3058 (C–H of imidazolium group), 2959 (C–H of CH_2), 2870 (C–H of CH_3), 1640 (C=N of imidazolium group), 1558–1453 (C=C and C–N of imidazolium group), 749 (Cl^-).

2.2. Poly(ionic liquids) syntheses

Polyurethane was prepared according to the following procedure (see Fig. 1): PTMG polyol (2000 g/mol) (0.04 mol), DMPA diol (0.11 mol) dissolved in NMP and DBTDL (0.1% wt) as catalyst, were dissolved in MEK (50 mL) in a five-necked flask. Then, HDI was added dropwise to the system and the reaction mixture was stirred at 60 °C for 2 h. The NCO/OH ratio of 1.05 (0.157 mol HDI/0.15 mol OH) was used. The second step was the addition into the reaction medium of the selected IL (see Fig. 1). In this step, the solid content was quantified as well as the acidity of the polymer (by titration with KOH 0.5 M). The acid number reached a value of 25 mgKOH/g (0.45 mmol of IL/g polymer). After that, in order to neutralize the carboxylic acid group, the system was cooled to 40 °C and IL (bmim Cl; TBAB or TBPB) was charged into the reactor. The system was kept at this temperature (40 °C) for 4 h, under stirring to obtain a PIL with the desired cation. The neutralization step occurred at a molar ratio COOH/IL = 1:1 Finally, films with a thickness close to 0.15 mm were produced by casting and dried under vacuum at 63 °C for 24 h.

2.3. Characterization of poly (ionic liquid)s

The structural elucidation of the samples was carried out by Fourier Transform Infrared (FTIR) and Proton Nuclear Magnetic Resonance (^{1}H NMR) spectroscopic techniques. FTIR spectra were recorded on a Perkin-Elmer Spectrum 100 spectrometer in ATR (Attenuated Total Reflection) mode. ^{1}H NMR spectra were obtained using a Bruker Avance DRX-400 spectrometer at 400 MHz in DMSO-d_6. Molecular weights were acquired from a Gel Permeation Chromatograph (GPC), equipped with a Waters 1515 pump and a Waters 2412 refractive index detector, using THF as eluent at a flow rate of 1 mL/min; samples to be analyzed were dissolved in DMSO and then diluted with THF. Differential Scanning Calorimetry (DSC) thermograms were attained by using a TA Instrument Q20 differential scanning calorimeter in the range of −90 °C–170 °C, or 200 °C at a heating rate of 10 °C/min under nitrogen. Thermogravimetric Analysis (TGA) was performed using a TA Instrument SDT-Q600 between 25 °C and 600 °C at a heating rate of 10 °C/min in a nitrogen atmosphere. Tensile tests (stress x strain curves) were carried out at 25 °C with rectangular shape films (12 mm long; 7 mm wide) with a thickness close to 0.15 mm, on a DMTA equipment (model Q800, TA Instruments) with 1 N/min. The Young Modulus of the materials was determined according to ASTM D638. The analyses were carried out in triplicate. The field emission scanning electron microscopy (FESEM) analyses were performed in FEI Inspect F50 equipment in secondary electrons (SE) mode. The AFM analyses were performed in Peak force tapping mode using a Bruker Dimension Icon PT equipped with a TAP150A probe (Bruker, resonance frequency of 150 kHz and 5 N m^{-1} spring constant). The equipment was calibrated prior to samples measurements. The scanned area of the images was 60 × 60 μm^2 with a resolution of 512 frames per area. The DMT Modulus map was derived from PeakForce.

2.4. Sorption measurements

The CO_2 sorption tests were gravimetrically assessed in a Magnetic Suspension Balance (MSB), (Rubotherm Prazisionsmesstechnik GmbH, 350 bar and 673.15 K). The materials sorption capability was isothermally assessed in the range of 0.8–50.0 bar pressure at 303.15 K. The apparatus details are described elsewhere [24,25]. The experimental procedure was detailed in our previous work [18].

2.5. Computer simulations

Molecular dynamics simulations were carried out by the PM7-MD method [26–31]. In PM7-MD, immediate forces acting on all atoms, including hydrogens, are found according to the PM7 semi-empirical Hamiltonian at every time-step. The motion of atomic nuclei is, therefore, directly correlated with the evolution of the system's electronic configuration. Quantum effects are reproduced in PM7-MD simulations, out of which inter- and intra-molecular electronic polarization is most important for the present work.

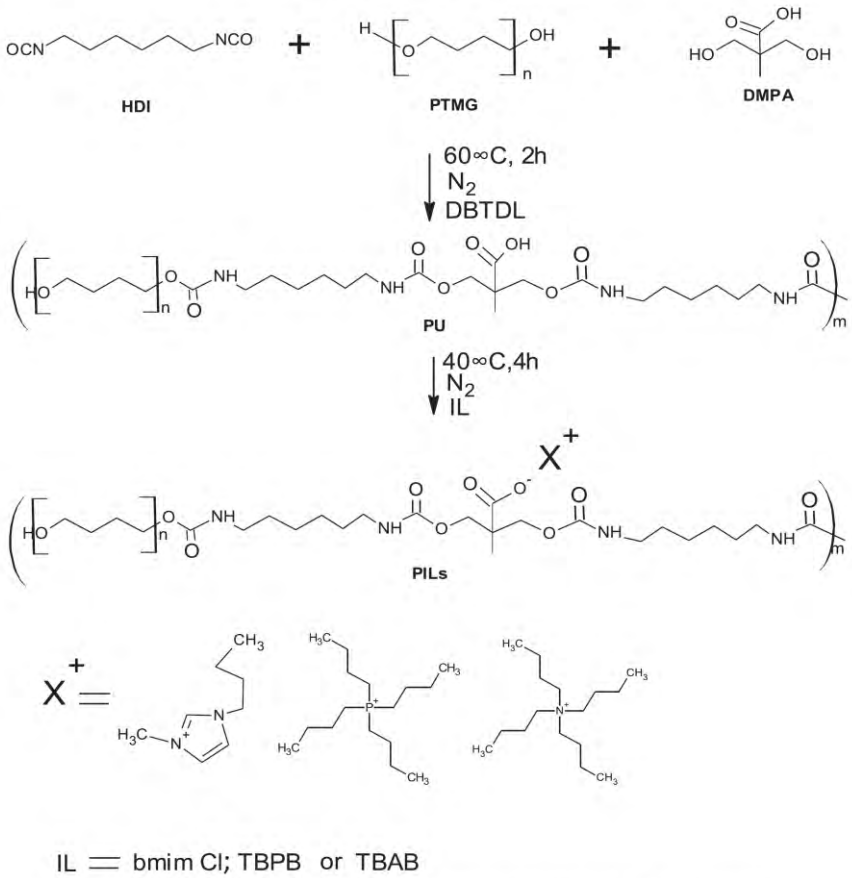

Fig. 1. Synthesis steps and proposed structures of anionic PILs synthesized with different cations (X^+).

The negatively charged oligomer containing three synthesized units, as depicted in Fig. 1, was neutralized by three cations. Three neutral systems were prepared containing: (1) bmim; (2) TBA; (3) TBP. All systems were simulated for 500 ps with a time-step of 0.5 fs at 300 K to sample the phase space in the vicinity of the oligomer surface and identify a preferential coordination site(s) in the oligomer for each cation. Constant temperature was maintained by the Andersen coupling procedure [32] with a relaxation time of 100 fs. Atom-atom spatial correlations were characterized by pair correlation functions (PCFs) for prospective coordination sites.

Density functional theory (DFT) with hybrid functional Becke-3-Lee-Yang-Parr [33–35] and 6-311G* atom-centered triple-zeta polarized basis set was used to optimize selected structures and validate PM7-MD simulations through comparison of intermolecular distances. The self-consistent field convergence criterion was set to 10^{-7} Hartree.

The Packmol code [36] was used to prepare initial coordinates of the systems. The VMD software [37] was used to visualize ionic trajectories. PCFs were computed by the in-home analysis tool.

3. Results and discussion

3.1. Polymer characterization

The molecular weight of the anionic polymeric materials were similar to the non-ionic polyurethane (PU (M_n = 210.500 g/mol; DPI = 1.7); PU-BMIM (M_n = 204.500; DPI = 2.1); PU-TBA (M_n = 195.800; DPI = 2.0); PU-TBP (M_n = 190.000; DPI = 2.0)). The molecular weight of the cation does not change considerably, since an ionic exchange reaction does not interfere with the polymer chain size. Fourier transform infrared spectroscopy (FT-IR) was employed to identify polymer formation and new hydrogen bonds between the ionic compounds. The IR spectra of all samples are presented in Fig. 2a as well as in the range of 3000–3500 cm^{-1} and 1200-2000 cm^{-1} in Fig. 2b and c, respectively.

The absence of the band at about 2270 cm^{-1} corresponding to N=C=O stretching vibration confirms the absence of free NCO group in the polymer structure, which indicates the completion of the urethane reaction [38].

Polyurethanes typically display two main N–H absorption bands, one associated with the non-bonded hydrogen (3440 cm^{-1}) and other with the bonded hydrogen (3320 cm^{-1}) [39,40]. The band corresponding to the N–H stretching of free groups near 3440 cm^{-1} was observed as a small shoulder. This suggests that the N–H groups participate in hydrogen bonding [39,41]. The augmentation in the band area at 3320 cm^{-1} with the incorporation of the cation tetrabutylphosphonium is certain indicating the increase of bonded H. An analogous wavenumber band area for the other samples spectra remained constant (see Fig. 2b). This different behavior related to the change in the intensity of the band

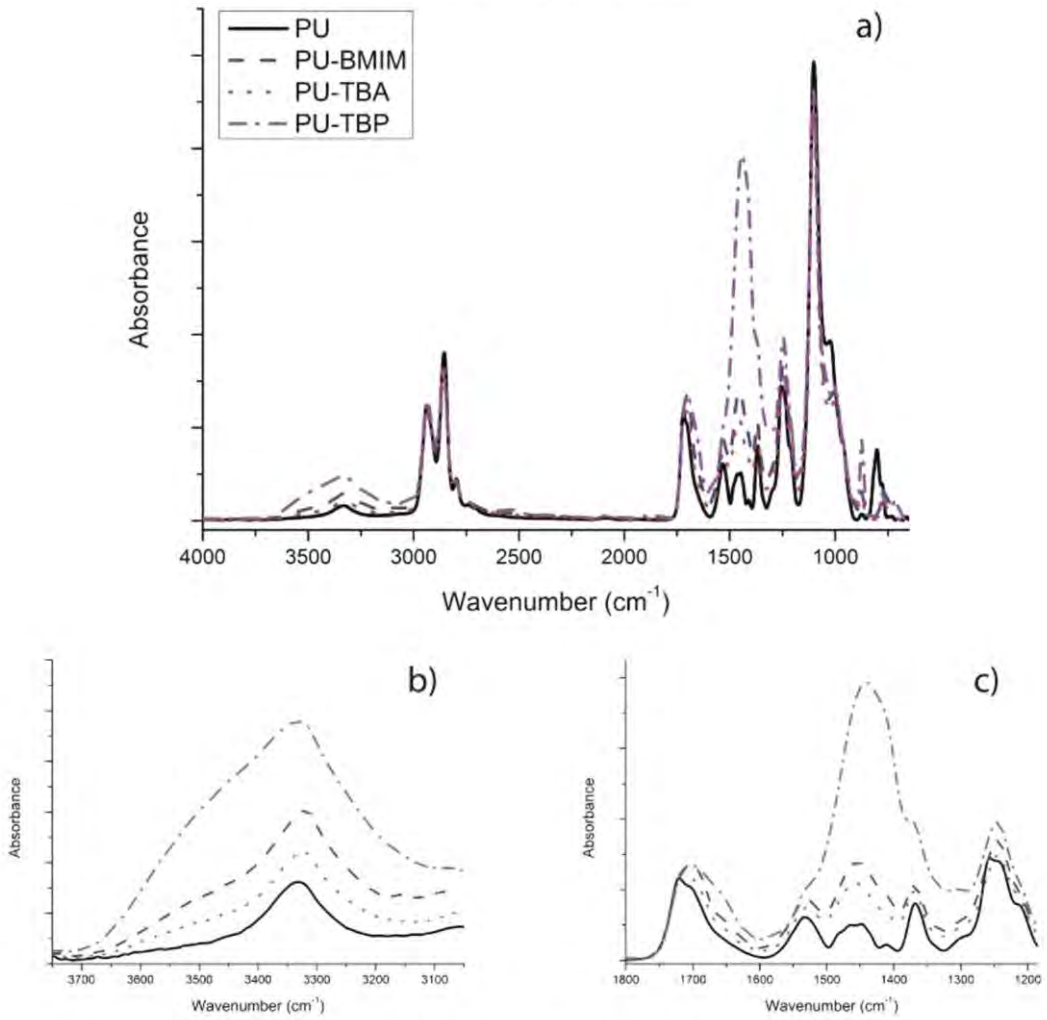

Fig. 2. FTIR spectra of polyurethane (PU) and PILs: (a) 660–4000 cm^{-1}, (b) 3000–3500 cm^{-1}, (c) 1200–2000 cm^{-1}.

area evidences dependence of the absorptivity coefficient on the strength of hydrogen bonding, which in turn varies upon presence of the cation, especially tetrabutylphosphonium.

The carbonyl stretching region in the spectrum of polyurethane also indicates the presence of bands, at about 1721 cm^{-1} and 1699 cm^{-1} associated with "free" (non-bonded hydrogen) carbonyl groups and bonded hydrogen to carbonyl groups, respectively [39]. In this region, a broad band is observed being assigned to superposition of the hydrogen bonded and free carbonyl group absorption. Increase of the band area and frequency decrease from 1720 cm^{-1} (PU) to 1702 cm^{-1} upon the cation addition (Fig 2c) indicate the hydrogen bond formation. The C=O bands from the carboxylic acid group (COOH) and the urethane group (NHCO) are in overlay [38,41] (Fig. 2c).

The synthesized PU presents COOH group from PTMG. It can create hydrogen bond both with hard segments and with C–O–C group of the soft segments [41]. After ionization, the carboxylic acid group (COOH) was transformed to the COO- group. Decrease in the band area of C–O–C group (1103 cm^{-1}) (Fig. 2a) was observed. Thus, the number of hydrogen bonds between soft and hard segments was reduced. The absorption range of –COO– (1470 cm^{-1}) [18,42,43] overlaps with that of $-CH_2$ and $-CH_3$ [43] (Fig. 2c). It was verified that after ionization the band shifts to lower frequency (from 1462 cm^{-1} to 1444 cm^{-1}) and significantly increases the area. The intensity increase after ionization indicates presence of the carboxylate ion (–COO–) in the PILs. The band intensity for TBP is more pronounced due to a larger diameter of the phosphorus atom and, consequently, a smaller electron density on this atom exhibiting the weakest possible cation-anion coordination, as corroborated by simulation results discussed later.

The IR spectra (Fig. 2a) also reveal others characteristic polyurethane adsorption bands: 2936 cm^{-1} (C–H of CH_2), 2858 cm^{-1} (C–H of CH_3), 1532 cm^{-1} (H–N), 1245 cm^{-1} (C–N and C–O of urethane), 1026 cm^{-1} (C–O–C) and 865 cm^{-1} (C–O–C) [18,44]. Accordingly, the structures of the synthesized polymers were analyzed by ^1H NMR. The different resonance peaks and their corresponding assignments are in accordance with literature [18,44] and were also compared with the starting materials spectra

from the Spectral Database for Organic Compounds (SDBS). A typical ^{1}H NMR spectrum of the sample PU-TBA is presented, for reference, in Fig. 3.

The peaks of the all NMR spectra showed the signals of the polyurethane chain, δ (ppm): 1.57 (2H, NH–CO–O–CH_2–$\underline{CH_2}$, m, of PTMG), 3.35 (2H, t, O–$\underline{CH_2}$–CH_2– of PTMG), 3.98 (2H, t, NH–⊖CO–O–$\underline{CH_2}$– of PTMG), 1.28 (2H, m,N–CH_2–CH_2-($\underline{CH_2}$)$_2$– of HDI),1.42 (2H, m, N–CH_2–$\underline{CH_2}$– of HDI), 3.00 (2H m,N–$\underline{CH_2}$–CH_2–, m, of HDI), 1.10 (3H, s,$\underline{CH_3}$ of DMPA), 4.08 (2 H,s, R–NH–⊖CO–O–$\underline{CH_2}$–C of DMPA), 7.10 (1H,s, NH urethane).

The presence of the TBA cation are assigned at δ (ppm): 3.25 (2H t, $CH_3CH_2CH_2\underline{CH_2}N$ of TBA), 1.63 (2H, m, $CH_3CH_2\underline{CH_2}CH_2N$ of TBA), 1,38 (2H, m,$CH_3\underline{CH_2}CH_2CH_2N$ of TBA), 1.02 (3H, t, $\underline{CH_3}CH_2CH_2CH_2N$ of TBA).

The presence of the bmim cation is manifested by δ (ppm): 9.22 (1H, s, NC$\underline{H}$N of bmim), 7.84 (1H, t, CH_3NCH$\underline{CH}$N of bmim), 7.77 (1H, t, CH_3NC$\underline{H}$CHN of bmim), 4.25 (2H, t, N$\underline{CH_2}$(CH_2)$_2CH_3$ of bmim), 3.91 (3H, s, N$\underline{CH_3}$ of bmim), 1.81 (2H, m, N$CH_2\underline{CH_2}CH_2CH_3$ of bmim), 1.30 (2H, m, N(CH_2)$_2\underline{CH_2}CH_3$ of bmim), 0.97 (3H, t, N(CH_2)$_3\underline{CH_3}$ of bmim).

The signals of TBP cation are assigned at δ (ppm): 2.25 (2H, m, $CH_3CH_2CH_2\underline{CH_2}$P of TBP), 1.55 (2H, m, $CH_3(\underline{CH_2})_2CH_2$P of TBP), 0.98 (3H, t, $\underline{CH_3}CH_2CH_2CH_2$P of TBP).

The DSC measurements were carried out to PILs and PU. The DSC curves of all samples (see Fig. 4) show an endothermic peak (PURE PU = 21 °C; PU-bmim = 22.2 °C; PU-TBP = 23.4 °C and PU-TBA = 21.5 °C), which represents the melting of the crystalline microphase. This behavior is due to the molecular weight (M_n = 2000) of soft segments (PTMG) which favors the crystallization. The same behavior was not evidenced for PTMG with lower molecular weight (M_n = 1000) [45,46].

The melting temperature of the microphase is not influenced by the cation insertion into the polymeric chain. The same behavior was observed elsewhere [40] for cationic polyurethane containing pendant trialkylphosphonium. The melting and crystallization enthalpy also presented a small variation (PU-ΔHm = 26.0 J/g and ΔHc = 22.5 J/g; samples PU-bmim, PU-TBP, PU-TBA presented values of ΔHm = 22.2 J/g and ΔHc = 21.2 J/g, ΔHm = 21.9 J/g and ΔHc = 19.5 J/g, ΔHm = 22.4 J/g and ΔHc = 19.7 J/g, respectively). Nevertheless, the crystallization temperatures of PU (−26.9 °C) and the poly(ionic liquid) PU-bmim (−26.9 °C) are similar, but the chains with the cations TBP and TBA presented a lower crystallization temperature (−30.6 °C and −30.3 °C, respectively).

Thermal stability of PU and PILs was investigated by thermogravimetric analysis (TGA) (see Table 1 and Fig. 5). The cation insertion decreased the thermal stability of anionic structures. The same behavior was not observed by Zhang et al. [40] for cationic structures. The insertion of TBP in the polymeric structure resulted in higher thermal stabilities. The TGA thermograms prove that they are stable up to 190 °C and 210 °C to PILs depending on the cation and 236 °C for PU. The TGA thermograms indicate two stages of thermal degradation processes.

In the first step, the decomposition temperatures correspond mainly to the degradation of hard segment, which occurs basically through the dissociation or breaking of the urethane bonds [47,48]. The second stage of thermal degradation is attributed to the decomposition of polyol, i.e. PTMG soft segments [49]. Meanwhile, PILs in this stage may go through the decomposition of the part related to the cation. Such decomposition has been reported in a temperature interval of 140–350 °C [50]. The final step of weight loss occurs in the temperature range 250–507 °C and could be due to the disintegration of the PU moiety into simpler molecules like CO_2 and ethers.

Fig. 6 shows SEM images of PU and the PILs. The PU microstructure exhibited a smooth surface without pores. The SEM images of the PILs are very similar to those obtained for PU.

We observed by AFM images (see Fig. 7) that the hard domains of PU (lighter regions) and the soft domains (dark regions) present

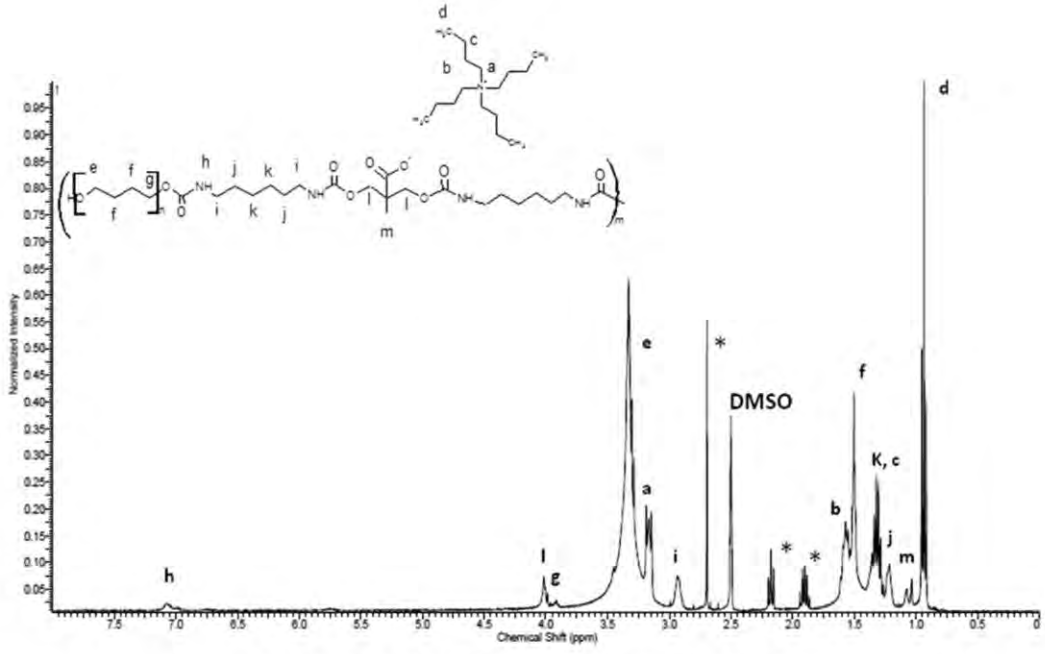

Fig. 3. 1H NMR spectrum for the PU-TBA. *: Residual N-methy-2-pyrrolidone (NMP) solvent.

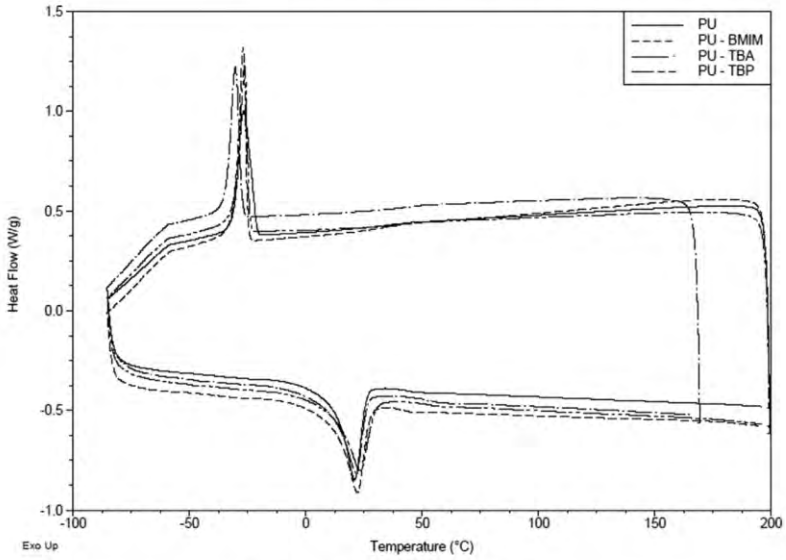

Fig. 4. DSC thermograms for PU and PILs.

Table 1
Temperature range obtained from derivative TGA curves of PU and PILs.

Sample	Degradation stage	T_{onset} (°C)	T_{endset} (°C)
PU	1	236	354
	2	354	493
PU-bmim	1	202	250
	2	250	493
PU-TBP	1	210	256
	2	256	488
PU-TBA	1	190	356
	2	356	507

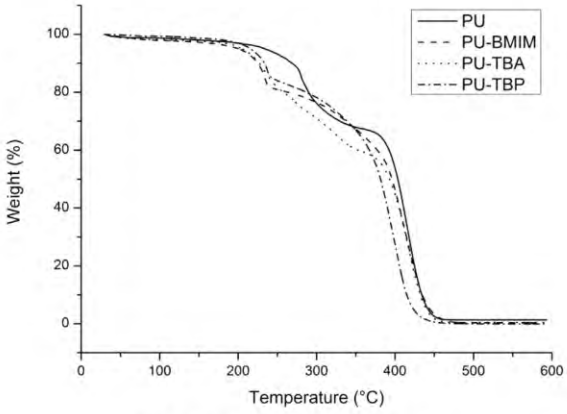

Fig. 5. TGA thermograms for PU and PILs.

some connectivity or continuity associated with them [40,51]. This behavior is probably due to the hydrogen bonding between hard/hard segments and hard/soft segments.

Upon cation addition to the polymeric chain, the morphology changes. In this case, the hard and soft segments reorganize changing their mutual miscibility resulting in an increased degree of microphase segregation. This behavior can influence mechanical properties of the materials [51].

The tensile properties of PU and the poly(ionic liquids) are presented in Fig. 8. The Young modulii are given in Fig. 9. The stress values increase with the cation addition (TBA and TBP).

The values of the Young modulus (See Fig. 9) increased in the following order: PU-bmim < PU < PU-TBA < PU-TBP. The poly(ionic liquid) with the imidazole cation presented the lower elastic modulus, probably thanks to a higher interaction of the imidazole ring with the carboxyl group. ILs PU-TBA and PU-TBP presented higher modulus of elasticity comparing with PU and PU-bmim. The changes evidenced by AFM and FTIR when the ionic compound is formed probably influence mechanical behavior of the poly(ionic liquids).

Zhang et al. [40] reported the synthesis of cationic polyurethanes containing pendant trialkylphosphonium. They evidenced that the addition of phosphonium into the polyurethanes resulted in several desirable advantages including improved microphase separation and enhanced mechanical performance compared to the non-charged polymer.

3.2. CO_2 sorption - experimental results

The results of CO_2 sorption obtained for the poly(ionic liquids) and PU are shown in Fig. 10. Also in Table 2 is presented a comparative study of CO_2 sorption of this work with different poly (ionic liquids) described in literature.

The CO_2 sorption results presented in Fig. 10 show typical physical adsorption shape curves (no chemical reaction takes place). It increases upon increasing CO_2 partial pressure [52,53]. PU presents a CO_2 sorption value of 7.4 $mgCO_2/g$ (0.82 bar) and 140 $mgCO_2/g$ (50 bar) due to the interaction between CO_2 and the polar groups (usually O, N) of the polymeric chains [18,54,55]. It can be seen in Fig. 10 that the cation plays a role in CO_2 sorption values. The CO_2 solubility was increased by the inclusion of the cation. For a pressure of 0.82 bar PU-bmim presented a CO_2 sorption of 9.4 $mgCO_2/g$, PU-TBP exhibited a value of 15.7 $mgCO_2/g$ and PU-TBA

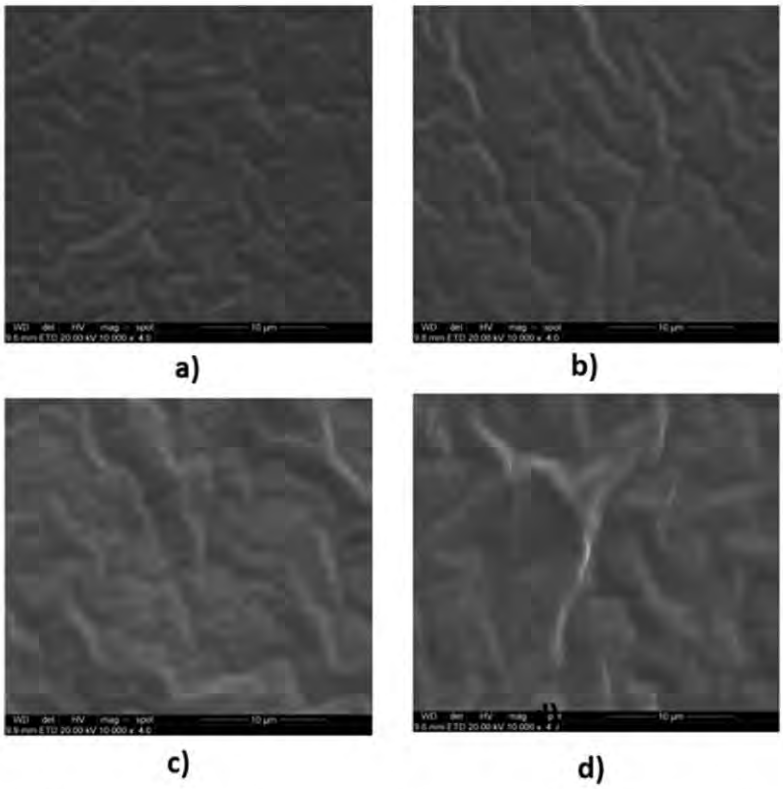

Fig. 6. Micrographs of the materials at magnification of 10000×: (A) PU, (B) PU-BMIM, (C) PU-TBP, (D) PUTBA.

a sorption capacity of 16.1 mgCO_2/g. The amounts of CO_2 sorption at 50 bar were 162 mgCO_2/g for the PU-bmim, 168 mgCO_2/g for PU-TBP and 226 mgCO_2/g for PU-TBA.

In order to examine the reusability of PILs, PU-TBA was subjected to five additional runs. The sorption was carried out at 303.15 K under 1 MPa CO_2 pressure. After each step, the CO_2 desorption was carried out under vacuum at 298.15 K for 6 h. The results for the six consecutive tests are shown in Fig. 11.

The CO_2 sorption capacity was slightly increased in the first three recycles, probably due to impurities withdrawal remaining constant for the next cycles. These results indicate that the PU-TBA has high stability and capacity of being reused. In order to obtain performance data for our PU-TBA and PU-TBP, the CO_2 sorption capacity was compared with other PILs described in literature (Table 2).

The CO_2 sorption values showed that the CO_2 uptake capacity of the PILs reported in literature are lower, as compared to PU-TAB and PU-TBP. This behavior is probably related with the weakest possible cation-anion coordination achieved by TBA and TBP, as described in Section 3.3. The results suggest that the novel anionic polyurethane using tetraalkylammonium and tetrabutylphosphonium as cations presents significant potential for carbon dioxide capture.

3.3. CO_2 sorption – simulation results

Simulations were conducted to understand the varying performance of the polymeric anion with the bmim, TBA, and TBP cations. Two reasons can be responsible for this. First, certain cations, e.g. the imidazolium-based ones, capture CO_2 with a reasonable efficacy. The electron deficient hydrogen atom located at the C-2 position is known to form a relatively weak hydrogen bond with the oxygen atom of CO_2. Second, the cation may play an adverse role provided that it blocks an active site in the anion and does not introduce alternative CO_2 binding sites. PCFs derived for selected atom pairs (Fig. 12) indicate a clear hydrogen bond, with a length $L_{PM7\text{-}MD} = 2.1$ Å, between the hydrogen atom of the imidazole ring and the oxygen atom of the carboxyl group. This predicted hydrogen bond from molecular dynamics appears in excellent agreement with the result of the structure optimization employing hybrid DFT (B3LYP), $L_{DFT} = 2.0$ Å. A small discrepancy, $\Delta L = L_{PM7\text{-}MD} - L_{DFT} = +0.1$ Å, can be fully explained by thermal expansion of the system upon heating up to 300 K. No distance correlations were found for the ester and imide groups (Fig. 12a). Therefore, the bmim cation blocks an important CO_2 binding site (the deprotonated carboxyl group, COO-) and decreases an overall performance of the compound, as follows from the experiment. In turn, neither TBA nor TBP exhibit such a behavior. The corresponding peaks, N–carboxyl and P–carboxyl, is fuzzy significantly in the range 3–4 Å. Importantly, all cations coordinate the carboxyl group of the polymeric anion, whereas other polar sites of the anion are largely ignored by all investigated cations. The heights of the PCFs corresponding to phosphorus of TBP are somewhat smaller as compared to the same heights in the case of TBA. This is due to a larger diameter of the phosphorus atom and, consequently, a smaller electron density on this atom.

The CO_2 capturing performance of [TBA][anion], mg/g, is better than that of [TBP][anion], since the mass of nitrogen (14 a.m.u) is over two times smaller than the mass of phosphorus (31 a.m.u). Our

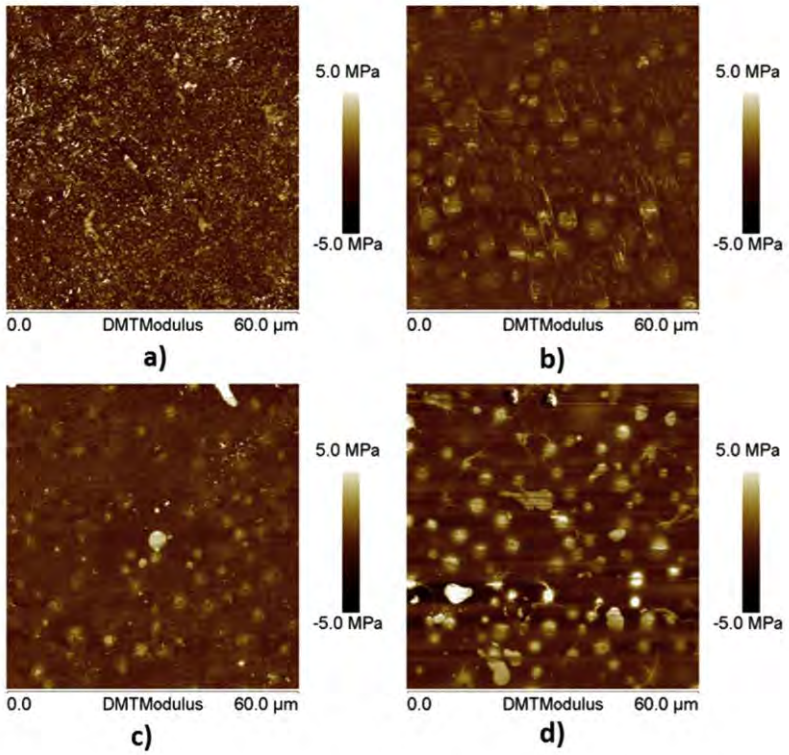

Fig. 7. DMT Modulus maps obtained by AFM images: (A) PU, (B) PU-bmim, (C) PU-TBP, (D) PU-TBA.

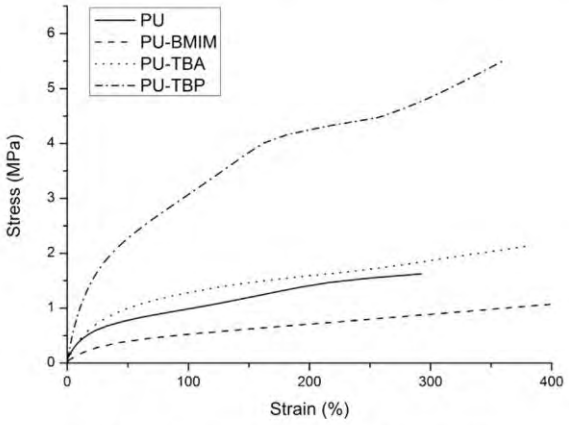

Fig. 8. Stress/Strain curves of pure PU and poly(ionic liquids).

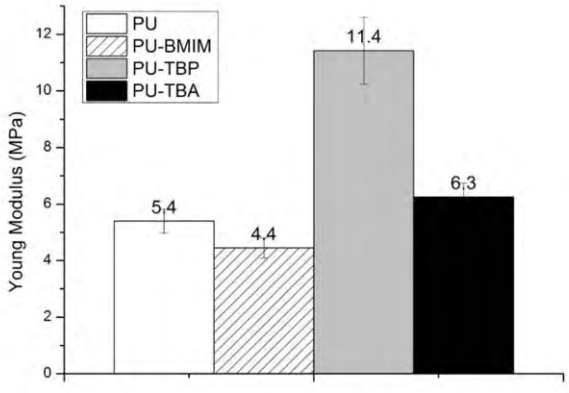

Fig. 9. Young modulus of pure PU and poly(ionic liquids).

investigation reveals that a successful compound for gas capture must exhibit the weakest possible cation-anion coordination and smaller molecular masses [56].

4. Conclusions

This study reveals experimentally and by simulation a new and simple concept for low-cost sorbents design. A successful compound for gas capture must exhibit the weakest possible cation-anion coordination and smaller molecular masses. The mechanical properties are influenced by cation insertion. The values of the Young modulus increased in the order PU-bmim < PU < PU-TBA < PU-TBP. The highest CO_2 sorption values were obtained for the anionic polyurethanes using tetrabutylammonium and tetrabutylphosphonium as cations. These new compounds show improved CO_2 sorption capacity, as compared to other PIL reported in the literature presenting significant potential for carbon dioxide capture.

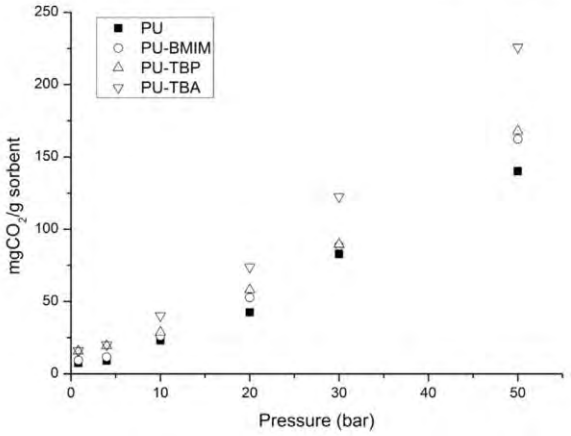

Fig. 10. Pure PU and poly(ionic liquids) sorption values at 303.15 °C.

Table 2
Comparison of PU-TBA and PU-TBP with different poly(ionic liquids) in terms of CO_2 sorption.

PIL	CO_2 sorption (mg/g)	Conditions (P, T)	Ref.
[PVBIT][a]	3.05	0.79 bar, 295.15 K	[7]
[PVBIH][b]	3.22	0.79 bar, 295.15 K	[7]
P([AMIM]BF_4-AN)[c]	14.30	1 bar, 273.15 K	[17]
P6 [BIEMA][Br][d]	3.34	1 bar, 278.15 K	[11]
P6 [BIEMA][acetate][e]	12.46	1 bar, 278.15 K	[11]
P[VBTEA][PF_6][f]	14.04	1 bar, 278.15 K	[5]
PU-TBP	15.70	0.82 bar, 303.15 K	This study
PU-TAB	16.10	0.82 bar, 303.15 K	This study

[a] Poly[1-(4-vinylbenzyl)-3-butylimidazolium tetrafluoroborate].
[b] Poly[(1-(4-vinylbenzyl)- 3-butylimidazolium hexafluorophosphate].
[c] Poly(ionic liquid)s based on the copolymer of 1-allyl-3-methylimidazolium tetrafluoroborate and acrylonitrile.
[d] Poly[2-(1-butylimidazolium-3-yl)ethyl methacrylate bromide].
[e] poly[2-(1-butylimidazolium-3-yl)ethyl methacrylate acetate].
[f] Poly(4-vinylbenzyltriethylammonium hexafluorophosfate.

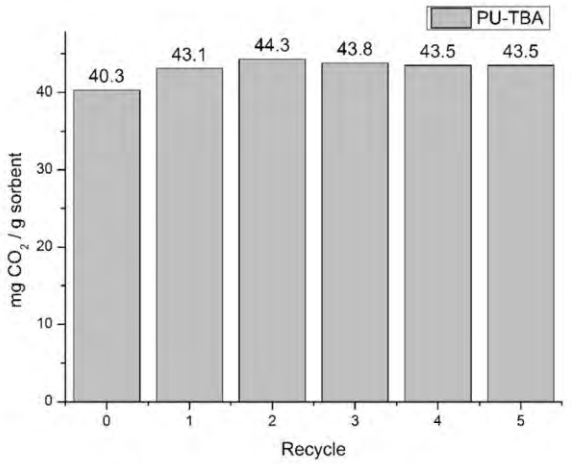

Fig. 11. CO_2 sorption/desorption tests for the PIL PU-TBA.

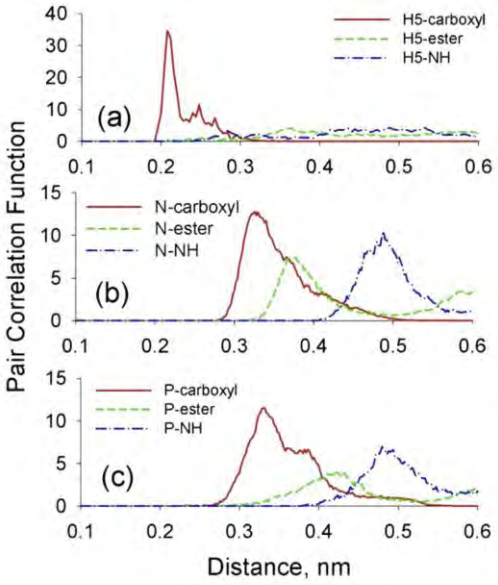

Fig. 12. Pair correlation functions for selected inter-molecular distances (see legends) in (a) [bmim][anion]; (b) [TBA][anion]; (c) [TBP][anion]. "H5" is an intrinsically acidic hydrogen atom of the imidazole ring; "P" and "N" are the central atoms of the TBA and TBP cations, respectively; "carboxyl" corresponds to the oxygen atoms of the negatively charged moiety of the polymeric anion (one per polymer unit); "ester" is the oxygen atoms in the –COO– group (two per polymer unit); "NH" is the nitrogen atom of the imide group (two per polymer unit).

Acknowledgments

The authors would like to thank PETROBRAS (grant number: 2014/00433-7) for financial support, Sandra Einloft and Rosane Ligabue thank CNPq for research scholarship. Franciele L. Bernard thanks Hewlett-Packard Brasil Ltda for scholarship.

"This work was achieved in cooperation with Hewlett-Packard Brasil Ltda. using incentives of Brazilian Informatics Law (Law no 8.2.48 of 1991)."

References

[1] H. Cheng, P. Wang, J. Luo, J. Fransaer, D.E. de Vos, Z.H. Luo, Poly(ionic liquid)-based nanocomposites and their performance in CO_2 capture, Ind. Eng. Chem. Res. 54 (2015) 3107–3115.
[2] S. Zulfiqar, M.I. Sarwar, D. Mecerreyes, Polymeric ionic liquids for CO_2 capture and separation: potential, progress and challenges, Polym. Chem. 6 (2015) 6435–6451.
[3] T.T.N. Bachelor, P. Toochinda, Development of low-cost amine-enriched solid sorbent for CO_2 capture, Environ. Technol. 33 (2012) 2645–2651.
[4] M. Ramdin, A. Amplianitis, S. Bazhenov, A. Volkov, V. Volkov, T.J.H. Vlugt, T.W. de Loos, Solubility of CO_2 and CH_4 in ionic liquids: ideal CO_2/CH_4 selectivity, Ind. Eng. Chem. Res. 53 (2014) 15427–15435.
[5] G. Yu, Q. Li, N. Li, Z. Man, C. Pu, C. Asumana, X. Chen, Synthesis of new crosslinked porous ammonium-based poly(ionic liquid) and application in CO_2 adsorption, Polym. Eng. Sci. 54 (2014) 59–63.
[6] S. Seo, L.D. Simoni, M. Ma, M.A. DeSilva, Y. Huang, M.A. Stadtherr, J.F. Brennecke, Phase-change ionic liquids for post combustion CO_2 capture, Energy Fuels 28 (2014) 5968–5977.
[7] J. Tang, W. Sun, H. Tang, M. Rodosz, Y. Shen, Enhanced CO_2 absorption of poly(ionic liquid)s, Macromolecules 38 (2005) 2037–2039.
[8] J. Yuan, D. Mecerreyes, M. Antonietti, Poly(ionic liquid)s: an update, Prog. Polym. Sci. 38 (2013) 1009–1036.
[9] F.L. Bernard, D.M. Rodrigues, B.B. Polesso, A.J. Donato, M. Seferin, V.V. Chaban, F. Dalla Vecchia, S. Einloft, New cellulose based ionic compounds as low-cost sorbents for CO_2 capture, Fuel Process. Technol. 149 (2016) 131–138.
[10] J. Yuan, M. Antonietti, Poly(ionic liquid)s: polymers expanding classical property profiles, Polymer 52 (2011) 1469–1482.

[11] E.I. Privalova, E. Karjalainen, M. Nurmi, P. Maki-Arvela, K. Eränen, H. Tenhu, D.Y. Murzin, J.P. Mikkola, Imidazolium-based poly(ionic liquid)s as new alternatives for CO_2 capture, Chem. Sus Chem. 6 (2013) 1500–1509.

[12] R. Sood, M.M. Obadia, B.P. Mudraboyina, B. Zhang, A. Serghei, J. Bernard, E. Drockenmuller, 1,2,3-Triazolium-based poly(acrylate ionic liquid)s, Polymer 55 (2014) 3314–3319.

[13] C. Liu, S. Wang, H. Zhou, C. Gao, W. Zhang, Thermoresponsive poly(ionic liquid): controllable RAFT synthesis, thermoresponse, and application in dispersion RAFT polymerization, J. Polym. Sci. Part A Polym. Chem. 64 (2015) 846–864.

[14] J. Tang, H. Tang, W. Sun, H. Plancher, M. Radosz, Y. Shen, Poly(ionic liquid)s: a new material with enhanced and fast CO_2 absorption, Chem. Commun. 54 (2005) 3325–3327.

[15] J. Tang, H. Tang, W. Sun, M. Radosz, Y. Shen, Poly(ionic liquid)s as New Materials for CO_2. absorption, J. Polym. Sci. Part A Polym. Chem. 43 (2005) 5477–5489.

[16] J. Tang, Y. Shen, M. Radosz, W. Sun, Isothermal carbon dioxide sorption in poly (ionic liquid) s, Ind. Eng. Chem. Res. 48 (2009) 9113–9118.

[17] J.M. Zhu, K.G. He, H. Zhang, F. Xin, Effect of swelling on carbon dioxide adsorption by poly(ionic liquid)s, Adsorpt. Sci. Technol. 30 (2012) 35–41.

[18] T.O. Magalhães, A.S. Aquino, F. Dalla Vecchia, F.L. Bernard, M. Seferin, S.C. Menezes, R. Ligabue, S. Einloft, Syntheses and characterization of new poly(ionic liquid)s designed for CO_2 capture, RSC Adv. 4 (2014) 18164–18170.

[19] C.H. Yu, C.H. Huang, C.S. Tan, A review of CO_2 capture by absorption and adsorption, Aerosol Air Qual. Res. 12 (2012) 745–769.

[20] J. Tang, H. Tang, W. Sun, M. Radosz, Y. Shen, Low-pressure CO_2 sorption in ammonium-based poly(ionic liquid)s, Polymer 46 (2005) 12460–12467.

[21] T. Welton, Room temperature ionic liquids – solvents for synthesis and catalysis, Chem. Rev. 99 (1999) 2071–2083.

[22] N. Jain, A. Kumar, S. Chauhan, S.M.S. Chauhan, Chemical and biochemical transformations in ionic liquids, Tetrahedron 61 (2005) 1015–1060.

[23] P. Wasserscheid, T. Welton (Eds.), Ionic Liquids in Synthesis, WILEY-VCH, Weinheim, 2008 ch.1.

[24] A. Blasig, J. Tang, X. Hu, Y. Shen, M. Radosz, Magnetic suspension balance study of carbon dioxide solubility in ammonium-based polymerized ionic liquids: poly(p-vinylbenzyltrimethyl ammonium tetrafluoroborate) and poly([2-(methacryloyloxy)ethyl] trimethyl ammonium tetrafluoroborate), Fluid Phase Equilib. 256 (2007) 75–80.

[25] F. Dreisbach, H.W. Lösch, Magnetic suspension balance for simultaneous measurement of a sample and the density of the measuring fluid, J. Therm. Anal. Cal. 62 (2000) 515–521.

[26] J.J.P. Stewart, Optimization of parameters for semiempirical methods VI: more modifications to the NDDO approximations and re-optimization of parameters, J. Mol. Model 19 (2013) 1–32.

[27] J.J.P. Stewart, Optimization of parameters for semiempirical methods V: modification of NDDO approximations and application to 70 elements, J. Mol. Model 13 (2007) 1173–1213.

[28] T. Clark, J.J.P. Stewart, MNDO-like semiempirical molecular orbital theory and its application to large systems, Comput. Methods Large Syst. Electron. Struct. Approaches Biotechnol. Nanotechnol. (2011) 259–286.

[29] A.S. Aquino, F.L. Bernard, J.V. Borges, L. Mafra, F. Dalla Vecchia, M.O. Vieira, R. Ligabue, M. Seferin, V.V. Chaban, E.J. Cabrita, S. Einloft, Rationalizing the role of the anion in CO_2 capture and conversion using imidazolium-based ionic liquid modified mesoporous silica, RSC Adv. 5 (2015) 64220–64227.

[30] V. Chaban, Hydrogen fluoride capture by imidazolium acetate ionic liquid, Chem. Phys. Lett. 625 (2015) 110–115.

[31] V. Chaban, The thiocyanate anion is a primary driver of carbon dioxide capture by ionic liquids, Chem. Phys. Lett. 618 (2015) 89–93.

[32] H.C. Andersen, Molecular dynamics simulations at constant pressure and/or temperature, J. Chem. Phys. 72 (1980) 2384–2393.

[33] A.D. Becke, Density-functional exchange-energy approximation with correct asymptotic-behavior, Phys. Rev. A 38 (1988) 3098–3100.

[34] C.T. Lee, W.T. Yang, R.G. Parr, Development of the colle-salvetti correlation-energy formula into a functional of the electron-density, Phys. Rev. B 37 (1988) 785–789.

[35] M.W. Schmidt, K.K. Baldridge, J.A. Boatz, S.T. Elbert, M.S. Gordon, J.H. Jensen, S. Koseki, N. Matsunaga, K.A. Nguyen, S. Su, T.L. Wundus, M. Dupuis, J.A. Montgomery Jr., General atomic and molecular electronic structure system, J. Comb. Chem. 14 (1993) 1347–1363.

[36] L. Martinez, R. Andrade, E.G. Birgin, J.M. Martinez, PACKMOL: a package for building initial configurations for molecular dynamics simulations, J. Comput. Chem. 30 (2009) 2157–2164.

[37] W. Humphrey, A. Dalke, K. Schulten, VMD: visual molecular dynamics, J. Mol. Graph. 14 (1996) 33–38.

[38] S.A. Chen, J.S. Hsu, Effects of emulsification on properties of quaternary ammonium ion-based polyurethane anionomer, Polym. Bull. 26 (1991) 429–436.

[39] M.M. Coleman, K.H. Lee, D.J. Skrovanek, P.C. Painter, Hydrogen bonding in polymers. 4. Infrared temperature studies of a simple polyurethane, Macromolecules 19 (1986) 2149–2157.

[40] M. Zhang, S.T. Hemp, M. Zhang, M.H. Allen Jr., R.N. Carmean, R.B. Moore, T.E. Long, Water-dispersible cationic polyurethanes containing pendant trialkylphosphoniums, Polym. Chem. 5 (2014) 3795–3803.

[41] S.A. Chen, J.S. Hsu, Polyurethane anionorners.I. Structure—property relationships, Polym 34 (1993) 2769–2775.

[42] T.C. Wen, Y.J. Wang, T.T. Cheng, C.H. Yang, The effect of DMPA units on ionic conductivity of PEG–DMPA–IPDI waterborne polyurethane as single-ion electrolytes, Polymer 40 (1999) 3979–3988.

[43] M.F. Rojas, F.L. Bernard, A. Aquino, J. Borges, F. Dalla Vecchia, S. Menezes, R. Ligabue, S. Einloft, Poly(ionic liquid)s as efficient catalyst in transformation of CO_2 to cyclic carbonate, J. Mol. Catal. A Chem. 392 (2014) 83–88.

[44] H.T. Lee, S.Y. Wu, R.J. Jeng, Effects of sulfonated polyol on the properties of the resultant aqueous polyurethane dispersions, Colloids Surf. A Physicochem. Eng. Asp. 276 (2006) 176–185.

[45] P. Król, Synthesis methods, chemical structures and phase structures of linear polyurethanes. Properties and applications of linear polyurethanes in polyurethane elastomers, copolymers and ionomers, Prog. Mater. Sci. 52 (2007) 915–1015.

[46] K. Kojio, S. Nakashima, M. Furukawa, Microphase-separated structure and mechanical properties of norbornane diisocyanate-based polyurethanes, Polymer 48 (2007) 997–1004.

[47] Z.S. Petrovic, Z. Zavargo, J.H. Flyn, W.J. Macknight, Thermal degradation of segmented polyurethanes, J. Appl. Polym. Sci. 51 (1994) 1087–1095.

[48] M. Barikani, N. Fazeli, M. Barikani, Study on thermal properties of polyurethane-urea elastomers prepared with different dianiline chain extenders, J. Polym. Eng. 33 (2013) 87–94.

[49] S. Pashaei, Siddaramaiah, A.A. Syed, Thermal degradation kinetics of polyurethane/organically modified montmorillonite clay nanocomposites by TGA, J. Macromol. Sci. A Pure Appl. Chem. 47 (2010) 777–783.

[50] Y. Hao, J. Peng, S. Hu, J. Li, M. Zhai, Thermal decomposition of allyl-imidazolium-based ionic liquid studied by TGA–MS analysis and DFT calculations, Thermochem. Acta 501 (2010) 78–83.

[51] R. Gao, M. Zhang, S. Wang, R.B. Moore, R.H. Colby, T.E. Long, Polyurethanes containing an imidazolium diol-based ionic-liquid chain extender for incorporation of ionic-liquid electrolytes, Macromol. Chem. Phys. 214 (2013) 1027–1036.

[52] A. Ahmady, M. Ali Hashim, M.K. Aroua, Absorption of carbon dioxide in the aqueous mixtures of methyldiethanolamine with three types of imidazolium-based ionic liquids, Fluid Phase Equilib. 309 (2011) 76–82.

[53] F.L. Bernard, F. Dalla Vecchia, M.F. Rojas, R. Ligabue, M.O. Vieira, E.M. Costa, Vitaly V. Chaban, S. Einloft, Anticorrosion protection by Amine–Ionic liquid mixtures: experiments and simulations, J. Chem. Eng. Data 61 (2016) 1803–1810.

[54] D.L. Tomasko, H. Li, D. Liu, X. Han, M.J. Wingert, L.J. Lee, K.W. Koelling, A review of CO_2 applications in the processing of polymers, Ind. Eng. Chem. Res. 42 (2003) 6431–6456.

[55] A.A. Gabrienko, A.V. Ewing, A.M. Chibiryaev, A.M. Agafontsev, K.A. Dubkov, S.G. Kazarian, New insights into the mechanism of interaction between CO_2 and polymers from thermodynamic parameters obtained by in situ ATR-FTIR spectroscopy, Phys. Chem. Chem. Phys. 18 (2016) 6465–6475.

[56] Csiro Advanced Coal Technology, Development of novel ionic liquids to capture CO_2. http://www.anlecrd.com.au/Default.aspx?SiteSearchID=995&ID=/search-results, 2012 (accessed 19.08.16).

4.2. Capítulo II: Poli(líquidos iônicos) aniônicos base poliuretano-imida

A síntese e caracterização de PLIs aniônicos base PU-imida são descritas neste capítulo, por meio do artigo intitulado *"Hybrid alkoxysilane-functionalized urethane-imide-based poly(ionic liquids) as a new platform for carbon dioxide capture*", submetido ao "Energy & Fuels" (comprovante de submissão Anexo A).Neste trabalho, foi investigado o efeito da concentração do grupo silano e do contra-cátion (imidazólio, fosfônio, amônio e pirrolidinio) sobre as propriedades térmicas, mecânicas morfológicas e capacidade de sorção de CO_2 dos PLIs base PU-imida. Os materiais obtidos foram caracterizados por FTIR, RMN, DSC, TGA, DMA e AFM. A capacidade de sorção e reuso no processo de captura foi determinada usando uma célula de decaimento de pressão na temperatura de 303,15°C e pressões de 0,8 e 10 bar. Também foram utilizados estudos de simulação para avaliar a interação entre o CO_2 os grupos funcionais presentes na estrutura dos PLIs. Os valores de sorção de CO_2 e estudos de simulação demostraram que o cátion tem um efeito importante sobre a afinidade pelo CO_2, enquanto que a concentração de silano não exerce impacto significativo. Estudos de simulação mostraram que o principal sítio de interação com o CO_2 é o COO^-, assim o uso de contra-cations que coordenem fracamente este sítio favorecem a sorção de CO_2. O PLI que demostrou boas propriedades térmicas, mecânicas e melhor desempenho de sorção foi o HPLI-02-TBA (33,1mg/g a 303,15 K e 0,82 bar). Este PLI exibiu elevada propriedade mecânica e alta capacidade de sorção de CO_2, quando comparado com PLIs base PU.

Hybrid alkoxysilane-functionalized urethane-imide-based poly(ionic liquids) as a new platform for carbon dioxide capture

Franciele L. Bernard[a,b], Barbara B. Polesso[c], Fabiana W. Cobalchini[c], Vitaly V. Chaban[d], Jailton F. do Nascimento[e], Felipe Dalla Vecchia[c] and Sandra Einloft [a,b*]

a) Post-Graduation Program in Materials Engineering and Technology. Pontifical Catholic University of Rio Grande do Sul – PUCRS.
b) School of Chemistry. Pontifical Catholic University of Rio Grande do Sul – PUCRS.
c) School of Engineering, Pontifical Catholic University of Rio Grande do Sul – PUCRS. Av. Ipiranga, 6681, Partenon, Porto Alegre Brazil, CEP: 90619-900.
d) Institute of Science and Technology (ICT), Federal University of São Paulo (UNIFESP); São José dos Campos, SP – Brazil.
e) Petrobras / CENPES. Ilha do Fundão Qd. 07; Rio de Janeiro – RJ, Brasil.
** Corresponding author: einloft@pucrs.br*

Graphical Abstract

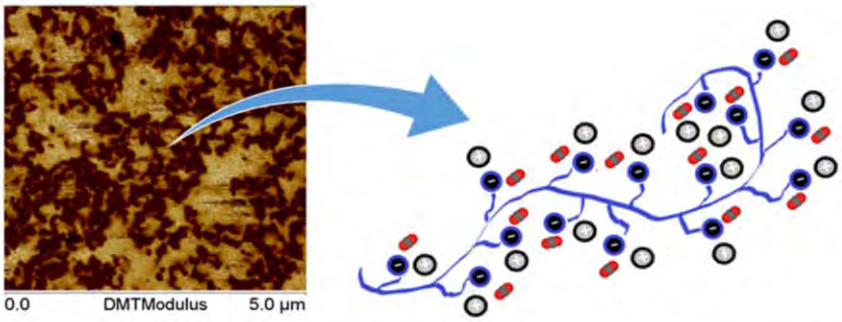

Abstract. Development of new and improvement of the existing materials for carbon dioxide (CO_2) capture is an urgent and significant goal for emission reduction. We hereby report synthesis of hybrid urethane-imide-based poly-ILs (HPILs) and their CO_2 capture capacities. The synthesized HPILs were characterized by FTIR, NMR, DSC, TGA, DMTA, AFM. CO_2 physisorption and reusability were assessed by the pressure-decay technique at a few conditions. Density functional theory calculations were used to identify binding energies between CO_2 and each center of HPILs. Cations of HPILs play an important role in CO_2 physisorption. The impact of the silane content was found to be relatively insignificant. Weakly coordinating cations foster better CO_2 sorption. The best performances were obtained for the tetrabutylammonium-based HPILs (33.1mg/g in HPIL-02-TBA and 31.7 mg/g in HPIL-06-TBA at 303.15 K and 0.82 bar). HPIL-02-TBA possesses the highest CO_2 sorption capacity out of all reported poly(ionic liquids) thus far and exhibits interesting thermal stability and competitive mechanical properties.

Keywords: poly ionic liquids, poly(urethane-imide)-based, hybrid, anionic, carbon dioxide; capture

1. Introduction

Fossil fuel burning is, allegedly, the largest human contribution to climate change due to heavy emissions of carbon dioxide (CO_2) [1–3]. Reduction of CO_2 emissions is necessary to mitigate global warming and unpredictable climate changes [2,4–6]. Carbon capture and storage (CCS) is an effective short-term solution to control CO_2 emissions from the industrial energy sources [2,5]. In this context, development of new, more efficient sorbents for CO_2 capture has become a major research focus in this field [4].

Room temperature ionic liquids (RTILs) are formally created by combining an organic cation and inorganic/organic anion. RTILs possess melting points below 100°C [5,7–9]. RTILs have been described as solvents to remove CO_2 from the flue gas [10–15]. Many RTILs exhibit unique physicochemical properties, including negligible vapor pressure, low flammability, high thermal stability, etc [16]. Physicochemical properties of RTILs can be finely tuned by combining hundreds of cations with hundreds of anions. Most RTILs are miscible with one another thanks to the prevailing electrostatic attraction between any cation and any anion. High viscosity and relatively low CO_2 sorption/desorption rates [15–18] are seen as drawbacks of RTILs. Recent success in polymerized RTILs (PILs) [16,17,19] motivates development of improved CO_2 sorbents.

PILs represent an emerging class of the polyelectrolyte species consisting of the RTIL monomers [4,5,19–22]. These polymers constitute a new, more versatile platform giving rise to a variety of high-performance sorbents [4,5,14–17,19,20,23]. PILs combine useful features of RTILs, e.g. tenability [5,19,20], with mechanical stability, processability, and adjustable macromolecular design of polymers [5,14,19,20,22,24]. CO_2 sorption and desorption in PILs are completely reversible and occur more quickly than in conventional RTILs [25,26]. PILs synthesis is conducted via two general procedures. The first one is a direct polymerization of the RTIL monomers [5]. In turn, the second one involves condensation reactions and/or polymer modification [5,22]. Polycondensation and modification of the existing polymers is more attractive because it utilizes commercially available

polymers of high molecular weight [22,27]. A few successful PILs for CO_2 capture were synthesized by this procedure: polyurethane (PU) [28–31], polybenzimidazoles [27,32], Cellulosic [33] and polyimides [22]. Multiple factors affect CO_2 solubility in PILs, e.g. ion structure, alkyl chain length, molecular weight, electron density distribution, moisture and polymeric macrostructure [4,5].

We have recently reported synthesis of cationic and anionic PU-based PILs introducing different cations imidazolium, phosphonium, and ammonium families [28–30]. Highest CO_2 sorption capacity was attained for anionic polyurethane using tetrabutylammonium (16.1 mgCO_2/g at 0.82 bar and 303.15K) as cation. This compound exhibited weak cation-anion coordination. These new compounds exhibit superior CO_2 sorption, as compared to other PILs. For example, PIL based on the copolymer of 1-allyl-3-methylimidazolium tetrafluoroborate and acrylonitrile presented a sorption value of 14.30 mgCO_2/g at 1 bar and 278.15K [16].

Development of organic-inorganic PILs was exemplified by Cheng et al. by immobilization of (p-vinylbenzyl)-triemethylammonium tetrafluoroborate and (p-vinylbenzyl)-triethylammonium hexafluorophosphate onto a mesoporous silica by surface-initiated atom-transfer radical polymerization[6].

In this work, several new hybrid anionic poly(urethane-imide)-based poly(ionic liquids) were obtained by condensation polymerization. Imide and silane groups were added to polyurethane chain in order to obtain HPILs with improved mechanical properties and sorption capacity. The following organic cations were used: imidazolium, ammonium, phosphonium, pyrrolidinium. We, furthermore, evaluate the impact of silane content on the polymeric properties and CO_2 sorption performance.

2. Experimental

2.1 Materials

Poly(tetramethylene ether) glycol (PTMG, M_n=2000 g/mol, Sigma-Aldrich), hexamethylene diisocyanate (HDI, 99%, Merck), dimethylol propionic acid (DMPA, 99%, Perstorp), 4,4'-oxydiphthalic anhydride (ODPA, 97%, Sigma Aldrich), 3-aminopropyltrimethoxysilane (APS, 97%, Sigma Aldrich) dibutyl tin dilaurate (DBTDL, Miracemanuodex), N-methyl-2-pyrrolidone (NMP, 99.92%, Neon), methylethylketone (MEK, 99%, Mallinckrodt), tetrahydrofuran (THF, 99%, Vetec), potassium hydroxide (KOH, ≥ 85%, Sigma-Aldrich) were used as purchased. Tetrabutylammonium bromide (TBAB, 99%, Acros Organics), tetrabutylphosphonium bromide (TBPB, 98%, Sigma Aldrich), 1-butyl-1-methylpyrrolidinium chloride (BMPYRR, 99%, Sigma Aldrich) were dried under vacuum during 12 hours at 60°C. 1-butyl-3-methylimidazolium chloride (bmimCl) was synthesized as described elsewhere [34,35]. The synthesized bmimCl was characterized by Fourier-transform infrared spectroscopy (FTIR) using Perkin-Elmer spectrophotometer model Spectrum 100 FT-IR with full attenuated reflectance (ATR), and by proton nuclear magnetic resonance (1H-NMR), in Varian spectrophotometer, VNMRS 300 MHz, using DMSO-d6 as solvent and glass tubes of diameter 5 mm. 1H-NMR (300 MHz, DMSOd6, 25°C), δ (ppm): 1.01 (m, CH_3), 1.29 (m, CH_2CH_3), 1.83 (m, CH_2), 3.97 (s, CH_3), 4.25 (t, CH_2N), 7.79 (s, H_5), 7.91 (s, H_4), 9.48 (s, H_2). FTIR v (cm^{-1}): 3141 (N-H of imidazole), 3058 (C-H of imidazole), 2959 (C-H of CH_2), 2870 (C-H of CH_3), 1640 (C=N of imidazole), 1558-1453 (C=C and C-N of imidazole), 749 (Cl^-).

2.2. Synthesis of hybrid poly(ionic liquid)s

Synthesis of HPILs was performed in three steps (Fig. 1), as described elsewhere [30,36–38]. Initially, the NCO-terminated PU pre-polymer was synthesized in five-necked flask at 65°C during 70 min using excess of diisocyanate (HDI), PTMG polyol, DMPA diol and DBTDL (0.1 wt%) as catalyst in the mixture of solvents (MEK and MNP, 1:1). The NCO/OH ratio of 2 (2 HDI/ PTMG 0.3 + DMPA 0.7) was used. At the next step, diisocyanate excess was neutralized with aromatic dianhydride and alkoxysilane (ODPA + APS) according to the following procedure: ODPA

temperature during 120 min providing a hybrid PU-imide solution. The synthesized hybrid PU-imide solution was labelled as PUIS-x, where x is APS fraction. For example, PUIS-02 means (PTMG + DMPA)/HDI/(ODPA + APS) = 1/2/(0.8 + 0.2), whereas PUIS-06 means (PTMG + DMPA)/HDI/(ODPA + APS) = 1/2/(0.4 + 0.6). The third step is addition of the selected RTIL (Fig. 1). The solid content and the polymer acidity were identified by titration with KOH 0.5 M. The acid number is 114 mgKOH/g (2 mmol of RTIL/g polymer). To neutralize carboxylic acid, the system was cooled down to 40°C and RTIL (bmimCl, TBAB, TBPB, BMPYRR) was loaded into the reactor. The system was kept at 40 °C during 240 min under stirring to obtain PILs. The neutralization step occurs at molar ratio COOH/IL = 1:1. Films around 0.15 mm thick were produced by casting. The films were post-cured at 150°C during 120 min under vacuum[36].

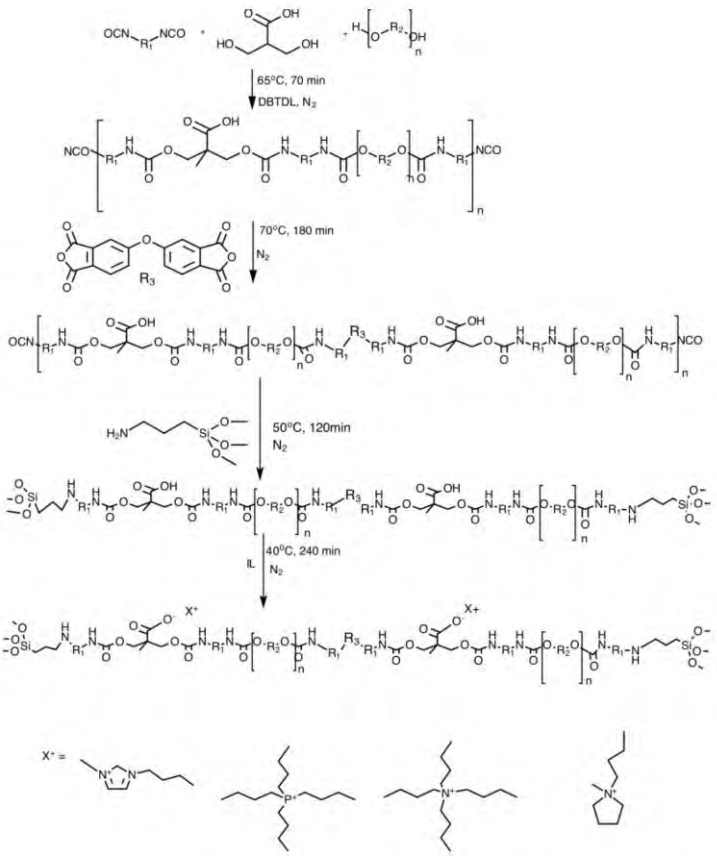

Figure 1. Synthesis steps to obtain the hybrid poly(uretane-imide)-based poly(ionic liquids).

2.3. Characterization of the hybrid poly(ionic liquids)

Structures of the products were identified by Fourier-transform infrared (FTIR) and ^{13}C-NMR spectroscopies. FTIR spectra were recorded on Perkin-Elmer Spectrum 100 spectrometer in ATR (attenuated total reflection) mode. The solid-state ^{13}C-NMR spectra were obtained using Bruker Avance DRX-400 spectrometer at 400 MHz. Differential Scanning Calorimetry (DSC) thermograms were obtained by TA Instrument Q20 differential scanning calorimeter in -90-170°C range with heating rate 10°C/min under nitrogen. Thermogravimetric analysis (TGA) was performed by TA Instrument SDT-Q600 between 25°C and 600°C at 10°C/min heating rate in nitrogen atmosphere. Tensile tests (stress × strain curves) were obtained at 25°C with rectangular-shaped films (12 × 7 × 0.15 mm) in DMTA equipment (model Q800, TA Instruments), 1 N/min. The Young modulus was determined according to ASTM D638. The analysis was conducted in triplicate. The field-emission scanning electron microscopy (FESEM) analysis was performed in FEI Inspect F50 equipment in the secondary electrons mode. The AFM analysis was performed in the peak force tapping mode by Bruker Dimension Icon PT equipped with TAP150A probe (Bruker, resonance frequency of 150 kHz and 5 N m^{-1} spring constant). The scanned area of the images was 5 × 5 μm^2 with resolution 512 frames per area. The DMT modulus map was derived from PeakForce. Average roughness (R_a), root mean square roughness (R_q), and maximum height roughness (R_{max}) were obtained from topography images (height).

2.4. Sorption measurements

The pressure-decay technique was used to determine CO_2 sorption capacity at T = 303.15 K and p_1 = 0.82 and p_2 = 10 bar. The dual-chamber gas sorption cell was similar to that of Koros et al [39]. Operation of such device was reported elsewhere [40,41]. Pressure in the sorption chamber and reservoir was measured with pressure transducer (±0.01 bar).

Samples (W_s = 1.0-1.5 g) were weighted and transferred to the sorption chamber. The system was subjected to 10^{-3} mbar vacuum at 25°C during 6 h. Afterwards, CO_2 (air liquid/99.998%) was introduced into the reservoir at specified pressure and was allowed to enter the sorption chamber, it was partially dissolved in the sample.

Gas solubility at equilibrium was determined from the difference between the initial and final number of moles of gas using Eqs. 1-2, respectively. Mass of gas dissolved in the sample is denoted as $W_{CO2/g}$

$$n_{CO_2} = \frac{p_i V gc}{Z_{(Pi,Ti)} R.T_i} - \frac{p_{eq}(Vt - V_p)}{Z_{(Peq,Teq)} R T_{eq}}, \quad (1)$$

$$w_{CO_2/g} = \frac{n_{CO_2} M}{Ws}, \quad (2)$$

where V_{gc} is volume of the gas chamber, p_i and T_i are pressure and temperature in the gas chamber, p_{eq} and T_{eq} are pressure and temperature at equilibrium. V_c is the sorption cell total volume and Z is the compressibility factor for the pure gas calculated by the Span-Wagner equations-of-state for CO_2 [42].

2.5. Computational Methodology

All binding energies and closest-approach distances were computed for the relaxed geometries. The geometry was considered relaxed when the energy difference between the two subsequent iterations in the LBGS procedure was inferior to 10^{-5} Hartree [43]. The electronic structure was obtained from hybrid density functional theory (DFT), B3LYP [44,45], using the split-valence triple-zeta polarized basis set with diffuse functions, 6-311+G*. The same basis set was employed to both relax the nuclear geometry and compute binding energy. The basis set superposition error was estimated using ghost atoms (counterpoise technique) and deducted from the reported results. Determination of each group's impact is useful for a thoughtful polymer design. Such analysis is currently available by means of computational chemistry only.

3. Results and discussion

3.2. Polymer characterization

Fig. 2 - 3 shows FTIR spectra of the hybrid PU-imide and hybrid poly(ionic liquids). No band at around 2270 cm^{-1} (N=C=O stretching vibration) indicates no free NCO group in the polymer structure [36,46].

The bands at 1780 cm^{-1} and 1707 cm^{-1} are attributed to the asymmetric and symmetric stretching vibration of C=O (imide groups), respectively. Therefore, the imide groups were successfully introduced into the PU chain [36,47,48]. The absorption band at 1625 cm^{-1} corresponds to C=O of the urethane group [47,48]. After conversion from molecular to ionic material, the bands got wider, indicating that more carbonyl groups participate in H-bonding [30]. New band at 962 cm^{-1} (O−Si−O) indicates reaction between -NCO of PU-imide and -NH_2 of APS [36]. The absorption bands at 1370 cm^{-1} are attributed to C–N stretching, while the band at 725 cm^{-1} corresponds to the imide ring deformation [36,46,47]. H-bonding was detected by FTIR (Fig. 2b - 3b). The N–H stretching band of the urethane group presents two main N–H absorption bands, one associated with non-bonded at 3440 cm^{-1} and another with bonded hydrogen at 3320 cm^{-1} [49,50]. The FTIR spectra contain a small shoulder at 3440 cm^{-1} and a dominant absorption band at 3320 cm^{-1}. This proves that the N-H groups participate in H-bonding [49,51]. The band area augmented at 3320 cm^{-1} upon coordination of the polymer chain by the cations. This observation indicates formation of additional H-bonds between the cation and the anion (Fig. 2a - 3a).

The FTIR spectra (Fig. 2 - 3) also reveal urethane-specific bands: 2936 (C-H of CH_2), 2858 (C-H of CH_3), 1550 (H-N), 1245 (C-N and C-O of urethane), 1104 (C-O-C), and 865 cm^{-1} (C-O-C) [28,30,52]. The C=O bands from the carboxylic acid group (COOH) and the urethane group (NHCO) are in overlay [51,53]. The asymmetric, 1550-1610 cm^{-1}, and symmetric, 1335-1420 cm^{-1}, stretching vibrations of COO are also present[54–56].

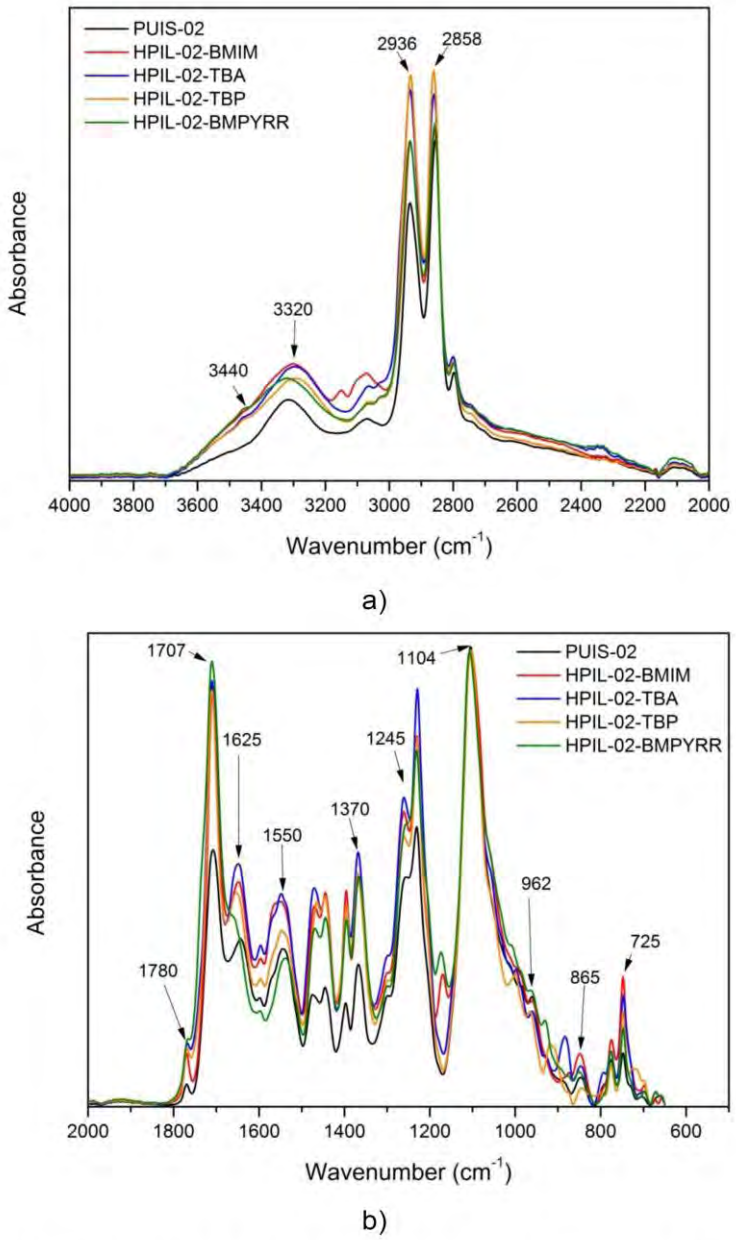

Figure 2. FTIR spectra of PUIS-02 and the corresponding HPILs; a) wavenumber from 4000 to 2000 cm^{-1} and (b) wavenumber from 2000 to 650 cm^{-1}.

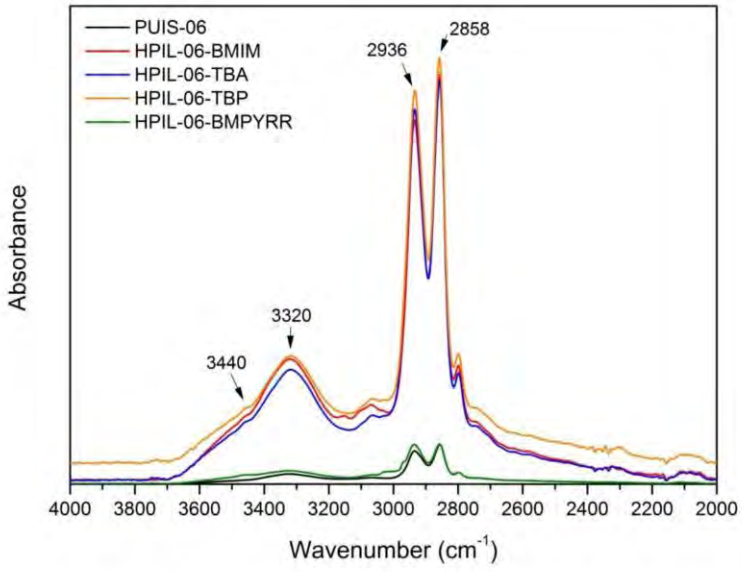

a)

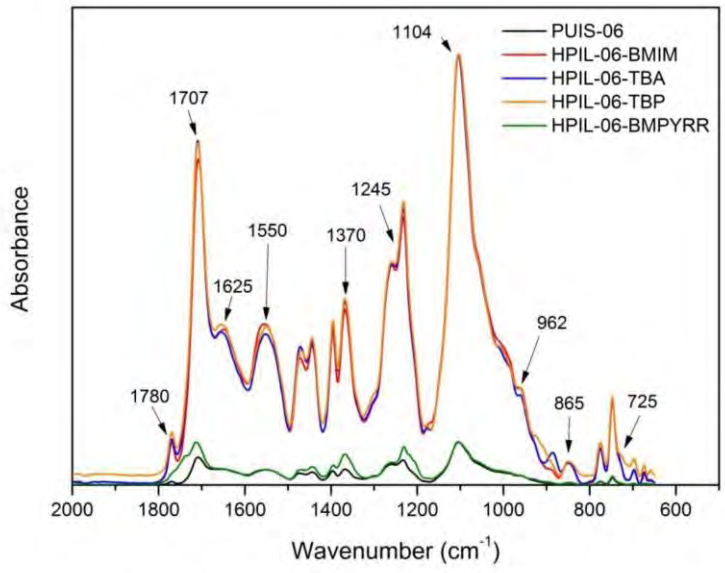

b)

Figure 3. FTIR spectra of PUIS-06 and the corresponding HPILs; a) wavenumber from 4000 to 2000 cm^{-1} and (b) wavenumber from 2000 to 650 cm^{-1}.

Typical ^{13}C-NMR spectrum of HPIL-06-TBP is shown in Fig. 4. Peaks at 167, 157, 156 ppm correspond to the carbonyl group and, thus, prove PU-imide polymer structure formation. The 167 ppm peak was assigned to

C=O of the imide groups. The 156 and 157 ppm peaks correspond to the carbonyl groups of urethane and urea, respectively [57,58]. Carbonyl groups of carboxylate of DMPA are responsible for the 175 ppm peak [58]. The aromatic carbon atoms of OPDA are revealed by a range of peaks, 120-173 ppm [59]. The 18 and 27 ppm peaks were attributed to CH_3 of DMPA and CH_2-C of PTMG, respectively [58]. The 71 ppm peak reveals CH_2 of PTMG next to the urethane bonds [58]. The 64 and 50 ppm peaks correspond to CH_2-O and C-CH_2-O of DMPA, respectively [58]. The carbon atoms of HDI linked to urethane bond, N-CH_2-CH_2-CH_2, were detected at 26, 31, and 41 ppm. Characteristic peaks of APS, -Si-CH_2-CH_2-CH_2-N, are located at 14, 24, and 41 ppm [60,61]. The 18 ppm peak corresponds to the methoxy groups of APS [61]. The TBP cation, P-CH_2-CH_2-CH_2-CH_3, provides peaks at 14, 18, 23, 24 ppm. The TBA cation, N-CH_2-CH_2-CH_2-CH_3 at 14, 18, 24, 59 ppm. Bmpyrr was detected by the following peaks: 14 (butyl-CH_3), 18 (butyl-CH_2), 21 (4-3 CH_2), 26 (butyl-CH_2), 48 (N-CH_3), 63 (N-CH_2); 64 ppm (5-2 N-CH_2) [62]. Bmim was detected by the following peaks: 14 (butyl-CH_3), 19 (butyl-CH_2), 31 (butyl-CH_2), 36 (N-CH_3), 51 (N-CH_2); 121 (C-4), 123 (C-5), 137 ppm (C-2) [63]. The peaks were assigned according to the Spectral Database for Organic Compounds[59].

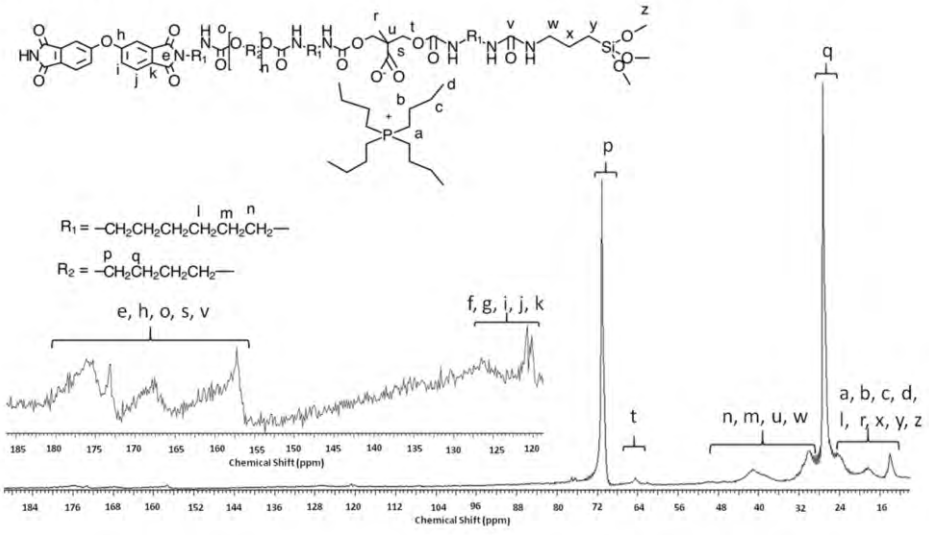

Figure 4. The solid-state ^{13}C-NMR spectra of HPUIS-06-TBP.

Surface morphologies were obtained by SEM (Fig. 5). A non-porous and relatively smooth morphology was observed in all films besides HPIL-06-TBA (Fig. 5h) and HPIL-06-BMPYRR (Fig. 5j) which present an irregular surface. This is due to cation (TBA and BMPYRR) on the polymeric chain of PUIS-06. Irregular surfaces may affect mechanical properties and, possibly, CO_2 sorption.

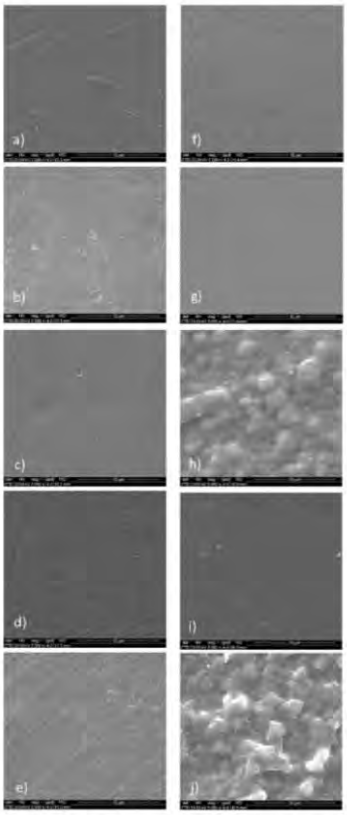

Figure 5. SEM Micrographs of the materials obtained with the 5000x magnification: (a) PUIS-02, (b) HPIL-02-BMIM, (c) HPIL-02-TBA, (d) HPIL-02-TBP, (e) HPIL-02-BMPYRR, (f) PUIS-06, (g) HPIL-06-BMIM, (h) HPIL-06-TBA, (i) HPIL-06-TBP, (j) HPIL-06-BMPYRR.

DSC thermograms for PU-imide and HPILs are shown in Fig. 6. PUIS-02, HPIL-02-BMIM, HPIL-02-BMPYRR, PUIS-06, HPIL-06-BMIM, and HPIL-06-BMPYRR provide endothermic peaks at +13.8, +7.8, -3.9, +11.3, +11.1, +8.5°C, respectively. These temperatures correspond to crystalline microphase melting (T_m) [30,64–66]. HPIL-02-TBA, HPIL-02-TBP, HPIL-

06-TBA, HPIL-06-TBP exhibit a single glass transition temperature (T_g): 11.0, 11.4, 10.4, 10.3°C, respectively. Thus, both silane and cation influence polymer chain mobility substantially. The increase of cross-linking, caused by an elevated silane content, reduces mobility of chains and limits crystallization of soft segments [67]. Reduction of T_m in HPIL-02-BMIM, HPIL-06-BMIM, HPIL-02-BMPYRR, HPIL-06-BMPYRR together with glass transitions in HPIL-02-TBA, HPIL-02-TBP, HPIL-06-TBA, HPIL-06-TBP suggest a strong interaction between the carboxyl group of the polymeric chain and the cations. This strong interaction results in the chain backbone organization. The cations containing a ring (BMIM and BMPYRR) foster crystallization of soft segments and chain backbone organization.

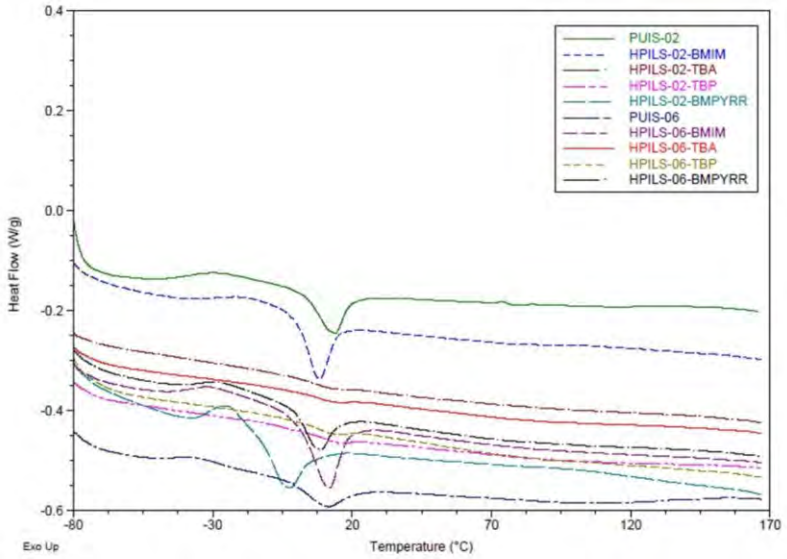

Figure 6. DSC thermograms for PUIS and hybrid poly(ionic liquids).

Thermogravimetric analysis (TGA) was performed to assess thermal stability of the synthesized materials (Table 1). All samples showed three thermal events (Fig. 7). The first event corresponds to PUIS and HPILs decomposition and occurs at about 175°C leading to around 5% mass loss. The mass loss is attributed to water evaporation, DMF, and residual low-molecular-weight monomers [57]. The second event is attributed to

urethane linkages decomposition [68]. The third event is degradation of the imide rings and the organic moiety of APS [67,68].

Degradation temperatures increase somewhat at the higher silane content. Compare 208 and 358 °C in PUIS-02 to 228 and 385°C in PUIS-06. This is due to the increase of cross-linking at higher silane content which decreases chain mobility and increases thermal stability [57,67]. Ionic PUIS-based materials are less thermally stable than their neutral precursors. The same behavior was reported in other PU-based PILs [32]. The residue consists of an inorganic content of the material [67,69]. The residue content increases as the silane content increases. Compare 14.8 wt% in PUIS-02 to 18.7 wt% in PUIS-06. The residue content decrease in the ionic materials (Table 1). To recapitulate, PUIS is stable above 200°C, whereas HPILs exhibit systematically lower thermal stabilities.

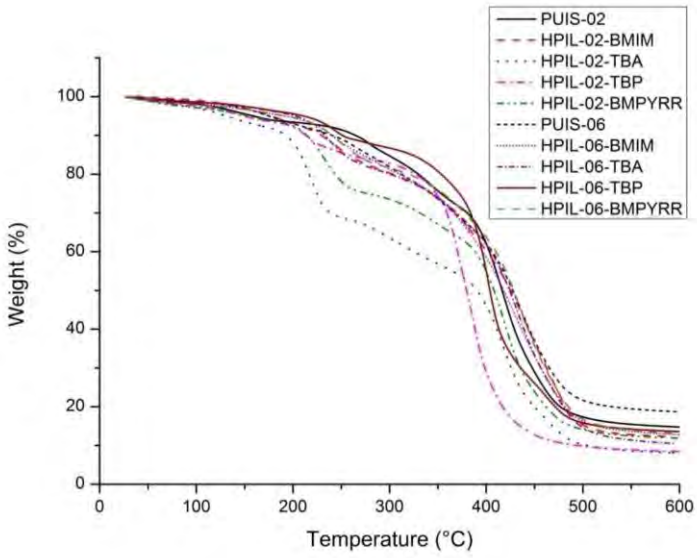

Figure 7. TGA thermograms for PUIS-02, PUIS-06 and the corresponding hybrid poly(ionic liquids).

Table 1. Results of thermal analyses of PUIS-2, PUIS-06 and the corresponding hybrid poly(ionic liquids).

Sample	Degradation stage	T_{onset} (°C)	T_{endset} (°C)	wt% remaining at 600°C
PUIS-02	*2*	208	358	
	3	358	524	14.8
HPIL-02-BMIM	*2*	194	300	
	3	300	572	12.1
HPIL-02-TBA	*2*	175	253	
	3	253	535	8.1
HPIL-02-TBP	*2*	184	268	
	3	268	522	8.5
HPIL-02-BMPYRR	*2*	178	276	11.8
	3	276	555	
PUIS-06	*2*	228	385	
	3	385	541	18.7
HPIL-06-BMIM	*2*	192	317	
	3	317	570	12.8
HPIL-06-TBA	*2*	185	289	
	3	289	580	10.4
HPIL-06-TBP	*2*	201	287	
	3	287	548	13.5
HPIL-06-BMPYRR	*2*	192	298	13.1
	3	298	573	

Surface morphology of the films was identified by atomic force microscopy (Figs. 8-9, Table 2). Surface structure changes occur with the increase of silane content and upon ionization of the material. One observes discontinuous lighter and darker regions in the images of DMT modulus. These patterns relate to microphase separation in the polymeric structure [70]. The microphase separation was observed upon silane content increase and upon the organic ionic introduction. Ionization of the materials fosters miscibility of hard and soft segments and, therefore,

improves microphase segregation [30,70]. Ionization is more important for microphase separation in the HPILs derived from PUIS-02. In turn, higher silane content influences microphase reorganization in HPILs. Height sensor images and roughness data of the surface suggest that the increase of the silane content reduces roughness of the films. Compare R_a = 37.1 in PUIS-02 to R_a = 9.71 in PUIS-06. Cross-linking improves film surface smoothness [70]. The roughness is smaller in the HPIL-02 series, as compared to their precursor, PUIS-02. The impacts of the cations show different strength: BMPYRR < BMIM < TBP < TBA. Film roughness in the HPIL-06 series is, however, larger than in PUIS-06 (Table 2).

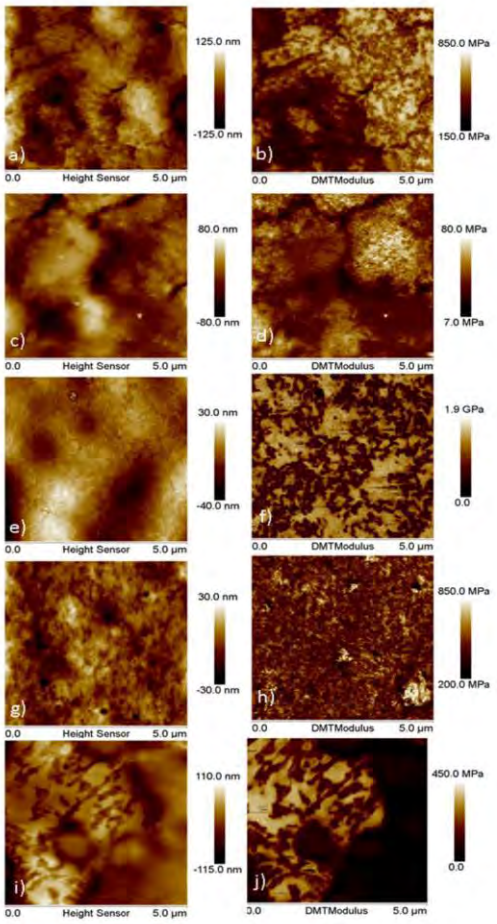

Figure 8. AFM height sensor images (left) and DMT modulus images (right): (a-b) PUIS-02, (c-d) HPIL-02-BMIM, (e-f) HPIL-02-TBA, (g-h) HPIL-02-TBP, (i-j) HPIL-02-BMPYRR.

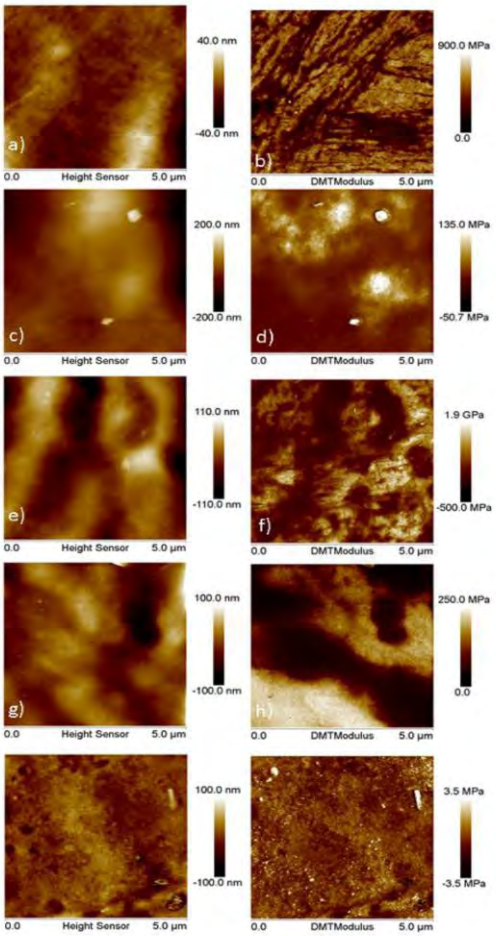

Figure 9. AFM height sensor images (left) and DMT modulus images (right): (a-b) PUIS-06, (c-d) HPIL-06-BMIM, (e-f) HPIL-06-TBA, (g-h) HPIL-06-TBP, (i-j) HPIL-06-BMPYRR.

Table 2. Average roughness (R_a); root-mean-square roughness (R_q); maximum height roughness (R_{max}) for the prepared films

Sample	R_a (nm)	R_q (nm)	R_{max} (nm)
PUIS-02	37.1	29.6	264.0
HPIL-02-BMIM	22.5	17.9	240.0
HPIL-02-TBA	10.6	8.2	92.2
HPIL-02-TBP	15.3	12.0	100.0
HPIL-02-BMPYRR	30.4	23.4	225.0
PUIS-06	9.71	7.32	74.2
HPIL-06-BMIM	34.9	19.3	498.0
HPIL-06-TBA	33.9	27.3	210.0
HPIL-06-TBP	27.2	21.2	271.0
HPIL-06-BMPYRR	55.9	44.8	521

Tensile properties and Young moduli (Figs. 10-11) indicate that higher silane content leads to larger Young moduli: 4.9 MPa in PUIS-02 and 16.8 MPa in PUIS-06. Therefore, a significant silane content is desirable to obtain competitive mechanical strengths and improve films rigidity [67,68,70]. Ionic materials exhibit better mechanical properties than their neutral precursors [30]. Furthermore, ionization significantly increases mechanical properties of HPIL-02 (56.4 MPa in HPIL-02-TBA). Ionization of PUIS-06 results in insignificant Young modulus increase, e.g. 21.8 MPa in HPIL-06-TBA.

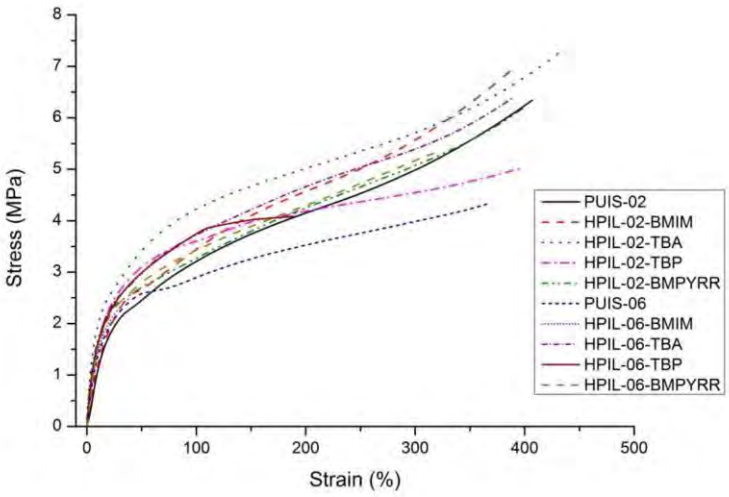

Figure 10. Stress/strain curves for the developed HPIL-based films.

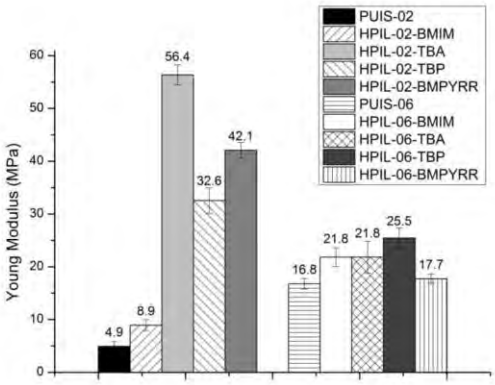

Figure 11. Young moduli for the developed HPIL-based films.

Figs. 12 describe CO_2 sorption by PUIS-02/PUIS-06 and the corresponding HPILs, whereas Table 3 compares them to the recently published results. The silane content increase in PU-imide leads to higher CO_2 sorption capacities. Compare 21.8 mg/g in PUIS-02 to 25.0 mg/g in

PUIS-06. Affinities to CO_2 of the ionized materials are even better. Ionization impact in PUIS-02 are more substantial than in PUIS-06. If cross-linking increases microvoid volume, due to a rigidity increase, this may complicate HPIL-CO_2 interactions [71].

The best CO_2 sorption values were obtained when TBA was used as a cation: 33.1 mg/g in HPIL-02-TBA and 31.7 mg/g in HPIL-06-TBA. Other cations (TBP, BMIM and BMPYRR) provide somewhat less efficient CO_2 sorption. This trend is in concordance with that observed in other PU-based PILs [30]. The electronic-structure simulations reveal that the cations exhibiting weaker coordination of the carboxyl group promote electrostatic binding of the CO_2 molecule and the carboxyl group [30].

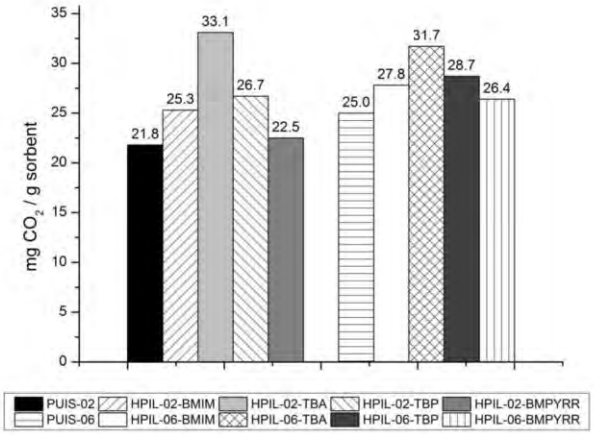

Figure 12. CO_2 sorption capacities of PUIS-2/PUIS-06 and the corresponding HPILs at 303.15 K and 0.82 bar.

Fig. 13 summarizes CO_2 sorption by PUIS-02 and the corresponding HPILs obtained at 10 bar and 303.15 K. The CO_2 sorption values are proportional to those at lower pressure. Again, the best result was recorded for the TBA containing HPILs, 61.0 mgCO_2/g.

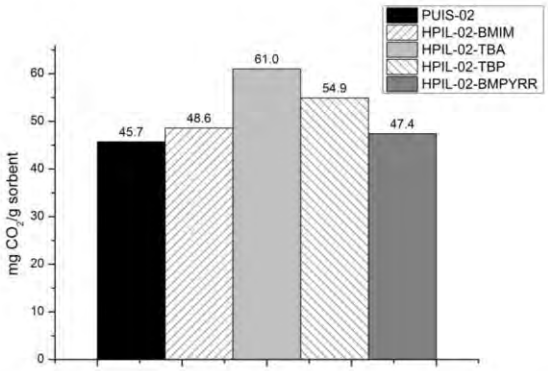

Figure 13. CO_2 sorption by the synthesized HPILs at 30°C and 10 bar.

At comparable temperatures and pressures, CO_2 sorption of developed HPILs are systematically higher (Table 3).

Table 3. Comparison of CO_2 sorption by HPIL-02-TBA with competitive poly(ionic liquids)

PIL	CO_2 sorption (mg/g)	Conditions (P, T)	Ref.
P[VBIT][BF_4][1]	3.05	0.79 bar, 295.15K	[23]
P[VBIH][PF_6][2]	3.22	0.79 bar, 295.15K	[23]
P([AMIM]BF_4-AN)[3]	14.30	1 bar, 273.15K	[16]
P6 [BIEMA][Br][4]	3.34	1 bar, 278.15K	[24]
P6 [BIEMA][acetate][5]	12.46	1 bar, 278.15K	[24]
P[VBTEA][PF_6][6]	14.04	1 bar, 278.15K	[17]
mpPIL	20.24	1 bar, 273.15 K	[21]
SiO_2-meso-([VBTMA]-[BF_4])	17.7	1 bar, 303.15K	[6]
PIL-8.1.BF_4	24.76	1bar, 273.15K	[31]
PU-TBP	15.70	0.82 bar, 303.15K	[30]
PU-TAB	16.10	0.82 bar, 303.15K	[30]
PUIS-02-TBA	33.1	0.82 bar, 303.15K	This study

[1]poly[1-(4-vinylbenzyl)-3-butylimidazolium tetrafluoroborate]; [2]poly[(1-(4-vinylbenzyl)- 3-butylimidazolium hexafluorophosphate]; [3]poly(ionic liquid)s based on the copolymer of 1-allyl-3-methylimidazolium tetrafluoroborate and acrylonitrile; [4]Poly[2-(1-butylimidazolium-3-yl)ethyl methacrylate bromide]; [5]poly[2-(1-butylimidazolium-3-yl)ethyl methacrylate acetate]; [6]poly(4-vinylbenzyltriethylammonium hexafluorophosfate.

Reusability of the developed class of HPILs was characterized by subjecting HPIL-02-TBA to six sorption/desorption cycles. CO_2 sorption was carried out at 303.15 K and 0.82 bar. CO_2 desorption was carried out under vacuum at 298.15 K during 6 hours. Sorption capacity of HPIL-02-TBA increased insignificantly (61.0 mgCO_2/g to 62.5 mgCO_2/g) over the first cycles (probably due to the removal of moisture) and remained constant over the last cycles. These results indicate that HPIL-02-TBA sorbent offers necessary stability.

3.3. Binding energies

The PU-based anion and the cations constituting the new HPILs are expected to contain a number of groups for binding CO_2. DFT calculations were used to identify the impact of those centers according to binding energies (Table 4). The most successful CO_2 capturing group is deprotonated carboxyl. Coordination of CO_2 by carboxyl brings -19 kJ mol^{-1} to the system. Since there are two carboxyl groups per polymer unit, their total impact amounts to -38 kJ mol^{-1} being noticeably higher than that of any other group. The imidazole group appeared also rather useful for CO_2 capture, -14 kJ mol^{-1}, thanks to the acidic hydrogen atom of the imidazole ring. Two bmim cations are required to compensate for a negative charge of each polymer unit. Since the CO_2 capturing experiments reveal a better performance of the TBA and TBP containing HPILs, 33.1 and 26.7 mgCO_2/g (Fig. 12), one concludes that imidazole decreases activity of carboxyl substantially, and vice versa. TBA and TBP belong to the non-coordinating cations, which do not block the carboxyl groups of the polyurethane anion. Interestingly, a somewhat poorer CO_2 affinity of TBP detected by the binding energy calculations is confirmed by the actual CO_2 capacities of the respective HPILs. In turn, the bmim and BMPYRR containing HPILs exhibit lower CO_2 capacities, 25.3 and 22.5 mg CO_2/g. Hence, these cation-anion combinations should be considered less efficient. Although the ether and amide groups perform rather modestly, the

polymer units contains a number of such groups, therefore, their integral impact per mole of polymer units appears substantial.

The TBA and TBP cations exhibit a marginal affinity to CO_2, -6.7 and -3.7 kJ mol^{-1}, respectively. In BMPYRR, the primary electron-deficient center, nitrogen, is sterically blocked by two alkyl groups, while maintaining four covalent bonds with carbon atoms in total. This structure results in a relatively modest value, -9.3 kJ mol^{-1}. Table 4 also summarizes binding energies of each polymer unit for the ease of further comparison, which is left as an exercise for an interested reader.

Table 4.Binding energies E_b and closest-approach distances r_{min} for a variety of neutral and ionic moieties participating in the CO_2 capture. Decomposition into the interacting moieties was performed according to conventional chemical logics.

Chemical Moiety	$-E_b$ (10^{-1} eV)	r_{min} (Å) (atom pair)
$-CH_2-COO^-$	1.97	2.54 (C_{CO2}-O)
$-CH_2-NH-CO-CH_2-$	0.93	2.89 (C_{CO2}-O)
$-CH_2-N(CO)_2-C_6H_3-$	0.83	2.95 (C_{CO2}-O)
$-CH_2-O-CH_2-$	1.04	2.75 (C_{CO2}-O)
$-C_6H_4-O-C_6H_4-$	0.46	3.18 (C_{CO2}-O)
$-CH_2-Si-(OCH_3)_3$	0.76	2.93 (C_{CO2}-O)
bmim	1.45	2.31 (O_{CO2}-H)
TBA	0.69	2.67 (O_{CO2}-H)
TBP	0.38	3.24 (O_{CO2}-H)
BMPYRR	0.96	2.62 (O_{CO2}-H)

Conclusions

We report new hybrid alkoxysilane-functionalized urethane-imide-based poly(ionic liquids) as a new efficient platform for CO_2 capture. The HPILs are expected to contain a number of functional groups to bind CO_2. DFT calculations were used to identify the impacts of those centers. TBA and TBP are non-coordinating cations living the polyurethane anion carboxyl groups more available. HPILs containing these cations exhibit the

highest affinities to CO_2. The best results were obtained for the TBA-based HPILs (33.1mg/g in HPIL-02-TBA and 31.7 mg/g in HPIL-06-TBA at 303.15 K and 0.82 bar). CO_2 sorption capacity of HPIL-02-TBA is the highest one from all reported poly(ionic liquids). Furthermore, the synthesized and characterized HPILs exhibit superior mechanical properties than anionic and cationic PU based PIL.

4. Acknowledgments

The authors would like to thank PETROBRAS for financial support; Sandra Einloft thanks CNPq for research scholarship. Franciele L. Bernard thanks Hewlett-Packard Brasil Ltda for scholarship. "This work was achieved in cooperation with Hewlett-Packard Brasil Ltda. using incentives of Brazilian Informatics Law (Law nº 8.2.48 of 1991)."

5. References

[1] V. Marjanović, M. Milovančević, I. Mladenović, Prediction of GDP growth rate based on carbon dioxide (CO_2) emissions, Journal of CO_2 Utilization. 16 (2016) 212–217. doi:10.1016/j.jcou.2016.07.009.

[2] J. Patricio, A. Angelis-Dimakis, A. Castillo-Castillo, Y. Kalmykova, L. Rosado, Region prioritization for the development of carbon capture and utilization technologies, Journal of CO_2 Utilization. 17 (2017) 50–59. doi:10.1016/j.jcou.2016.10.002.

[3] A. Rafiee, M. Panahi, K.R. Khalilpour, CO_2 utilization through integration of post-combustion carbon capture process with Fischer-Tropsch gas-to-liquid (GTL) processes, Journal of CO_2 Utilization. 18 (2017) 98–106. doi:10.1016/j.jcou.2017.01.016.

[4] S. Zulfiqar, M.I. Sarwar, D. Mecerreyes, Polymeric ionic liquids for CO_2 capture and separation: potential, progress and challenges, Polym. Chem. (2015) 6435–6451. doi:10.1039/C5PY00842E.

[5] L.C. Tome, I.M. Marrucho, Ionic liquid-based materials: a platform to design engineered CO_2 separation membranes, Chemical Society Reviews. 45 (2016) 2785–2824. doi:10.1039/C5CS00510H.

[6] H. Cheng, P. Wang, J. Luo, J. Fransaer, D.E. De Vos, Z.H. Luo, Poly(ionic liquid)-based nanocomposites and their performance in CO_2 capture, Industrial and Engineering Chemistry Research. 54 (2015) 3107–3115. doi:10.1021/ie505014h.

[7] J.S. Wilkes, A Short History of Ionic Liquids - From Molten Salts to Neoteric Solvents, Green Chemistry. 4 (2002) 73–80. doi:10.1039/b110838g.

[8] J.D. Figueroa, T. Fout, S. Plasynski, H. McIlvried, R.D. Srivastava, Advances in CO_2 capture technology-The U.S. Department of Energy's Carbon Sequestration Program, International Journal of Greenhouse Gas Control. 2 (2008) 9–20. doi:10.1016/S1750-5836(07)00094-1.

[9] Z. Xue, Z. Zhang, J. Han, Y. Chen, T. Mu, Carbon dioxide capture by a dual amino ionic liquid with amino-functionalized imidazolium cation and taurine anion, International Journal of Greenhouse Gas Control. 5 (2011) 628–633. doi:10.1016/j.ijggc.2011.05.014.

[10] L.A. Blanchard, Z. Gu, J.F. Brennecke, High-Pressure Phase Behavior of Ionic Liquid / CO_2 Systems, J. Phys. Chem. B. 105 (2001) 2437–2444. doi:10.1021/jp003309d.

[11] J.L. Anthony, E.J. Maginn, J.F. Brennecke, Solubilities and Thermodynamic Properties of Gases in the Ionic Liquid 1- n -Butyl-3-methylimidazolium Hexafluorophosphate, The Journal of Physical Chemistry B. 106 (2002) 7315–7320. doi:10.1021/jp020631a.

[12] C. Cadena, J.L. Anthony, J.K. Shah, T.I. Morrow, J.F. Brennecke, E.J. Maginn, Why is CO_2 so Soluble in Imidazolium-Based Ionic Liquids, Journal of the American Chemical Society. 126 (2004) 5300–5308. doi:10.1021/ja039615x.

[13] S.D. Kenarsari, D. Yang, G. Jiang, S. Zhang, J. Wang, A.G. Russell, Q. Wei, M. Fan, Review of recent advances in carbon dioxide separation and capture, RSC Advances. 3 (2013) 22739–22773. doi:10.1039/C3RA43965H.

[14] L.C. Tomé, D. Mecerreyes, C.S.R. Freire, L.P.N. Rebelo, I.M. Marrucho, Pyrrolidinium-based polymeric ionic liquid materials: New perspectives for CO_2 separation membranes, Journal of Membrane Science. 428 (2013) 260–266. doi:10.1016/j.memsci.2012.10.044.

[15] M.A. Sedghamiz, A. Rasoolzadeh, M.R. Rahimpour, The ability of artificial neural network in prediction of the acid gases solubility in different ionic liquids, Journal of CO_2 Utilization. 9 (2015) 39–47. doi:10.1016/j.jcou.2014.12.003.

[16] J.M. Zhu, K.G. He, H. Zhang, F. Xin, C. Engineering, Effect of Swelling on Carbon Dioxide Adsorption by Poly (ionic liquid) s, (2011) 35–42.

[17] G. Yu, Q. Li, N. Li, Z. Man, C. Pu, C. Asumana, X. Chen, Synthesis of New Crosslinked Porous Ammonium- Based Poly (ionic liquid) and Application in CO_2 Adsorption, Polymer Engineering and Science. (2014) 2–6. doi:10.1002/pen.

[18] F.L. Bernard, F. Dalla Vecchia, M.F. Rojas, R. Ligabue, M.O. Vieira, E.M. Costa, V. V. Chaban, S. Einloft, Anticorrosion Protection by Amine-Ionic Liquid Mixtures: Experiments and Simulations, Journal of Chemical and Engineering Data. 61 (2016) 1803–1810. doi:10.1021/acs.jced.5b00996.

[19] W. Qian, J. Texter, F. Yan, Frontiers in poly(ionic liquid)s: syntheses and applications, Chem. Soc. Rev. (2017). doi:10.1039/C6CS00620E.

[20] J. Yuan, M. Antonietti, Poly(ionic liquid)s: Polymers expanding classical property profiles, Polymer. 52 (2011) 1469–1482. doi:10.1016/j.polymer.2011.01.043.

[21] A. Wilke, J. Yuan, M. Antonietti, J. Weber, Enhanced carbon dioxide adsorption by a mesoporous poly(ionic liquid), ACS Macro Letters. 1 (2012) 1028–1031. doi:10.1021/mz3003352.

[22] A.S. Shaplov, S.M. Morozova, E.I. Lozinskaya, P.S. Vlasov, A.S.L. Gouveia, L.C. Tomé, I.M. Marrucho, Y.S. Vygodskii, Turning into poly(ionic liquid)s as a tool for polyimide modification: synthesis, characterization and CO_2 separation properties, Polym. Chem. 7 (2016) 580–591. doi:10.1039/C5PY01553G.

[23] J. Tang, W. Sun, H. Tang, M. Radosz, Y. Shen, Enhanced CO_2 absorption of poly(ionic liquid)s, Macromolecules. 38 (2005) 2037–2039. doi:10.1021/ma047574z.

[24] E.I. Privalova, E. Karjalainen, M. Nurmi, P. Mäki-arvela, K. Eränen, Imidazolium-Based Poly (ionic liquid) s as New Alternatives for CO_2 Capture, ChemSusChem. (2013) 1500–1509. doi:10.1002/cssc.201300120.

[25] J. Tang, H. Tang, W. Sun, M. Radosz, Y. Shen, Low-pressure CO_2 sorption in ammonium-based poly(ionic liquid)s, Polymer. 46 (2005) 12460–12467. doi:10.1016/j.polymer.2005.10.082.

[26] A. Blasig, J. Tang, X. Hu, Y. Shen, M. Radosz, Magnetic suspension balance study of carbon dioxide solubility in ammonium-based polymerized ionic liquids: Poly(p-vinylbenzyltrimethyl ammonium tetrafluoroborate) and

poly([2-(methacryloyloxy)ethyl] trimethyl ammonium tetrafluoroborate), Fluid Phase Equilibria. 256 (2007) 75–80. doi:10.1016/j.fluid.2007.03.007.

[27] R.S. Bhavsar, S. Kumbharkar, A.S. Rewar, U.K. Kharul, Polybenzimidazole based film forming polymeric ionic liquids: Synthesis and effects of cation-anion variation on their physical properties, Polymer Chemistry. (2014) 4083–4096. doi:10.1039/C3PY01709E.

[28] T.O. Magalhaes, A.S. Aquino, F. Dalla Vecchia, F.L. Bernard, M. Seferin, S.C. Menezes, R. Ligabue, S. Einloft, Syntheses and characterization of new poly(ionic liquid)s designed for CO_2 capture, RSC Adv. 4 (2014) 18164–18170. doi:10.1039/c4ra00071d.

[29] M. Fernández, L.Á. Carreño, F. Bernard, R. Ligabue, S. Einloft, Poly(ionic liquid)s Nanoparticles Applied in CO_2 Capture, Macromolecular Symposia. 368 (2016) 98–106. doi:10.1002/masy.201500148.

[30] F.L. Bernard, B.B. Polesso, F.W. Cobalchini, A.J. Donato, M. Seferin, R. Ligabue, V. V. Chaban, J.F. do Nascimento, F. Dalla Vecchia, S. Einloft, CO_2 capture: Tuning cation-anion interaction in urethane based poly(ionic liquids), Polymer. 102 (2016) 199–208. doi:10.1016/j.polymer.2016.08.095.

[31] S.M. Morozova, A.S. Shaplov, E.I. Lozinskaya, D. Mecerreyes, H. Sardon, S. Zulfiqar, F. Suaez-García, Y.S. Vygodskii, Ionic Polyurethanes as a New Family of Poly(ionic liquid)s for Efficient CO_2 Capture, (2017). doi:10.1021/acs.macromol.6b02812.

[32] S.C. Kumbharkar, R.S. Bhavsar, U.K. Kharul, Film forming polymeric ionic liquids (PILs) based on polybenzimidazoles for CO_2 separation, RSC Advances. 4 (2014) 4500. doi:10.1039/c3ra44632h.

[33] F.L. Bernard, D.M. Rodrigues, B.B. Polesso, A.J. Donato, M. Seferin, V. V. Chaban, F.D. Vecchia, S. Einloft, New cellulose based ionic compounds as low-cost sorbents for CO_2 capture, Fuel Processing Technology. 149 (2016) 131–138. doi:10.1016/j.fuproc.2016.04.014.

[34] T. Welton, Room-Temperature Ionic Liquids. Solvents for Synthesis and Catalysis, Chemical Reviews. 99 (1999) 2071–2084. doi:10.1021/cr980032t.

[35] N. Jain, A. Kumar, S. Chauhan, S.M.S. Chauhan, Chemical and biochemical transformations in ionic liquids, Tetrahedron. 61 (2005) 1015–1060. doi:10.1016/j.tet.2004.10.070.

[36] J. Song, G. Chen, Y. Ding, J. Shi, Y. Liu, Preparation and characterization

of epoxy resin modified with alkoxysilane- functionalized poly (urethane-imide) by the sol – gel process, (2011) 1594–1599. doi:10.1002/pi.3120.

[37] M. Lin, Y. Shu, W. Tsen, F. Chuang, Synthesis of polyurethane – imide (PU – imide) copolymers with different dianhydrides and their properties, 445 (1999) 433–445.

[38] C. Chen, M. Tsai, I. Tseng, A. Hsu, T.-C. Liu, S. Huang, Composition, thermal and tensile properties of polyurethane-urea-silica hybrids, (2013) 9729–9738. doi:10.1039/c3ra23186k.

[39] W.J. Koros, D.R. Paul, Design considerations for measurement of gas sorption in polymers by pressure decay, Journal of Polymer Science: Polymer Physics Edition. 14 (1976) 1903–1907. doi:10.1002/pol.1976.180141014.

[40] S. TAKISHIMA, K. NAKAMURA, M. SASAKI, H. MASUOKA, Dilation and solubility in carbon dioxide+poly (vinyl acetate) system at high pressures., Journal of The Japan Petroleum Institute. 33 (1990) 332–336. doi:10.1627/jpi1958.33.332.

[41] V.M. Shah, B.J. Hardy, S.A. Stern, Solubility of carbon dioxide, methane, and propane in silicone polymers: Effect of polymer side chains, Journal of Polymer Science Part B: Polymer Physics. 24 (1986) 2033–2047. doi:10.1002/polb.1986.090240910.

[42] W. Span, R; Wagner, A new EOS for CO_2 covering the fluid region from the triple point temperature to 1100K at pressures up to 800MPa.pdf, Journal of Physical and Chemical Reference Data. 25 (1996) 1509–1596. doi:10.1063/1.555991.

[43] D.F. Shanno, Conditioning of Quasi-Newton Methods for Function Minimization, Mathematics of Computation. 24 (1970) 647. doi:10.2307/2004840.

[44] A.D. Becke, Density-functional exchange-energy approximation with correct asymptotic behavior, Physical Review A. 38 (1988) 3098–3100. doi:10.1103/PhysRevA.38.3098.

[45] C. Lee, W. Yang, R.G. Parr, Development of the Colle-Salvetti correlation-energy formula into a functional of the electron density, Physical Review B. 37 (1988) 785–789. doi:10.1103/PhysRevB.37.785.

[46] H. Deligöz, T. Yalcınyuva, S. Özgümüs, A novel type of Si-containing poly(urethane-imide)s: synthesis, characterization and electrical properties, European Polymer Journal. 41 (2005) 771–781.

doi:10.1016/j.eurpolymj.2004.11.007.

[47] D. Gnanasekaran, P. Ajit Walter, A. Asha Parveen, B.S.R. Reddy, Polyhedral oligomeric silsesquioxane-based fluoroimide-containing poly(urethane-imide) hybrid membranes: Synthesis, characterization and gas-transport properties, Separation and Purification Technology. 111 (2013) 108–118. doi:10.1016/j.seppur.2013.03.035.

[48] D. Liu, S. Zeng, Q. Hu, C. Yi, Z. Xu, Synthesis and properties of highly branched poly(urethane–imide) via A2 + B3 approach, Polymer Bulletin. 64 (2010) 877–890. doi:10.1007/s00289-009-0178-0.

[49] M.M. Coleman, K.H. Lee, D.J. Skrovanek, P.C. Painter, Hydrogen bonding in polymers. 4. Infrared temperature studies of a simple polyurethane, Macromolecules. 19 (1986) 2149–2157. doi:10.1021/ma00162a008.

[50] M. Zhang, S.T. Hemp, M. Zhang, M.H. Allen, R.N. Carmean, R.B. Moore, T.E. Long, Water-dispersible cationic polyurethanes containing pendant trialkylphosphoniums, Polym. Chem. 5 (2014) 3795–3803. doi:10.1039/C3PY01779F.

[51] S.-A. Chen, J.-S. Hsu, Polyurethane anionomers. I. Structure-property relationships, Polymer. 34 (1993) 2769–2775. doi:10.1016/0032-3861(93)90119-U.

[52] H.-T. Lee, S.-Y. Wu, R.-J. Jeng, Effects of sulfonated polyol on the properties of the resultant aqueous polyurethane dispersions, Colloids and Surfaces A: Physicochemical and Engineering Aspects. 276 (2006) 176–185. doi:10.1016/j.colsurfa.2005.10.034.

[53] S.-A. Chen, J.-S. Hsu, Effects of emulsification on properties of quaternary ammonium ion-based polyurethane anionomer, Polymer Bulletin. 26 (1991) 429–436. doi:10.1007/BF00302611.

[54] M.A. Pérez-Limiñana, F. Arán-Aís, A.M. Torró-Palau, A. César Orgilés-Barceló, J. Miguel Martín-Martínez, Characterization of waterborne polyurethane adhesives containing different amounts of ionic groups, International Journal of Adhesion and Adhesives. 25 (2005) 507–517. doi:10.1016/j.ijadhadh.2005.02.002.

[55] S.M. Cakic, J. V. Stamenkovic, D.M. Djordjevic, I.S. Ristic, Synthesis and degradation profile of cast films of PPG-DMPA-IPDI aqueous polyurethane dispersions based on selective catalysts, Polymer Degradation and Stability. 94 (2009) 2015–2022. doi:10.1016/j.polymdegradstab.2009.07.015.

[56] H. Honarkar, M. Barmar, M. Barikani, Synthesis, characterization and properties of waterborne polyurethanes based on two different ionic centers, Fibers and Polymers. 16 (2015) 718–725. doi:10.1007/s12221-015-0718-1.

[57] P. Liu, Q. Zhang, L. He, Q. Xie, H. Ding, Thermal and mechanical properties of poly(urethane-imide)/epoxy/silica hybrids, Journal of Applied Polymer Science. (2010) n/a-n/a. doi:10.1002/app.32322.

[58] H. Daemi, M. Barikani, M. Barmar, Compatible compositions based on aqueous polyurethane dispersions and sodium alginate, Carbohydrate Polymers. 92 (2013) 490–496. doi:10.1016/j.carbpol.2012.09.046.

[59] National Institute of Advanced Industrial Science and Technology (AIST), Spectral Database for Organic Compounds (SDBS), (n.d.). http://sdbs.db.aist.go.jp/sdbs/cgi-bin/direct_frame_top.cgi (accessed April 4, 2017).

[60] J. Guo, B.N. Nguyen, L. Li, M.A.B. Meador, D.A. Scheiman, M. Cakmak, Clay reinforced polyimide/silica hybrid aerogel, Journal of Materials Chemistry A. 1 (2013) 7211. doi:10.1039/c3ta00439b.

[61] S. Lu, D. Tu, X. Li, R. Li, X. Chen, A facile “ship-in-a-bottle” approach to construct nanorattles based on upconverting lanthanide-doped fluorides, Nano Research. 9 (2016) 187–197. doi:10.1007/s12274-015-0979-4.

[62] C. Jagadeeswara Rao, K.A. Venkatesan, K. Nagarajan, T.G. Srinivasan, P.R. Vasudeva Rao, Electrochemical behavior of europium (III) in N-butyl-N-methylpyrrolidinium bis(trifluoromethylsulfonyl)imide, Electrochimica Acta. 54 (2009) 4718–4725. doi:10.1016/j.electacta.2009.03.074.

[63] S.A. Dharaskar, K.L. Wasewar, M.N. Varma, D.Z. Shende, C. Yoo, Synthesis, characterization and application of 1-butyl-3-methylimidazolium tetrafluoroborate for extractive desulfurization of liquid fuel, Arabian Journal of Chemistry. 9 (2016) 578–587. doi:10.1016/j.arabjc.2013.09.034.

[64] P. KROL, Synthesis methods, chemical structures and phase structures of linear polyurethanes. Properties and applications of linear polyurethanes in polyurethane elastomers, copolymers and ionomers, Progress in Materials Science. 52 (2007) 915–1015. doi:10.1016/j.pmatsci.2006.11.001.

[65] M.F. Rojas, F.L. Bernard, A. Aquino, J. Borges, F.D. Vecchia, S. Menezes, R. Ligabue, S. Einloft, Poly(ionic liquid)s as efficient catalyst in transformation of CO_2 to cyclic carbonate, Journal of Molecular Catalysis A: Chemical. 392 (2014) 83–88. doi:10.1016/j.molcata.2014.05.007.

[66] K. Kojio, S. Nakashima, M. Furukawa, Microphase-separated structure and mechanical properties of norbornane diisocyanate-based polyurethanes, Polymer. 48 (2007) 997–1004. doi:10.1016/j.polymer.2006.12.057.

[67] H. Sardon, L. Irusta, P. Santamaría, M.J. Fernández-Berridi, Thermal and mechanical behaviour of self-curable waterborne hybrid polyurethanes functionalized with (3-aminopropyl)triethoxysilane (APTES), Journal of Polymer Research. 19 (2012) 9956. doi:10.1007/s10965-012-9956-8.

[68] D. Gnanasekaran, B.S.R. Reddy, Cost effective poly(urethane-imide)-POSS membranes for environmental and energy-related processes, Clean Technologies and Environmental Policy. 15 (2013) 383–389. doi:10.1007/s10098-012-0500-7.

[69] K.K. Jena, S. Sahoo, R. Narayan, T.M. Aminabhavi, K. Raju, Novel hyperbranched waterborne polyurethane-urea/silica hybrid coatings and their characterizations, Polymer International. 60 (2011) 1504–1513. doi:10.1002/pi.3109.

[70] K.M. Seeni Meera, R. Murali Sankar, S.N. Jaisankar, A.B. Mandal, Physicochemical Studies on Polyurethane/Siloxane Cross-Linked Films for Hydrophobic Surfaces by the Sol–Gel Process, The Journal of Physical Chemistry B. 117 (2013) 2682–2694. doi:10.1021/jp3097346.

[71] J. Tang, Y. Shen, M. Radosz, W. Sun, Isothermal carbon dioxide sorption in poly(ionic liquid)s, Industrial and Engineering Chemistry Research. 48 (2009) 9113–9118. doi:10.1021/ie900292p.

4.3. Capítulo III: Poli(líquidos iônicos) aniônicos base celulose

O artigo intitulado "*New cellulose based ionic compounds as low-cost sorbents for CO_2 capture*" publicado na Fuel Processing Technology apresentado neste capítulo, descreve a obtenção de PLIs aniônicos celulósicos e sua avaliação para sorção de CO_2. Para síntese dos PLIs utilizou-se celulose extraída da casca de arroz. A celulose foi modificada com ácido cítrico e funcionalizada com quatro diferentes cátions de líquidos iônicos (Cloreto de 1-butil-3-metilimidazólio; Brometo de tetrabutilfosfínio, Brometo de tetrabutilamônio e Cloreto de 1-butil-1-metilpirrolidinio). Os compostos obtidos foram caracterizados por FTIR, DRX, TGA, BET e MEV-FEG. A capacidade de sorção foi determinada utilizando uma microbalança termogravimétrica por Suspensão Magnética de alta precisão (PTGA), na temperatura de 25°C e pressões de 0,1 – 3 MPa. Estudos de simulações ab initio foram empregados para compreender o efeito do cátion e dos grupos funcionais presentes na estrutura da celulose modificada sobre a sorção de CO_2. Estes compostos exibiram valores de sorção elevados, boa estabilidade térmica e capacidade de reutilização no processo de captura. O uso de resíduos para obtenção da celulose e a pequena quantidade de LIs utilizados na modificação permitiu a obtenção de sorventes de baixo custo para captura de CO_2. Resultados experimentais e de simulação revelaram que o CO_2 interage de forma mais efetiva com o grupo carboxilato, e, em menor grau com os grupos polares da estrutura da celulose. O melhor desempenho foi obtido para o PLI CL-TBA (44 mgCO_2/g em 0,1 MPa).

Fuel Processing Technology 149 (2016) 131–138

Contents lists available at ScienceDirect

Fuel Processing Technology

journal homepage: www.elsevier.com/locate/fuproc

Research article

New cellulose based ionic compounds as low-cost sorbents for CO_2 capture

Franciele L. Bernard [a,b], Daniela. M. Rodrigues [c], Barbara B. Polesso [c], Augusto J. Donato [b], Marcus Seferin [a,b], Vitaly V. Chaban [d], Felipe Dalla Vecchia [c], Sandra Einloft [a,b,*]

[a] Post-Graduation Program in Materials Engineering and Technology, Pontifical Catholic University of Rio Grande do Sul — PUCRS, Brazil
[b] School of Chemistry, Pontifical Catholic University of Rio Grande do Sul — PUCRS, Brazil
[c] School of Engineering, Pontifical Catholic University of Rio Grande do Sul — PUCRS, Av. Ipiranga, 6681, Partenon, Porto Alegre CEP: 90619-900, Brazil
[d] Institute of Science and Technology (ICT), Federal University of São Paulo (UNIFESP), São José dos Campos, SP, Brazil

ARTICLE INFO

Article history:
Received 26 January 2016
Received in revised form 4 April 2016
Accepted 9 April 2016
Available online xxxx

Keywords:
Modified cellulose
Ionic compounds
Low-cost sorbents
Carbon dioxide capture
Quantum mechanical simulations

ABSTRACT

Supporting ionic liquids in solid materials is a promising solution to address CO_2 capture. Cellulose is a versatile and low-cost material. The support of different ionic liquids cations on cellulose extracted from rice husk is an excellent strategy for CO_2 capture. This study reports chemical modification of cellulose fibers extracted from rice husk with different ionic liquids cations and its potential for CO_2 capture. The obtained ionic compounds were characterized by FTIR, XRD, FESEM, TGA and BET. CO_2 sorption capacity was gravimetrically assessed in a Magnetic Suspension Balance (MSB). In addition, ab Initio calculations were performed. First, the carboxylate groups are responsible for the CO_2 capture process. Second, the cation maintains the CO_2 binding sites of the anion partially or fully non-occupied, improving the CO_2-ionic compound affinity. The best result for CO_2 sorption was obtained for the ionic compound CL-TBA of 71 $mgCO_2/g$ at 3 MPa and 25 °C. At lower pressures, this compound presents a high CO_2 sorption value (44 $mgCO_2/g$ at 0.1 MPa). We conclude that these ionic compounds deserve further attention in the post-combustion process.

1. Introduction

An increasing level of carbon dioxide concentration in the atmosphere related to fossil fuels processing and utilization contributes to global warming considerably. Carbon capture and storage technologies appear among the key technologies to reduce CO_2 emissions and mitigate the effects of climate change [1]. Chemical absorption processes using aqueous amine solutions have been extensively studied and used in industry for decades. However, they have some operational drawbacks, such as large amount of energy required for the amine regeneration process [2,3], amines degradation/evaporation, and equipment corrosion [2–4]. Ionic liquids have been proposed as the next generation of solvents for a selective CO_2 separation [5]. These compounds are versatile and less harmful to the environment than conventional organic solvents [6–10]. They present unique properties, such as negligible vapor pressure, non-flammability, high thermal stability, and tunability (myriad of possible combinations of cations and anions [2,3,5]). Nevertheless, these solvents suffer from high viscosity and high production costs, when compared to aqueous amines solutions [5,11,12]. Implementing ionic moieties of ionic liquids into solid materials can provide a solution of these problems. This pathway has attracted the attention of researchers in the last decade. Solid sorbents, typically studied for CO_2 capture are metal organic frameworks (MOFs) [1], mesoporous materials [13,14], activated carbon [15,16], polymeric and inorganic membranes [17], poly(ionic liquids) [18–20], covalent organic frameworks (COFs) [21], silica nanoparticles encapsulating amine-functionalized ionic liquids [22], etc. Functionalized cellulose containing amino groups has also been recently considered for CO_2 capture [23].

Cellulose is a versatile, low-cost material that undergoes chemical changes primarily by the hydroxyl groups [24]. Cellulose constitutes ca. 33% of rice husk [25], Brazil belonging to the 10 largest world rice producers [26]. The present utilization of the rice husk is far from being optimal [25,27]. Strategies to use these low-cost materials for CO_2 capture will foster emergence of green technologies and sustainable development.

The main aim of this study was to investigate chemical modification of cellulose fibers, extracted from rice husk, with different cations of ionic liquids and subsequent CO_2 capture of the developed materials. Quantum mechanical simulations were employed to reveal a role of each moiety of the ionic compounds in CO_2 capture.

2. Materials and methods

2.1. Materials

The rice husks were donated by Cooperativa Arrozeira Extremo Sul Ltda. The obtained material was washed with distilled water and dried

* Corresponding author at: Post-Graduation Program in Materials Engineering and Technology, Pontifical Catholic University of Rio Grande do Sul — PUCRS, Brazil.
E-mail address: einloft@pucrs.br (S. Einloft).

http://dx.doi.org/10.1016/j.fuproc.2016.04.014
0378-3820/

in an oven at 100 °C for 8 h. The dried husk was grounded in a knife mill. The fraction that passed through the 20 mesh sieve (0.841 mm) was collected. Anhydrous citric acid (CA, 99.5% Synth), sodium hydroxide (NaOH, 97% Vetec), hydrogen peroxide (H_2O_2, 35%, Neon), sulphuric acid (H_2SO_4, F. Maia, P. A), N,N–dimethylformamide (DMF, 99.5%, Merck) and ethanol (CH_3CH_2OH, 99%, Vetec) were used as purchased. Tetrabutylammonium bromide (TBAB, 99%, Acros Organics), tetrabutylphosphonium bromide (TBPB, 98%, Sigma Aldrich), and 1-butyl-1-methylpyrrolidinium chloride (BMPYRR, 99%, Fluka) were dried under vacuum at 60 °C for 12 h. 1-butyl-3-methylimidazolium chloride (BMIM Cl) was synthesized as described in literature [28–30]. BMIM Cl was characterized by Fourier transform infrared spectroscopy (FTIR), using a Perkin-Elmer spectrophotometer model Spectrum 100 FT-IR with full attenuated reflectance model (ATR), as well as by proton nuclear magnetic resonance (^{1}H NMR) on a Varian Spectrophotometer, model VNMRS 300 MHz, using DMSO-d_6 as solvent, in accordance with the literature. 1H NMR (300 MHz, DMSO-d_6, 25 °C) δ (ppm): 1.01 (m, CH_3), 1.29 (m, CH_2CH_3), 1.83 (m, CH_2), 3.97 (s, CH_3), 4.25 (t, CH_2N), 7.79 (s, H5), 7.91 (s, H4), 9.48 (s, H2). FTIR ν (cm^{-1}): 3141 (N—H of imidazole group), 3058 (C—H of imidazole group), 2959 (C—H of methylene), 2870 (C—H of methyl), 1640 (C═N of imidazole group), 1558–1453 (C═C and C—N of imidazole group), 749 (Cl^-).

2.2. Cellulose extraction

The cellulose extraction procedure was adapted from literature procedures [25,31]. The material was treated with 4 wt% NaOH at 90 °C for 2 h to remove lignin and hemicellulose of the rice husk fibers. The acid hydrolysis treatment was conducted on the fibers after alkali treatment using 10.0 mol/L H_2SO_4 at 50 °C for 40 min under continuous stirring. Afterwards, bleaching was carried out by addition of 16 v/v% H_2O_2 and 5 wt% NaOH solution in 1:1 proportion (v/v) at 55 °C for 2 h to remove the remaining lignin. The rice husk:solution ratio was 0.05 g/mL. Each step was repeated five times. The solid was filtered and washed with distilled water until neutral pH was achieved and dried in oven at 50 °C after each treatment. The detailed procedure used for determining cellulose content is available in Technical Association of Pulp and Paper Industry (TAPPI standard T203 OS-74). The extracted cellulose content from rice husk was 75 wt%.

2.3. Cellulose chemical modification

Cellulose chemical modification was performed in two stages. The first stage was modification with citric acid (Fig. 1). The second step was attachment of the cationic moiety (Fig. 2). The modification with citric acid was performed by a similar procedure described elsewhere [32,33]. The cellulose was poured into a flask containing 1.2 mol/L aqueous solution of citric acid to obtain 100 g L^{-1} cellulose solution. This solution was stirred for 0.5 h at room temperature. The cellulose was separated by filtration and placed into an oven at 120 °C and kept constant for 1.5 h. After cooling, the cellulose was washed with distilled water in proportion of 200 mL/g several times to remove any excess of citric acid and dried at 55 °C for 24 h. The concentration of carboxylic groups (mol·mg^{-1}) introduced into the modified cellulose was determined by back titration [34,35], by the treatment of the material (0.1 g) with 100 mL of an aqueous solution of NaOH (0.02 mol/L) for 1 h under constant stirring. The materials were separated by filtration, and the solution was titrated with HCl (0.02 mol/L).

The functionalization reaction is described elsewhere [18]. In a Schlenk flask, under N_2 atmosphere, 1 g of citric-acid-modified cellulose was added to the ionic liquid (molar ratio COOH/IL = 1:1) dissolved in 15 mL of dimethylformamide (DMF). The mixture was stirred at 40 °C for 2 h. The materials were separated by filtration, washed repeatedly with distilled water and ethanol and dried at 55 °C for 24 h. The concentration of ionic liquid introduced into the modified cellulose was determined by back titration by treating the material (0.1 g) with 100 mL of an aqueous HCl solution (0.02 mol/L) for 1 h under constant stirring. Then, the materials were separated by filtration and the solution was titrated with NaOH (0.02 mol/L) (Fig. 2).

2.4. Characterization

The synthesized materials were characterized by Universal Attenuated Total Reflectance sensor (UATR-FTIR) using a Perkin-Elmer Model 100 FTIR Spectrum, in the range 4000–650 cm^{-1}. The field emission scanning electron microscopy (FESEM) analyses were performed in FEI Inspect F50 equipment in secondary electrons (SE) mode. Thermogravimetric Analysis (TGA) was performed using a TA Instruments SDT-Q600 between 25 and 600 °C with a heating rate of 10 °C/min in nitrogen atmosphere. The specific surface area (SBET) and pore size were calculated from nitrogen sorption data using Brunauer-Emmett-Teller (BET) at −196 °C (Micromeritics, ASAP 2420). Powder X-ray diffraction (XRD) pattern was recorded on a Bruker-AXS D8 ADVANCE diffractometer operated at 40 kV and 20 mA using Cu Kα radiation (λ = 1.5406 Å) in the range (3–40°) with step of 0.02 and scanning time of 1.0 min. Eq. (1) was used to calculate the crystallinity index of the materials (CrI) by the Segal method [36].

$$\mathrm{CrI} = \frac{I_{002} - I_{AM}}{I_{002}} \times 100 \quad (1)$$

where I_{002} is maximum intensity of the 002 peak and I_{AM} is intensity scattered by the amorphous part of the sample. The diffraction peak for plane (002) is located at diffraction angle around 2θ = 22° and intensity scattered by the amorphous part is measured as the lowest intensity at diffraction angle around 2θ = 18° [25].

2.5. Ab initio calculations

The binding energies and equilibrium geometries of ions and molecules were computed from hybrid density functional theory (HDFT) using Becke-3-Lee-Yang-Parr (B3LYP) approach [37,38]. The atom-

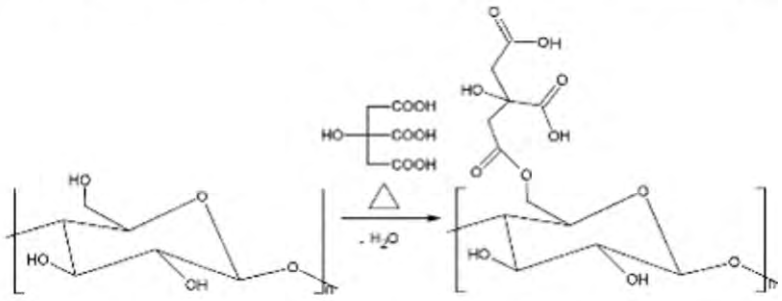

Fig. 1. Schematic representation of the carboxylic groups introduced onto the cellulose surface.

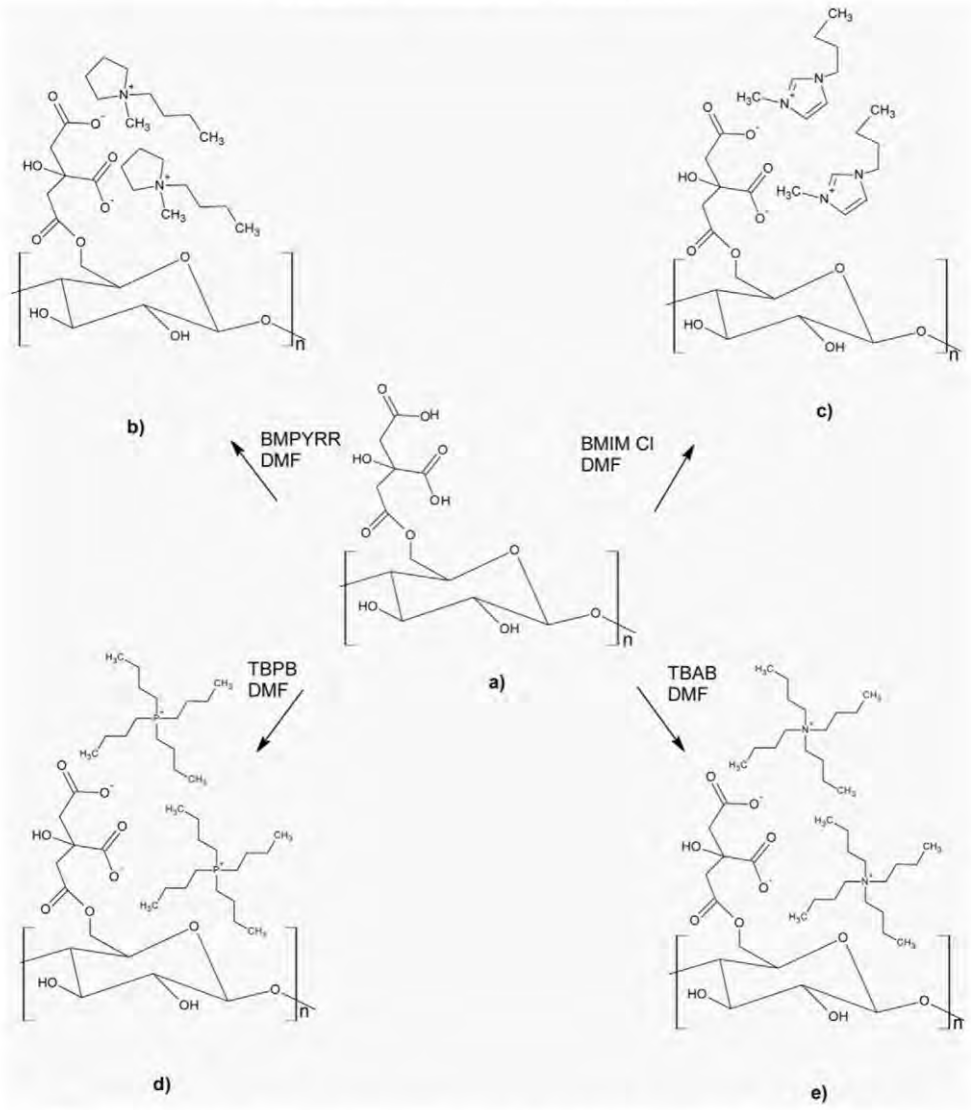

Fig. 2. Ionic compounds obtained from cellulose modification: (a) CL-CA; (b) CL-BMPYRR; (c) CL-BMIM; (d) CL-TBP; (e) CL-TBA.

centered split-valence double-zeta polarized 6-31G(d) basis set was used for all atoms (carbon, hydrogen, oxygen) at all stages of the calculations. The basis set superposition errors (BSSE) were estimated by the counterpoise method and deducted from the reported binding energies. The self-consistent field convergence criterion was set to 10^{-8} Eh. The geometry convergence criterion was set to 0.12 kJ mol^{-1} nm^{-1} for the largest force. The successful location of the stationary point (local minimum) was ensured by analyzing vibrational frequencies.

2.6. Gas adsorption measurements

Pure gas sorption (CO_2) in the samples were gravimetrically assessed in a Magnetic Suspension Balance (MSB) (Rubotherm Prazisionsmesstechnik GmbH, 35 MPa and 400 °C) equipped with a single sinker device for absorbate density determination and thermostatized with an oil bath (Julabo F25/± 1 °C). The apparatus details are described elsewhere [39–41]. When compared to other gravimetrical sorption methods, the MSB device allows high-pressure sorption measurements since the sample can be potted into a closed chamber coupled to an external accurate balance (accuracy of ± 10 μg). The samples (0.06 to 0.09 g) were weighted and transferred to the MSB sample container. The system was subjected to a 10^{-7} MPa vacuum at the temperature of the sorption measurement, 25 °C, for 24 h (constant weight was achieved within this time). The gas (CO_2, Air Liquide/99.998%) was admitted into the MSB pressure chamber up to the desired pressure, 0.1–3 MPa. In this study, pressure gauge with an accuracy of 10^{-3} MPa was used to control system pressure. The gas solubility in the samples for each isotherm and pressure considered was measured for 3–4 h until no more weight increasing for gas sorption was observed. At this step of gas solubility in the samples, the weight reading from

Table 1
Specific surface area, ionic liquid loading and crystallinity.

Samples	SBET (m^2/g)	Ionic liquid loading (mol)/mg	Crystallinity (%)
Cellulose	0.2398	–	87
CL-CA	0.4575	–	84
CL-BMIM	0.6984	1.57×10^{-6}	89
CL-TBP	0.6430	1.16×10^{-6}	88
CL-TBA	1.7370	0.68×10^{-6}	87
CL-BMPYRR	0.5901	0.95×10^{-6}	89

the microbalance at pressure P and temperature T was recorded as $W_t(P,T)$. The mass of absorbed gas in the sample (W) was calculated using the following (Eq. (2)):

$$W = \left[W_t(P,T) - W_{sc}(P,T) + \rho_g(P,T)\cdot\left(V_{sc}(T) + V_s(T)\right)\right] - W_s(vac,T) \quad (2)$$

where $W_{sc}(P,T)$ is the weight of sample container, $\rho_g(P,T)$ stands for gas density, directly measured with the MSB coupled single-sinker device, $V_{sc}(T)$ is the volume of the sample container, determined from a buoyancy experiment when no sample is charged into the sample container, $V_s(T)$ the specific solid sample volume, $W_s(vac,T)$ is the weight of samples under vacuum and the term $\rho_g(P,T)\cdot(V_{sc}(T)+V_s(T))$ represents the buoyancy force. In this work, the solubility in the sample was treated as excess solubility.

3. Results

3.1. Specific surface area measurements

The determined concentration of carboxylic functions of CL-CA sample was 2.15×10^{-6} (mol/mg); this result is close to the previously known investigations [42]. Table 1 shows surface area data, ionic liquid loading and crystallinity for each sample. Even if the presence of the countercation increases surface area, the obtained values for all ionic materials are small. We highlight that the amount of ionic liquid loaded is low, indicating the possibility of the capture process cost reduction. Crystallinity value obtained in the samples is discussed in Section 3.2.

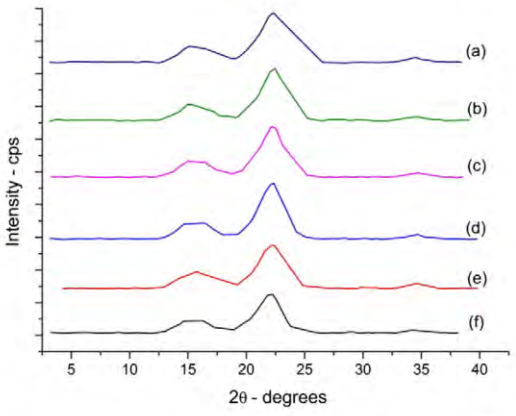

Fig. 3. XRD pattern of cellulose and modified cellulose samples: (a) CL-TBP; (b) CL-TBA; (c) CL-BMIM; (d) CL-BMPYRR; (e) cellulose; (f) CL-CA.

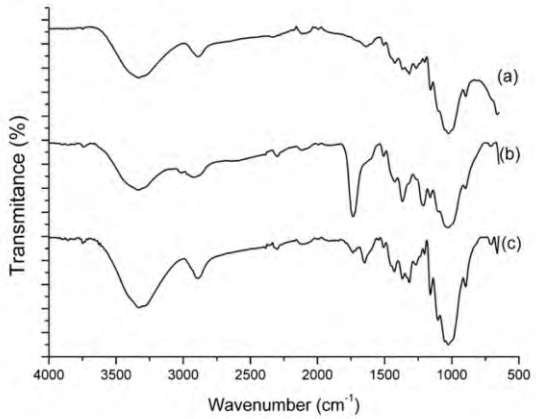

Fig. 4. FTIR spectra of: (a) cellulose, (b) cellulose modified with citric acid and (c) ionic compound CL- BMPYRR.

3.2. X-ray diffraction (XRD)

Fig. 3 shows X-ray diffraction profile of the synthesized cellulose based ionic compounds and that of the extracted cellulose. All samples exhibit typical cellulose peaks around $2\theta = 16°$, 22.6° and 35° [25].

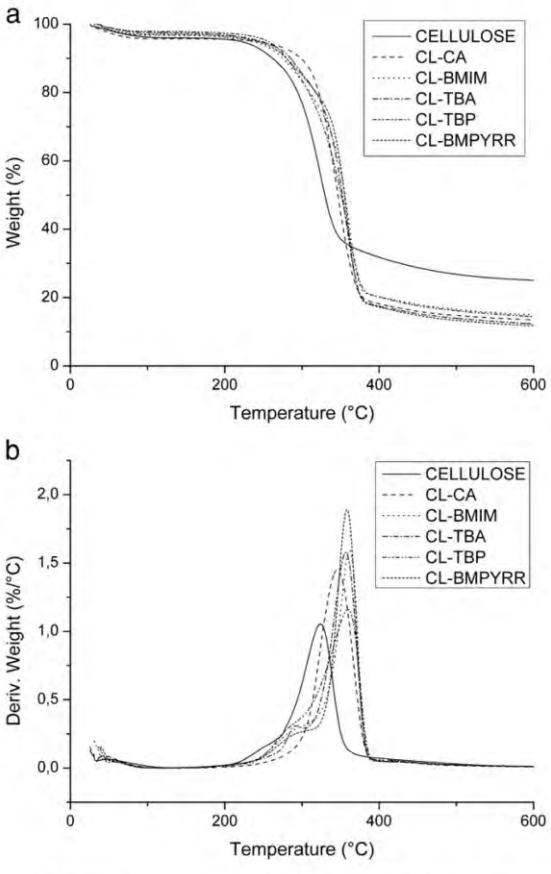

Fig. 5. (a) TG and (a) DTG curves for cellulose and modified cellulose samples.

The crystallinity index (CrI) of the cellulose was ca. 87%, whereas for the sample CL-CA CrI was ca. 84%. The presence of the counter cation does not affect considerably the crystallinity of the samples when compared with cellulose and CL-CA samples (Table 1).

3.3. Spectroscopic characterization

The FTIR spectra of all samples (Fig. 4) showed a broadband located at 3330–3340 cm^{-1}, attributed to the stretching of —OH groups, band near 2920 cm^{-1} related to the C—H stretching, band at 1160 cm^{-1} corresponding to C—O—C asymmetrical bridge stretching, broadbands around 1050 cm^{-1} and 890 cm^{-1} related to the C—H and C—O stretching vibration of the cellulose structure [25,27]. Having compared spectra for the citric acid modified cellulose (Fig. 4b) and cellulose (Fig. 4a), we identified a strong band at 1740 cm^{-1} attributed to the carboxylic acid (—COOH). This evidences introduction of citric acid into the cellulose chain [24].

Fig. 4c presents FTIR for the ionic compound CL-BMPYRR. A new band at 1648 cm^{-1}, which is present in all ionic compounds, suggests formation of carboxylates. In turn, band at 1740 cm^{-1} corresponds to the unreacted carboxylic acid [24,43].

3.4. Thermogravimetric Analysis (TGA)

The Thermogravimetric Analysis (TGA) was performed in order to characterize thermal stability of the synthesized material. Fig. 5 presents the TG and DTG curves obtained for all materials. All samples showed two thermal events. The earlier weight loss was ca. 4% and T_{onset} below 100 °C attributed to water vaporization [25]. The later weight loss is attributed to cellulose degradation (T_{onset} of 289 °C and T_{max} of 324 °C), being 71%. The modified samples presented a higher thermal stability than cellulose (citric acid modified samples T_{onset} = 318 °C and T_{max} = 346 °C; samples CL-BMIM, CL-TBP, CL-TBA and CL-BMPYRR presented values of T_{onset} = 330 °C and T_{max} = 362 °C; T_{onset} = 314 °C and T_{max} = 359 °C, T_{onset} = 324 °C and T_{max} = 357 °C; T_{onset} = 333 °C and T_{max} = 358 °C, respectively) and weight loss around 84%. This behavior is associated with the reduction of the cellulose weight as a result of the chemical modification with citric acid and the ionic

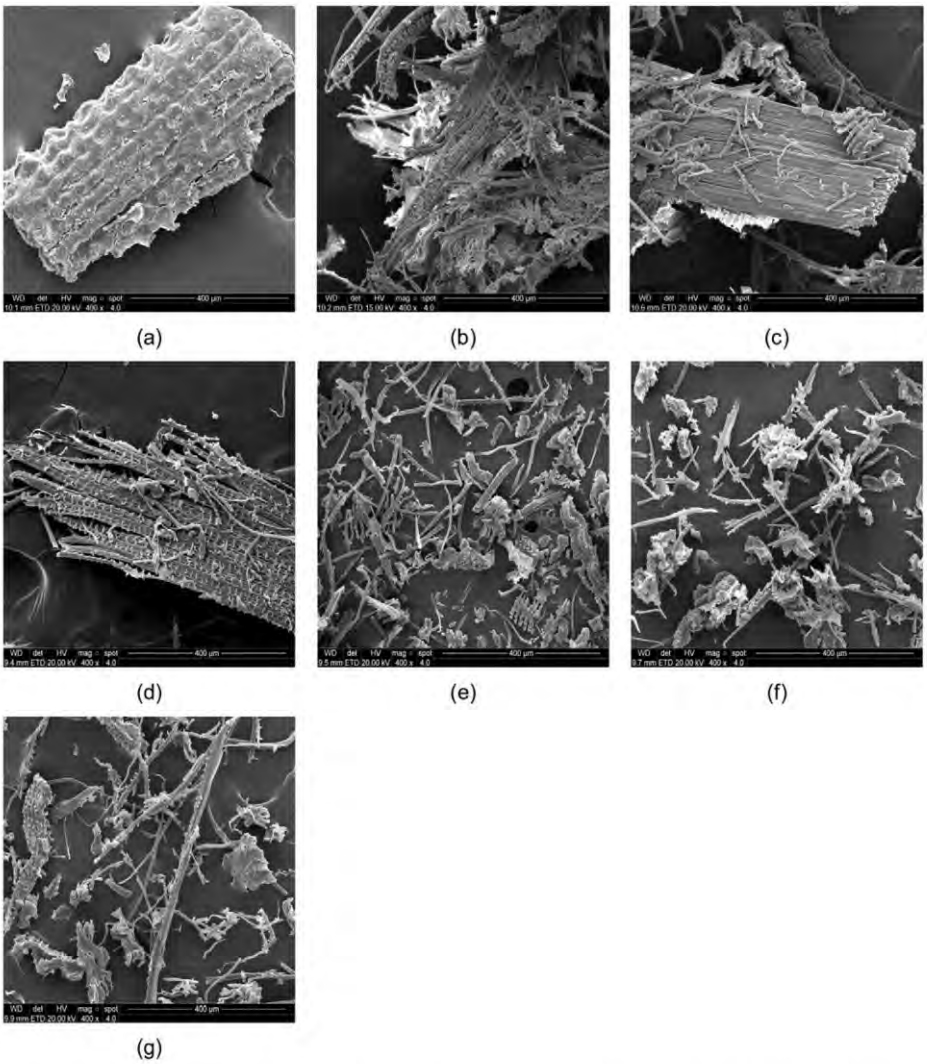

Fig. 6. Micrographs of the materials: (a) rice husk fibers, (b) cellulose, (c) CL-CA, (d) CL-BMIM, (e) CL-TBA, (f) CL-TBP, (g) CL-BMPYRR.

liquids cations. When comparing the DTG curves (Fig. 5b) of cellulose and the acid citric modified sample with the ionic compounds (CL-BMIM; CL-TBP; CL-BMPYRR and CL-TBA), a new shoulder is observed, possibly due to the anion–cation interaction.

3.5. Field emission scanning electron microscopy (FESEM)

Using FESEM, Fig. 6 exemplifies different effects on the rice husk surface after cellulose extraction as well as chemical modification. Fig. 6a shows the smooth compacted surface of the untreated rice husk fiber. Fig. 6b shows the same after bleaching. Cellulose exists in the form of bundles of fibers. The FESEM micrograph of chemically modified cellulose fibers with citric acid (Fig. 6c) showed similar morphology to that shown by the sample after bleaching treatment (Fig. 6b). The chemical modification of cellulose with the ionic liquid led to separation of the fiber bundles into individual fibers and provided an apparent reduction of the average size of cellulose particles (see Fig. 6 e, f and g) with the exception for BMIM cation (see Fig. 6d). This behavior might contribute to the increase of CO_2 adsorption, due to the increased contact surface.

3.6. Quantum mechanical simulations

The BMPYRRR, TBP and TBA cations do not coordinate CO_2. They are used as weakly coordinating counter-ions for the modified cellulose. The cations of this sort are expected not to form strong cation-anion bonds and, therefore, to maintain the CO_2 binding sites of the anion partially or fully non-occupied. In turn, the BMIM cation coordinates CO_2 thanks to a weak hydrogen bond originating from the intrinsically acidic hydrogen atom of the imidazole ring and the oxygen atom of CO_2. The CO_2 capture ability of BMIM was thoroughly previously investigated [11,44,45]. An elementary unit of the polymeric anion possesses 11 oxygen atoms constituting eight prospective binding sites (Fig. 7): two carboxylate groups, three hydroxyl groups, two ether groups, and one ester group. Such an abundance of coordinating sites (polar and relatively groups) attracts an interest to the cellulose derived anions. Somewhat different chemical environment permits to consider the mentioned groups as unique sites in relation to CO_2. For systematicity, we used the tetramethylammonium cation to represent a weakly coordinating organic cation in all calculations.

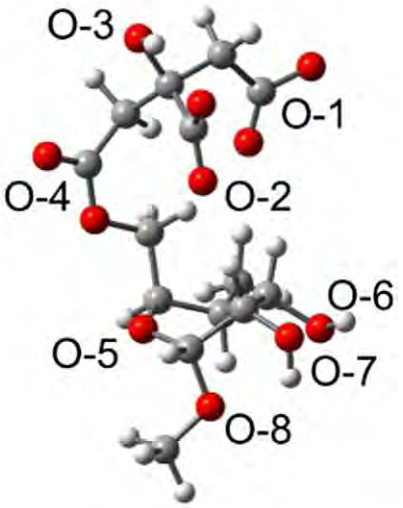

Fig. 7. The CO_2 binding sites of the modified cellulose moiety: carbon atoms are grey, hydrogen atoms are white, oxygen atoms are red. (For interpretation of the references to color in this figure legend, the reader is referred to the web version of this article.)

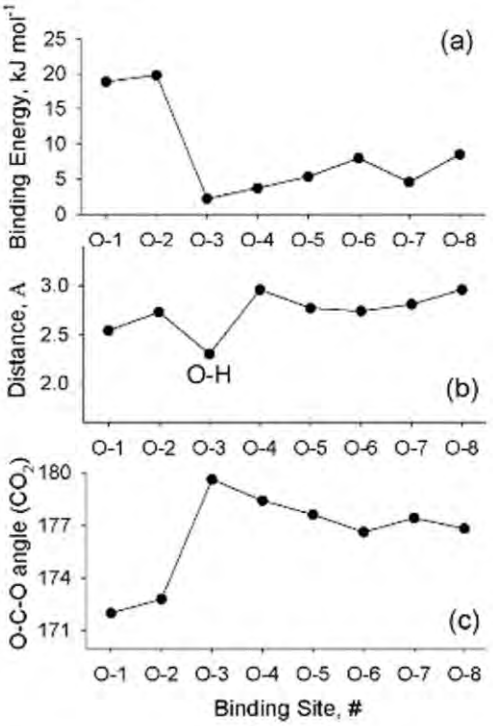

Fig. 8. Primary characteristics of the CO_2 physisorption process: (a) binding energy; (b) closest-approach distance; (c) CO_2 deviation from its genuine linearity due to binding. In most cases, the closest-approach distance is carbon-oxygen, except at O-3, in which oxygen of CO_2 coordinates hydrogen of hydroxyl.

Specific contributions of the O-x, where x = 1…8, sites cannot be clearly derived from the experiment, but can be obtained from the HDFT calculations in terms of binding energies, closest-approach distances, and selected characteristic angles (Fig. 8, Table 2). We investigated 8 local minima by initially putting CO_2 in the vicinity of the desired binding site and applying a geometry optimization procedure to locate a stationary point for every configuration. The strongest CO_2 binding is observed at the O-2 site (see Fig. 9). This is due to the simultaneous attraction to the carboxyl and hydroxyl groups of the citric acid moiety and despite steric hindrance preventing a tight coordination of the carbon atom of CO_2 by the carboxyl group. Compare r(C—O) = 2.54 Å (O-1) to r(C—O) = 2.73 Å (O-2). The ester, ether and hydroxyl groups, per se, perform poorly and the respective binding energy in no case exceeds 10 kJ mol^{-1}. In the meantime, the ether groups, O-5 and O-8, appear somewhat more successful among others. This conclusion is in concordance with the recent experimental study [46], in which

Table 2
The oxygen (CO_2)–carbon (cellulose) distances, carbon (CO_2)–oxygen (cellulose)–carbon (cellulose) non-valence angles, BSSE, BSSE percentage with respect to the computed binding energy.

Site, #	r(O—C), Å	angle (C—O—C), °	BSSE, kJ mol^{-1}	BSSE, %
O-1	4.0	140.7	14.8	44.0
O-2	3.7	120.9	17.0	46.2
O-3	3.9	102.6	4.60	67.1
O-4	3.9	131.4	7.52	66.9
O-5	3.4	120.2	8.57	61.6
O-6	3.7	125.9	8.52	51.6
O-7	3.3	108.9	9.57	67.8
O-8	3.9	135.3	15.3	64.1

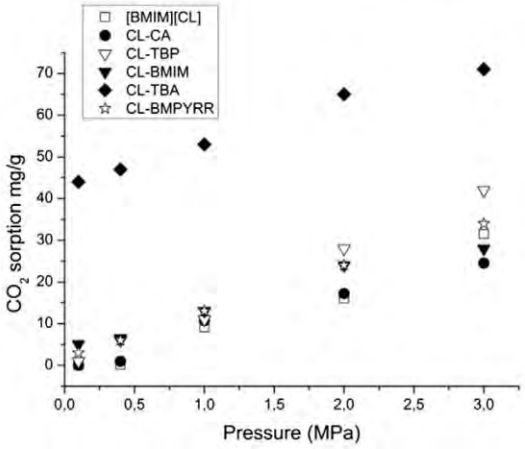

Fig. 9. CO_2 sorption for the ionic compounds, cellulose and the ionic liquid [BMIM] [Cl].

higher density of carboxylate and ether groups per adsorbent particle was linked to better CO_2 capture. Note that chemical environment matters significantly in the process of gas molecule binding and the impact of neighboring groups cannot be fully isolated. For instance, oxygen of CO_2 coordinates hydrogen of hydroxyl at O-3; nevertheless, this pattern is not implemented either in O-6 or O-7 (also hydroxyl group containing sites of the modified cellulose). The reason for that is formation of intramolecular hydrogen bond between the hydroxyl groups at the O-6 and O-7 positions. Consequently, both groups are located above the ring (*cis*-conformation) and are insufficiently available to oxygen of CO_2. Compare the depicted closest-approach distances in Fig. 8b.

The CO_2 molecule in vacuum is linear, with the O-C-O angle equaling to 180°. Binding perturbs an original shape of CO_2, the magnitude of perturbation being proportional to the binding energy (Fig. 8). Whereas the O-C-O angle is 172° at O-2 and 173° at O-1, this same angle exceeds 177° in all other cases. The weakest binding, at O-3, coincides ideally with the most linear CO_2 shape.

The BSSEs constitute a significant portion of the binding energies (Table 2). Their contribution increases when the binding energy decreases and becomes less electrostatic in nature. See the cases of hydroxyl and ether groups. Using a larger basis set generally favors smaller BSSE, which nevertheless needs to be estimated and deducted.

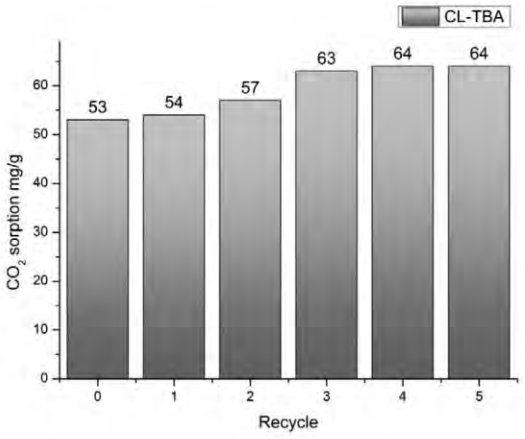

Fig. 10. CO_2 sorption/desorption tests for the ionic compound CL-TBA.

3.7. Gas sorption measurements

The experimental results of CO_2 sorption by the synthesized materials are shown in Fig. 9. The sorption behavior for the ionic liquid [BMIM] [Cl] at the same experimental conditions is also presented. Note that in Fig. 9 the CO_2 sorption values for modified cellulose with citric acid (CL-CA) were similar to those found for the ionic liquid [BMIM] [Cl]. However, the sorption of CO_2 was slightly higher in the CL-BMIM sample, suggesting that the system [BMIM] cation-cellulose improves the affinity with CO_2. As suggested by the quantum mechanical simulations, the CO_2 interacts quite strongly with the cellulose chain. The effect of the countercation in increasing CO_2 sorption is evident when comparing the results for CO_2 sorption of the ionic compounds (CL-BMIM; CL-TBP; CL-BMPYRR and CL-TBA) with the sample without countercation (CL-CA). These results suggest that the solubility of CO_2 in these materials is mainly influenced by the interaction of the countercation with the cellulose chain and by the surface area (CL-TBP 0.6430 m^2/g and CL-TBA 1.7370 m^2/g). An amount of ionic liquid loading (Table 1) is weaker. Quantum mechanical simulations evidenced that the CO_2 interacts with the cellulose chain mainly by O-1 and O-2. Hence, the cation plays a stabilizing role in the ionic compound system. The weakly coordinating countercations for the modified cellulose stabilize the system maintaining the CO_2 binding sites of the anion partially or fully non-occupied, increasing CO_2-philicity of the ionic compound. The best result for CO_2 sorption was obtained for the ionic compound CL-TBA of 71 $mgCO_2/g$ at 3 MPa and 25 °C, but as depicted in Fig. 9, even at lower pressures, this compound presents a high CO_2 sorption value (44 $mgCO_2/g$ at 0.1 MPa). The low surface area values explain this behavior. The sorption capacity at low pressures is dependent on the CO_2 interaction with the ionic compound, while at higher pressures the low specific surface area do not facilitate the CO_2 sorption. The usage of industrial wastes, such as fly ash derived materials for CO_2 sorption, are described elsewhere [47]. Maroto-Valer et al. [48] reported different materials obtained by modification of fly ashes (AC) aiming to introduce chemical adsorption sites as well as evaluate their sorption capacity. The specific surface areas of the products are considerably higher when compared to our results (AC untreated 818 m^2/g; AC treated with MEA 241 m^2/g and cellulose 0.2398 m^2/g; CL-TBA 1.7370 m^2/g). Even with low specific surface areas, the results obtained for CO_2 sorption of AC treated with MEA varied from 68.6 mg CO_2/g sorbent to 5.5 $mgCO_2/g$ depending on the MEA content. When AC was modified with MDEA and DEA, lower values were found when compared to MEA (30 °C, at ca. 0.240 MPa with flow rate of 100 mL/min). These values are lower, as compared with those found in the present work.

3.8. Recycling experiments for CL-TBA

In order to examine the reusability of PILs, CL-TBA was subjected to five more runs. The sorption was carried out at 25 °C under a 1 MPa CO_2 pressure. After each step, the CO_2 desorption was carried out under vacuum at 25 °C for 8 h. The results for the six consecutive tests are shown in Fig. 10. The CO_2 sorption capacity was slightly increased in the first three recycles, probably due to impurities withdrawal remaining constant for the next cycles. These results indicate that the CL-TBA has high stability and capacity of being reused.

4. Conclusions

The chemical modification of cellulose extracted from rice husk with different ionic liquid cations was performed and the potential for CO_2 capture of these materials was evaluated. The quantum mechanical simulations and the experimental results revealed the role of each moiety of the ionic compounds in the gas capture process. The abundance of coordinating sites attracts an interest to the cellulose-derived anions, since CO_2 interacts with the cellulose chain. The presence of the countercation in increasing the CO_2 solubility was evidenced and the best result

for CO_2 sorption was obtained for the ionic compound CL-TBA of 71 mgCO_2/g at 3 MPa and 25 °C. Weakly coordinating countercations for the modified cellulose stabilize the system maintaining the CO_2 binding sites of the anion partially or fully non-occupied, improving the CO_2-philicity of the ionic compound. Our results present a new sustainable CO_2 capture option that can add value to a waste being also affordable to be used in post-combustion process. However, the sorbents should be further tested under more representative post-combustion conditions.

Acknowledgments

This work was performed in cooperation with Hewlett-Packard Brasil Ltda. (PROFACC 2016) using incentives of Brazilian Informatics Law (Law no. 8.2.48 of 1991). The authors would like to thank Cooperativa Arrozeira Extremo Sul Ltda. for donating the rice husk, Sandra Einloft thanks CNPq for research scholarship. Franciele L. Bernard thanks Hewlett-Packard Brasil Ltda. for scholarship.

References

[1] K. Sumida, D.L. Rogow, J.A. Mason, T.M. McDonald, E.D. Bloch, Z.R. Herm, T. Bae, J.R. Long, Carbon dioxide capture in metal organic frameworks, Chem. Rev. 112 (2012) 724–781.
[2] M. Sarmah, B.P. Baruah, P. Khare, A comparison between CO_2 capturing capacities of fly ash based composites of MEA/DMA and DEA/DMA, Fuel Process. Technol. 106 (2013) 490–497.
[3] J.M. Ketzer, R.S. Iglesias, S. Einloft, Reducing greenhouse gas emission with CO_2 capture and geological storage(Org.) in: W. Chen, J. Seiner, T. Suzuki, M. Lackner (Eds.), Handbook of Climate Change Mitigation, 1, Springer Science + Business Media, New York 2012, pp. 1405–1440.
[4] B. Ali, B. Si Ali, R. Yusoff, M.K. Aroua, Carbon steel corrosion behaviors in carbonated aqueous mixtures of monoethanolamine and 1-n-butyl-3-methylimidazolium tetrafluoroborate, Int. J. Electrochem. Sci. 7 (2012) 3835–3853.
[5] S.D. Kenarsari, D. Yang, G. Jiang, S. Zhang, J. Wang, A.G. Russell, Q. Wei, M. Fan, Review of recent advances in carbon dioxide separation and capture, RSC Adv. 3 (2013) 22739–22773.
[6] M. Koei, Ionic Liquids in Chemical Analysis, CRC Press, 2009.
[7] M.W. Arshad, CO_2 Capture Using Ionic Liquids, Department of Chemical and Biochemical Engineering Technical, University of Denmark, Denmark, 2009 (148 pp.).
[8] L. Li, N. Zhao, W. Wei, Y. Sun, A review of research progress on CO_2 capture, storage, and utilization in Chinese Academy of Sciences, Fuel 108 (2013) 112–130.
[9] M. Ramdin, T.W. Loos, T.J.H. Vlugt, State-of-the-art of CO_2 capture with ionic liquids, Ind. Eng. Chem. Res. 51 (2012) 8149–8177.
[10] M.E. Boot-Handford, J.C. Abanades, E.J. Anthony, M.J. Blunt, S. Brandani, N. Mac Dowell, J.R. Fernández, M.C. Ferrari, R. Gross, J.P. Hallett, R.S. Haszeldine, P. Heptonstall, A. Lyngfelt, Z. Makuch, E. Mangano, R.T.J. Porter, M. Pourkashanian, G.T. Rochelle, N. Shah, J.G. Yaoa, P.S. Fennell, Carbon capture and storage update, Energy Environ. Sci. 7 (2014) 130–189.
[11] A. Ahmady, M. Ali Hashim, M.K. Aroua, Absorption of carbon dioxide in the aqueous mixtures of methyldiethanolamine with three types of imidazolium-based ionic liquids, Fluid Phase Equilib. 309 (2011) 76–82.
[12] S. Kumar, J. Hyun Cho, L. Moon, Ionic liquid-amine blends and CO_2BOLs: prospective solvents for natural gas sweetening and CO_2 capture technology—a review, Int. J. Greenhouse Gas Control 20 (2014) 87–116.
[13] A.S. Aquino, F.L. Bernard, J.V. Borges, L. Mafra, F. Dalla Vecchia, M.O. Vieira, R. Ligabue, M. Seferin, Vitaly V. Chaban, E.J. Cabrita, S. Einloft, Rationalizing the role of the anion in CO_2 capture and conversion using imidazolium-based ionic liquid modified mesoporous silica, RSC Adv. 5 (2015) 64220.
[14] M.M. Wan, H.Y. Zhu, Y.Y. Li, J. Ma, S. Liu, J.H. Zhu, Novel CO_2-capture derived from the basic ionic liquids orientated on mesoporous materials, ACS Appl. Mater. Interfaces 6 (2014) 12947–12955.
[15] M. Kacem, M. Pellerano, A. Delebarre, Pressure swing adsorption for CO_2/N_2 and CO_2/CH_4 separation: Comparison between activated carbons and zeolites performances, Fuel Process. Technol. 138 (2015) 271–283.
[16] A. Erto, A. Silvestre-Albero, J. Silvestre-Albero, F. Rodríguez-Reinoso, M. Balsamo, A. Lancia, F. Montagnaro, Carbon-supported ionic liquids as innovative adsorbents for CO_2 separation from synthetic flue-gas, J. Colloid Interface Sci. 448 (2015) 41–50.
[17] J.D. Carruthers, M.A. Petruska, E.A. Sturm, S.M. Wilson, Molecular sieve carbons for CO_2 capture, Microporous Mesoporous Mater. 154 (2011) 62–67.
[18] T.O. Magalhães, A.S. Aquino, F. Dalla Vecchia, F.L. Bernard, M. Seferin, S.C. Menezes, R. Ligabue, S. Einloft, Syntheses and characterization of new poly(ionic liquid)s designed for CO_2 capture, RSC Adv. 4 (2014) 18164–18170.
[19] G. Yu, Q. Li, N. Li, Z. Man, C. Pu, C. Asumana, X. Chen, Synthesis of new crosslinked porous ammonium-based poly(ionic liquid) and application in CO_2 adsorption, Polym. Eng. Sci. 54 (2014) 59–63.
[20] S. Zulfiqar, M.I. Sarwar, D. Mecerreyes, Polymeric ionic liquids for CO_2 capture and separation: potential, progress and challenges, Polym. Chem. 6 (2015) 6435–6451.
[21] Y. Zeng, R. Zou, Y. ZhaoCovalent, Organic frameworks for CO_2 capture, Adv. Mater. 1-19 (2016).
[22] G.E. Romanos, P.S. Schulz, M. Bahlmann, P. Wasserscheid, A. Sapalidis, F.K. Katsaros, C.P. Athanasekou, K. Beltsios, N.K. Kanellopoulos, CO_2 capture by novel supported ionic liquid phase systems consisting of silica nanoparticles encapsulating amine-functionalized ionic liquids, J. Phys. Chem. C 118 (2014) 24437–24451.
[23] C. Gebald, J.A. Wurzbacher, P. Tingaut, T. Zimmermann, A. Steinfeld, Amine-based nanofibrillated cellulose as adsorbent for CO_2 capture from air, Environ. Sci. Technol. 45 (2011) 9101–9108.
[24] P. de Cuadro, T. Belt, K.S. Kontturi, M. Reza, E. Kontturi, T. Vuorinen, M. Hughes, Cross-linking of cellulose and poly(ethylene glycol) with citric acid, React. Funct. Polym. 90 (2015) 21–24.
[25] N. Johar, I. Ahmad, A. Dufresne, Extraction, preparation and characterization of cellulose fibers and nanocrystals from rice husk, Ind. Crop. Prod. 37 (2012) 93–99.
[26] USDA - United States Department of Agriculture, Foreign agricultural service reports, http://apps.fas.usda.gov2015 (accessed 11.01.16).
[27] S.M.L. Rosa, N. Rehman, M.I.G. de Miranda, S.M.B. Nachtigall, C.I.D. Bica, Chlorine-free extraction of cellulose from rice husk and whisker isolation, Carbohydr. Polym. 87 (2012) 1131–1138.
[28] T. Welton, Room-temperature ionic liquids. Solvents for synthesis and catalysis, Chem. Rev. 99 (1999) 2071–2084.
[29] N. Jain, A. Kumar, S. Chauhan, S.M.S. Chauhan, Chemical and biochemical transformations in ionic liquids, Tetrahedron 61 (2005) 1015–1060.
[30] P. Wasserscheid, T. Welton, In Ionic Liquids in Synthesis, eds.; WILEY-VCH: Weinheim, 2008, ch.1.
[31] K.B.R. Teodoro, E.M. Teixeira, A.C. Corrêa, A. Campos, J.M. Marconcini, L.H.C. Mattoso, Whiskers de fibra de sisal obtidos sob diferentes condições de hidrólise ácida: efeito do tempo e da temperatura de extração, Polímeros 21 (2011) 280–285.
[32] R.F. Rodrigues, R.L. Trevenzoli, L.R.G. Santos, V.A. Leão, V.R. Botaro, Heavy Metals Sorption on Treated Wood Sawdust, Eng. Sanit. Ambient. Rio de Janeiro, 2006.
[33] B. Zhu, T. Fan, D. Zhang, Adsorption of copper ions from aqueous solution by citric acid modified soybean straw, J. Hazard. Mater. 153 (2008) 300–308.
[34] O. Karnitz, L.V.A. Gurgel, J.C.P. De Melo, V.R. Botaro, T.M.S. Melo, R.P.F. Gil, L.F. Gil, Adsorption of heavy metal ion from aqueous single metal solution by chemically modified sugarcane bagasse, Bioresour. Technol. 98 (2007) 1291–1297.
[35] L.V.A. Gurgel, O.K. Júnior, R.P. de Freitas Gil, L.F. Gil, Adsorption of Cu (II), Cd (II), and Pb (II) from aqueous single metal solutions by cellulose and mercerized cellulose chemically modified with succinic anhydride, Bioresour. Technol. 99 (2008) 3077–3083.
[36] L. Segal, L. Creely, A.E. Martin, C.M. Conrad, An empirical method for estimating the degree of crystallinity of native cellulose using X-ray diffractometer, Text. Res. J. 29 (1959) 786–794.
[37] A.D. Becke, Density-functional exchange-energy approximation with correct asymptotic-behavior, Phys. Rev. A 38 (1988) 3098–3100.
[38] C.T. Lee, W.T. Yang, R.G. Parr, Development of the Colle-Salvetti correlation-energy formula into a functional of the electron-density, Phys. Rev. B 37 (1988) 785–789.
[39] A. Blasig, J. Tang, X. Hu, Y. Shen, M. Radosz, Magnetic suspension balance study of carbon dioxide solubility in ammonium-based polymerized ionic liquids: Poly(p-vinylbenzyltrimethyl ammonium tetrafluoroborate) and poly([2-(methacryloyloxy)ethyl] trimethyl ammonium tetrafluoroborate), Fluid Phase Equilib. 256 (2007) 75–80.
[40] F. Dreisbach, H.W. Lösch, Magnetic suspension balance for simultaneous measurement of a sample and the density of the measuring fluid, J. Therm. Anal. Calorim. 62 (2000) 515–521.
[41] F. Dreisbach, W.H. Lösch, P. Harting, Highest pressure adsorption equilibria data: measurement with magnetic suspension balance and analysis with a new adsorbent/adsorbate-volume, Adsorption 8 (2002) 95–109.
[42] F. Gellerested, P. Gatenholm, Surface properties of lignocellulosic fibers bearing carboxylic groups, Cellulose 6 (1999) 103–121.
[43] H.S. Altundoğana, A. Topdemira, M. Çakmakb, N. Baha, Hardness removal from waters by using citric acid modified pine cone, J. Taiwan Inst. Chem. Eng. 58 (2016) 219–225.
[44] I. Bahadur, K. Osman, C. Coquelet, P. Naidoo, D. Ramjugernath, Solubilities of carbon dioxide and oxygen in the ionic liquids methyl trioctyl ammonium bis(trifluoromethylsulfonyl)imide, 1-butyl-3-methyl imidazolium bis (trifluoromethylsulfonyl)imide, and 1-butyl-3-methyl imidazolium methyl sulfate, J. Phys. Chem. B 119 (2015) 1503–1514.
[45] R. Ishizuka, N. Matubayasi, K.M. Tu, Y. Umebayashi, Energetic contributions from the cation and anion to the stability of carbon dioxide dissolved in imidazolium-based ionic liquids, J. Phys. Chem. B 119 (2015) 1579–1587.
[46] Y. Li, W.J. Huang, D.X. Zheng, Y. Mi, L. Dong, Solubilities of CO_2 capture absorbents 2-ethoxyethyl ether, 2-butoxyethyl acetate and 2-(2-ethoxyethoxy)ethyl acetate, Fluid Phase Equilib. 370 (2014) 1–7.
[47] A. Kaithwas, M. Prasad, A. Kulshreshtha, S. Verma, Industrial wastes derived solid adsorbents for CO_2 capture: a mini review, Chem. Eng. Res. Des. 90 (2012) 1632–1641.
[48] M.M. Maroto-Valer, Z. Lu, Y. Zhang, Z. Tang, Sorbents for CO_2 capture from high carbon fly ashes, Waste Manag. 28 (2008) 2320–2328.

4.4. Capítulo IV: Poli (líquidos iônicos) catiônicos base celulose

O artigo intitulado "*Cellulose based poly(ionic liquids): Tuning cation-anion interaction to improve carbon dioxide sorption*" submetido a Fuel (comprovante de submissão Anexo B), descrito neste capitulo apresenta a produção de PLIs catiônicos a partir da celulose extraída da casca de arroz. Foi investigado o efeito da combinação de dois cátions (imidazólio e o amónio) com quatro diferentes contra – ânions (([Cl^-], [BF_4^-], [PF_6^-] ou [Tf_2N^-]). Os PLIs sintetizadas foram caracterizados por RMN, XPS, FTIR, TGA e MEV-FEG. A capacidade de sorção de CO_2 avaliada pela técnica de decaimento da pressão a 298,15 K e pressões de 0,1 - 3,0 Mpa. A capacidade de sorção/dessorção também foi investigada. A coordenação competitiva átomo-átomo foi investigada por simulação PM7-MD. Os PLIs sintetizados mostraram boa estabilidade térmica e uma elevada capacidade de sorção de CO_2 influenciada diretamente pelo contra-ânion. O maior valor de sorção foi encontrado para PIL [$CelEt_3N$] [PF_6] (38 mg / g a 0,1 MPa e 168 mg / g a 3 MPa a 298,15 K). Os ciclos de sorção/dessorção de CO_2 evidenciaram a estabilidade destes materiais durante o processo de sorção de CO_2.

Cellulose based poly(ionic liquids): Tuning cation-anion interaction to improve carbon dioxide sorption

Franciele L. Bernard[a,b], Rafael B. Duczinski[a], Marisol F. Rojas[d], Maria Carolina C. Fialho[c], Luz Ángela Carreño[d], Vitaly V. Chaban[e] Felipe Dalla Vecchia[a,c] and Sandra Einloft[a,b*]

a) Post-Graduation Program in Materials Engineering and Technology. Pontifical Catholic University of Rio Grande do Sul – PUCRS.
b) School of Chemistry. Pontifical Catholic University of Rio Grande do Sul – PUCRS.
c) School of Engineering, Pontifical Catholic University of Rio Grande do Sul – PUCRS. Av. Ipiranga, 6681, Partenon, Porto Alegre Brazil, CEP: 90619-900.
d)School of Chemistry, Universidad Industrial de Santander, Street 9, 27 Bucaramanga, Colombia
e) Institute of Science and Technology (ICT), Federal University of São Paulo (UNIFESP); São José dos Campos, SP – Brazil.

** Corresponding author: einloft@pucrs.br*

Graphic Abstract

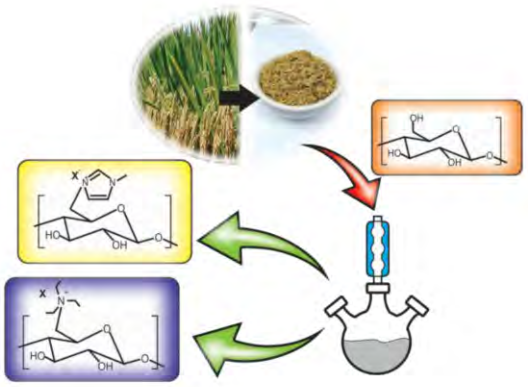

Abstract

Mitigation of climate change is an urgent agenda. Development of materials from agroindustrial residue to be used as sorbents for CO_2 capture is a significant goal to be achieved both for environmental protection and resource utilization. In this work, cationic cellulosic PILs using cellulose extracted from rice husk were synthesized. Imidazolium and ammonium were evaluated as cation combined with

different counter- anions ($[Cl]^-$, $[BF_4]^-$, $[PF_6]^-$ or $[Tf_2N]^-$). Synthesized PILs were characterized by NMR, XPS, DRX, FTIR, TGA and FESEM. Reusability and CO_2 sorption capacity were performed by pressure decay-technique. Competitive atom-atom coordination was investigated by PM7-MD simulations. PILs showed a high CO_2 sorption capacity directly influenced by anion. At 3 MPa of CO_2 pressure the sorption capacity increases in the following order for both cations $[Cl]^- < [BF_4]^- < [TF_2N]^- < [PF_6]^-$. Simulation results suggest that TF_2N blocks important CO_2 binding sites. The best sorption value was found for PIL $[CeIEt_3N][PF_6]$ of 38 mg/g at 0.1MPa and 168 mg/g at 3MPa at 298.15K.The recycling experiments of CO_2 sorption demonstrated a good reusability of synthesized PILs for CO_2 sorption.

1. Introduction

Carbon capture technologies emerge as one of the main strategies to reduce CO_2 emissions and mitigate the climate change effect[1–11]. Development of versatile materials for CO_2 separation from exhausted gases has become one of the main research niches in this area.[6,8,12,13]

Amines aqueous solutions stand out as the benchmark solvent for CO_2 separation from exhaust gases[14–19] and natural gas[14,15,17,20]. However the use of this solvents presents operational drawbacks such as high energy consumption in regeneration stage, corrosive products formation as well as additional operational costs due to solvents substitution as a consequence of degradation[14,16,18,19,21].

Poly (ionic liquids) or polymeric ionic liquids (PILs) have shown potential for CO_2 capture [11,20–24]. These functional polymers present an ionic liquid (IL) moiety on each repeated unit [8,12,22]. ILs polymerization resulted in increased CO_2 capture efficiency. PILs present higher CO_2 sorption capacity, faster sorption/ desorption kinetics once compared to ILs [27]. PILs synthesis is carried out following these main routes: IL monomers direct radical polymerization,

polycondensation and/or polymers modification [8,28,29]. Among these routes the latter is extremely attractive allowing the use of commercially available polymers [8,28,29].

Different PILs obtained via polycondensation and/or polymers modification has been reported as well as their use in CO_2 capture. Literature describe PILs based on polybenzimidazoles [29–31], polyimides [28], poly(ether ketone)s [32] and polyurethane [33–35].

Cellulose is a versatile low cost natural polymer.[36,37] The possibility of its structure undergo chemical modification by reaction with available hydroxyl groups allows its application in several areas [36–38]. World rice crop is estimated at 500 million tons per year. The rice husk is the main agroindustrial residue generated in this cereal processing [39,40]. The use of this residue as raw material source for extracting cellulose can contribute significantly to the environment protection. In addition, if used in PILs synthesis it may reduce waste generation and produce low cost sorbents [41].

We have recently reported the synthesis of cellulose based anionic PILs and their ability to capture CO_2[41]. PILs were obtained by chemical modification of cellulose fibers extracted from rice husk. Four different ionic liquids (IL) counter-cations were introduced (imidazolium, phosphonium, ammonium and pyrrolidinium) [41]. Cellulose based PILs were presented as a promising approach for CO_2 capture. Yet, counter-cation introduction into cellulose structure promoted increased CO_2 solubility and a completely reversible CO_2 sorption/desorption process. The best sorption result was obtained with ammonium as counter-cation (CL-TBA) [41].

A different approach was used to obtain cellulosic PILs in this work. Unlike our first work cationic cellulosic PILs were synthesized. PILs were obtained with imidazolium or ammonium cation, using different counter- anions ($[Cl^-]$, $[BF_4^-]$, $[PF_6^-]$ or $[Tf_2N^-]$). In addition, PM7-MD simulations were used to understand the competitive atom-atom coordination.

2. Experimental Section

2.1 Materials

Rice husk was donated by Cooperativa Arrozeira Extremo Sul Ltda. Sodium hydroxide (NaOH, 97% Vetec), hydrogen peroxide (H2O2, 35%, Neon), sulphuric acid (H_2SO_4, F.Maia, P.A), Thionyl chloride ($SOCl_2$, 99%, Aldrich), ammonium hydroxide solution (30-32%, Vetec) 1-Methylimidazole (Aldrich, 99.0%), Triethylamine (99%, Vetec), Lithium(I) bis(trifluoromethanesulfonyl)imide ($LiTf_2N$, 99%, Aldrich), Sodium tetrafluoroborate ($NaBF_4$, 98 %, Aldrich), Sodium hexafluorophosphate ($NaPF_6$, 98%, Aldrich) and N,N –dimethylformamide (DMF, 99.5%, Merck) were used as received

2.2 Cellulose extraction and modification

Cellulose fibers extraction procedure from rice husk was adapted from literature [42,43]. Fibers were obtained by submitting rice husk to alkali (NaOH) and acid (H_2SO_4) treatments followed by bleaching (H_2O_2/ NaOH). Cellulose extraction details are well reported elsewhere.[41]

Cellulosic based Poly (ionic liquid)s (PILs) syntheses were performed in a three step process as shown in Figure 1. The experimental procedure was based on literature.[44–47] Initially, cellulose was chemically modified with $SOCl_2$ to obtain chlorinated cellulose (6-chloro-6-deoxycellulose, CDC) (Figure 1a). A sample of 10 g of cellulose fiber was suspended in DMF (200 mL) followed by the slow addition of 35 mL of thionyl chloride ($SOCl_2$) at 80°C under mechanical stirring. After the addition was complete, the reaction was kept for 2.5 h at 90 °C. The viscous solution was cooled to room temperature and poured into iced water (500 mL) under stirring. The precipitated (CDC) was treated with several aliquots of ammonium hydroxide solution and washed with water to bring the pH to neutral. The CDC was then separated by filtration and dried under vacuum at 60°C. In the next step, a sample of CDC (4g) was reacted with 40 mL of 1-Methylimidazole (at 100°C) or Triethylamine (at 80°C) and kept under stirring for 24 h. The cellulose

based PILs ([Celmim][Cl] or [CelEt$_3$N][Cl]) obtained from this reaction were precipitated using methanol and then dried under vacuum at 60 °C. Finally, to exchange chloride from ([Celmim][Cl] or [CelEt$_3$N]][Cl]) by another anion, lithium or sodium salt of the corresponding anion was used. The ion exchange step was performed at room temperature with stirring for 24 h using saturated solution of LiTf$_2$N, NaBF$_4$ or NaPF$_6$ (Figure 1b).

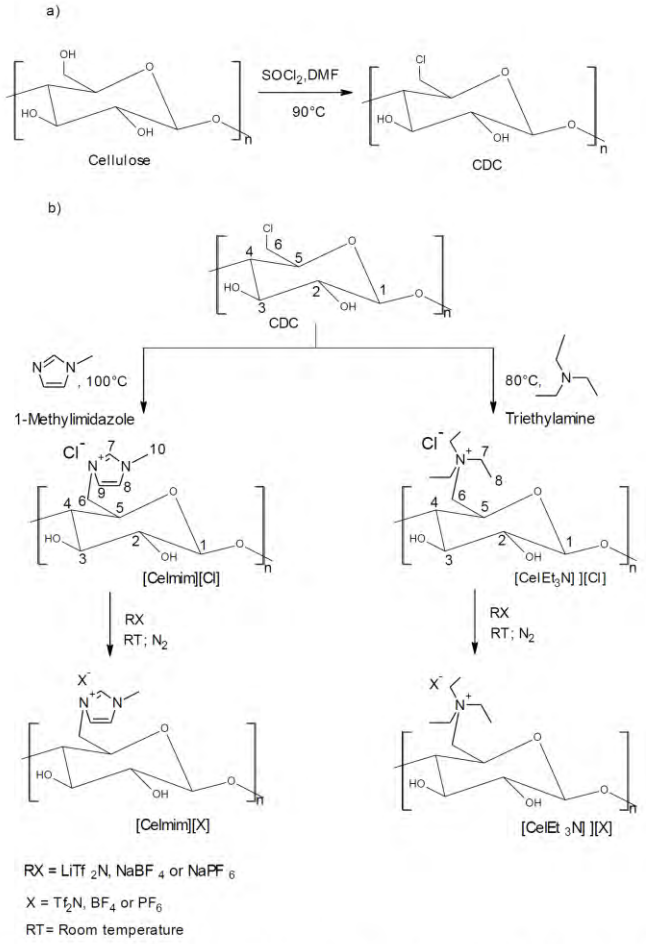

Figure 1. Synthesis steps and proposed structures of obtained materials: (a) 6-chloro-6-deoxycellulose (CDC); (b) Cellulosic poly (ionic liquids).

2.3 Characterization

The synthesized materials were characterized by Universal Attenuated Total Reflectance sensor (UATR-FTIR) using Perkin-Elmer 100 FTIR Spectrum, 4000-650 cm^{-1} range. The solid-state ^{13}C NMR spectra were obtained by Bruker Avance DRX-400 spectrometer at 400 MHz. Field emission scanning electron microscopy (FESEM) analyses were performed by FEI Inspect F50 equipment in secondary electrons (SE) mode. Thermogravimetric Analysis (TGA) was performed using TA Instruments SDT-Q600 between 25 and 500°C with a heating rate of 10°C/min in a nitrogen atmosphere. Powder X-ray diffraction (XRD) pattern was recorded by Bruker-AXS D8 ADVANCE diffractometer operated at 40 kV voltage and 20 mA current using Cu Kα radiation (λ = 1.5406 Å), 3 ~ 40° range with 0.02 step and 1.0 min scanning time. To evaluate the surface composition of the cellulosic poly (ionic liquids), survey scans were carried out by XPS/ISS/UPS-ACenteno surface characterization platform built by SPECS (Germany). The platform is equipped with PHOIBOS 150 2D-DLD energy analyzer. A monochromatic Al Kα X-ray source (FOCUS 500) operated at 200 W was used for measurements. The pass-through energy of the hemispherical analyzer was set at 100 eV for the general spectra and 60 eV for high resolution spectra. The surface charge compensation was monitored with a Flood Gun device (FG 15/40-PS FG500) operated at 58 μA and 2 eV. High-resolution spectra of the elements found were recorded for quantification, CasaXPS software was used for spectral analysis and curve fitting using C-C signal position at 285 eV as reference [47–49].

2.4 Sorption measurements

CO_2 sorption capacity was assessed by pressure-decay technique at 298,15 K and 0.1-3 MPa using a dual-chamber gas sorption cell [50]. Operation of such device was reported elsewhere [51,52]. Samples (W_s = 1.0-1.5 g) were weighted, moved to sorption chamber and subjected to 10^{-3} mbar vacuum at 298.15°C during 1 h. CO_2 (air liquid/99.998%) was

carried out into reservoir at desired pressure and allowed to enter the sorption chamber.

Gas sorption at equilibrium was determined from the difference between the initial and final number of moles of gas using Eqs. 1-2, respectively. The gas mass adsorbed in the sample is denoted as $W_{CO2/g}$

$$n_{CO_2} = \frac{p_i V gc}{Z_{(Pi,Ti)} R.T_i} - \frac{p_{eq}(Vt - V_p)}{Z_{(Peq,Teq)} RT_{eq}}, \quad (1)$$

$$w_{CO_2/g} = \frac{n_{CO2} M}{Ws}, \quad (2)$$

where V_{gc} is volume of the gas chamber, p_i and T_i are pressure and temperature in the gas chamber, p_{eq} and T_{eq} are pressure and temperature at equilibrium. V_c is total volume of the sorption cell, Z is compressibility factor for the pure gas calculated by the Span-Wagner equations-of-state for CO_2 (Equation: converging the fluid region at the triple-point temperature up to 1100K at pressures up to 800 MPa).[53]

2.5 Computer simulations

Semi-empirical molecular dynamics simulations, PM7-MD,[54–62] were employed to investigate atom-atom coordination. The wave function convergence criterion was set to 10-7 Hartree with the Slater basis set. The equations-of-motion were propagated with a time-step of 0.5 fs during 4.0 ns for each system, of which first 0.5 ns were disregarded as equilibration. Equilibration was controlled by simultaneous monitoring of thermodynamic and structure properties. All simulated systems were maintained at 300 K by means of Andersen thermostat.[63] The simulated systems consisted of 2 to 8 monomers (Figure 1) and no qualitative dependence of the structure distributions on the system size was identified. Empirical corrections for van der Waals interactions and hydrogen bonding interactions were applied on-the-fly.[54,64,65] PM7-MD simulations were extensively used before, including for the CO_2 capture problems,[55–57] and provided satisfactory to excellent correspondence with the experimental results.

Gabedit 2.8,[66] Packmol,[67] and VMD 191 [68] were used as supplementary utilities. All other operations were performed in the software developed by V.V.C.

3. Results and discussion

Structures of 6-chloro-6-deoxycellulose CDC, [Celmim] [Cl] and [CelEt$_3$N] [Cl] synthesized materials were confirmed by ^{13}CNMR (Figure 2), XPS analysis (Figure 3) and UATR-FTIR (Figure 4).

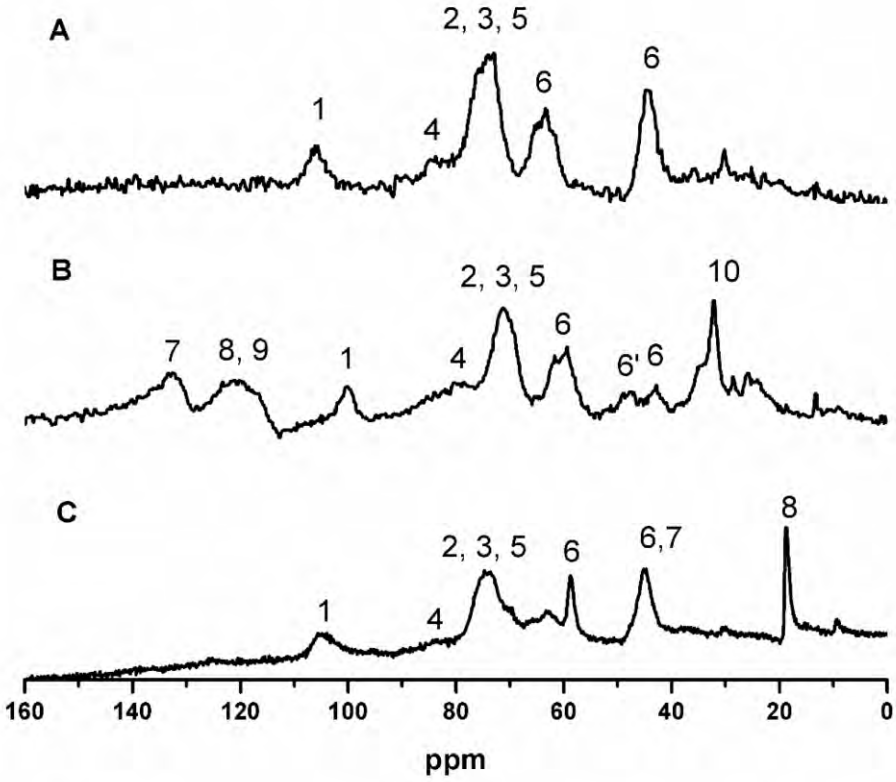

Figure 2.^{13}C NMR spectra of CDC (A), [Celmim][Cl](B) and[CelEt$_3$N][Cl](C) .

Resonance signals shown in Figure 2 and their assignments were compared to literature[44] and to starting materials spectra using the Spectral Database for Organic Compounds (SDBS)[69]. The six carbons atoms of CDC presented peaks

showed in spectrum: carbon 1 (O-C-O) at 105 ppm, carbon 4 (C-O) at 83 ppm, carbons 2, 3 e 5 (secondary carbons bonded to -CH or –OH) at 73 ppm are in overlay. For carbon 6 two peaks were revealed at 63 ppm, attributed to primary carbon bonded to –OH and at 44 ppm attributed to partial exchange of –OH group by Cl. Formation of [Celmim][Cl] was confirmed at 50 ppm peak attributed to the partial replacement of Cl group by the imidazole cation at carbon 6. Imidazolium was detected by the following peaks: carbon 7 was revealed at 142 ppm (NCN); carbon 8 and 9 at 127 ppm (CH-CH-N) and carbon 10 at 34 ppm (CH_3N). For [CelN222][Cl] sample a new peak at 18 ppm (CH_3-CH_2-N) and also the increase in peak intensity at 44 ppm indicating the overlap of carbon 6 (CH_2-N or CH_2-Cl) with carbon 7 (CH_2-N of triethylamine) was observed.

Surface composition analysis confirms that cellulosic poly (ionic liquids) were obtained. Survey spectra of cellulose and cellulosic PILs are shown in Figure 3. Their elemental composition and elements ratio are shown in Table 1. The calculated elements ratio obtained from the proposed structure are also shown. The cellulose extracted is not completely pure, since the C/O ratio is higher than the theoretical value [47], probably due to residual lignin, hemicellulose, wax and other impurities [42,48]. In chlorinated cellulose (CDC), the C/O ratio decreased showing that impurities were removed from surface in the treatment with $SOCl_2$/DMF. A small amount of sulfur impurities and a chlorine excess from $SOCl_2$ is observed both in CDC and in cellulosic PILs. In some of these, Si impurities come from de SiO_2 of rice husk[70] and the Na from $NaBF_4$ salt. In cellulosic PILs the ratio C/N is higher than the calculated, showing that probably the reaction with 1-methylimidazole and triethylamine was not given on all halogenated carbons. In cellulosic PILs the presence of the atoms from the ILs anions is observed. However, the C/F, C/P, C/B and C/S ratio were higher than expected because, as discussed previously, there is a smaller amount of available cations than projected. From deconvoluted high resolution carbon C 1s and Cl 2p spectra the relative amounts of carbon bond types were calculated and the organically bound chlorine and inorganic chloride were differentiate [71]; the results are shown in Table 2. The cellulose C 1s spectrum showed three signals at 285.0, 286.7, 288.0 and 289.9 eV,

assigned as C1 (C-C, C-H mainly from lignin), C2 (C-O, C-OH from cellulose), C3 (O-C-O, C=O from either cellulose or lignin) and C4 (O=C-O), respectively [48,49,71,72]. A high percentage of C1 was found, which confirms lignin presence [48,71,73]. For the CDC, the amount of C1 decreases, confirming impurities removal. In CDC and cellulosic PILs it was not possible to differentiate other carbon types as they appear at binding energies similar to those of cellulose, which is in greater proportion[74]. It is possible to observe for [CeImim][Tf_2N] and [$CeIEt_3N$] [Tf_2N] a signal C5 at 293 eV corresponding to C-F_3 of the anion [75]. However, for [$CeIEt_3N$] [Tf_2N] this signal has a low intensity related to the lower amount of fluoride found on this one. In the CDC Cl 2p spectrum we found a high amount of organically bound chlorine at 200 eV and a low amount of inorganic chloride, whereas in all cellulosic PILs spectra the organically bound chlorine decreases considerably, even to zero for [$CeIEt_3N$][BF_4], and an inorganic chloride at 198 eV was predominant [71]. This confirms that ion exchange did not took place in all halogenated carbons and that excess chlorine is due to inorganic chlorine. N 1s and S 2p High-resolution spectra for [CeImim][Tf_2N] and [$CeIEt_3N$] [Tf_2N] allowed to identify clearly the nitrogen from the cation (at 400.1 eV) and from the anion (at 397.6 eV), as well as the sulfur of the anion (at 167.2 eV) and from the impurity (at 162.3 eV) [76,77].

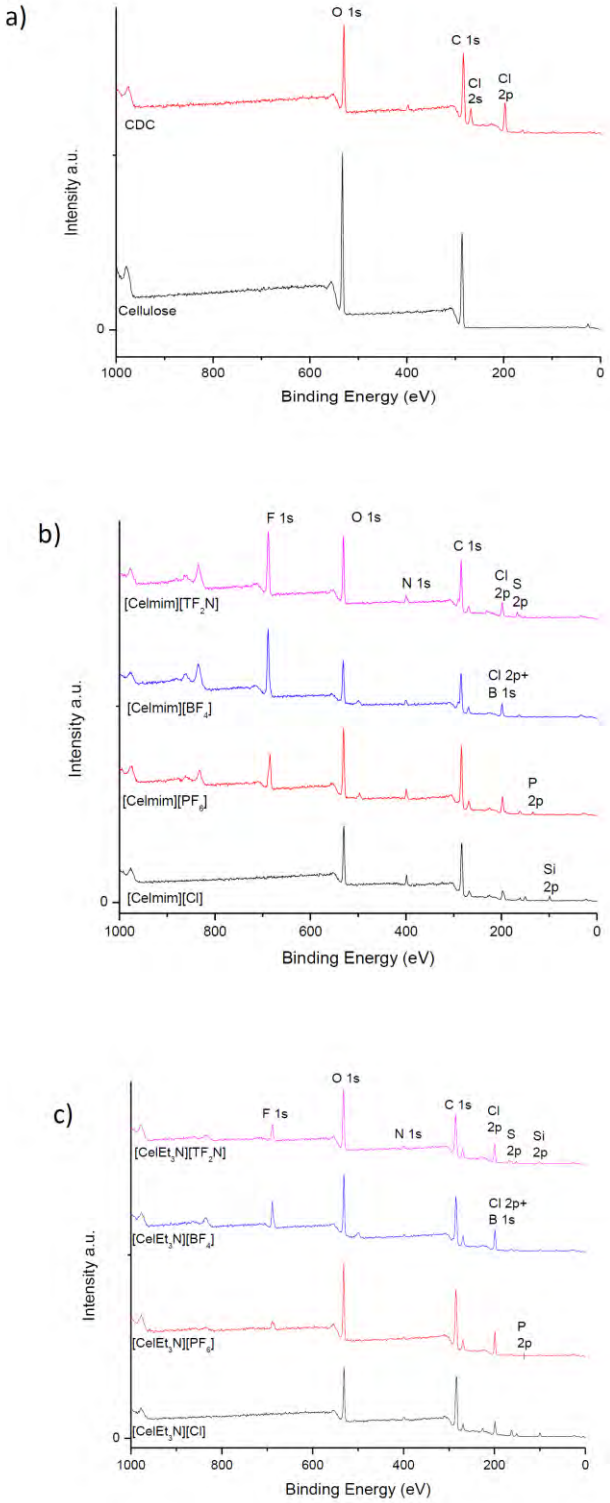

Figure 3. Survey spectra of cellulose and CDC(a), and cellulosic PILs with cation [Celmim] (b) and [CelEt$_3$N] (c).

Table 1. Surface composition and element ratio of cellulose and cellulosic PILs from survey XPS spectra.

Sample	Surface composition (at.%)										Element ratio[a]													
	C	O	N	Cl	F	S	P	B	Na	Si	C/O		C/N		C/Cl		C/F		C/P		C/B		C/S	
											exp	cal	exp	cal	exp	cal	exp	cal	exp	cal	exp	cal	exp	cal
Cellulose	64.5	35.5									1.8	1.2												
CDC	40.4	39.7	2.4	15.8		2.1					1.0	1.5			2.6	6.0								
[Celmim][Cl]	41.4	38.4	6.3	8.8		2.2				3.0	1.1	2.5	6.6	5.0	4.7	10								
[Celmim][PF_6]	51.4	22.2	4.9	5.4	11.8	1.6	1.5		1.1		2.3	2.5	10.5	5.0	9.5	--	4.4	1.7	34.1	10.0				
[Celmim][TF_2N]	26.4	28.1	3.5	5.9	32.7	3.4					0.9	1.5	7.5	4.0	4.5	--	0.8	2.0					7.9	6.0
[Celmim][BF_4]	44.6	16.4	2.7	10.9	22.7	0.9		0.5	1.3		2.7	2.5	16.3	5.0	4.1	--	2.0	2.5			87.1	10.0		
[$CelEt_3N$][Cl]	65.3	20.2	2.2	5.6		3.2				3.4	3.2	3.0	29.3	12.0	11.6	12.0								
[$CelEt_3N$][PF_6]	62.0	25.2	1.3	7.1	3.5	0.7	0.3				2.5	3.0	49.2	12.0	8.7	--	17.6	2.0	213.6	12.0				
[$CelEt_3N$][TF_2N]	55.4	27.7	2.3	5.1	5.3	2.5				1.7	2.0	1.8	23.8	7.0	10.9	--	10.4	2.3					10.4	7.0
[$CelEt_3N$][BF_4]	50.4	21.4	1.2	16.4	7.9	1.1		0.6		1.0	2.3	3.0	40.9	12.0	3.1	--	6.4	3.0			83.9	12.0		

[a] Calculated elements ratio obtained from the proposed structure

Table 2. Carbon type and chlorine percentages in cellulose and cellulosic PILs from high resolution XPS spectra.

Sample	Carbon type composition (at. %)					Chlorine (at. %)	
	C1	C2	C3	C4	C5	Cl 1	Cl 2
Cellulose	28.5	57.3	11.3	2.9		--	--
CDC	17.9	40.7	32.5	8.9		28.4	71.6
[Celmim][Cl]	27.1	48.0	22.9	2.0		74.7	25.3
[Celmim][PF_6]	14.4	59.6	26.0	ND		64.5	35.6
[Celmim][TF_2N]	12.9	65.4	10.0	ND	11.7	64.5	35.5
[Celmim][BF_4]	21.7	53.9	12.4	ND	11.9	74.6	25.4
[CelEt$_3$N][Cl]	45.0	36.6	15.0	3.4		66.3	33.7
[CelEt$_3$N][PF_6]	21.9	43.8	28.7	5.5		66.6	33.4
[CelEt$_3$N][TF_2N]	28.3	28.2	39.7	3.8		69.1	30.9
[CelEt$_3$N][BF_4]	14.8	48.8	31.7	3.3	1.4	100.0	0.0

C1 (C-C, C-H), C2 (C-O, C-OH), C3 (O-C-O, C=O), C4 (O=C-O), C5 (C-F_3), Cl 1 (inorganic chloride), Cl 2 (organically bound chlorine).

Typical infrared spectra of cellulose, chlorinated cellulose (CDC), [Celmim][Cl] and [CelEt$_3$N][Cl] are shown in Figure 4. IR spectra of all samples exhibited characteristic bands of cellulose structure: 3330 - 3340 cm^{-1} (stretching of –OH groups), 2920 cm^{-1} (C–H stretching vibrations), 1369 cm^{-1} (C-H bending), 1160 cm^{-1} (C–O–C asymmetrical bridge stretching), 1050 cm^{-1} (C-O stretching vibration) and 890 cm^{-1} (C-H stretching vibration). [42,78,79]. Yet, the appearance of a band near 1640 cm^{-1} corresponding to C=C stretching of aromatic rings, attributed to lignin and a band around 1700-1725 cm^{-1} attributed to ester and acetyl groups in residual hemicellulose [42,78,79] was observed corroborating XPS findings.

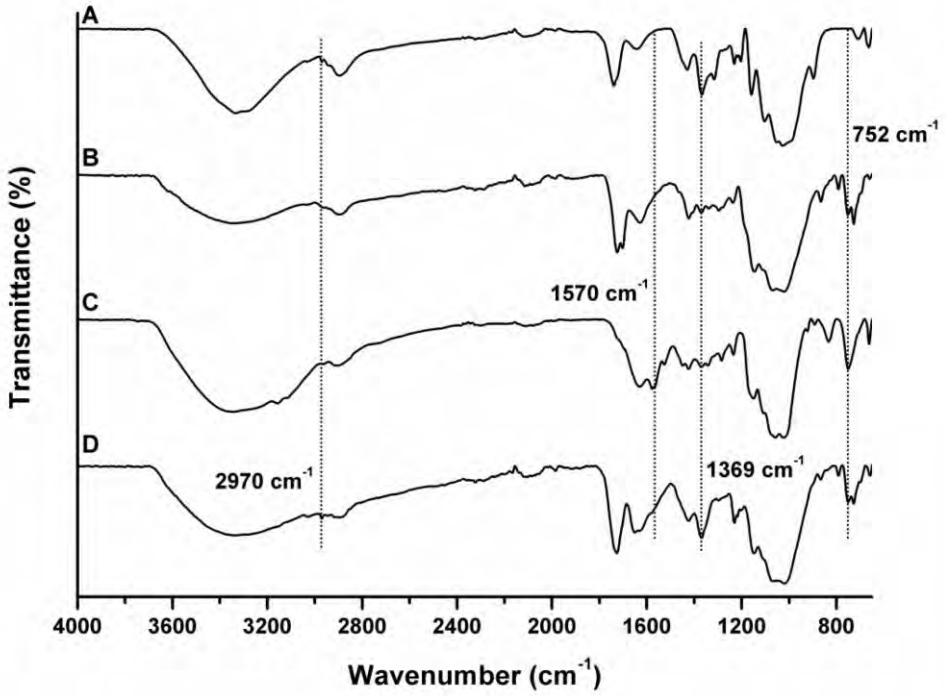

Figure 4. FT-IR spectra of the materials: (a) cellulose, (b) CDC, (c) [Celmim][Cl] and (d) [CelEt$_3$N][Cl].

New bands were observed after the cellulose chemical modification (Figure 4). The CDC spectrum (Figure 4b) showed the appearance of two new bands near 752 e 723 cm^{-1} related to stretching vibration of C-Cl bond [44–46]. The C-Cl appearing in CDC was also confirmed by XPS and ^{13}CNMR analysis. The spectrum obtained for imidazole based PILs revealed bands at 1570 cm^{-1} and 1060 cm^{-1} attributed to C=C stretching and C–N of imidazolium ring, respectively (Figure 4c).[44] For ammonium based PILs one can observe peaks intensification at 1369 cm^{-1} (C-H bending), 2970 (C–H stretching of -CH_2) and 2940 cm^{-1} (C–H stretching of -CH_3) associated to ammonium cation alkyl chains[69] (Figure 4d). The exchange of $[Cl]^-$ anion for $[PF_6]^-$ or $[Tf_2N]^-$ provided the appearance of new bands: near to 840 cm^{-1} attributed to hexafluorophosphate anion[80,81], around 790 cm^{-1} (C–S) and 846 cm^{-1} (N–S) attributed to (trifluoromethanesulfonyl) imide anion[34]. The band near to 1050 cm^{-1} of tetrafluoroborate anion $[BF_4]^-$ [81] is in overlay with the band of C-H of cellulose structure.

Structural level changes may be assessed by X-ray diffraction (Figure 5 and 6). Figure 5 shows the diffractograms for cellulose extracted from rice husk (a), CDC (b) and cellulosic PILs [Celmim][Cl] (c) and [CelEt_3N][Cl] (d). Cellulose showed typical peaks of microcrystalline cellulose around 2θ = 16°, 22.6° and 35° [42,44]. Changes in X-ray diffractograms profile for all samples were observed after functionalization (Figure 6). This behavior was also verified by Chen et al., 2015 [44]. Drastic crystallinity reductions were observed after cellulose functionalization (Figure 6). This indicates that cellulosic based PLIs and CDC have an amorphous structure [44].

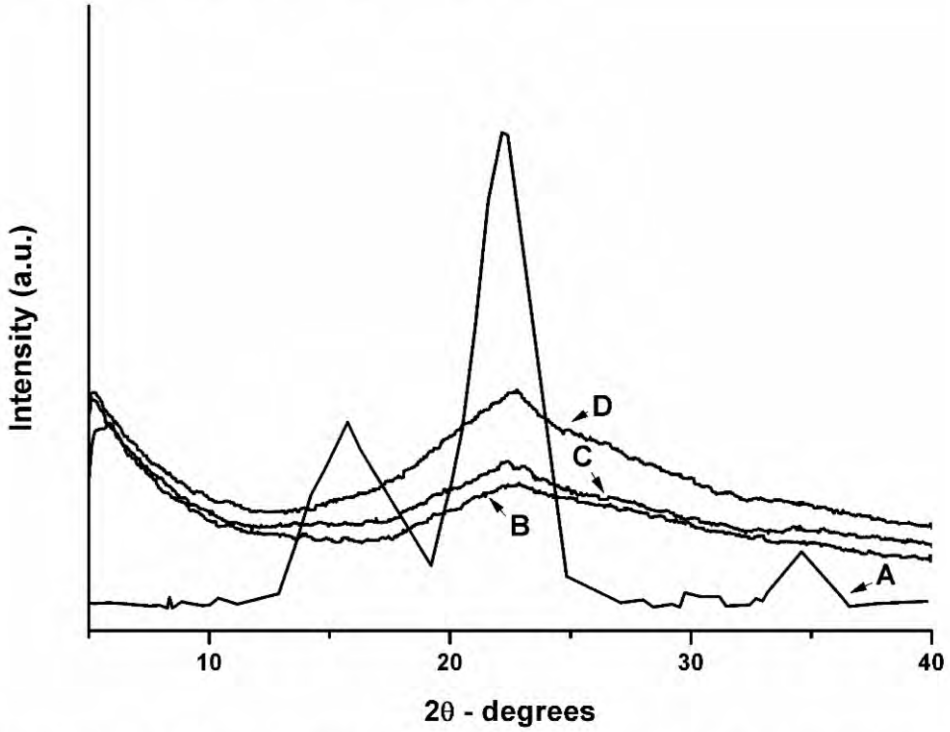

Figure. 5. XRD pattern of cellulose and modified cellulose samples: (a) cellulose, (b) CDC, (c) [CelEt_3N][Cl] and (d) [Celmim][Cl].

The effect of cation side chain size and anion type on structural conformation of cellulosic PILs may be seen in Figure 5 and 6. It may be highlighted that the longer the side chain size of the inserted cation, the lower is the crystalline peak intensity. PIL [CelEt_3N][Cl] evidenced lower crystalline peak intensity once compared to [Celmim][Cl] (Figure 5). When

the $[Cl]^-$ anion exchange was performed by $[BF_4]^-$, $[PF_6]^-$ or $[Tf_2N]^-$, a distinct behavior was evidenced for the different cations (Figure 6). Insertion of larger anions to $[Celmim]^+$ further reduced the packaging degree of molecules, whereas for $[CelEt_3N]^+$ cation the insertion of larger anions seems to contribute to a more ordered assembly (Figure 6).

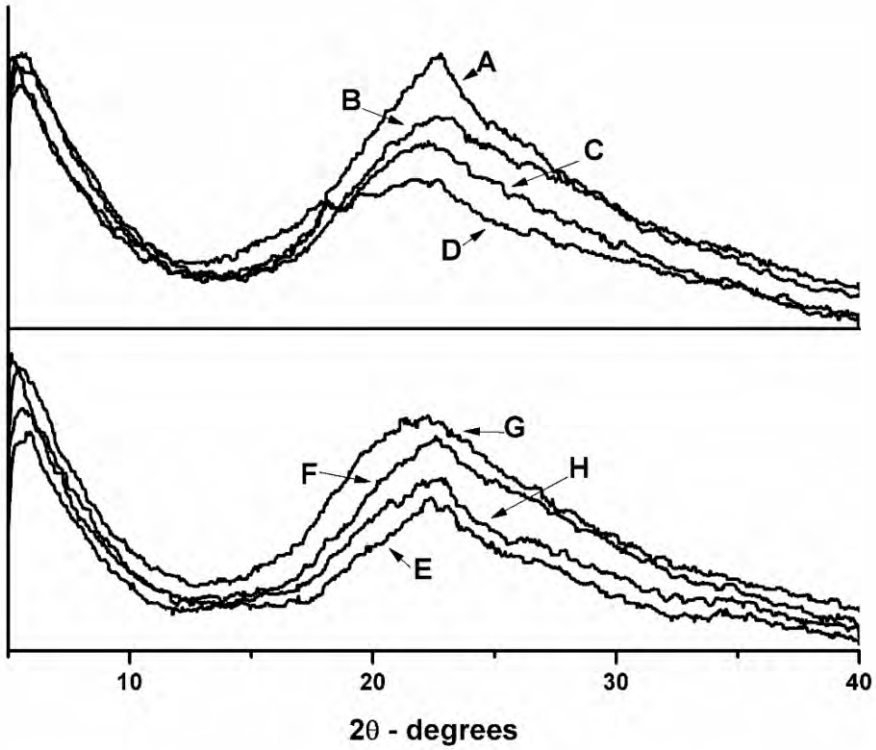

Figure. 6. XRD pattern of PILs: (a) [Celmim][Cl]; (b) $[Celmim][BF_4]$; (c) $[Celmim][PF_6]$; (d) $[Celmim][TF_2N]$; (e) $[CelEt_3N][Cl]$; (f) $[CelEt_3N][BF_4]$; (g) $[CelEt_3N][PF_6]$; (h) $[CelEt_3N][TF_2N]$.

Cellulose, CDC and PILs morphology were investigated by FESEM (Figure 7). As expected the pure cellulose exhibited a typical fibrous-looking surface. This morphology was significantly altered in functionalized cellulose samples. Chemical modification resulted in fiber compaction and agglomeration, evidenced in all PILs and CDC (Figure 7).

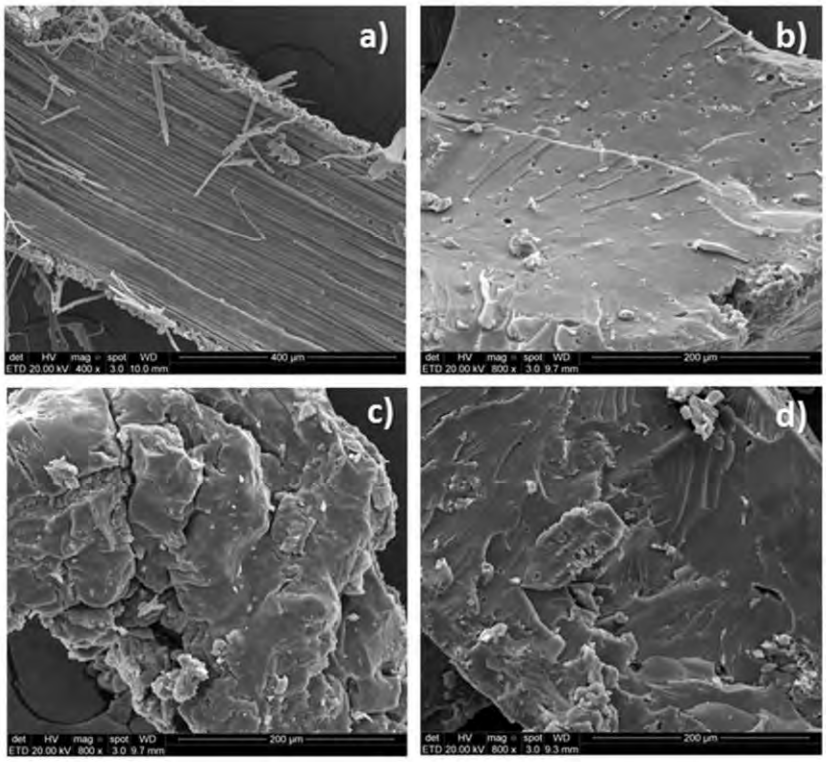

Figure 7. Micrographs of the materials: (a) cellulose, (b) CDC, (c) [Celmim][Cl] and (d) [CelEt$_3$N][Cl].

Thermogravimetric curves of cellulose and PILs are shown in Figure 8. Cellulose presented an initial mass loss inferior to 5% (T_{1onset} of 44°C and T_{1max} of 63°C) attributed to physically absorbed water on surface[42]. Yet, a decomposition event with mass loss of 91% (T_{2onset} of 313°C and T_{2max} of 334°C), attributed to structure degradation was evidenced[42] (Figure 8). All PILs presented two thermal events: the first stage with mass loss of 38 % ($T_{1\ onset}$ at 207°C and T_{1max} at 210°C) for [Celmim] [Cl] and 54% (T_{1onset} at 186°C and T_{1max} at 197°C) for [CelEt$_3$N] [Cl] is attributed to imidazolium or ammonium group loss allied to condensation of the carbon -OH groups of carbons 2 and 3 [44,45,82]. The second stage with mass loss of 20% (T_{2onset} at 266°C and T_{2max} at 270°C) for [Celmim] [Cl] and 12% (T_{2onset} at 387°C and $T_{2\ max}$ at 437°C) for [CelEt$_3$N] [Cl] is attributed to cellulose fibers degradation [44,45] (Figure 8). Exchange of anion $[Cl]^-$ by fluorinated anions resulted in increased thermal stability for ammonium PILs ($[BF_4]^-$ = T_{1onset} at 204°C and T_{1max} at 208°C; $[PF_6]^-$ =; T_{1onset} at 203°C and T_{1max} at

210°C; $[TF_2N]^-$ =; T_{1onset} at 204°C and T_{1max} at 213°C) whereas for imidazolium PILS the thermal stability remained almost constant with the anion exchange ($[BF_4]^-$ = T_{1onset} at 203°C and T_{1max} at 208°C; $[PF_6]^-$ =; T_{1onset} at 198°C and T_{1max} at 200°C; $[TF_2N]^-$ =T_{1onset} at 205°C and T_{1max} at 212°C) (Figure 8).

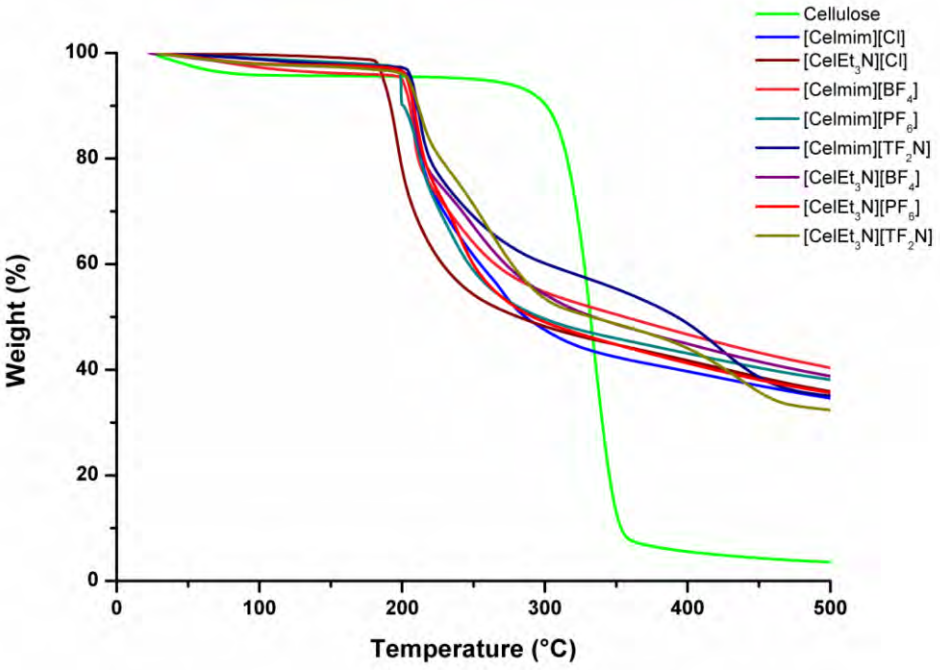

Figure. 8. TGA thermograms of cellulose and PILs

Experimental results of CO_2 sorption for all synthesized PILs as well as for cellulose are shown in Figure 9. Table 3 presents a parallel for CO_2 sorption values of PIL $[CelEt_3N][PF_6]$ relative to PILs described in literature.

It may be evidenced from Figure 9 that cellulose structure ionization promotes increased CO_2 affinity. This behavior was also observed in anionic cellulosic PILs[41]. Cellulose presented CO_2 sorption capacity of 20 mg/g at low pressure (0.1MPa) and 88 mg/g at higher pressures (3 MPa). Cellulose sorption capacity is related to the CO_2 affinity by polar groups (ether, ester and hydroxyl groups) of cellulose structure[41]. PILs presented superior sorption capacity once compared to cellulose (Figure 9). PILs [Celmim][Cl] and $[CelEt_3N][Cl]$

presented similar CO_2 sorption capacity at low pressure (27 mg/g and 26 mg/g, respectively). At higher pressure a different behavior was observed. PIL [Celmim][Cl] presented sorption capacity of 113 mg/g and [CelEt$_3$N][Cl] 89 mg/g. Anion effect for CO_2 sorption capacity may also be observed (Figure 9). The exchange of $[Cl]^-$ anion for fluorinated ones increased the CO_2 affinity. At higher CO_2 pressures (3 Mpa), sorption capacity increases in the following order for both cations: $[Cl]^- < [BF_4]^- < [TF_2N]^- < [PF_6]^-$. Preferential affinity of CO_2 for ionic liquids containing the anion $[TF_2N]$ rather than other anions with lower fluorination ($[BF_4]^-$, $[PF_6]^-$) is well known [83]. For cationic cellulosic PILs a different behavior was evidenced since the anion $[PF_6]^-$ provided higher performance. It is probable due to the size of $[TF_2N]^-$ causing steric effect and making it more difficult to CO_2 interact with polar groups present in cellulose structure, resulting in CO_2 sorption capacity reduction. This was also observed using semi-empirical molecular dynamics simulations (Figure 10).

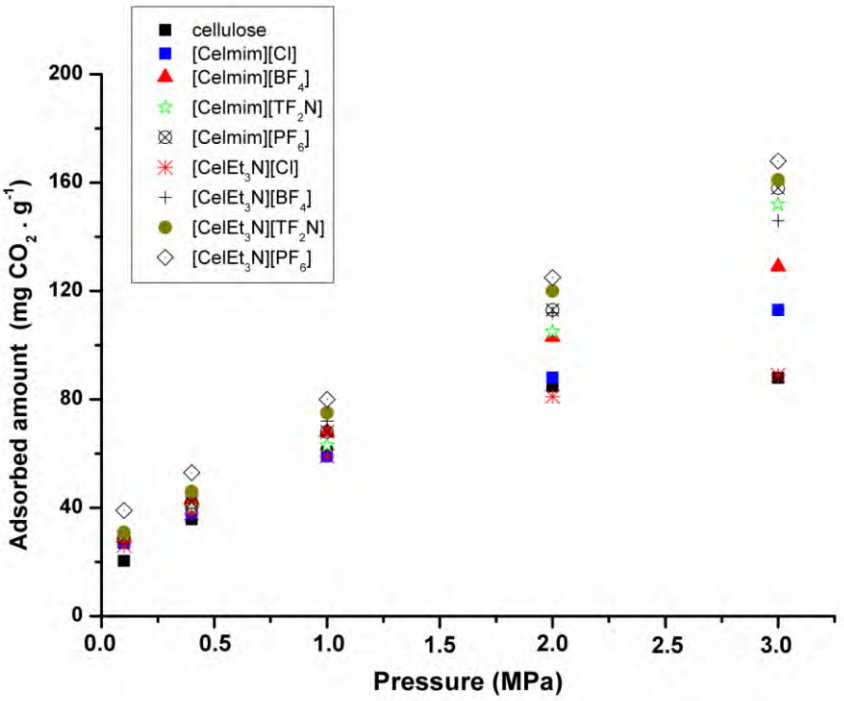

Figure 9. CO_2 sorption for cellulose and PILs.

To corroborate experimental observations, competitive atom-atom coordination (Figure 10) was investigated by the PM7-MD simulations, as described in the methodology. The simulations suggest that different CO_2 sorption capacities of [Celmim][PF_6] and [Celmim][NTF_2] are driven by the cation-anion coordination peculiarities. Due to its bulky structure and significantly polar moieties, the NTF_2 anion is located near the most CO_2-philic groups of imidazole and cellulose. This effect can also be seen for the PF_6 anion, in which case it is, however, less pronounced (Figure 10). The corresponding peaks for NTF_2 are somewhat higher and sharper. In particular, the acidic hydrogen atom of the imidazole ring and two hydroxyl groups of cellulose are blocked. The distance between NTF_2 and the hydroxyl groups of cellulose, 0.21 nm, suggests formation of a strong hydrogen bond. According to the PM7-MD simulations, coordination of CO_2 by these moieties is not feasible. Note that, unlike fluorine atoms of PF_6, are well distributed in space and can approach several CO_2-philic sites of the cationic cellulose simultaneously.

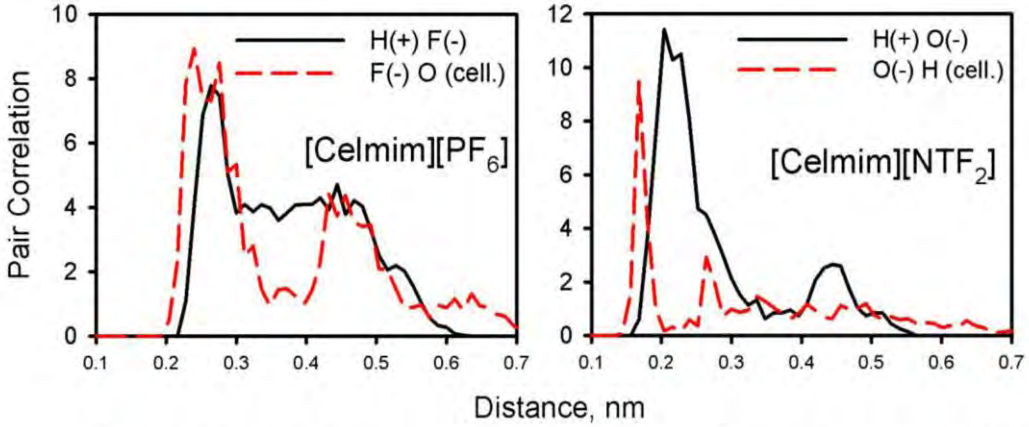

Figure 10. Selected pair correlation functions obtained from the PM7-MD simulations. The strongest spatial correlations between the anion (-), cationic (+) and neutral (cellulose) moieties are presented for comparison.

Table 3 presents CO_2 sorption values for PILs described in literature and PIL [CelEt$_3$N][PF$_6$]. As one may see PIL [CelEt$_3$N][PF$_6$] exhibited higher sorption value when compared to PILs obtained via direct radical polymerization (P[VBIT][BF$_4$]; P[VBIH][PF$_6$]; P([AMIM]BF$_4$-AN); P6 [BIEMA][Br]), as well as polyurethane based PILs (PIL-8.1.BF$_4$; PU-TAB). It can also be verified in Table 3 a comparison between the CO_2 sorption performance of [CelEt$_3$N][PF$_6$] and the anionic cellulosic PIL CL-TBA at different pressures (0.1 MPa and 3 MPa). At low pressure the [CelEt$_3$N][PF6] exhibited sorption capacity comparable to CL-TBA and at high pressure higher CO_2 sorption capacity.

Table 3. Comparison of [CelEt$_3$N][PF$_6$] with different poly(ionic liquids) in terms of CO_2 sorption.

PIL	CO_2 sorption (mg/g)	Conditions (P, T)	Ref.
P[VBIT][BF$_4$]	3.05	0.79 bar, 295.15K	[84]
P[VBIH][PF$_6$]	3.22	0.79 bar, 295.15K	[84]
P([AMIM]BF4-AN)	14.30	0.1 MPa, 273.15K	[85]
P6 [BIEMA][Br]	3.34	0.1 MPa, 278.15K	[86]
P[VBTEA][PF$_6$]	14.04	0.1 MPa, 278.15K	[87]
PIL-8.1.BF$_4$	24.76	0.1 MPa, 273.15K	[88]
PU-TAB	16.10	0.082 MPa, 303.15K	[33]
PU-TAB	123.0	3 MPa, 303.15K	[33]
CL-TBA	44	0.1MPa, 298.15 K	[41]
CL-TBA	71	3 MPa, 298.15 K	[41]
[CelEt$_3$N][PF$_6$]	38	0.1MPa, 298.15 K	This study
[CelEt$_3$N][PF$_6$]	168	3 MPa, 298.15 K	This study

In order to evaluate the reuse capacity of PIL [CelEt$_3$N][PF$_6$] five CO_2 sorption/desorption cycles were performed (Figure 11). Sorption was evaluated at 298,15 k and 0.1 MPa and desorption under vacuum at 298,15 k and 1h. Sorption/desorption values evidenced that CO_2 was completely removed in 1h and sorption values were constant in all five cycles (Figure 11). This result evidenced the capacity of this material to be used in CO_2 capture processes.

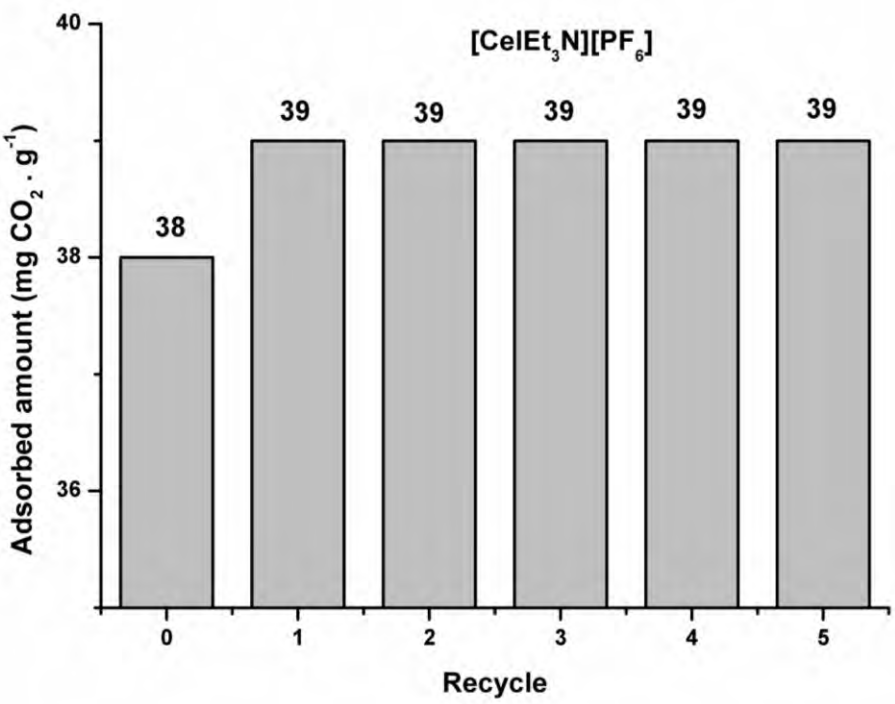

Figure 11. CO_2 sorption/desorption tests for [$CelEt_3N$][PF_6].

4. Conclusions

Cationic cellulosic PILs obtained from rice husk cellulose extraction showed a high CO_2 sorption capacity when compared to anionic cellulosic PILs and other PILs reported in literature. The anion fluorination promotes CO_2 sorption capacity increase, however the use of voluminous fluorinated anions may impair the CO_2 interaction with polar groups of cellulose structure. The best sorption result was found for PIL [$CelEt_3N$][PF_6].

5. Acknowledgments

The authors would like to thank Cooperativa Arrozeira Extremo Sul Ltda for donating rice husk and to Surface Science Laboratory of the Guatiguará Technological Park, for XPS analysis. Sandra Einloft thanks CNPq for research scholarship. Franciele L. Bernard thanks Hewlett-Packard Brasil Ltda for scholarship. This work was achieved in cooperation with Hewlett-Packard Brasil Ltda. using incentives of Brazilian Informatics Law (Law nº 8.2.48 of 1991).

6. References

[1] Songolzadeh M, Soleimani M, Takht Ravanchi M, Songolzadeh R. Carbon dioxide separation from flue gases: A technological review emphasizing reduction in greenhouse gas emissions. The Scientific World Journal 2014;2014. doi:10.1155/2014/828131.

[2] Olajire AA. CO_2 capture and separation technologies for end-of-pipe applications - A review. Energy 2010;35:2610–28. doi:10.1016/j.energy.2010.02.030.

[3] Figueroa JD, Fout T, Plasynski S, McIlvried H, Srivastava RD. Advances in CO_2 capture technology-The U.S. Department of Energy's Carbon Sequestration Program. International Journal of Greenhouse Gas Control 2008;2:9–20. doi:10.1016/S1750-5836(07)00094-1.

[4] Watabe T, Yogo K. Isotherms and isosteric heats of adsorption for CO_2 in amine-functionalized mesoporous silicas. Separation and Purification Technology 2013;120:20–3. doi:10.1016/j.seppur.2013.09.011.

[5] Mondal MK, Balsora HK, Varshney P. Progress and trends in CO_2 capture/separation technologies: A review. Energy 2012;46:431–41. doi:10.1016/j.energy.2012.08.006.

[6] Yaumi AL, Abu Bakar MZ, Hameed BH. Recent advances in functionalized composite solid materials for carbon dioxide capture. Energy 2017. doi:10.1016/j.energy.2017.02.053.

[7] Bruhn T, Naims H, Olfe-Kräutlein B. Separating the debate on CO_2 utilisation from carbon capture and storage. Environmental Science and Policy 2016;60:38–43. doi:10.1016/j.envsci.2016.03.001.

[8] Tome LC, Marrucho IM. Ionic liquid-based materials: a platform to design engineered CO2 separation membranes. Chemical Society Reviews 2016;45:2785–824. doi:10.1039/C5CS00510H.

[9] Leeson D, Mac Dowell N, Shah N, Petit C, Fennell PS. A Techno-economic analysis and systematic review of carbon capture and storage (CCS) applied to the iron and steel, cement, oil refining and pulp and paper industries, as well as other high purity sources. International Journal of Greenhouse Gas Control 2017;61:71–84. doi:10.1016/j.ijggc.2017.03.020.

[10] Wuebbles DJ, Jain AK. Concerns about climate change and the role of fossil fuel use. Fuel Processing Technology 2001;71:99–119. doi:10.1016/S0378-3820(01)00139-4.

[11] Shafeeyan MS, Wan Daud WMA, Houshmand A, Arami-Niya A. The application of response surface methodology to optimize the amination of activated carbon for the preparation of carbon dioxide adsorbents. Fuel 2012;94:465–72. doi:10.1016/j.fuel.2011.11.035.

[12] Zulfiqar S, Sarwar MI, Mecerreyes D. Polymeric ionic liquids for CO_2 capture and separation: potential, progress and challenges. Polym Chem 2015:6435–51. doi:10.1039/C5PY00842E.

[13] Xiong YB, Wang H, Wang YJ, Wang RM. Novel imidazolium-based poly(ionic liquid)s: Preparation, characterization, and absorption of CO_2. Polymers for Advanced Technologies 2012;23:835–40. doi:10.1002/pat.1973.

[14] Singto S, Supap T, Idem R, Tontiwachwuthikul P, Tantayanon S, Al-Marri MJ, et al. Synthesis of new amines for enhanced carbon dioxide (CO_2) capture performance: The effect of chemical structure on equilibrium solubility, cyclic capacity, kinetics of absorption and regeneration, and heats of absorption and regeneration. Separation and Purification Technology 2016;167:97–107. doi:10.1016/j.seppur.2016.05.002.

[15] Hairul NAH, Shariff AM, Bustam MA. Process behaviour in a packed absorption column for high pressure CO2 absorption from natural gas using PZ+AMP blended solution. Fuel Processing Technology 2017;157:20–8. doi:10.1016/j.fuproc.2016.11.008.

[16] Seo S, Simoni LD, Ma M, DeSilva MA, Huang Y, Stadtherr MA, et al. Phase-Change Ionic Liquids for Postcombustion CO2 Capture. Energy & Fuels 2014;28:5968–77. doi:10.1021/ef501374x.

[17] Perry RJ, Davis JL. CO_2 Capture Using Solutions of Alkanolamines and Aminosilicones. Energy & Fuels 2012;26:2512–7. doi:10.1021/ef201963m.

[18] Liang Z (Henry), Rongwong W, Liu H, Fu K, Gao H, Cao F, et al. Recent progress and new developments in post-combustion carbon-capture technology with amine based solvents. International Journal of Greenhouse Gas Control 2015;40:26–54. doi:10.1016/j.ijggc.2015.06.017.

[19] Ramezani R, Mazinani S, Di Felice R, Darvishmanesh S, Van der Bruggen B. Selection of blended absorbents for CO_2 capture from flue gas: CO_2 solubility, corrosion and absorption rate. International Journal of Greenhouse Gas Control 2017;62:61–8. doi:10.1016/j.ijggc.2017.04.012.

[20] Kazemi A, Kazemi Joujili A, Mehrabani-Zeinabad A, Hajian Z, Salehi R. Influence of CO_2 Residual of Regenerated Amine on the Performance of Natural Gas Sweetening Processes Using Alkanolamine Solutions. Energy & Fuels 2016;30:4263–73. doi:10.1021/acs.energyfuels.6b00295.

[21] García-Abuín A, Gómez-Díaz D, Navaza JM. New processes for amine regeneration. Fuel 2014;135:191–7. doi:10.1016/j.fuel.2014.06.067.

[22] Qian W, Texter J, Yan F. Frontiers in poly(ionic liquid)s: syntheses and applications. Chem Soc Rev 2017. doi:10.1039/C6CS00620E.

[23] Yuan J, Antonietti M. Poly(ionic liquid)s: Polymers expanding classical property profiles. Polymer 2011;52:1469–82. doi:10.1016/j.polymer.2011.01.043.

[24] Tang J, Tang H, Sun W, Radosz M, Shen Y. Poly(ionic liquid)s as new materials for CO2 absorption. Journal of Polymer Science Part A: Polymer Chemistry 2005;43:5477–89. doi:10.1002/pola.21031.

[25] Bara Jason E. , Hatakeyama Evan S. , Gin Douglas L. NRD. Improving CO_2 permeability in polymerized room-temperature ionic liquid gas separation membranes through the formation of a solid composite with a room-temperature ionic liquidy. Polymers for Advanced Technologies 2008;19:1415–20.

[26] Yu G, Man Z, Li Q, Li N, Wu X, Asumana C, et al. Reactive & Functional Polymers New crosslinked-porous poly-ammonium microparticles as CO_2 adsorbents. Reactive & Functional Polymers 2013;73:1058–64. doi:10.1016/j.reactfunctpolym.2013.04.005.

[27] Tang J, Tang H, Sun W, Plancher H, Radosz M, Shen Y. Poly(ionic liquid)s: a new material with enhanced and fast CO_2 absorption. Chemical Communications (Cambridge, England) 2005:3325–7. doi:10.1039/b501940k.

[28] Shaplov AS, Morozova SM, Lozinskaya EI, Vlasov PS, Gouveia ASL, Tomé LC, et al. Turning into poly(ionic liquid)s as a tool for polyimide modification: synthesis, characterization and CO_2 separation properties. Polym Chem 2016;7:580–91. doi:10.1039/C5PY01553G.

[29] Bhavsar RS, Kumbharkar S, Rewar AS, Kharul UK. Polybenzimidazole based film forming polymeric ionic liquids: Synthesis and effects of cation-anion variation on their physical properties. Polymer Chemistry 2014:4083–96. doi:10.1039/C3PY01709E.

[30] Kumbharkar SC, Bhavsar RS, Kharul UK. Film forming polymeric ionic liquids (PILs) based on polybenzimidazoles for CO_2 separation. RSC Advances 2014;4:4500. doi:10.1039/c3ra44632h.

[31] Bhavsar RS, Kumbharkar SC, Kharul UK. Polymeric ionic liquids (PILs): Effect of anion variation on their CO_2 sorption. Journal of Membrane Science 2012;389:305–15. doi:10.1016/j.memsci.2011.10.042.

[32] Kammakakam I, Won H, Nam S, Bum H, Kim T. Alkyl imidazolium-functionalized cardo-based poly (ether ketone) s as novel polymer membranes for O_2 / N_2 and CO_2 / N_2 separations. Polymer 2013;54:3534–41. doi:10.1016/j.polymer.2013.05.006.

[33] Bernard FL, Polesso BB, Cobalchini FW, Donato AJ, Seferin M, Ligabue R, et al. CO_2 capture: Tuning cation-anion interaction in urethane based poly(ionic liquids). Polymer 2016;102:199–208. doi:10.1016/j.polymer.2016.08.095.

[34] Magalhaes TO, Aquino AS, Dalla Vecchia F, Bernard FL, Seferin M, Menezes SC, et al. Syntheses and characterization of new poly(ionic liquid)s designed for CO2 capture. RSC Adv 2014;4:18164–70. doi:10.1039/c4ra00071d.

[35] Fernández M, Carreño LÁ, Bernard F, Ligabue R, Einloft S. Poly(ionic liquid)s Nanoparticles Applied in CO_2 Capture. Macromolecular Symposia 2016;368:98–106. doi:10.1002/masy.201500148.

[36] Cuadro P De, Belt T, Kontturi KS, Reza M, Kontturi E, Vuorinen T, et al. Reactive & Functional Polymers Cross-linking of cellulose and poly (ethylene glycol) with citric acid. REACTIVE AND FUNCTIONAL POLYMERS 2015;90:21–4. doi:10.1016/j.reactfunctpolym.2015.03.007.

[37] Bandera D, Sapkota J, Josset S, Weder C, Tingaut P, Gao X, et al. Reactive & Functional Polymers Influence of mechanical treatments on the properties of cellulose nanofibers isolated from microcrystalline cellulose. Reactive and Functional Polymers 2014;85:134–41. doi:10.1016/j.reactfunctpolym.2014.09.009.

[38] Salimi H, Aryanasab F, Reza A. Designing syntheses of cellulose and starch derivatives with basic or cationic N -functions : part I — cellulose derivatives. Polymers for Advanced Technologies 2016. doi:10.1002/pat.3599.

[39] Nascimento P, Marim R, Carvalho G, Celso R, Cid G, Celso R, et al. Nanocellulose Produced from Rice Hulls and its Effect on the Properties of Biodegradable Starch Film 2015;19:1–8. doi:10.1590/1980-5373-MR-2015-0423.

[40] Lau LC, Lee KT, Mohamed AR. Simultaneous SO_2 and NO removal using sorbents derived from rice husks: An optimisation study. Fuel 2011;90:1811–7. doi:10.1016/j.fuel.2010.12.009.

[41] Bernard FL, Rodrigues DM, Polesso BB, Donato AJ, Seferin M, Chaban V V., et al. New cellulose based ionic compounds as low-cost sorbents for CO_2 capture. Fuel Processing Technology 2016;149:131–8. doi:10.1016/j.fuproc.2016.04.014.

[42] Johar N, Ahmad I, Dufresne A. Extraction, preparation and characterization of cellulose fibres and nanocrystals from rice husk. Industrial Crops and Products 2012;37:93–9. doi:10.1016/j.indcrop.2011.12.016.

[43] Teodoro KBR, Teixeira E de M, Corrêa AC, Campos A de, Marconcini JM, Mattoso LHC. Whiskers de fibra de sisal obtidos sob diferentes condições de hidrólise ácida: efeito do tempo e da temperatura de extração. Polímeros 2011;21:280–5. doi:10.1590/S0104-14282011005000048.

[44] Chen Q, Peng C, Xie H, Zhao Z kent, Bao M. Cellulosic poly(ionic liquid)s: synthesis, characterization and application in the cycloaddition of CO_2 to epoxides. RSC Adv 2015;5:44598–603. doi:10.1039/C5RA05667E.

[45] da Silva Filho EC, de Melo JCP, Airoldi C. Preparation of ethylenediamine-anchored cellulose and determination of thermochemical data for the interaction between cations and basic centers at the solid/liquid interface. Carbohydrate Research 2006;341:2842–50. doi:10.1016/j.carres.2006.09.004.

[46] Silva Filho EC, Santos Júnior LS, Silva MMF, Fonseca MG, Santana SAA, Airoldi C. Surface cellulose modification with 2-aminomethylpyridine for copper, cobalt, nickel and zinc removal from aqueous solution. Materials Research 2013;16:79-87. doi:10.1590/S1516-14392012005000147.

[47] Samadi A, Kemmerlin RK, Husson SM. Polymerized ionic liquid sorbents for CO2 separation. Energy and Fuels 2010;24:5797–804. doi:10.1021/ef101027s.

[48] Fras L, Johansson LS, Stenius P, Laine J, Stana-Kleinschek K, Ribitsch V. Analysis of the oxidation of cellulose fibres by titration and XPS. Colloids and Surfaces A: Physicochemical and Engineering Aspects 2005;260:101–8. doi:10.1016/j.colsurfa.2005.01.035.

[49] Morsi SM, Pakzad A, Amin A, Yassar RS, Heiden PA. Chemical and nanomechanical analysis of rice husk modified by ATRP-grafted oligomer. Journal of Colloid and Interface Science 2011;360:377–85. doi:10.1016/j.jcis.2011.04.065.

[50] Koros WJ, Paul DR. Design considerations for measurement of gas sorption in polymers by pressure decay. Journal of Polymer Science: Polymer Physics

Edition 1976;14:1903–7. doi:10.1002/pol.1976.180141014.

[51] Shah VM, Hardy BJ, Stern SA. Solubility of carbon dioxide, methane, and propane in silicone polymers: Effect of polymer side chains. Journal of Polymer Science Part B: Polymer Physics 1986;24:2033–47. doi:10.1002/polb.1986.090240910.

[52] Takishima s,Makamura k,MasakiM, Masuoka H. Dilation and solubility in carbon dioxide+poly (vinyl acetate) system at high pressures. Journal of The Japan Petroleum Institute 1990;33:332–6. doi:10.1627/jpi1958.33.332.

[53] Span, R; Wagner W. A new EOS for CO_2 covering the fluid region from the triple point temperature to 1100K at pressures up to 800MPa.pdf. Journal of Physical and Chemical Reference Data 1996;25:1509–96. doi:10.1063/1.555991.

[54] Stewart JJP. Optimization of parameters for semiempirical methods VI: More modifications to the NDDO approximations and re-optimization of parameters. Journal of Molecular Modeling 2013;19:1–32. doi:10.1007/s00894-012-1667-x.

[55] Aquino A, Bernard F, Borges J, Mafra L, Vecchia F, Oliveira M, et al. Rationalizing the role of the anion in CO_2 capture and conversion using imidazolium-based ionic liquid modified mesoporous silica. RSC Adv 2015;5:64220–7. doi:10.1039/C5RA07561K.

[56] Chaban V. The thiocyanate anion is a primary driver of carbon dioxide capture by ionic liquids. Chemical Physics Letters 2015;618:89–93. doi:10.1016/j.cplett.2014.11.008.

[57] Bernard FL, Dalla Vecchia F, Rojas MF, Ligabue R, Vieira MO, Costa EM, et al. Anticorrosion Protection by Amine-Ionic Liquid Mixtures: Experiments and Simulations. Journal of Chemical and Engineering Data 2016;61:1803–10. doi:10.1021/acs.jced.5b00996.

[58] Chaban V. Hydrogen fluoride capture by imidazolium acetate ionic liquid. Chemical Physics Letters 2015;625:110–5. doi:10.1016/j.cplett.2015.02.041.

[59] Andreeva NA, Chaban V V. Electrostatic charge confinement using bulky tetraoctylammonium cation and four anions. Chemical Physics Letters 2016;649:44–7. doi:10.1016/j.cplett.2016.02.034.

[60] Andreeva NA, Chaban V V. Understanding weakly coordinating anions: tetrakis (pentafluorophenyl)borate paired with inorganic and organic cations. Journal of Molecular Modeling 2017;23:86. doi:10.1007/s00894-017-3275-2.

[61] Stewart JJP. Application of the PM6 method to modeling the solid state. Journal of Molecular Modeling 2008;14:499–535. doi:10.1007/s00894-008-0299-7.

[62] Stewart JJP. Application of the PM6 method to modeling proteins. Journal of Molecular Modeling 2009;15:765–805. doi:10.1007/s00894-008-0420-y.

[63] Andersen HC. Molecular dynamics simulations at constant pressure and/or temperature. The Journal of Chemical Physics 1980;72:2384–93. doi:10.1063/1.439486.

[64] Grimme S, Antony J, Ehrlich S, Krieg H. A consistent and accurate ab initio parametrization of density functional dispersion correction (DFT-D) for the 94

elements H-Pu. The Journal of Chemical Physics 2010;132:154104. doi:10.1063/1.3382344.

[65] Korth M, Pitoňák M, Řezáč J, Hobza P. A transferable H-bonding correction for semiempirical quantum-chemical methods. Journal of Chemical Theory and Computation 2010;6:344–52. doi:10.1021/ct900541n.

[66] Allouche A-R. Gabedit-A graphical user interface for computational chemistry softwares. Journal of Computational Chemistry 2011;32:174–82. doi:10.1002/jcc.21600.

[67] Martínez L, Andrade R, Birgin EG, Martínez JM. PACKMOL: A package for building initial configurations for molecular dynamics simulations. Journal of Computational Chemistry 2009;30:2157–64. doi:10.1002/jcc.21224.

[68] Humphrey W, Dalke A, Schulten K. VMD: Visual Molecular Dynamics. Journal of Molecular Graphics 1996;14:33–8. doi:10.1016/0263-7855(96)00018-5.

[69] National Institute of Advanced Industrial Science and Technology (AIST). Spectral Database for Organic Compounds (SDBS) n.d. http://sdbs.db.aist.go.jp/sdbs/cgi-bin/direct_frame_top.cgi (accessed April 4, 2017).

[70] Wang X, Lu Z, Jia L, Chen J. Physical properties and pyrolysis characteristics of rice husks in different atmosphere. Results in Physics 2016;6:866–8. doi:10.1016/j.rinp.2016.09.011.

[71] Reeve DW, Tan Z. The Study of Carbon-chlorine Bonds in Bleached Pulp with X-ray Photoelectron Spectroscopy. Journal of Wood Chemistry and Technology 1998;18:417–26. doi:10.1080/02773819809349589.

[72] Park BD, Wi SG, Lee KH, Singh AP, Yoon TH, Kim YS. X-ray photoelectron spectroscopy of rice husk surface modified with maleated polypropylene and silane. Biomass and Bioenergy 2004;27:353–63. doi:10.1016/j.biombioe.2004.03.006.

[73] Zhong L, Fu S, Li F, Zhan H. Chlorine dioxide treatment of sisal fibre: Surface lignin and its influences on fibre surface characteristics and interfacial behaviour of sisal fibre/phenolic resin composites. BioResources 2010;5:2431–46. doi:10.1016/j.compositesa.2010.09.004.

[74] Foelske-Schmitz A, Weingarth D, Kötz R. XPS analysis of activated carbon supported ionic liquids: Enhanced purity and reduced charging. Surface Science 2011;605:1979–85. doi:10.1016/j.susc.2011.07.016.

[75] Moulder JF, Stickle WF, Sobol PE, Bomben KD. Handbook of X-ray Photoelectron Spectroscopy. Perkin-Elmer Corporation; 1992.

[76] Santos AR, Blundell RK, Licence P. XPS of guanidinium ionic liquids: a comparison of charge distribution in nitrogenous cations. Phys Chem Chem Phys 2015;17:11839–47. doi:10.1039/C5CP01069A.

[77] Hammer T, Reichelt M, Morgner H. Influence of the aliphatic chain length of imidazolium based ionic liquids on the surface structure. Physical Chemistry Chemical Physics 2010;12:11070. doi:10.1039/c004415f.

[78] Rosa SML, Rehman N, De Miranda MIG, Nachtigall SMB, Bica CID. Chlorine-free extraction of cellulose from rice husk and whisker isolation. Carbohydrate Polymers 2012;87:1131–8. doi:10.1016/j.carbpol.2011.08.084.

[79] Soni B, Hassan EB, Mahmoud B. Chemical isolation and characterization of different cellulose nanofibers from cotton stalks. Carbohydrate Polymers 2015;134:581–9. doi:10.1016/j.carbpol.2015.08.031.

[80] Marcilla R, Blazquez JA, Rodriguez J, Pomposo JA, Mecerreyes D. Tuning the solubility of polymerized ionic liquids by simple anion-exchange reactions. Journal of Polymer Science, Part A: Polymer Chemistry 2004;42:208–12. doi:10.1002/pola.11015.

[81] Yu G, Man Z, Li Q, Li N, Wu X, Asumana C, et al. New crosslinked-porous poly-ammonium microparticles as CO2 adsorbents. Reactive and Functional Polymers 2013;73:1058–64. doi:10.1016/j.reactfunctpolym.2013.04.005.

[82] Erdmenger T, Vitz J, Wiesbrock F, Schubert US. Influence of different branched alkyl side chains on the properties of imidazolium-based ionic liquids. Journal of Materials Chemistry 2008;18:5267. doi:10.1039/b807119e.

[83] Muldoon MJ, Aki SNVK, Anderson JL, Dixon JK, Brennecke JF. Improving carbon dioxide solubility in ionic liquids. Journal of Physical Chemistry B 2007;111:9001–9. doi:10.1021/jp071897q.

[84] Tang J, Sun W, Tang H, Radosz M, Shen Y. Enhanced CO 2 absorption of poly(ionic liquid)s. Macromolecules 2005;38:2037–9. doi:10.1021/ma047574z.

[85] Zhu JM, He KG, Zhang H, Xin F, Engineering C. Effect of Swelling on Carbon Dioxide Adsorption by Poly (ionic liquid) s 2011:35–42.

[86] Privalova EI, Karjalainen E, Nurmi M, Mäki-Arvela P, Eränen K, Tenhu H, et al. Imidazolium-Based Poly(ionic liquid)s as New Alternatives for CO 2 Capture. ChemSusChem 2013;6:1500–9. doi:10.1002/cssc.201300120.

[87] Yu G, Li Q, Li N, Man Z, Pu C, Asumana C, et al. Synthesis of New Crosslinked Porous Ammonium- Based Poly (ionic liquid) and Application in CO 2 Adsorption. Polymer Engineering and Science 2014:2–6. doi:10.1002/pen.

[88] Morozova SM, Shaplov AS, Lozinskaya EI, Mecerreyes D, Sardon H, Zulfiqar S, et al. Ionic Polyurethanes as a New Family of Poly(ionic liquid)s for Efficient CO 2 Capture 2017. doi:10.1021/acs.macromol.6b02812.

4.5. Capítulo V: Aminas e polieteraminas suportadas em celulose

O estudo relatado no artigo "*Development of Inexpensive Cellulose-Based Sorbents for Carbon Dioxide*" e submetido para o Brazilian Journal of Chemical Engineering (comprovante de submissão Anexo C), descreve o potencial para captura de CO_2 de fibras de celulose extraídas da casca de arroz, modificadas quimicamente com diferentes aminas e polieteraminas. Os compostos obtidos foram caracterizados por diferentes técnicas (FTIR, DRX, TGA, BET e MEV-FEG). Concentrações baixas de aminas e polieteraminas ($2x10^{-6}$ mol/mg) foram suportadas nas fibras de celulose. A capacidade de sorção de CO_2 foi avaliada gravimetricamente por uma balança de suspensão magnética. As simulações mecânicas quânticas e os resultados experimentais revelaram que a quimisorção é favorecida por grupos -NH- e $-NH_2$. O melhor resultado de sorção de CO_2 foi alcançado para a celulose modificada com amina CL-D-400 (409 μmol CO_2 / g a 1 bar e 1091 μmol CO_2 / g a 10 bar).

Development of Inexpensive Cellulose-Based Sorbents for Carbon Dioxide

Franciele L. Bernard [a,b], Daniela. M. Rodrigues [c], Barbara B. Polesso [c], Vitaly V. Chaban [d] , Marcus Seferin [a,b]Felipe Dalla Vecchia [c] and Sandra Einloft [a,b*]

a) Post-Graduation Program in Materials Engineering and Technology. Pontifical Catholic University of Rio Grande do Sul – PUCRS.
b) School of Chemistry. Pontifical Catholic University of Rio Grande do Sul – PUCRS.
c) School of Engineering, Pontifical Catholic University of Rio Grande do Sul – PUCRS. Av. Ipiranga, 6681, Partenon, Porto Alegre Brazil, CEP: 90619-900.
d) Institute of Science and Technology (ICT), Federal University of São Paulo (UNIFESP); São José dos Campos, SP – Brazil.

** Corresponding author: einloft@pucrs.br*

Abstract

Aqueous amine solutions are benchmark solvents for CO_2 capture and their operational drawbacks are well-known. In order to overcome these problems, the support of amines on solid materials appears as an option for CO_2 capture. Cellulose is a versatile and low-cost material that can be used as a support. This study reports chemical modification of cellulose fibers extracted from rice husk with different amines and their potential for CO_2 capture. The obtained compounds were characterized by different techniques. The CO_2 sorption capacity was gravimetrically assessed in a Magnetic Suspension Balance. Quantum mechanical simulations and experimental results revealed that -NH- and -NH_2 represent major working sites of the employed compounds. The best result for CO_2 sorption was attained for the amine-modified cellulose CL-D-400 with a sorption capacity of 409 µmol CO_2/g at 1 bar and 1091 µmol CO_2/g at 10 bar with amine concentrations as low as 2×10^{-6} mol/mg.

Keywords: cellulose, rice husk, CO_2 capture, amines, simulation.

1. Introduction

The CO_2 concentration in the atmosphere is increasing every year, as well as global warming and its effect on climate change (Barbosa, Damasceno e Hori, 2016; Chan *et al.*, 2016; Hussain, Farrukh e Minhas, 2015; Nouri e Ebrahim, 2016; Seo *et al.*, 2014). Preventing the growth of carbon dioxide emissions in atmosphere is essential for achieving the global warming reduction target(Dutcher, Fan e Russell, 2015). Different strategies have been considered and adopted by several countries aiming to reduce the CO_2 emissions, such as the improvement of energy efficiency, increasing the use of low carbon fuels or nuclear energy, renewable energy development, geo-engineering approaches and CO_2 capture and storage (CCS)(Garcés *et al.*, 2013; Leung, Dennis Y C, Caramanna e Maroto-Valer, 2014). Among these different strategies, CCS is considered crucial because it reduces the CO_2 emission from large emission sources(Arias *et al.*, 2016; Garðarsdóttir *et al.*, 2015; Kamarudin e Alias, 2013; Leung, Dennis Y.C., Caramanna e Maroto-Valer, 2014).

Chemical absorption using amine aqueous solutions is a benchmark technology for CO_2 capture (Arias *et al.*, 2016; Bachelor e Toochinda, 2012; Kamarudin e Alias, 2013). However, it has some operational drawbacks, such as high power consumption required for solvent regeneration, equipment corrosion (Gray *et al.*, 2005; Kamarudin e Alias, 2013), degradation/evaporation of amines [10], the need of a large-volume absorber (Yu, Huang e Tan, 2012), besides additional operating costs due to substitution of solvents(Seo *et al.*, 2014).

To overcome the drawbacks of chemical absorption, the impregnation and grafting of amines on solids have been suggested in literature (Bachelor e Toochinda, 2012; Gray *et al.*, 2005; Knowles *et al.*, 2005; Lima, Gomes e Lucena, 2015; Yu, Huang e Tan, 2012). Unfortunately, many of these commercial sorbents remain prohibitively expensive (Bachelor e Toochinda, 2012). This generates the necessity of developing inexpensive sorbents for CO_2 capture. As alternatives for obtaining low-cost sorbents, impregnation of agricultural wastes with amines has been suggested. Some examples are

bagasse, rice straw, industrial residues, such as mullite, fly ash and other oxygen rich sorbents(Bachelor e Toochinda, 2012; Gray *et al.*, 2004). Strategies to use residues for CO_2 capture will foster emergence of green technologies and sustainable development.

Brazil is among the ten largest rice producers in the world. By 2017, it produced about 11 759 096 tons of rice (IBGE- Grupo de Coordenação de Estatísticas Agropecuárias, 2017). Rice husk (RH) is a major agricultural waste generated as a byproduct during the rice milling stage(Rosa *et al.*, 2012) while cellulose constitutes about 33% of rice husk (Johar, Ahmad e Dufresne, 2012).

Cellulose is the most abundant natural polymer (Zhang *et al.*, 2016). It is a low-cost versatile material, thermodynamically stable, presenting crystalline structure and numerous hydrogen bonds (K. Shukla *et al.*, 2013). Cellulose undergoes functionalization primarily through the hydroxyl groups(Cuadro, de *et al.*, 2015; K. Shukla *et al.*, 2013).

Previous studies have been conducted on nanofibrillated cellulose modification using aminosilanes for CO_2 capture from the air (Gebald *et al.*, 2011, 2013). Commercially fibrillated cellulose suspension was used in that work. Hereby, we investigated chemical modification of cellulose fibers, extracted from the rice husk, with different amines. The potential of the newly developed compounds for CO_2 capture was characterized. Quantum mechanical simulations were employed to elucidate the impact of different functional groups on CO_2 sorption.

2. Experimental Section

2.1 Materials

The rice husks were donated by Cooperativa Arrozeira Extremo Sul Ltda. The material was washed with distilled water and dried in an oven at 100°C for 8h. The dried husk was grounded in a knife mill. The fraction that passed through the 20 mesh sieve (0.841 mm) was collected. Anhydrous citric acid (CA, 99.5% Synth), sodium hydroxide (NaOH, 97% Vetec), hydrogen peroxide

(H_2O_2, 35%, Neon), N,N-dimethylformamide (DMF, 99.5%, Merck) ethanol (CH_3CH_2OH, 99%, Vetec), hydrazine (32.04 g/mol, HYD, aqueous solution 65%), ethylenediamine (60.10 g/mol, EDA, 99%, Vetec) JEFFAMINE® M-2005 (Mn = 2000 g/mol , Huntsman), JEFFAMINE® D-4000 (Mn = 4000 g/mol, Huntsman), JEFFAMINE® D-400 (Mn = 430 g/mol Huntsman), JEFFAMINE® EDR-148 (Mn = 148 g/mol, Huntsman) were used as purchased.

2.2 Cellulose extraction

The cellulose extraction was adapted from literature procedures(Johar, Ahmad e Dufresne, 2012; Teodoro *et al.*, 2011). The rice husk was treated with 4 wt% NaOH at 90°C for 2h to remove lignin and hemicellulose of the rice husk fibers. The acid hydrolysis treatment was conducted on the fibers after alkali treatment using 10.0 mol L^{-1} H_2SO_4 at 50°C for 40 min under continuous stirring. Afterwards, bleaching was carried out by addition of 16% (v/v) H_2O_2 and 5 wt% NaOH solution in a 1:1 proportion (v/v) at 55°C for 2h to remove the remaining lignin. The rice husk:solution ratio was 0.05 g/mL. Each step was repeated for five times. The solid was filtered and washed with distilled water until neutral pH was achieved and dried at 50°C in the oven after each treatment.

2.3 Cellulose chemical modification

Cellulose chemical modification was performed in two stages. The first was modification with citric acid (Figure 1). The second step was functionalization with amines (Figure 2). The modification with citric acid was performed by a similar procedure described elsewhere(Rodrigues *et al.*, 2006; Zhu, Fan e Zhang, 2008). The cellulose was poured into a flask containing 1.2 mol/L aqueous solution of citric acid to obtain 100g/L cellulose solution. This solution was stirred for 0.5h at room temperature. The temperature was increased up to 120°C and kept constant 1.5h under stirring. After cooling, the cellulose was washed with distilled water in the proportion of 200 mL/g for several times to remove any excess of citric acid and dried at 55°C for 24h. The

concentration of carboxylic groups (mol mg^{-1}) introduced into the modified cellulose was determined by back titration (Gurgel *et al.*, 2008; Karnitz *et al.*, 2007; Shang *et al.*, 2016), by treating the material (0.1 g) with 100 mL of an aqueous solution of NaOH (0.02 mol/L) for 1h under constant stirring. The materials were separated by filtration and the solution was titrated with HCl (0.02 mol/L).

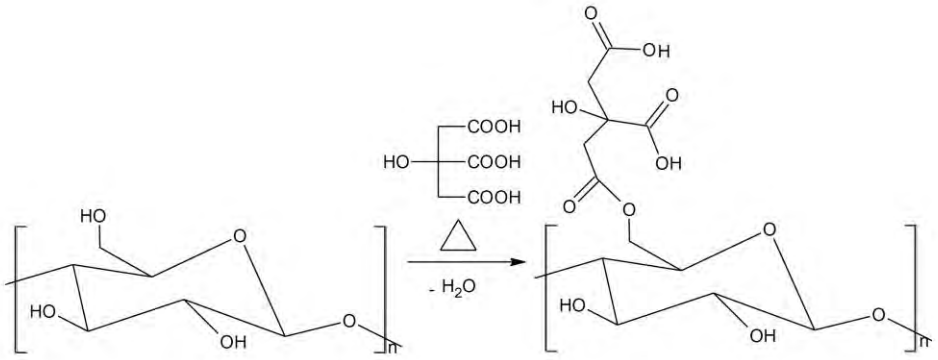

Figure 1. Schematic representation of the carboxylic acid functions introduced on the cellulose surface.

The amine functionalization reaction is described elsewhere(Bernard *et al.*, 2016; Magalhaes *et al.*, 2014). In a Schlenk flask, under N_2 atmosphere 1g of citric acid modified cellulose was added to the amine (molar ratio COOH/AMINE = 1:1) dissolved in 15 mL of dimethylformamide (DMF). The mixture was stirred at 40°C for 2h. The materials were separated by filtration, washed repeatedly with distilled water and ethanol and dried at 55°C for 24h. The concentration of amine (mol mg^{-1}) introduced into the modified cellulose was determined by back titration, by treating the material (0.1 g) with 100 mL of an aqueous HCl solution (0.02 mol/L) for 1 hour under constant stirring. The materials were separated by filtration and the solution was titrated with NaOH (0.02 mol/L)(Gurgel *et al.*, 2008; Karnitz *et al.*, 2007) (see Figure 2).

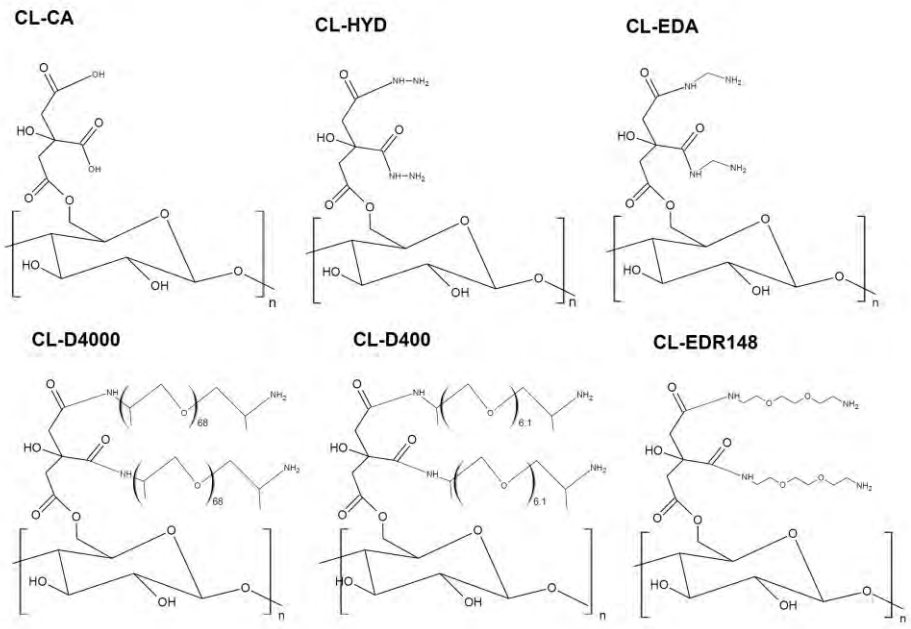

Figure 2 – Schematic representation of amines-modified cellulose.

2.4 Characterization

The synthesized materials were characterized by Universal Attenuated Total Reflectance sensor (UATR-FTIR) using Perkin-Elmer Model 100 FTIR Spectrum, in the range 4000-650 cm^{-1}. Field emission scanning electron microscopy (FESEM) analyses were performed in FEI Inspect F50 equipment in secondary electrons (SE) mode. Thermogravimetric Analysis (TGA) was performed using TA Instruments SDT-Q600 between 25°C and 600°C with a heating rate of 10°C/min in nitrogen atmosphere. Specific surface area and pore size were calculated from nitrogen sorption data using Brunauer-Emmett-Teller (BET) at -196°C (Micromeritics, ASAP 2420). Powder X-ray diffraction (XRD) pattern was recorded on Bruker-AXS D8 ADVANCE diffractometer operated at 40 kV and 20 mA using Cu Kα radiation (λ = 1.5406 Å) in the range 3-40° with a step of 0.02° and scanning time of 1.0 min. The Segal method (Eq. 1) was used

to calculate the sample crystallinity index (CrI) of the samples (Segal *et al.*, 1959).

$$\mathrm{CrI} = \frac{I_{002} - I_{AM}}{I_{002}} X\ 100\ (1)$$

where I_{002} is the maximum intensity of the 002 peak and I_{AM} is the intensity scattered by the amorphous part of the sample. The diffraction peak for plane (002) is located at diffraction angle around 2θ = 22° and the intensity scattered by the amorphous part is measured as the lowest intensity at a diffraction angle around 2θ = 18° (Johar, Ahmad e Dufresne, 2012).

2.5 Ab Initio Calculations

Thermodynamics of the reactions was estimated using molecular partition functions obtained from the numerical ab initio calculations and subsequent vibration frequency analysis. The Gaussian-X composite schemes proposed by Curtiss and coworkers (Curtiss *et al.*, 1998; Curtiss, Redfern e Raghavachari, 2007) were used. For an interested reader, we compared G-3 with its simplified modification G-3-MP2, as well as a newer method, G-4-MP2. The term 'MP2' in the method designation means that the MP4 stage in the original composite method (G-3, G-4) was substituted by the MP2 stage(Curtiss *et al.*, 1999).The reported results correspond to a

n ideal gas approximation. Gibbs free energy, enthalpy and entropy of each process, computed at given external conditions, are based on the Hess law of constant heat summation and known relations between these thermodynamic quantities.

Binding energies were computed using the Becke-3-LYP hybrid density functional(Becke, 1988; Lee, Yang e Parr, 1988) with the 6-311+G* atom-centered split-valence triple-zeta basis set. Both polarization and diffuse functions are included in this basis set for higher accuracy of the theoretical results. The basis set superposition error was excluded through the counterpoise approach. The geometries of the molecules were appropriately optimized prior to computing binding energies at the requested level of theory.

2.6 Gas adsorption measurements

Pure gas sorption (CO_2) in the samples was gravimetrically assessed in a Magnetic Suspension Balance (MSB), (Rubotherm Prazisionsmesstechnik GmbH, 35MPa and 400°C) equipped with a single sinker device for absorbate density determination and thermostatized with an oil bath (Julabo F25/± 0.1°C). The apparatus details are described elsewhere (Blasig *et al.*, 2007; Dreisbach e Lösch, 2000). When compared to other gravimetrical sorption methods, the MSB device has the advantage of allowing high-pressure sorption measurements since the sample can be potted into a closed chamber coupled to an external precise accurate balance (accuracy of ±10 μg). The samples (0.06 to 0.09 g) were weighted and transferred to the MSB sample container, and the system was subjected to 10^{-7} MPa vacuum at the temperature of the sorption measurement, 25°C, for 24 hours (constant weight was achieved in this time). The gas (CO_2, Air Liquide / 99.998 %) was admitted into the MSB pressure chamber up to the desired pressure, 0.1-3 MPa. In this study, pressure gauge with an accuracy of 10^{-3} MPa was used to control the system pressure. The gas solubility in the samples for each isotherm and pressure considered was measured during 3-4 hours until no more weight increasing for gas sorption was observed. At this step of gas solubility in the samples, the weight reading from the microbalance at pressure P and temperature T is recorded as 〖W〗_t (P,T). The mass of the adsorbed gas in the sample (W) was calculated using the following equation (2):

$$W = \left[W_t(P,T) - W_{sc}(P,T) + \rho_g(P,T)\cdot\left(V_{sc}(T) + V_s(T)\right)\right] - W_s(vac,T) \quad (2)$$

where W_{sc} (P,T) is the weight of sample container, ρ_g (P,T) stands for gas density, directly measured with the MSB coupled single-sinker device, dismissing the application of any equation of state to calculate the gas sorption, V_{sc} (T) is the volume of the sample container, determined from a buoyancy experiment when no sample is charged into the sample container, V_s (T) the specific solid sample volume, W_s (vac,T) is the weight of samples under vacuum and the term $\rho_g(P,T)\cdot\left(V_{sc}(T) + V_s(T)\right)$ represents the buoyancy force. In this work, the solubility in the sample was treated as the excess solubility.

3. Results and discussion

3.1 Specific surface area, amine load and cristallinity

Table 1 shows surface area data, amine loading and crystallinity for each sample. It can be seen that the amine functionalization caused a small increase in surface area with the exception of CL-M-2005 and CL-D-4000 samples. The determined concentration of carboxylic functions of CL-CA sample was 2.15×10^{-6} (mol/mg). Our result is close to the previous report [38]. The concentration of the loaded amines ranged from 2.00×10^{-6} to 2.04×10^{-6} (mol/mg) indicating that almost all supplied carboxyl groups were reacted. The corresponding crystallinity values are discussed in section 3.2.

Table 1: Specific surface area, amine loading and crystallinity.

Sample	SBET (m^2/g)	Amine loading (mol/mg)	Crystallinity (%)
CELLULOSE	0.2398	-	87
CL-CA	0.4575	-	84
CL-HYD	0.6579	$2.00\ x10^{-6}$	91
CL-EDA	0.5753	$2.04\ x10^{-6}$	88
CL-M2005	ND	$2.02\ x10^{-6}$	_
CL-D400	0.3113	$2.03\ x10^{-6}$	63
CL-D4000	ND	$2.01x10^{-6}$	_
CL- EDR 148	0.5831	$2.03\ x10^{-6}$	86

*ND (Not Determined).

3.2 X-ray diffraction (XRD)

Figure 3 shows the X-ray diffraction profile of the extracted cellulose and modified cellulose samples. All samples exhibit typical cellulose peaks around 2θ = 16°, 22.6° and 35°(Johar, Ahmad e Dufresne, 2012; Zhang *et al.*, 2016). The patterns indicated that the obtained cellulose presented a typical form of cellulose I since there was no doublet in the main peak at 2θ = 22.6°(Li *et al.*, 2009). One can also observe a change in the profile of the x-ray diffraction patterns after the chemical modification. The samples that were modified with amines containing higher molecular weight side chain presented less defined peaks indicating a lower organization once compared with cellulose and the samples obtained with amines containing lower molecular weight side chains. The crystallinity index values (Table 1) highlight that cellulose modified with low-

molecular-weight amines (CL-HYD; CL-EDA, CL-EDR-148) present higher crystallinity values. The Compound CL-D-400 functionalizated with JEFFAMINE® D-400 (Mn = 430 g/mol) showed considerable decrease in crystallinity.. The samples synthesized with higher-molecular-weight amines (CL-M-2005 and CL-D-4000) exhibited skewed peaks, which indicate that new assembly is formed via inserted side chain.These results indicate that the bigger the size of the inserted side chain the smaller the crystallinity of the sample, probably due to the reduction in the packing degree of cellulose molecules caused by side chains.

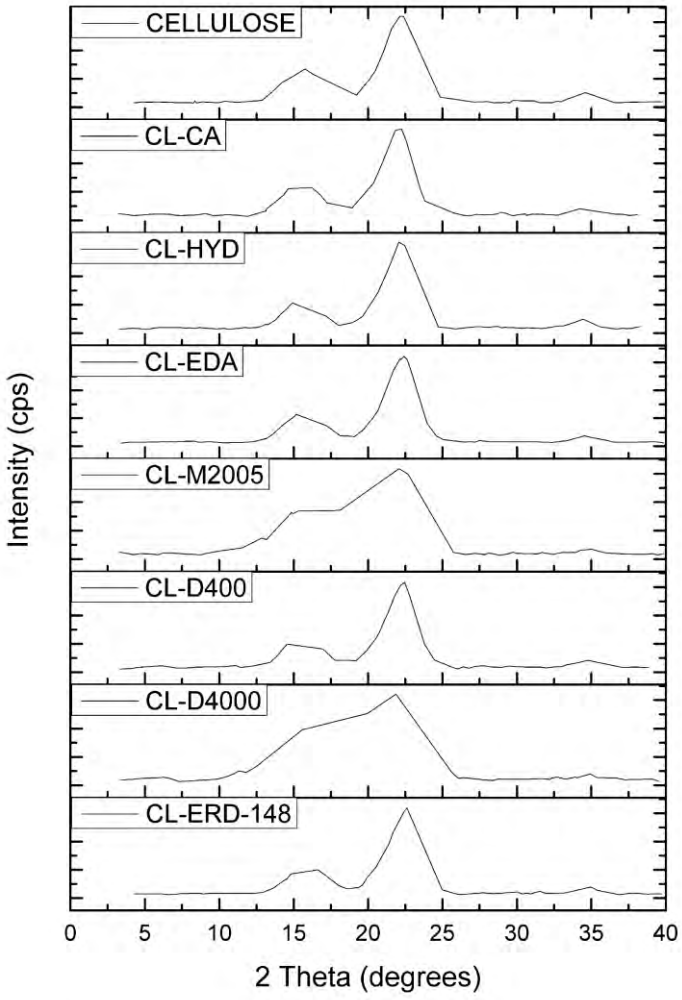

Figure 3. XRD pattern of cellulose and modified celluloses samples.

3.3 Spectroscopic characterization

The infrared spectra of cellulose in all samples (Figure 4-a, b and c) showed a broadband located at 3330 - 3340 cm^{-1}, attributed to the stretching of the OH groups, band near 2920 cm^{-1} related to C-H stretching, band at 1160 cm^{-1} corresponding to C-O-C asymmetrical bridge stretching, broadbands around 1050 cm^{-1} and 890 cm^{-1} related to the C-H and C-O stretching vibration of the cellulose structure(Johar, Ahmad e Dufresne, 2012; Rosa *et al.*, 2012). Having compared spectra for cellulose (Figure 4a) and citric acid modified cellulose (Figure 4b), we identified a strong band at 1740 cm^{-1} attributed to the carboxylic acid (X-COOH). This evidences introduction of citric acid into the cellulose chain (Cuadro, de *et al.*, 2015). Figure 4c presents the FTIR for CL-400 sample. A reduction in intensity of the carboxyl group absorption band (1740 cm^{-1}) due to the chemical modification with amines was observed. A new band at 1454 cm^{-1}, characteristic of the symmetric bending of primary amines (NH_2) and at 2869 cm^{-1} relative to the CH_2 stretching modes of the amine chains(Yu, Le e Cheng, 2012). A shoulder at 3286 cm^{-1} is evidenced which may be attributed to amine N-H stretching vibrations(Yu, Le e Cheng, 2012).

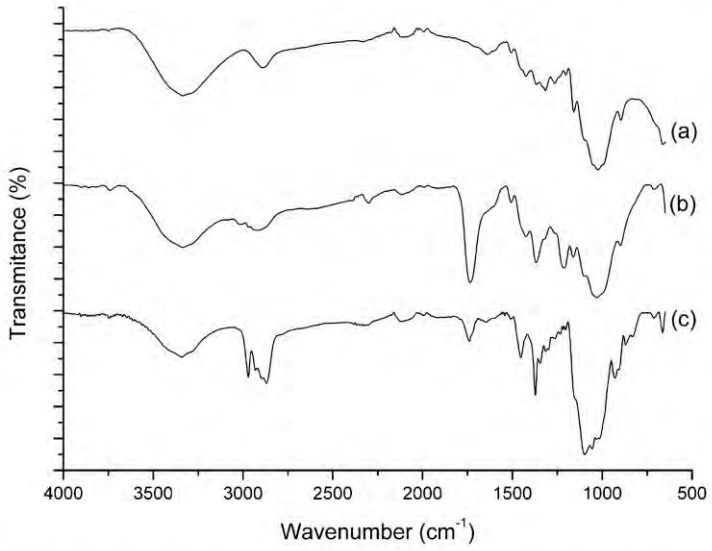

Figure 4. FTIR spectra of: (a) cellulose, (b) citric acid modified cellulose and (c) CL-D400.

3.4 Thermogravimetric Analysis (TGA)

Figure 5 presents TG and DTG curves obtained for all materials. All samples showed two thermal events. The earlier weight loss was ca. 4% and t_{onset} below 100°C, attributed to water vaporization [17]. The later weight loss attributed to cellulose degradation (t_{onset} of 289°C and T_{max} of 324°C) being 71%. The modified samples presented a higher thermal stability than cellulose. Degradation temperatures varied from t_{onset} 318°C to 360°C and T_{max} of 346°C to 392°C with a weight loss around 83%.

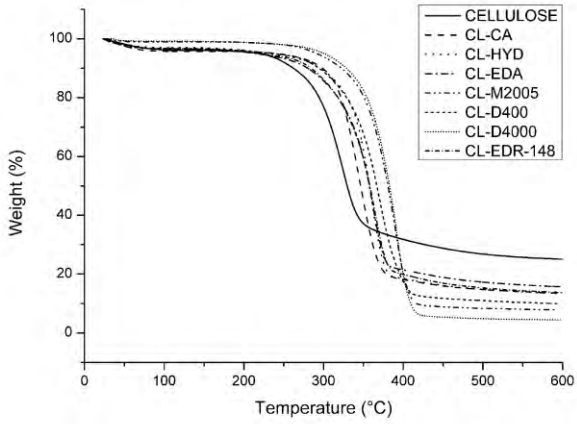

(a)

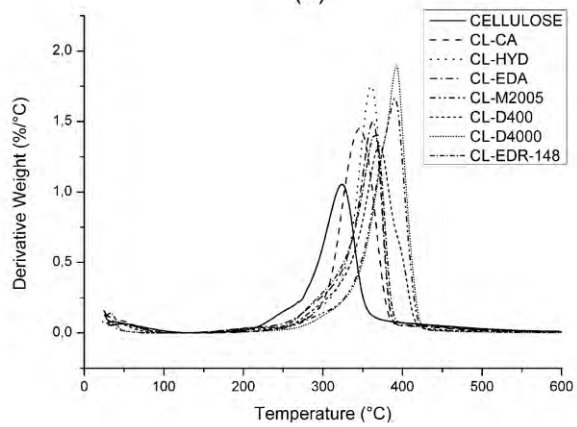

(b)

Figure.5 TG (a) and DTG (b) curves for cellulose and modified celluloses samples

3.5 Field emission scanning electron microscopy (FESEM)

Figure 6 exemplifies different effects on rice husk surface after cellulose extraction as well as chemical modification. The cellulose extraction in the form of bundles of fiber (Figure 6b) can be highlighted when comparing with the smooth compact surface of the untreated rice husk (Figure 6a). Citric acid modified cellulose (Figure 6c) showed similar morphology to that shown by the sample after bleaching treatment (Figure 6b). Amine modification of cellulose samples led to a separation of fiber bundles, especially sample CL-D-400 (Figure 6g). This may contribute to the increase of contact surface area and, consecutively, to CO_2 sorption.

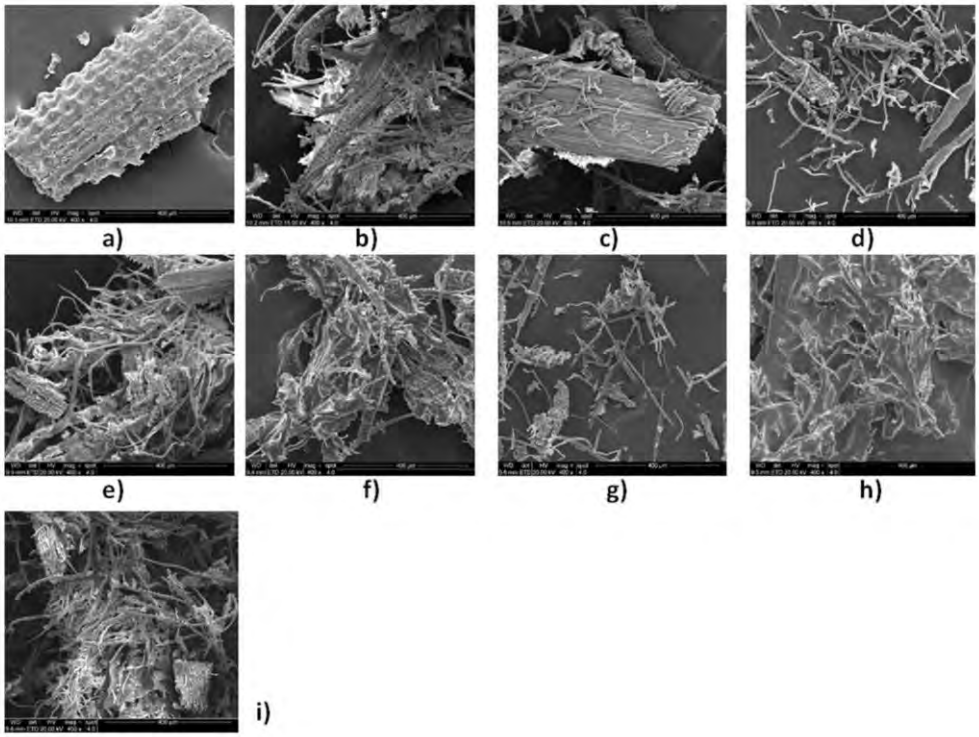

Figure 6. Micrographs of the materials: (a) rice husk fibers, (b) CELLULOSE, (c) CL-CA, (d) CL-HYD, (e) CL-EDA, (f) CL-M2005, (g) CL-D-400, (h) CL-D-4000, (i) CL-EDR-148.

3.6 Gas sorption measurements

Table 2 presents the experimental results for CO_2 sorption at 1 bar and 10 bar for the synthesized materials. Note that at both pressures all amine-functionalized samples presented higher sorption values when comparing with the citric acid modified cellulose (CL-CA).

The experimental results corroborate the thermodynamic potentials obtained by simulation (see section 3.7), which indicated that for CL-CA sample occurs only via physisorption, CO_2 is adsorbed due to electrostatic interactions. However, for samples functionalized with NH and NH_2 groups, chemisorption occurs. It is well-known that the interaction between the basic surface and acidic CO_2 molecules results in the formation of surface ammonium carbamates under anhydrous conditions (Yu, Le e Cheng, 2012). Among the amines modified cellulose samples, the best CO_2 sorption result was obtained for the sample functionalized with CL-D-400, whereas the worst result was recorded in the case of CL-D-4000. The micrograph images (Figure 6g) showed a better separation of fiber bundles for the sample CL-D-400. This can improve the interaction of CO_2 with the cellulose chain groups. For the CL-D-4000 sample, (Figure 6h) a higher compaction of the fibers is observed, which can hinder the interaction with CO_2. More detailed discussion regarding the interaction of the compounds with CO_2 is available in section 3.7.

Table 2. Sorption values for cellulose and amine modified cellulose samples at 25°C.

Sample	10 bar $\mu molCO_2/g$	1 bar $\mu molCO_2/g$
CL-CA	243	0.227
CL-HYD	864	287
CL-EDA	1045	346
CL-EDR-148	961	330
CL-D-400	1091	409
CL-D-4000	777	264
CL-M-2005	961	334

The CO_2 sorption capacity of the amine modified cellulose described in this study was lower when compared with commercial solid adsorbents (1800-2000 µmol/g) of surface areas of 1000 to 1700 m^2/g (Gray *et al.*, 2004). However, the cellulose used in this study originates from an agricultural residue and presents a low amount of amine (2×10^{-6} mol/mg) when compared to literature (concentrations of 10-20% (w/w)) (Bachelor e Toochinda, 2012). For example, the sorption results at 1 bar and 30°C found were 351 µmol CO_2/g (for bagasse enriched with 20% of DEA) and 329 µmol CO_2/g (for rice chaff). These results are similar to the obtained for CL-EDA (346 µmol CO_2/g) and lower than the sorption values obtained for the sample CL-D-400 (409 µmol CO_2/g) using lower amine concentrations of around 2×10^{-6}(mol/mg).

In order to examine the reusability of the best material, CL-D-400 was subjected to five additional runs. The sorption was carried out at 25°C under 1 bar of CO_2 pressure. The CO_2 desorption was carried out at 100 °C. At the end, a loss of 5% in the sorption capacity was observed.

3.7 Quantum mechanical simulations

Our experimental results (Table 2 with gas-capture results) indicate that all employed compounds, except CL-CA, exhibit a similar performance. Pressure increase leads to better CO_2 capture, while the order of the compounds efficacies persists. A poor performance of CL-CA is due to absence of chemisorption in this case and weak attraction of the CO_2 molecule to the protonated acetate group. Indeed, the computed binding energy for this case amounts to just 7 kJ mol^{-1}. The other results can be rationalized via computation of thermodynamic potentials for chemisorption of the molecular fragments (Figure 7), which represent the major working sites, -NH- and -NH_2, of the employed compounds.

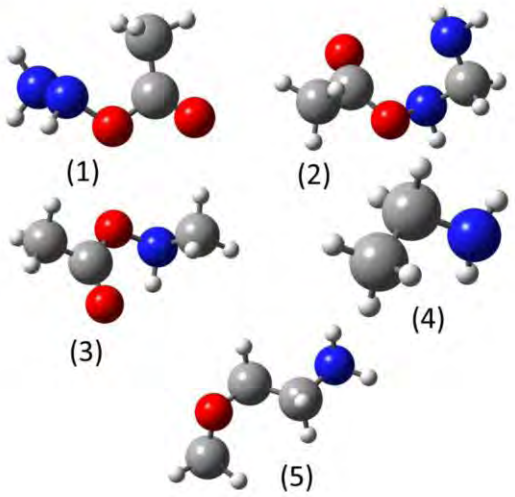

Figure 7. Optimized structures of molecular fragments, which are responsible for CO_2 capture in the modified cellulose species.

Thermodynamic potentials (Figure 8) were used to rationalize the experimentally observed performances of the cellulose based compounds. The depicted potentials correspond to the chemisorption reactions, but omitting subsequent solvation and ionization in aqueous media. This is done for simplicity of discussion and straightforward comparison. For instance, a total free energy of ethylamine is 20 kJ mol^{-1}, due to hydrogen bonds between the products of chemisorption and media. Johnson and coworkers (Xie *et al.*, 2010) thoroughly investigated the mechanism of CO_2 chemisorption by the primary amine and presented extensive evidence that the two-step pathway via a zwitterion intermediate is most energetically favorable and, thus, most expected at the working conditions.

The trend of enthalpy completely repeats the trend of free energy (Figure 8). The entropic contribution is similar in all cases. Therefore, the chemical environment (in particular, non-covalent binding energy) is responsible for the difference between the considered molecular fragments. The best performance was found in CL-D-400 and CL-EDA. This is confirmed theoretically by the thermodynamics of fragment 2, whose free energy and enthalpy are lowest. The chemisorption is conducted both through the amide and amine groups and their high concentrations in the compounds. The performance of CL- D-4000 is

worse, since that compound contains lots of ether groups, which are not efficient for the CO_2 fixation. The ether group itself attracts CO_2 weakly. The binding energy corresponding to this process is 8 kJ mol^{-1}. The impact of a few available carboxylate groups is even smaller, 4 kJ mol^{-1} in terms of binding energy. The performance of CL-HYD is inferior to that of CL-EDA, because the amide group cannot bind CO_2 in the -NH-NH_2 configuration. The resulting compound is unstable (according to the stationary-point-search simulations) and, therefore, is never formed. In turn, separating -NH- and -NH_2 by one or two methylene groups allows to achieve a more decent CO_2 capture.

It is noteworthy that the gas-phase thermodynamics provides a correct account of the reactions occurring in the condensed phase allowing to rate large molecules with multiple binding sites. This fact also suggests that intra-molecular interactions are more important than inter-molecular ones upon chemical adsorption. All methods, G-3, G-3-MP2, G-4-MP2, for thermodynamic potentials provide very similar results.

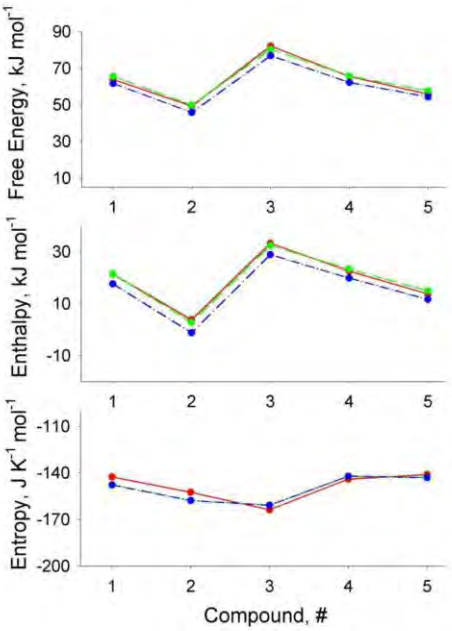

Figure 8. Free energy (top), enthalpy (center) and entropy (bottom) for CO_2 capture through chemisorption at –NH_2 by the molecular fragments depicted in Figure 7. The results from the G-4-MP2 method are red solid lines, from the G-

3-MP2 method are green dashed lines, from the G-3 method are blue dash-dotted lines.

Since a total number of molecules decreases upon chemisorption, pressure increase shifts this reaction rightwards. Figure 9 depicts an effect of pressure up to 1000 MPa. The latter brings the 34 kJ mol^{-1} free energy increase. An approximate shift of the chemisorption equilibrium constant can be estimated from the following relationship: $K^i = \exp(-G^i/R \times T)$, where T is temperature, R is gas constant, G^i is free energy at given conditions. These calculations allow to determine to which extent it is economically feasible to invest in the high-pressure apparatus. The calculated effect of pressure is in concordance with our experimental results. In all systems, higher pressure results in a significantly better CO_2 fixation.

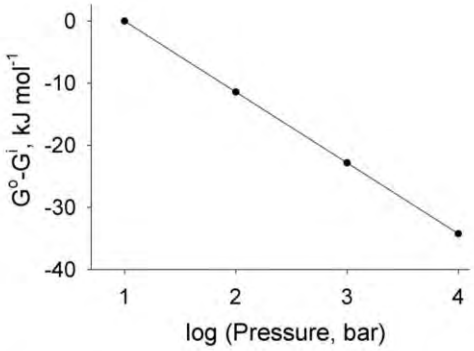

Figure 9. Free energy decrease due to elevation of external pressure. The thermodynamics of the CO_2 capture reaction by ethyl amine was considered for an example.

4. Conclusion

The chemical modification of cellulose fibers, extracted from the rice husk with different amines was performed. The potential of the obtained compounds for use as sorbents for CO_2 capture evaluated. The quantum mechanical simulations and the experimental results revealed the role of each moiety of the new compounds in the gas capture process. A poor performance of CL-CA was noticed due to the absence of chemisorption in this case and a relatively weak

attraction of the CO_2 molecule to the protonated acetate group. The best performance was found in CL-D-400 (CL-D - 400 (409 μmol CO_2/g at 1 bar). This result is confirmed theoretically by the thermodynamics of fragment 2, whose free energy and enthalpy are lowest. The chemisorption is conducted both through the amide and amine groups, therefore, their high concentrations in the compounds are important. On the other side, when a higher-molecular-weight amine was used (CL-D-4000) the performance was worse, since that compound contained lots of ether groups, which are not efficient for the CO_2 fixation. The performance of CL-HYD is inferior to that of CL-EDA, because the amide group cannot chemically bind CO_2 in the -NH-NH_2 configuration. In turn, separating -NH- and -NH_2 by one or two methylene groups allows to achieve a more decent CO_2 capture. Higher pressure results in a significantly better CO_2 fixation. The use of an industrial residue, cellulose, as a material for CO_2 capture is a promising environmental solution, besides being a low-cost option.

Acknowledgments

This work was achieved in cooperation with Hewlett-Packard Brasil Ltda. using incentives of Brazilian Informatics Law (Law nº 8.2.48 of 1991).The authors would like to thank Cooperativa Arrozeira Extremo Sul Ltda for donate the rice husk and Huntsman Perfomance Products – Brazil for donate the JEFFAMINEs, Sandra Einloft thanks CNPq for research scholarship. Franciele L. Bernard thanks Hewlett-Packard Brasil Ltda for scholarship.

5. References

Arias, A. M.; Mores, P. L.; Scenna, N. J.; Mussatl, S. F. Optimal design and sensitivity analysis of post-combustion CO_2 capture process by chemical absorption with amines. Journal of Cleaner Production, 115, 315–331 (2016).

Bachelor, T. T. N.; Toochinda, P. Development of low-cost amine-enriched solid sorbent for CO2 capture. Environmental Technology, 33 (23) 2645–2651 (2012).

Barbosa, R. C.; Damasceno, J. J. R.; Hori, C. E. The use of a high limestone content mining waste as a sorbent for CO_2 capture. Brazilian Journal of Chemical Engineering, 33 (3) 599–606 (2016).

Becke, A. D. Density-functional exchange-energy approximation with correct asymptotic behavior. Physical Review A, 38(6) 3098–3100, 1 (1988).

Bernard, F. L.; Rodrigues, D. M.; Polesso, B. B.; Donato, A. J.; Seferin, M.; Chaban, V. V.; Vecchia, F. D.; Einloft, S. New cellulose based ionic compounds as low-cost sorbents for CO_2 capture. Fuel Processing Technology, 149, 131–138 (2016).

Blasig, A.; Tang, J.; Hu, X.; Shen, Y.; Radosz, M. Magnetic suspension balance study of carbon dioxide solubility in ammonium-based polymerized ionic liquids: Poly(p-vinylbenzyltrimethyl ammonium tetrafluoroborate) and poly([2-(methacryloyloxy)ethyl] trimethyl ammonium tetrafluoroborate). Fluid Phase Equilibria, 256 (1–2), 75–80 (2007).

Chan, W. N.; Walter, A.; Sugiyama, M. I.; Borges, G. C. Assessment of CO_2 Emission Mitigation For a Brazilian Oil Refinery. Brazilian Journal of Chemical Engineering, 33 (4) 835–850, (2016).

Cuadro, P. DE; Belt, T.; Kontturi, K. S.; Reza, M.; Kontturi, E.; Vuorinen, T.; Hughes, M. Cross-linking of cellulose and poly(ethylene glycol) with citric acid. Reactive and Functional Polymers, 90, 21–24 (2015).

Curtiss, L. A.; Raghavachari, K.; Redfern, P. C.; Rassolov, V.; Pople, J. A. Gaussian-3 (G3) theory for molecules containing first and second-row atoms. The Journal of Chemical Physics, 109 (18), 7764–7776, (1998).

Curtiss, L. A.; Redfern, P. C.; Raghavachari, K. Gaussian-4 theory using reduced order perturbation theory. The Journal of Chemical Physics, 127 (12) 124105 (2007).

Curtiss, L. A.; Redfern, P. C.; Raghavachari, K.; Rassolov, V.; Pople, J. A. Gaussian-3 theory using reduced Mo/ller-Plesset order. The Journal of Chemical Physics, 110 (10) 4703–4709 (1999)

Dreisbach, F.; Lösch, H. W. Magnetic Suspension Balance For Simultaneous Measurement of a Sample and the Density of the Measuring Fluid. Journal of Thermal Analysis and Calorimetry, 62, (2) 515–521(2000).

Dutcher, B.; Fan, M.; Russell, A. G. Amine-Based CO_2 Capture Technology Development from the Beginning of 2013—A Review. ACS Applied Materials & Interfaces, 7 (4) 2137–2148 (2015).

Garcés, S. I.; Villarroel-Rocha, J.; Sapag, K.; Korili, S. A.; Gil, A. Comparative Study of the Adsorption Equilibrium of CO_2 on Microporous Commercial Materials at Low Pressures. Industrial & Engineering Chemistry Research, 52 (20) 6785–6793, (2013).

Garðarsdóttir, S. Ó.; Normann, F.; Andersson, K.; Johnsson, F. Postcombustion CO_2 Capture Using Monoethanolamine and Ammonia Solvents: The Influence of CO_2 Concentration on Technical Performance. Industrial & Engineering Chemistry Research, 54 (2) 681–690 (2015).

Gebald, C.; Wurzbacher, J. A.; Tingaut, P.; Steinfeld, A. Stability of Amine-Functionalized Cellulose during Temperature-Vacuum-Swing Cycling for CO_2 Capture from Air. Environmental Science & Technology, 47 (17) 10063–10070, (2013).

Gebald, C.; Wurzbacher, J. A.; Tingaut, P.; Zimmermann, T.; Steinfeld, A. Amine-Based Nanofibrillated Cellulose As Adsorbent for CO_2 Capture from Air. Environmental Science & Technology, 45 (20) 9101–9108 (2011).

Gray, M. L.; Soong, Y.; Champagne, K. J.; Baltrus, J.; Stevens, R. W.; Toochinda, P.; Chuang, S. S. C. CO_2 capture by amine-enriched fly ash carbon sorbents. Separation and Purification Technology, 35(1) 31–36 (2004).

Gray, M. L.; Soong, Y.; Champagne, K. J.; Pennline, H.; Baltrus, J. P.; Stevens, R. W.; Khatri, R.; Chuang, S. S. C.; Filburn, T. Improved immobilized carbon dioxide capture sorbents. Fuel Processing Technology, 86, (14–15),1449–1455, (2005).

Gurgel, L. V. A.; Júnior, O. K.; Gil, R. P. De F.; Gil, L. F. Adsorption of Cu(II), Cd(II), and Pb(II) from aqueous single metal solutions by cellulose and

mercerized cellulose chemically modified with succinic anhydride. Bioresource Technology, 99, (8) 3077–3083 (2008).

Hussain, A.; Farrukh, S.; Minhas, F. T. Two-Stage Membrane System for Post-combustion CO 2 Capture Application. Energy & Fuels, 29 (10) 6664–6669, (2015).

IBGE- GRUPO DE COORDENAÇÃO DE ESTATÍSTICAS AGROPECUÁRIAS. Levantamento Sistemático da Produção Agrícola. Disponível em: <http://www.ibge.gov.br/home/estatistica/indicadores/agropecuaria/lspa/lspa_201702_5.shtm>. Acesso em: 28 mar. 2017.

Johar, N.; Ahmad, I.; Dufresne, A. Extraction, preparation and characterization of cellulose fibres and nanocrystals from rice husk. Industrial Crops and Products, 37 (1) 93–99, 2012.

K. Shukla, S.; Bharadvaja, A.; C. Dubey, G.; Tiwari, A. Preparation And Characterization Of Cellulose Derived From Rice Husk For Drug Delivery. Advanced Materials Letters, 4(9) 714–719, (2013).

Kamarudin, K. S. N.; Alias, N. Adsorption performance of MCM-41 impregnated with amine for CO2 removal. Fuel Processing Technology, 106, 332–337 (2013).

Karnitz, O.; Gurgel, L. V. A.; Melo, J. C. P. DE; Botaro, V. R.; Melo, T. M. S.; Freitas Gil, R. P. de; Gil, L. F. Adsorption of heavy metal ion from aqueous single metal solution by chemically modified sugarcane bagasse. Bioresource Technology, 98 (6) 1291–1297 (2007).

Knowles, G. P.; Graham, J. V.; Delaney, S. W.; Chaffee, A. L. Aminopropyl-functionalized mesoporous silicas as CO2 adsorbents. Fuel Processing Technology, 86 (14–15) 1435–1448, (2005).

Lee, C.; Yang, W.; Parr, R. G. Development of the Colle-Salvetti correlation-energy formula into a functional of the electron density. Physical Review B, 37 (2) 785–789, (1988).

Leung, D. Y. C.; Caramanna, G.; Maroto-valer, M. M. An overview of current

status of carbon dioxide capture and storage technologies. Renewable and Sustainable Energy Reviews, 39 426–443, (2014).

LI, R.; Fei, J.; Cai, Y.; LI, Y.; Feng, J.; Yao, J. Cellulose whiskers extracted from mulberry: A novel biomass production. Carbohydrate Polymers, 76 (1)p. 94–99, mar. 2009.

Lima, A. E. O.; Gomes, V. A. M.; Lucena, S. M. P. Theoretical study of CO_2:N_2 adsorption in faujasite impregnated with monoethanolamine. Brazilian Journal of Chemical Engineering, 32 (3) 663–669 (2015).

Magalhaes, T. O.; Aquino, A. S.; Dalla Vecchia, F.; Bernard, F. L.; Seferin, M.; Menezes, S. C.; Ligabue, R.; Einloft, S. Syntheses and characterization of new poly(ionic liquid)s designed for CO_2 capture. RSC Adv., 4 (35). 18164–18170, (2014).

Nouri, S. M. M.; Ebrahim, H. A. Effect of sorbent pore volume on the carbonation reaction of lime with CO_2. Brazilian Journal of Chemical Engineering, 33 (2) 383–389 (2016).

Rodrigues, R. F.; Trevenzoli, R. L.; Santos, L. R. G.; Leão, V. A.; Botaro, V. R. Heavy metals sorption on treated wood sawdust. Engenharia Sanitaria e Ambiental, 11 (1) (2006).

Rosa, S. M. L.; Rehman, N.; Miranda, M. I. G. DE; Nachtigall, S. M. B.; Bica, C. I. D. Chlorine-free extraction of cellulose from rice husk and whisker isolation. Carbohydrate Polymers, 87 (2) 1131–1138, (2012).

Segal, L.; Creely, J. J.; Martin, A. E.; Conrad, C. M. An Empirical Method for Estimating the Degree of Crystallinity of Native Cellulose Using the X-Ray Diffractometer. Textile Research Journal, 29 (10) 786–794 (1959).

Seo, S.; Simoni, L. D.; Ma, M.; Desilva, M. A.; Huang, Y.; Stadtherr, M. A.; Brennecke, J. F. Phase-Change Ionic Liquids for Postcombustion CO 2 Capture. Energy & Fuels, 28 (9) 5968–5977 (2014).

Shang, W.; Sheng, Z.; Shen, Y.; AI, B.; Zheng, L.; Yang, J.; Xu, Z. Study on oil absorbency of succinic anhydride modified banana cellulose in ionic liquid.

Carbohydrate Polymers, 141 135–142, (2016).

Teodoro, K. B. R.; Teixeira, E. De M.; Corrêa, A. C.; Campos, A. De; Marconcini, J. M.; Mattoso, L. H. C. Whiskers de fibra de sisal obtidos sob diferentes condições de hidrólise ácida: efeito do tempo e da temperatura de extração. Polímeros, 21 (4) 280–285, (2011).

Xie, H.-B.; Zhou, Y.; Zhang, Y.; Johnson, J. K. Reaction Mechanism of Monoethanolamine with CO_2 in Aqueous Solution from Molecular Modeling. The Journal of Physical Chemistry A, 114, (43) 11844–11852, (2010).

YU, C.; Huang, C.; Tan, C. A Review of CO_2 Capture by Absorption and Adsorption. 745–769, (2012).

Yu, J.; Le, Y.; Cheng, B. Fabrication and CO_2 adsorption performance of bimodal porous silica hollow spheres with amine-modified surfaces. RSC Advances, 2 (17) 6784, (2012).

Zhang, K.; Sun, P.; Liu, H.; Shang, S.; Song, J.; Wang, D. Extraction and comparison of carboxylated cellulose nanocrystals from bleached sugarcane bagasse pulp using two different oxidation methods. Carbohydrate Polymers, 138 237–243, (2016).

Zhu, B.; Fan, T.; Zhang, D. Adsorption of copper ions from aqueous solution by citric acid modified soybean straw. Journal of Hazardous Materials, 153 (1–2) 300–308 (2008).

5. DISCUSSÕES GERAIS

5.1. Comparativo entre os melhores materiais de cada grupo

A partir dos resultados e discussões apresentados na seção 4 foram selecionados os melhores materiais obtidos de cada grupo: CL-TBA, [CelEt$_3$N][PF$_6$], CL-D400; PU-TBA, PU-TBP e HPIL-02-TBA. A capacidade de sorção de CO_2 foi utilizada como fator principal para seleção destes materiais. A aparência física dos materiais é ilustrada na Figura 5.1 e um comparativo entre os principais resultados é mostrado na Tabela 5.1. Os resultados experimentais obtidos para o teste de dessorção utilizando temperatura ou vácuo, também foram incluídos na Tabela 5.1. Neste teste, após a realização do ensaio de sorção na célula de decaimento de pressão, a amostra foi submetida a vácuo ou aquecimento. Em seguida, esta amostra foi re-submetida a um ensaio de sorção e a partir da diferença entre o CO_2 capturado no primeiro e no segundo ensaio, a quantidade de CO_2 dessorvido da amostra foi determinado.

Filmes de Poli (líquidos iônicos) translúcidos foram obtidos a partir de PU ou PU-imida (Fig. 5.1d-f). Os PLIs base PU-imida apresentaram coloração levemente amarela, resultante do dianidrido utilizada na síntese (Fig. 5.1f). Todos os materiais sintetizados a partir da celulose apresentaram-se sob a forma de pó, as amostras de celulose modificadas com o ácido cítrico (Fig. 5.1a e Fig. 5.1c) exibiram coloração amarela e as modificadas com cloreto de tionila, coloração marrom escura (Fig.5.1b).

Figura 5.1. Imagens ópticas obtidas para os melhores materiais de cada grupo: a) CL-TBA, b) [CelEt3N][PF6]; c) CL-D400; d) PU-TBA; e) PU-TBP e f) HPIL-02-TBA.

A Tabela 5.1 apresenta um comparativo entre os resultados de estabilidade térmica, módulo de Young, sorção e dessorção de CO_2 obtidos para as melhores amostras de cada grupo. Todas as amostras demostraram boa estabilidade térmica. O PLI base PU-imida mostrou módulo de Young superior aos obtidos com os PLIs base PU. Os valores de sorção de CO_2, obtidos a baixa pressão (~0.1Mpa) demostraram o desempenho superior dos PLIs celulósicos (CL-TBA e [CelEt3N][PF6]). Por outo lado, com o aumento da pressão (1MPa), os melhores resultados de sorção foram alcançados com o PLI celulósico [$CelEt_3N$][PF_6] e com o PLI base PU-imida HPIL-02-TBA.

Os testes de dessorção realizados com vácuo demostraram a capacidade de reciclo dos PLIs. Este comportamento não foi evidenciado para a amostra CL-D400, onde a reação entre o grupo -NH_2 e o CO_2 pode produzir carbamato de amônio (ABOUDI; VAFAEEZADEH, 2015), reduzindo assim a capacidade de sorção deste material ao longo do processo. Para todos os PLIs a substituição de vácuo por

temperatura durante os testes de dessorção gerou uma retenção de CO_2 na amostra (10,5% a 17%). A diminuição da temperatura de dessorção de CO_2 da amostra CL-D400 de 100°C para 50°C reduziu a capacidade de sorção de CO_2 em 58,5% (Tabela 5.1). Em geral, os PLIs demostraram maior potencial para captura quando comparados com o CL-D400.

Tabela 5.1. Principais resultados obtidos para as amostras selecionadas em cada grupo.

Amostra	$T_{(onset)}$°C	Módulo de Young	Sorção de CO_2 (mg/g) ~0,1MPa	Sorção de CO_2 (mg/g) 1 MPa	CO_2 dessorvido (%)		Material pertencente ao Capítulo
					Condições: vácuo; T. amb; Tempo 1h	Condições: 50°C e Tempo 1h	
CL-TBA	324	-	44,0*	53,0*	100	84,5	III
$[CelEt_3N][PF_6]$	203	-	38,0*	80,0*	100	89.5	IV
PU-TBA	190	6,3	16,1**	49,1**	100	84,6	I
PU-TBP	210	11,4	15,7**	43,7**	100	86,5	I
HPIL-02-TBA	175	56,4	33,1**	61,0**	100	83,0	II
CL-D400	318	-	18,0*	48*	95***	41,5	V

*Temperatura = 25°C; **Temperatura = 30°C; *** condição de dessorção diferente = 100°C sem uso de vácuo.

Apesar dos PLIs sintetizados neste trabalho terem demostrado valores de sorção de CO_2 superiores a diversos PLIs relatados na literatura (TANG et al., 2005a; ZHU et al., 2011; PRIVALOVA et al., 2013; MOROZOVA et al., 2017), a capacidade de sorção destes PLIs não superou a alcançada com o uso da solução aquosa de 30% m/m de MEA (0,45 mol/mol = 324mg CO_2/g MEA á 1 atm e 25°C) (RINPRASERTMEECHAI et al., 2012), solvente tradicionalmente empregado em plantas de captura. Entretanto, o uso destes PLIs oferece algumas vantagens em comparação às aminas, tais como a ausência da formação de produtos corrosivos, a reciclabilidade, e a baixa necessária para a regeneração. Também cabe ressaltar que a comparação destes PLIs com aminas deve considerar outros fatores que não

foram abordados neste trabalho, como por exemplo o custo de fabricação destes sorventes, a capacidade seletiva, entre outros.

6. CONCLUSÕES

Nesta secção, as conclusões serão divididas em três blocos: PLIs aniônicos base PU e PU-imida, PLIs celulósicos aniônicos e catiônicos e aminas suportadas em celulose.

Os resultados obtidos para os PLIs aniônicos base PU e PU-imida evidenciaram que o contra-cátion desempenha um papel importante sobre a solubilidade do CO_2, estabilidade térmica, propriedades mecânicas e morfologia dos PLIs. Ensaios experimentais de sorção/dessorção de CO_2 demonstraram a capacidade de reutilização destes materiais. Estudos computacionais revelaram que o grupo carboxílico desprotonado (COO^-) é um importante sítio de interação com o CO_2, e que os cátions TBA e TBP exercem uma coordenação mais fraca sobre este sítio comparada com o imidazólio. A coordenação fraca favorece a interação entre o CO_2 e o grupo carboxilato (COO^-), contribuindo para o aumento da capacidade de sorção de CO_2. A comparação dos resultados de sorção de CO_2 obtidos para os PLIs base PU e PU-imida mostraram que o aumento da presença de grupos polares na cadeia polimérica promove a melhora da capacidade de sorção de CO_2. Para os PLIs base PU-imida observou-se que concentrações menores dos grupos silanos favorece a interação entre o PLIs e o CO_2.

O uso da celulose extraída da casca de arroz como base para o desenvolvimento de sorventes para captura de CO_2, demonstrou ser uma opção promissora, pois permite a redução de resíduos agroindústrias e pode contribuir para a obtenção de sorventes de baixo custo.

Os PLIs celulósicos aniônicos e catiônicos demonstraram-se estáveis termicamente e reutilizáveis no processo de captura de CO_2. Para os PLIs aniônicos o método empregado para obtenção destes compostos permite uma capacidade de

sorção elevada, com o uso de uma pequena quantidade de líquido iônico. A investigação realizada por simulação computacional revelou que o CO_2 interage de forma mais efetiva com o grupo carboxilato, e, em menor grau com os grupos polares da estrutura da celulose. Os cátions BMPYRR, TBP e TBA são usados como contra-íons de coordenação fraca, mantendo os locais de atração do CO_2 parcialmente ou totalmente livres. Por sua vez, o cátion BMIM coordena o CO_2, devido a uma ligação de hidrogênio fraca proveniente do átomo de hidrogênio ácido do anel imidazólio com o átomo de oxigênio do CO_2. A capacidade de sorção de CO_2 dos PLIs catiônicos é influenciada pelo contra-ânion, os resultados mostraram também que a fluoração do ânion pode proporcionar o aumento da sorção de CO_2. Porém, o uso de ânions fluorados volumosos pode prejudicar a interação do CO_2 com os grupos polares da estrutura e reduzir a capacidade de sorção de CO_2.

A modificação química da celulose com aminas e polieteraminas promoveu resultados de sorção de CO_2 menores que os obtidos com os PLIs celulósicos e PLIs aniônicos base PU. A introdução de grupos amidas e aminas proporcionaram o aumento da estabilidade térmica e da capacidade de solubilidade de CO_2 da celulose. Estudos de simulação revelaram que a quimisorção é favorecida por grupos -NH- e -NH_2. Aliado a isso, os testes experimentais de sorção de CO_2 evidenciaram que a concentração destes grupos pode influenciar a solubilidade.

Para os PLIs, os ensaios de dessorção efetuados com o uso de temperatura (50°C) demonstraram a possibilidade de utilização de calor residual de processo para a realização da etapa de dessorção. Isto pode representar uma vantagem em relação a soluções aquosas de aminas que necessitam de alta quantidade de calor para etapa de regeneração.

Dentre todos os materiais sintetizados neste trabalho, os PLIs celulósicos CL-TBA e [CelEt_3N][PF_6] e com o PLI base PU-imida HPIL-02-TBA demostraram maior afinidade pelo CO_2, aliado a boa estabilidade térmica e reciclabilidade.

7. REFERÊNCIAS BIBLIOGRÁFICAS

ABOUDI, J.; Vafaeezadeh, M. Efficient and reversible CO_2 capture by amine functionalized-silica gel confined task-specific ionic liquid system. **Journal of Advanced Research**, v. 6, n. 4, p. 571–577, 2015.

AKI, S. N. V. K.; Mellein, B. R.; Saurer, E. M.; Brennecke, J. F. High-Pressure Phase Behavior of Carbon Dioxide with Imidazolium-Based Ionic Liquids. **The Journal of Physical Chemistry B**, v. 108, n. 52, p. 20355–20365, 2004.

ANTHONY, J. L.; Anderson, J. L.; Maginn, E. J.; Brennecke, J. F. Anion Effects on Gas Solubility in Ionic Liquids: The Journal of Physical Chemistry B. **The Journal of Physical Chemistry B**, v. 109, n. 13, p. 6366–6374, 2005.

ARIAS, A. M.; Mores, P. L.; Scenna, N. J.; Mussati, S. F. Optimal design and sensitivity analysis of post-combustion CO_2 capture process by chemical absorption with amines. **Journal of Cleaner Production**, v. 115, p. 315–331, 2016.

BABAMOHAMMADI, S.; Shamiri, A.; Aroua, M. K. A review of CO_2 capture by absorption in ionic liquid-based solvents. **Reviews in Chemical Engineering**, v. 31, n. 4, p. 383–412, 2015.

BACHELOR, T. T. N.; Toochinda, P. Development of low-cost amine-enriched solid sorbent for CO_2 capture. **Environmental Technology**, v. 33, n. 23, p. 2645–2651, 2012.

BARA, J. E.; Gabriel, C. J.; Hatakeyama, E. S.; Carlisle, T. K.; Lessmann, S.; Noble, R. D.; GIN, D. L. Improving CO_2 selectivity in polymerized room-temperature ionic liquid gas separation membranes through incorporation of polar substituents. **Journal of Membrane Science**, v. 321, n. 1, p. 3–7, 2008.

BARA, J. E.; Lessmann, S.; Gabriel, C. J.; Hatakeyama, E. S.; Noble, R. D.; Gin, D. L. Synthesis and Performance of Polymerizable Room-Temperature Ionic Liquids as Gas Separation Membranes. **Industrial & Engineering Chemistry Research**, v. 46, n. 16, p. 5397–5404, 2007.

BARA J. E. , Hatakeyama Evan S. , Gin Douglas L., N. R. D. Improving CO_2 permeability in polymerized room-temperature ionic liquid gas separation membranes through the formation of a solid composite with a room-temperature ionic liquidy. **Polymers for Advanced Technologies**, v. 19, p. 1415–1420, 2008.

BHAVSAR, R. S.; Kumbharkar, S. C.; Kharul, U. K. Polymeric ionic liquids (PILs): Effect of anion variation on their CO_2 sorption. **Journal of Membrane Science**, v. 389, p. 305–315, 2012.

BHAVSAR, R. S.; Kumbharkar, S.; Rewar, A. S.; Kharul, U. K. Polybenzimidazole based film forming polymeric ionic liquids: Synthesis and effects of cation-anion variation on their physical properties. **Polymer Chemistry**, p. 4083–4096, 2014.

BLASIG, A.; Tang, J.; Hu, X.; Shen, Y.; Radosz, M. Magnetic suspension balance study of carbon dioxide solubility in ammonium-based polymerized ionic liquids: Poly(p-vinylbenzyltrimethyl ammonium tetrafluoroborate) and poly([2-(methacryloyloxy)ethyl] trimethyl ammonium tetrafluoroborate). **Fluid Phase Equilibria**, v. 256, n. 1–2, p. 75–80, 2007.

BRUHN, T.; Naims, H.; Olfe-kräutlein, B. Separating the debate on CO_2 utilisation from carbon capture and storage. **Environmental Science and Policy**, v. 60, p. 38–43, 2016.

CADENA, C.; Anthony, J. L.; Shah, J. K.; Morrow, T. I.; Brennecke, J. F.; Maginn, E. J. Why is CO_2 so Soluble in Imidazolium-Based Ionic Liquids? **Journal of the American Chemical Society**, v. 126, n. 16, p. 5300–5308, 2004.

CARLISLE, T. K.; Bara, J. E.; Lafrate, A. L.; Gin, D. L.; Noble, R. D. Main-chain imidazolium polymer membranes for CO_2 separations: An initial study of a new ionic liquid-inspired platform. **Journal of Membrane Science**, v. 359, n. 1–2, p. 37–43, 2010.

CARLISLE, T. K.; Wiesenauer, E. F.; Nicodemus, G. D.; Gin, D. L.; Noble, R. D. Ideal CO_2 /Light Gas Separation Performance of Poly(vinylimidazolium) Membranes and Poly(vinylimidazolium)-Ionic Liquid Composite Films. **Industrial & Engineering Chemistry Research**, v. 52, n. 3, p. 1023–1032, 2013.

CHENG, H.; Wang, P.; Luo, J.; Fransaer, J.; DE Vos, D. E.; Luo, Z. H. Poly(ionic liquid)-based nanocomposites and their performance in CO_2 capture. **Industrial and Engineering Chemistry Research**, v. 54, n. 12, p. 3107–3115, 2015.

DAI, Z.; Noble, R. D.; Gin, D. L.; Zhang, X.; Deng, L. Combination of ionic liquids with membrane technology: A new approach for CO_2 separation. **Journal of Membrane Science**, v. 497, p. 1–20, 2016.

FANG, W.; Luo, Z.; Jiang, J. CO_2 capture in poly(ionic liquid) membranes: atomistic insight into the role of anions. **Physical Chemistry Chemical Physics**, v. 15, p. 651–658, 2013.

FERNÁNDEZ, M.; Carreño, L. Á.; Bernard, F.; Ligabue, R.; Einloft, S. Poly(ionic liquid)s Nanoparticles Applied in CO $_2$ Capture. **Macromolecular Symposia**, v. 368, n. 1, p. 98–106, 2016.

FIGUEROA, J. D.; Fout, T.; Plasynski, S.; Mcilvried, H.; Srivastava, R. D. Advances in CO_2 capture technology-The U.S. Department of Energy's Carbon Sequestration Program. **International Journal of Greenhouse Gas Control**, v. 2, n. 1, p. 9–20, 2008.

GARCES, S. I.; Villarroel-rocha, J.; Sapag, K.; Korili, S. A.; Gil, A. Comparative Study of the Adsorption Equilibrium of CO_2 on Microporous Commercial Materials at Low Pressures. **Industrial & Engineering Chemistry Research**, v. 52, p. 6785–6793, 2013.

HASIB-UR-RAHMAN, M.; Siaj, M.; Larachi, F. Ionic liquids for CO_2 capture-Development and progress. **Chemical Engineering and Processing: Process Intensification**, v. 49, n. 4, p. 313–322, 2010.

HORNE, W. J.; Andrews, M. A.; Shannon, M. S.; Terrill, K. L.; Moon, J. D.; Hayward, S. S.; BARA, J. E. Effect of branched and cycloalkyl functionalities on CO_2 separation performance of poly(IL) membranes. **Separation and Purification Technology**, v. 155, p. 89–95, 2014.

KENARSARI, S. D.; Yang, D.; Jiang, G.; Zhang, S.; Wang, J.; Russell, A. G.; Wei, Q.; Fan, M. Review of recent advances in carbon dioxide separation and capture. **RSC Advances**, v. 3, n. 45, p. 22739–22773, 2013.

KETZER, J. M.; Iglesias, R. S.; Einloft, S. Reducing Greenhouse Gas Emissions with CO_2 Capture and Geological Storage. In: **Handbook of Climate Change Mitigation and Adaptation**. New York, NY: Springer New York, 2015. p. 1–40.

KUMBHARKAR, S. C.; Bhavsar, R. S.; Kharul, U. K. Film forming polymeric ionic liquids (PILs) based on polybenzimidazoles for CO2 separation. **RSC Advances**, v. 4, n. 9, p. 4500, 2014.

LEUNG, D. Y. C.; Caramanna, G.; Maroto-valer, M. M. An overview of current status of carbon dioxide capture and storage technologies. **Renewable and Sustainable Energy Reviews**, v. 39, p. 426–443, 2014.

MAGALHAES, T. O.; Aquino, A. S.; Dalla Vecchia, F.; Bernard, F. L.; Seferin, M.; Menezes, S. C.; Ligabue, R.; Einloft, S. Syntheses and characterization of new poly(ionic liquid)s designed for CO_2 capture. **RSC Adv.**, v. 4, n. 35, p. 18164–18170, 2014.

MARKEWITZ, P.; Kuckshinrichs, W.; Leitner, W.; Linssen, J.; Zapp, P.; Bongartz, R.; Schreiber, A.; Müller, T. E. Worldwide innovations in the development of carbon capture technologies and the utilization of CO_2. **Energy & Environmental Science**, v. 5, n. 6, p. 7281, 2012.

MECERREYES, D. Polymeric ionic liquids: Broadening the properties and applications of polyelectrolytes. **Progress in Polymer Science (Oxford)**, v. 36, n. 12, p. 1629–1648, 2011.

MONDAL, M. K.; Balsora, H. K.; Varshney, P. Progress and trends in CO_2 capture/separation technologies: A review. **Energy**, v. 46, n. 1, p. 431–441, 2012.

MONTZKA, S. A.; Dlugokencky, E. J.; Butler, J. H. Non-CO_2 greenhouse gases and climate change. **Nature**, v. 476, n. 7358, p. 43–50, 2011.

MOROZOVA, S. M.; Shaplov, A. S.; Lozinskaya, E. I.; Mecerreyes, D.; Sardon, H.; Zulfiqar, S.; Suaez-garcía, F.; Vygodskii, Y. S. Ionic Polyurethanes as a New Family of Poly(ionic liquid)s for Efficient CO_2 Capture. 2017.

NOAA – NATIONAL ORGANIC & ATMOSPHERIC ADMINISTRATION. **Trends in Atmospheric carbon Dioxide – Mauna Loa**.

OLAJIRE, A. A. CO_2 capture and separation technologies for end-of-pipe applications - A review. **Energy**, v. 35, n. 6, p. 2610–2628, 2010.

PENNLINE, H. W.; Luebke, D. R.; Jones, K. L.; Myers, C. R.; Morsi, B. I.; Heintz, Y. J.; Ilconich, J. B. Progress in carbon dioxide capture and separation research for gasification-based power generation point sources. **Fuel Processing Technology**, v. 89, n. 9, p. 897–907, 2008.

PRIVALOVA, E. I.; Karjalainen, E.; Nurmi, M.; Mäki-arvela, P.; Eränen, K. Imidazolium-Based Poly (ionic liquid) s as New Alternatives for CO 2 Capture. **ChemSusChem.**, p. 1500–1509, 2013.

PRIVALOVA, E. I.; Mäki-arvela, P.; Murzin, D. Y.; Mikkhola, J. P. Capturing CO_2: conventional versus ionic-liquid based technologies. **Russian Chemical Reviews**, v. 81, n. 5, p. 435–457, 31 maio 2012.

QIAN, W.; Texter, J.; Yan, F. Frontiers in poly(ionic liquid)s: syntheses and applications. **Chem. Soc. Rev.**, 2017.

RAMDIN, M.; Amplianitis, A.; Bazhenov, S.; Volkov, A.; Volkov, V.; Vlugt, T. J. H.; De Loos, T. W. Solubility of CO_2 and CH_4 in Ionic Liquids: Ideal CO_2 /CH_4 Selectivity. **Industrial \& Engineering Chemistry Research**, v.53 p. 15427–15435, 2014.

RAMDIN, M.; De loos, T. W.; Vlugt, T. J. H. State-of-the-art of CO_2 capture with ionic liquids. **Industrial and Engineering Chemistry Research**, v. 51, p. 8149–8177, 2012.

RINPRASERTMEECHAI, S.; Chavadej, S.; Rangsunvigit, P.; Kulprathipanja, S. Carbon Dioxide Removal from Flue Gas Using Amine-Based Hybrid Solvent Absorption. v. 6, n. 4, p. 284–288, 2012.

RIVERA-TINOCO, R.; Bouallou, C. Comparison of absorption rates and absorption capacity of ammonia solvents with MEA and MDEA aqueous blends for CO_2 capture. **Journal of Cleaner Production**, v. 18, n. 9, p. 875–880, 2010.

SADEGHPOUR, M.; Yusoff, R.; Aroua, M. K. Polymeric ionic liquids (PILs) for CO_2 capture. **Reviews in Chemical Engineering**, v. 0, n. 0, 2016.

SEO, S.; Simoni, L. D.; Ma, M.; Desilva, M. A.; Huang, Y.; Stadtherr, M. A.; BRENNECKE, J. F. Phase-Change Ionic Liquids for Postcombustion CO_2 Capture. **Energy & Fuels**, v. 28, n. 9, p. 5968–5977, 2014.

SHAPLOV, A. S.; Morozova, S. M.; Lozinskaya, E. I.; Vlasov, P. S.; Gouveia, A. S. L.; Tomé, L. C.; Marrucho, I. M.; Vygodskii, Y. S. Turning into poly(ionic liquid)s as a tool for polyimide modification: synthesis, characterization and CO_2 separation properties. **Polym. Chem.**, v. 7, n. 3, p. 580–591, 2016.

SIMONS, K.; Nijmeijer, K.; Bara, J. E.; Noble, R. D.; Wessling, M. How do polymerized room-temperature ionic liquid membranes plasticize during high pressure CO_2 permeation? **Journal of Membrane Science**, v. 360, n. 1–2, p. 202–209, 2010.

SONGOLZADEH, M.; Soleimani, M.; Takht Ravanchi, M.; Songolzadeh, R. Carbon dioxide separation from flue gases: A technological review emphasizing reduction in greenhouse gas emissions. **The Scientific World Journal**, v. 2014, n. Figure 1, 2014.

TANG, J.; Shen, Y.; Radosz, M.; Sun, W. Isothermal carbon dioxide sorption in poly(ionic liquid)s. **Industrial and Engineering Chemistry Research**, v. 48, n. 20, p. 9113–9118, 2009.

TANG, J.; Sun, W.; Tang, H.; Radosz, M.; Shen, Y. Enhanced CO_2 absorption of poly(ionic liquid)s. **Macromolecules**, v. 38, n. 6, p. 2037–2039, 2005a.

TANG, J.; Tang, H.; Sun, W.; Plancher, H.; Radosz, M.; Shen, Y. Poly(ionic liquid)s: a new material with enhanced and fast CO_2 absorption. **Chemical communications (Cambridge, England)**, n. 26, p. 3325–3327, 2005b.

TANG, J.; Tang, H.; Sun, W.; Radosz, M.; Shen, Y. Poly(ionic liquid)s as new materials for CO_2 absorption. **Journal of Polymer Science Part A: Polymer Chemistry**, v. 43, n. 22, p. 5477–5489, 2005c.

TANG, J.; Tang, H.; Sun, W.; Radosz, M.; Shen, Y. Low-pressure CO_2 sorption in ammonium-based poly(ionic liquid)s. **Polymer**, v. 46, n. 26, p. 12460–12467, 2005d.

TOME, L. C.; Aboudzadeh, M. A.; Rebelo, L. P. N.; Freire, C. S. R.; Mecerreyes, D.; Marrucho, I. M. Polymeric ionic liquids with mixtures of counter-anions: a new straightforward strategy for designing pyrrolidinium-based CO_2 separation membranes. **Journal of Materials Chemistry A: Materials for Energy and Sustainability**, v. 1, n. 35, p. 10403–10411, 2013.

TOMÉ, L. C.; Isik, M.; Freire, C. S. R.; Mecerreyes, D.; Marrucho, I. M. Novel pyrrolidinium-based polymeric ionic liquids with cyano counter-anions: HIGH performance membrane materials for post-combustion CO_2 separation. **Journal of Membrane Science**, v. 483, p. 155–165, 2015.

TOME, L. C.; Marrucho, I. M. Ionic liquid-based materials: a platform to design engineered CO_2 separation membranes. **Chemical Society Reviews**, v. 45, n. 10, p. 2785–2824, 2016.

TOMÉ, L. C.; Mecerreyes, D.; Freire, C. S. R.; Rebelo, L. P. N.; Marrucho, I. M. Pyrrolidinium-based polymeric ionic liquid materials: New perspectives for CO2 separation membranes. **Journal of Membrane Science**, v. 428, p. 260–266, 2013.

WANG, M.; Joel, A. S.; Ramshaw, C.; Eimer, D.; Musa, N. M. Process intensification for post-combustion CO2 capture with chemical absorption: A critical review. **Applied Energy**, v. 158, p. 275–291, 2015.

WATABE, T.; Yogo, K. Isotherms and isosteric heats of adsorption for CO 2 in amine-functionalized mesoporous silicas. **SEPARATION AND PURIFICATION TECHNOLOGY**, v. 120, p. 20–23, 2013.

WILKES, J. S. A Short History of Ionic Liquids - From Molten Salts to Neoteric Solvents. **Green Chemistry**, v. 4, n. 2, p. 73–80, 2002.

XIONG, Y. B.; Wang, H.; Wang, Y. J.; WANG, R. M. Novel imidazolium-based poly(ionic liquid)s: Preparation, characterization, and absorption of CO_2. **Polymers for Advanced Technologies**, v. 23, n. 5, p. 835–840, 2012.

YANG, H.; Xu, Z.; Fan, M.; Gupta, R.; Slimane, R. B.; Bland, A. E.; Wright, I. Progress in carbon dioxide separation and capture: A review. **Journal of Environmental Sciences**, v. 20, n. 1, p. 14–27, 2008.

YAUMI, A. L.; Abu Bakar, M. Z.; Hameed, B. H. Recent advances in functionalized composite solid materials for carbon dioxide capture. **Energy**, 2017.

Yu, C.; Huang, C.; Tan, C. A Review of CO_2 Capture by Absorption and Adsorption. p. 745–769, 2012.

YU, G.; Li, Q.; Li, N.; Man, Z.; Pu, C.; Asumana, C.; Chen, X. Synthesis of New Crosslinked Porous Ammonium- Based Poly (ionic liquid) and Application in CO_2 Adsorption. **Polymer engineering and science**, p. 2–6, 2014.

YUAN, J.; Antonietti, M. Poly(ionic liquid)s: Polymers expanding classical property profiles. **Polymer**, v. 52, n. 7, p. 1469–1482, 2011.

YUAN, J.; Mecerreyes, D.; Antonietti, M. Poly(ionic liquid)s: An update. **Progress in Polymer Science**, v. 38, n. 7, p. 1009–1036, 2013.

Zhu, J. M.; He, K. G.; Zhang, H.; Xin, F.; Engineering, C. Effect of Swelling on Carbon Dioxide Adsorption by Poly (ionic liquid) s. n. July, p. 35–42, 2011.

Zulfiqar, S.; Sarwar, M. I.; Mecerreyes, D. Polymeric ionic liquids for CO_2 capture and separation: potential, progress and challenges. **Polym. Chem.**, p. 6435–6451, 2015a.

ANEXO A

Fwd: Energy & Fuels - Manuscript ID ef-2017-02027c

Sandra Mara Oliveira Einloft

sex 14/07/2017 14:22

Para:Franciele L Bernard <franciele.bernard@pucrs.br>;

Fugi um pouco da reunião e mandei...

Sandra

Início da mensagem encaminhada

De: Energy & Fuels <onbehalfof+admin-journals+services.acs.org@manuscriptcentral.com>
Data: 14 de julho de 2017 14:14:11 BRT
Para: einloft@pucrs.br
Assunto: Energy & Fuels - Manuscript ID ef-2017-02027c
Responder A: admin-journals@services.acs.org

14-Jul-2017

RE: Energy & Fuels
Manuscript ID: ef-2017-02027c
Manuscript Type: Article
Manuscript Title: Hybrid alkoxysilane-functionalized urethane-imide-based poly(ionic liquids) as a new platform for carbon dioxide capture
Author(s): Bernard, Franciele L.; Polesso, Barbara; Cobalchini, Fabiana; Chaban, Vitaly; do Nascimento, Jailton; Dalla Vecchia, Felipe; Einloft, Sandra
Corresponding Author: Prof. Dr. Sandra Einloft
Corresponding Author's email: einloft@pucrs.br

Dear Sandra Einloft:

Your manuscript has been successfully submitted to Energy & Fuels.
Title: "Hybrid alkoxysilane-functionalized urethane-imide-based poly(ionic liquids) as a new platform for carbon dioxide capture"
Authors: Bernard, Franciele L.; Polesso, Barbara; Cobalchini, Fabiana; Chaban, Vitaly; do Nascimento, Jailton; Dalla Vecchia, Felipe; Einloft, Sandra
Manuscript ID: ef-2017-02027c.

Please reference the above manuscript ID in all future correspondence or when calling the office for questions. If there are any changes in your contact information, please log in to ACS Paragon Plus at http://paragonplus.acs.org/login and select "Edit Your Account" to update that information.

You can view the status of your manuscript by checking your "Authoring Activity" tab on ACS Paragon Plus after logging in to http://paragonplus.acs.org/login.

Thank you for submitting your manuscript to Energy & Fuels.

Sincerely,

Energy & Fuels Editorial Office

PLEASE NOTE: This email message, including any attachments, contains confidential information related to peer review

ANEXO B

Editor handles JFUE-D-17-02026

Fuel <eesserver@eesmail.elsevier.com>

sáb 27/05/2017 03:48

Para: Sandra Mara Oliveira Einloft <Einloft@pucrs.br>;

Cc: Franciele L Bernard <franciele.bernard@pucrs.br>; rafael.duczinski@acad.pucrs.br <rafael.duczinski@acad.pucrs.br>; marisolfernandezrojas@gmail.com <marisolfernandezrojas@gmail.com>; maria.fialho@acad.pucrs.br <maria.fialho@acad.pucrs.br>; luzangelacarreno@gmail.com <luzangelacarreno@gmail.com>; vvchaban@gmail.com <vvchaban@gmail.com>; Felipe Dalla Vecchia <felipe.vecchia@pucrs.br>;

Fuel
Ref: JFUE-D-17-02026
Title: Cellulose based poly(ionic liquids): Tuning cation-anion interaction to improve carbon dioxide sorption
Authors: Franciele Bernard; Rafael Duczinsky; Marisol Rojas; Maria Fialho; Luz Angela Carreno; Vitaly Chaban; Felipe Dalla Vecchia; Sandra Einloft
Article Type: Research paper

Dear Dr. Einloft,

Your submission entitled "Cellulose based poly(ionic liquids): Tuning cation-anion interaction to improve carbon dioxide sorption" will be handled by Principal Editor Eric Suuberg, ScD.

You may check on the progress of your paper by logging on to the Elsevier Editorial System as an author. The URL is https://ees.elsevier.com/jfue/.

Your username is: einloft@pucrs.br
If you need to retrieve password details, please go to: http://ees.elsevier.com/jfue/automail_query.asp

Thank you for submitting your work to this journal. Please do not hesitate to contact me if you have any queries.

Kind regards,

Fuel

****

For further assistance, please visit our customer support site at http://help.elsevier.com/app/answers/list/p/7923. Here you can search for solutions on a range of topics, find answers to frequently asked questions and learn more about EES via interactive tutorials. You will also find our 24/7 support contact details should you need any further assistance from one of our customer support representatives.

ANEXO C

Brazilian Journal of Chemical Engineering - Manuscript ID BJCE-2017-0182

Brazilian Journal of Chemical Engineering <onbehalfof+rgiudici+usp.br@manuscriptcentral.com>

dom 09/04/2017 20:45

Para:Sandra Mara Oliveira Einloft <Einloft@pucrs.br>;

Cc:Franciele L Bernard <franciele.bernard@pucrs.br>; daniela.maffi@acad.pucrs.br <daniela.maffi@acad.pucrs.br>; barbara.polesso@acad.pucrs.br <barbara.polesso@acad.pucrs.br>; vvchaban@gmail.com <vvchaban@gmail.com>; Marcus Seferin <seferin@pucrs.br>; Felipe Dalla Vecchia <felipe.vecchia@pucrs.br>; Sandra Mara Oliveira Einloft <Einloft@pucrs.br>;

09-Apr-2017

Dear Dr. Einloft:

Your manuscript entitled "Development of Inexpensive Cellulose-Based Sorbents for Carbon Dioxide" has been successfully submitted online and is presently being given full consideration for publication in the Brazilian Journal of Chemical Engineering.

Your manuscript ID is BJCE-2017-0182.

Please mention the above manuscript ID in all future correspondence or when calling the office for questions. If there are any changes in your street address or e-mail address, please log in to ScholarOne Manuscripts at https://mc04.manuscriptcentral.com/bjce-scielo and edit your user information as appropriate.

You can also view the status of your manuscript at any time by checking your Author Center after logging in to https://mc04.manuscriptcentral.com/bjce-scielo.

Thank you for submitting your manuscript to the Brazilian Journal of Chemical Engineering.

Sincerely,
Brazilian Journal of Chemical Engineering Editorial Office